Impact Load Effects on Post-Installed Anchors: An Experimental Investigation

by

Aliu Abdul-Hamid

A thesis submitted to the Faculty of Graduate and Postdoctoral Affairs in partial fulfillment of the requirements for the degree of

Master of Applied Science

in

Civil Engineering

Carleton University
Ottawa, Ontario

Abstract

The experimental study was carried out to assess the suitability of three proprietary post-installed anchors from Simpson Inc. for use under high strain-rate loading, such as blast loadings, in both tension and in shear. The anchors investigated included two torque-controlled expansion anchors (Strong Bolt® 2, Wedge-All®) and a screw anchor (Titen HD®) . While three different diameters (6.4 mm, 9.5 mm and 12.7 mm) of the Strong Bolt® 2 and Titen HD® anchors were investigated, only two diameters (9.5 mm and 12.7 mm) of Wedge-All® anchors were investigated.

The anchor capacities under static loading conditions with average strain rate of 3.0×10^{-4} /s were compared with those for impact-loads with average strain rate of 1 /s to define a Dynamic Increase Factor (DIF). The failure modes under both conditions were also assessed to ascertain the change as the loading rate increased.

For tensile loading, the results show that the Wedge-All® and 6.4-mm diameter Strong Bolt® 2 anchors may not be suitable for dynamic loading conditions. The Titen HD® as well as the 9.5-mm and 12.7-mm diameter Strong Bolt® 2 anchors are suitable for high strain-rate loading of up to 1 /s.

The torque-controlled expansion anchors failed predominantly in pull-through failure mode under the high strain-rate loading conditions even though they failed in a variety (steel fracture failure, concrete breakout and beam splitting) of modes under static loading condition. The Titen HD® anchors failed predominantly in a mixed pull-out and concrete breakout mode under both static and high strain-rate loading conditions.

Under high strain rate shear loading, the 9.5-mm and 12.7-mm diameter anchors (Strong Bolt® , Wedge-All® and Titen HD) were found to be suitable for dynamic loading

conditions. The predominant failure modes for anchors under shear loading, both under static loading and high strain-rate, was steel fracture failure.

Dynamic increase factors (DIF) of 1.1 and 1.2 are recommended for Titen HD and the 9.5-mm and 12.7-mm diameter Strong Bolt 2 anchors respectively for high strain rate up to 1 /s under tension loading. A DIF of 1.2 is recommended for the Titen HD anchors while DIFs of 1.0 and 1.2 are recommended for the 9.5-mm diameter and 12.7-mm diameter respectively for Strong Bolt 2 and Wedge-All anchors under shear loading up to strain rate of 1.0 /s.

Acknowledgements

I would like to acknowledge the incalculable academic and financial contribution of my supervisor, Dr. Abass Braimah in directing me to get this work done. The contribution of the laboratory personnel, including Stanley Conley, Jason Arnot and Stephen Vickers were instrumental in completing the experimental work. The anchors for the tests were provided by Simpson Inc through Fred Tai and Benoit Pelletier, whom I duly want to acknowledge, and the financial contribution from the Natural Sciences and Engineering Research Council (NSERC) through the Engage Grant Program.

On the personal level, I would like to mention the support from my family – my wife, Nimatu and our two children, Wunsaha and Suglo, including my mother and my late father, throughout this journey.

Finally, as a person of faith, I would like to acknowledge the extreme mercies from the almighty God in seeing me through this process.

Table of Contents

List of Tables

List of Illustrations

List of Symbols

A_e	Projected area of breakout concrete	[mm^2]
A_{se}	Effective tensile area of steel anchor	[mm^2]
A_{sv}	Effective shear area of steel anchor	[mm^2]
c_1	Anchor edge distance	[mm]
c_{ac}	Anchor critical edge distance	[mm]
d	Anchor diameter	[mm]
d_h	Anchor head diameter	[mm]
d_w	Washer diameter	[mm]
E_c	Concrete elastic modulus	[MPa]
E_s	Steel elastic modulus	[MPa]
f'_c	Concrete cylinder compressive strength	[MPa]
f'_{cc}	Concrete cube compressive strength	[MPa]
f_t	Static concrete tensile strength	[MPa]
f_{td}	Dynamic concrete tensile strength	[MPa]
f_{uta}	Steel ultimate strength	[MPa]
f_y	Steel yield strength	[MPa]
G_f	Total specific fracture energy	[N/mm]
h	Concrete beam depth	[mm]
h_{ef}	Anchor effective embedment depth	[mm]
h_{nom}	Anchor nominal embedment depth	[mm]
h_t	Anchor thread pitch	[mm]
h_s	Distance from tip of anchor to start of pitch	[mm]
k_1	Calibration factor for concrete tensile strength	[N/A]
k_2	Calibration factor for projected breakout area	[N/A]
k_3	Calibration factor for size-effect	[N/A]
k_n	Effective calibration factor/effectiveness factor	[N/A]
k_{np}	Effective pryout factor	[N/A]
l	Effective bearing length of anchor in shear	[mm]
N_u	Tensile capacity of anchor loaded in tension	[N]
V_u	Shear capacity of anchor loaded in shear	[N]
ε	Strain	[N/A]
$\dot{\varepsilon}$	Strain rate	[/s]
$\dot{\varepsilon_s}$	Static strain rate	[/s]
λ	Concrete unit weight factor	[N/A]
τ_k	Characteristic bond strength for bonded anchors	[N/mm^2]

List of Abbreviations

ACI	American Concrete Institute
ASTM	American Society for Testing and Materials
CCD	Concrete Capacity Design
CSA	Canadian Standards Association
DIF	Dynamic Increase Factor
DLR	Dynamic Load Ratio
DoD	Department of Defense
ICC-ES	International Code Council Evaluation Services
LVDT	Linear Vertical Deferential Transformer
SI	Systeme International (International System of Units)
UFC	Unified Facilities Criteria

1 Chapter: Introduction

1.1 Background and Research Motivation

The demand for more flexibility in planning, design, construction and strengthening of concrete structures has resulted in the increased use of metallic anchoring systems. From holding base plates of foundation in steel column erection to ensuring machinery is adequately fixed on factory floors, anchors are used.

Anchoring system are classified into two broad groups: cast-in-place and post-installed. As the name connotes, the former is attached to formwork and then adequately designed and mixed concrete is poured to cure with the anchor in place. These types of anchors include headed studs, bent bars, and straight deformed bars [1]. The heads in headed studs provide a bearing surface at the anchor head-concrete interface, enhancing the anchor's resistance to pull-out. Deformed bars may be used without a positive bearing surface provided adequate embedment is provided to develop the anchor material strength [1]. Hooked bars also have positive bearing surfaces in addition to development length to ensures adequate anchor capacity is achieved.

Post-installed anchors on the other hand may be installed in cured concrete at any point in the life of the concrete structure. Post-installed anchors are generally classified into two broad groups: mechanical and bonded. Mechanical anchors achieve strength through friction, bearing, keying or a combination of these at contact interfaces between anchor and concrete substrate. Bonded anchors on the other hand employ organic and inorganic materials to achieve strength through bonding and micro-keying actions with concrete substrate.

The behavior of anchors under static loading conditions have had considerable attention in the past decades. The Canadian [2] and American Design Codes [3], [4] present design procedures developed in accordance with the Concrete Capacity Design (CCD) [5] method which catalogues the capacity of anchors under tensile and shear conditions under static loading.

Though on individual basis, the behavior of steel and concrete have been evaluated at high strain rates – rates corresponding to those seen under impulsive and dynamic loading, the response of post-installed anchors to such conditions have not been adequately evaluated. It is therefore imperative that more research of post-installed anchors under these conditions be conducted to aid in their design, as the anchors are integral in the design of structures subjected to impulse type loading, especially blast-resistant window anchorages.

1.2 Research Objectives

The overall objective of the research presented in this thesis is to assess the behavior of three different types of post-installed anchors – Titen HD®, Strong-Bolt® 2 and Wedge-All®, manufactured by Simpson® Inc., under impulsive loads and to propose dynamic increase factors (DIF), defined as the ratio of the failure load under the impulsive condition to the failure loads under static conditions, for anchorage systems design. Particularly, the study is aimed at:

I. Assessing the ultimate tensile and shear capacities of the anchors at the manufacturer's suggested embedment depths under static and impulsive conditions.
II. Comparing the modes of failure associated with static and dynamic loading conditions.

III. Proposing appropriate DIF from the DLR for use in design under dynamic or impulsive load conditions.

2 Chapter: Literature Review

2.1 Introduction

Terrorist attacks on structures around the world have shown that most injuries from the attacks, apart from casualties or fatalities resulting from direct collapse of structural components, are caused by flying glass [6], [7]. In this regard, buildings, particularly government buildings and those in regular use by state and high-profile officials are often retrofitted with anti-shatter film to mitigate injuries and fatalities due to the glass shard hazard. To maintain the integrity of fenestrations, adequate connection should be ensured between window frames and main structural members. It is required that window frames and their anchorage be designed to resist dynamic blast loads subjected to window glass lite assuming the resulting dynamic loading would not fracture the glass [7] and will be transmitted to the anchorage systems. Conventional window anchors often lack the strength to resist the imposed dynamic blast loads, resulting in dislodgement of retrofitted windows and their projection into the interior of buildings with a potential to cause fatal injuries to occupants. Post-installed anchors are recommended for upgrading anchorage of window frames to the structure of the façade. However, the design of post-installed anchors and anchors in general requires comprehensive knowledge and understanding of their behavior under dynamic loads produced by explosions. A review of the literature has shown that most of the research work to date has concentrated on static or quasi-static behavior of steel anchors in concrete [8-20], . Information on behavior of anchors under dynamic loading conditions is quite limited, and most of the information is based on the individual properties of concrete and steel under high strain rate. Bischoff and Perry [21] assessed the experimental techniques and methods of measurement used in investigating compressive

behavior of concrete at high strain-rates. They observed that increase in plain concrete compressive strength primarily depends on the loading rate and follows a bilinear relationship on a linear-logarithmic scale. They also observed a 50 to 85% increase in the compressive strength of plain concrete at strain rates of about 10 /s. Cowell [22] reported an increase of 18 to 65% in the tensile strength of concrete and in some cases up to 70% under increased loading rates of up to 2000 MPa-/s in the case of tensile loading and 14000 MPa/s in the case of compressive loading. Malvar and Crawford [23], [24] in a literature review of the DIF for concrete and reinforcing steel reported that at strain rates of up to 1000 /s, significant increase of more than 50% could be achieved for steel, by more than 200% for concrete in compression, and more than 600% for concrete in tension.

Post-installed anchors are classified based on the load transfer mechanism into mechanical and bonded anchors. Mechanical anchors transfer load by friction, keying, bearing or a combination of these. Bonded anchors on the other hand transfer load through bond between steel anchor and the bonding agent and between bonding agent and substrate material [25][26]. Braimah et al. [25] and Ahmed and Braimah [27] investigated the behavior of adhesive steel anchors under impulse-type loading and behavior of undercut anchors subjected to high strain rate loading. For the adhesive anchors under impulse type loading, different substrate materials as well as angles of installation were investigated. DIF values of 1.2 and 2.5 were recommended for 90^{o} and 45^{o} installation angles for limestone substrate and 1.2 and 3.2 respectively for concrete substrate material. For undercut anchors, a maximum DIF in tension of 1.6 was recommended at strain rate of 10^{3} /s [25]. Solomos and Berra [28] employed Split-Hopkinson Pressure Bar (SHPB) [29] to investigate the behavior of anchors in concrete under dynamic tensile loading and found

that increase in anchor capacity was in the order of 1.07 to 1.67 times the capacity under static loading. Rodriguez et al. [8], [30] investigated the behavior of anchors in uncracked concrete under dynamic tensile loading and observed that wedge type anchors (expansion anchors) failed in either pull-out or pulled through mode from the concrete substrate under dynamic loading conditions. The authors recommended that the anchors be evaluated further to determine their seismic adequacy. Rodriguez et al. also found out that grouted anchors pulled out of cracked concrete under dynamic conditions. Fujikake et al. [31] observed that the dynamic cone resistance of adhesive anchors is closely related with the dynamic tensile strength of concrete.

Anchors may be loaded in tension, shear or a combination of the two. The capacities of anchors under these loading conditions should be adequately known to the design engineer. The CCD method [5] is widely accepted and has become the basis for design recommended in the Building Code Requirement for Structural Concrete (ACI 318 [3]), the Code Requirement for Nuclear Safety (ACI 349 [4]) and Appendix D of the Canadian Concrete Design Handbook (CSA A23.3-14 [2]). Anchor capacities according to the CCD method depend on the tensile capacity of concrete along a 35° failure cone as well as the effective embedment depth of the steel anchor. In ACI 349-85, which was the basis of design prior to the adoption of the CCD method, the capacity was expressed as a function of the square of the effective depth of a concrete cone with base diameter equal to two times the effective depth and resulting in a 45° failure cone. Report of ACI Committee 355 [32] provides the guidelines for the qualification of post-installed mechanical anchors for use in concrete, but makes little distinction for screw anchors. AC 193 [33] from the International Code Council (ICC) Evaluation Services provides the acceptance criteria for mechanical

anchors, where specification for screw anchors are presented. The standard terminologies and test methods for anchors in concrete are also outlined in American Society for Testing and Materials (ASTM) E2265-17 [34] and E488/E488M-15 [35] respectively.

2.2 Anchor Types in Concrete

Anchorage in concrete can be divided into two main categories, Cast-in-place and Post-installed. Fig.2.1 shows categorization of anchors used in concrete based on their mode of installation.

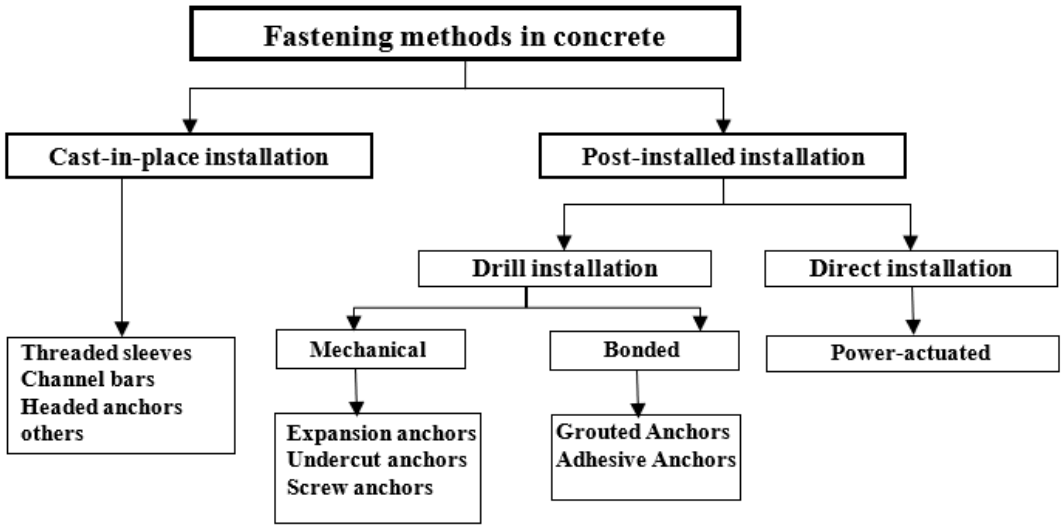

Fig.2.1: Fastening Methods in Concrete [26]

On the basis of load transfer mechanism, post-installed anchors may be sub-divided into mechanical (interlocking and friction) and bonded anchors [26]. Mechanical interlock involves transfer of load by means of bearing and interlock between anchor and base material. This mode of load transfer is encountered in headed anchors, anchor channels, undercut anchors and screw anchors. Expansion anchors rely on friction between the anchor and walls of the hole in substrate material to transfer applied loads. The friction

force is enhanced as a result of the expansion of the anchor during the installation process and is in a state of equilibrium with the applied tensile load [26].

2.2.1 Bonded Anchors

Bonded anchors are post-installed anchors whose main load transfer mechanism is achieved by the bond formed between the steel anchor and substrate material through a bonding agent. They resist tension loads by adhesion and micro-keying of the bonding material to the anchor rod or dowel and to the sides of the drilled hole [26]. Bonded anchors include adhesive and grouted anchors. An adhesive anchor is a steel element inserted into a drilled hole in hardened concrete with a structural adhesive acting as a bonding agent between the concrete and the steel [36]. In the installation process, the diameter of the drilled hole is typically about 1.5 mm larger than the diameter of the steel element. Adhesive anchors are available in glass or foil capsule using organic or inorganic compounds or a mixture of the two in either pre-packaged cartridge systems or bulk injection systems [26], [36]. A grouted anchor may be a threaded rod, deformed bar, headed bolt, or threaded rod with or without nut at the embedded end installed in a large drilled hole[36]. Typically, the hole size for grouted anchors is approximately twice the diameter of the anchor and is drilled with a core drill [36]. Grouted anchors are generally limited to vertical installations owing to the large hole diameters. As in adhesive anchors, grouted products may be inorganic, organic, or a mixture of the two. Fig. 2.2 shows the types of bonded anchor systems. The primary difference between adhesive and grouted anchors when a polymer-based material is used is the introduction of a filler material (such as fine sand) into the bond mixture of the grouted system [37].

The study of the behavior of bonded anchors under load and their design under static conditions are captured in the works of Cattaneo and Muciaccia [38], Chen [39], Nilforoush [9], Eligehausen and Cook [36]. Nilforoush et al. [20] investigated the long term performance of adhesive bonded anchors for up to 28 years and found that the long-term performance of adhesive anchors were substantially impaired by outdoor conditions such as temperature and humidity variations.

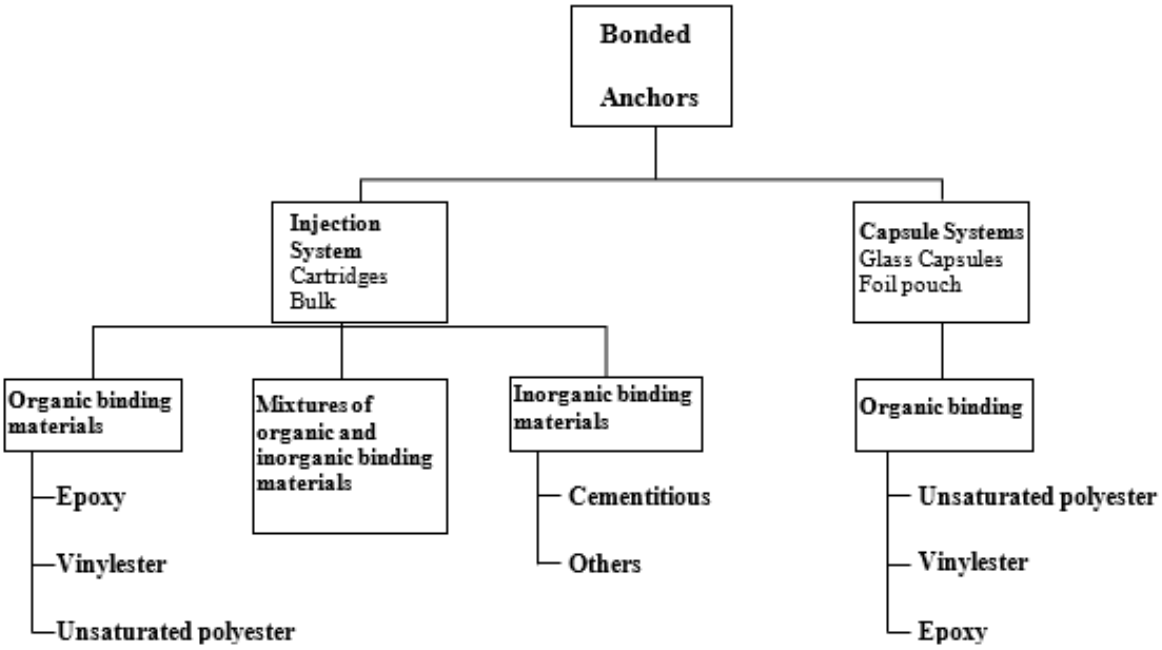

Fig. 2.2: Classification of Bonded Anchor Systems [26]

Under high rates of strain, Braimah et al. [25] conducted experimental tests on two different diameters of adhesive anchors, under two different substrate material and at different angles of orientation to the anchoring surface and recommended different values of DIFs for each type of application. Fujikake et al. [31] observed that the ultimate cone and bond capacities of adhesive anchors increased with loading rates. The dynamic cone resistance of bonded anchors was closely related to the dynamic tensile strength of concrete and the average dynamic bond strength at a given loading rate was independent of the embedment

depth. The authors proposed an empirical equation to evaluate the dynamic cone capacity and bond resistance for the anchors.

2.2.2 Undercut Anchors

Undercut anchors are anchors with parts that spread into and mechanically interlock with concrete base material. In the installation process, a cylindrical hole is first drilled and then followed by the undercutting process before or during the installation of the anchor [5]. The undercutting process is achieved by creating a notch of a specified dimension at a defined location either by using a special drilling apparatus or by undercutting action of the anchor itself [26]. The undercutting shape can take a form that widens towards the bottom of the hole. Fig. 2.3 shows different forms of undercut anchors.

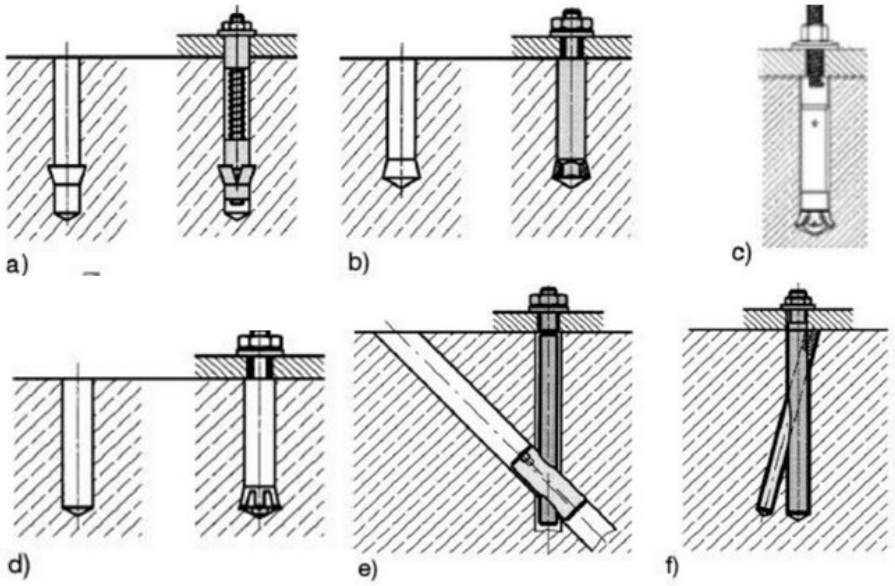

Fig. 2.3: Undercut Anchor Types - a) Reverse Undercut b) to d) Forward Undercut e) and f) other Interlocking Systems[26]

Undercut anchors are a subject of many research works, including Marco et al. [40] who observed that though concrete properties and undercut anchor system's tensile capacity may be affected by the type of coarse aggregate, the provisions of the CCD method

adequately predict anchor tensile capacities with no modification based on coarse aggregate types. Primavera et al. [41] observed through experimental investigation that while tensile capacities of anchors increased with increasing compressive strength, consistent with the ACI 349-85 and CCD methods, failure cone angles ranging from 21° to 28° were considerably smaller than the failure cone angles of the two design methods. Asmus [42] investigated the factors influencing splitting forces of mechanical undercut anchors and observed that the load-bearing area was the major factor as it relates the splitting pressure to the tensile force. He also observed that for anchor cone angles less than 20°, the splitting forces increase with increasing cone angles. Ahmed and Braimah [27] investigated the behavior of undercut anchors under high strain rate loading using numerical modelling techniques and observed that the tensile capacity of anchors increased with increasing strain rate and observed a maximum DIF of 1.6 at a strain rate of 10^3 /s.

2.2.3 Expansion Anchors

Expansion anchors produce expansion forces and thereby holding forces in the concrete base material. The base of the anchor is cone-shaped (mandrel) and shrouded with an expansion sleeve (expansion clip). During installation, the mandrel at the end of the anchor is drawn into the expansion clip, generating the expansion/frictional forces against the walls of the hole in the substrate material.

Expansion anchor can be categorized as torque-controlled and displacement-controlled anchors. Torque-controlled anchors require a specified amount of installation torque to be applied to activate the anchor mechanism. Conversely, displacement-controlled anchors require a pre-set axial displacement of an expansion plug in the anchor sleeve to activate the anchor mechanism. The expansion forces generated in displacement-controlled anchors

are more than those generated in torque-controlled anchors [26]. Fig. 2.4 shows the general working principles of expansion anchors.

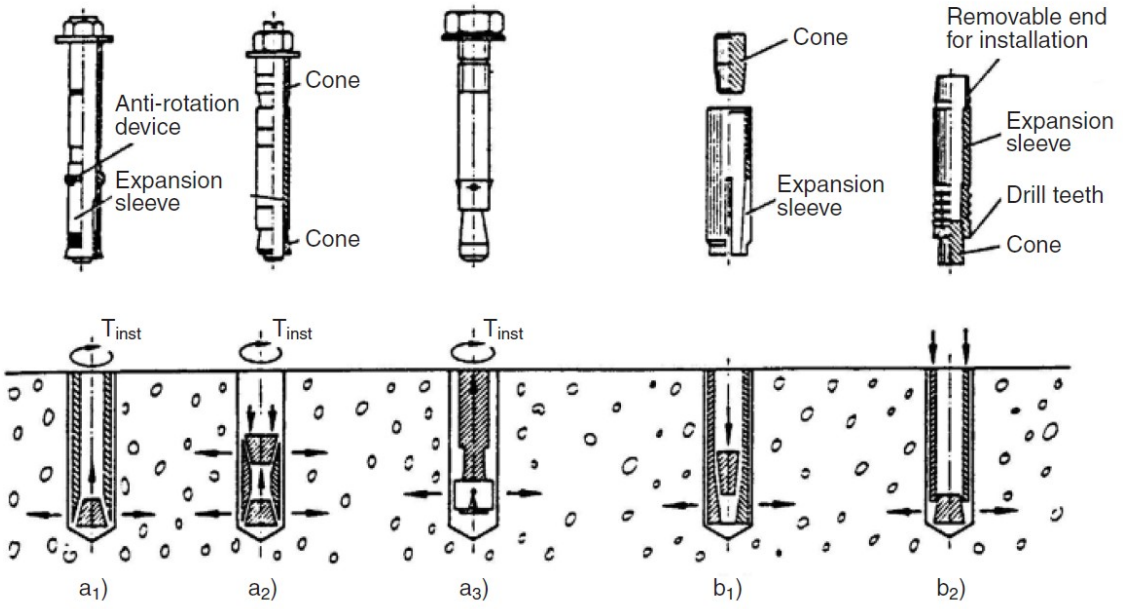

Fig. 2.4: Working Principles of Expansion Anchors – a_1) to a_3) Torque-Controlled, b_1) and b_2) Displacement-Controlled [26]

Follow-up expansion [26], an additional draw-in of the expansion cone of the anchor into the expansion sleeve during loading, is a phenomenon associated with torque controlled expansion anchors. The additional displacement occurs when the external load on the anchor completely balances out the pretressing forces induced in the anchor during the initial installation process. Further movement of the cone into the sleeve generates additional friction which resists the increasing imposed load.

The behavior of expansion anchors has been a subject of investigation by many researchers. Delhomme et al. [43] investigated the influence of tightening torque on the pull-out behavior of expansion anchors and concluded that a pre-tension load has no influence on the pull-out strength of a single expansion anchor installed far away from the edge of the

concrete. They observed however that under-torqueing may lead to unsatisfactory load-displacement behavior of the anchor system under serviceability conditions. Eligehausen [44] identified anchor pull-out, concrete cone, concrete splitting and steel rupture as the predominant failure modes for expansion anchors and proposed equations for determining the anchor capacities for each mode. Melcher et al. [45] presented the results of the actual behavior of expansion anchors to loading and concluded that equations for anchor capacities based on the CCD method [5] give a better prediction compared to the equations based on the ACI 349-85 method [4].

The long term performance of expansion anchors simulated under freeze-thaw conditions were investigated by Kwon et al. [19] who observed a change in failure mode from pull-out in the short term to concrete cone failure in long-term freeze-thaw samples leading to a reduction in capacity. The study reported that though the compressive strength of concrete generally reduced by 20%, the tensile capacity of the anchors was reduced by 50%, an appropriate reduction factor was therefore recommended for design purposes. The behavior of expansion anchors under seismic, cyclic, and high-strain rates has been investigated by only a few researchers. Muciaccia [46] reviewed the design criteria for post-installed anchors and presented an experimental investigation of anchor groups located far away from edges in low-strength, uncracked concrete. The author reported that when capacity design criteria is employed to preclude anchor failure, no significant difference is detected between anchor behavior and established steel-to-steel connections. Rodriguez et al.[8] carried out tensile tests on post-installed anchors and observed that tensile capacities and modes of failure under dynamic conditions were at least as high as

the capacities under quasi-static conditions, except for wedge-type expansion anchors which tend to pull out or pull through under dynamic loading.

2.2.4 Screw Anchors

Concrete screw anchors are manufactured with threads that cut into concrete during the installation process and provide mechanical interlock which helps in transfer of loads from the anchor to the concrete. The installation of screw anchors follows a simple process of screwing the anchor into the concrete after a cylindrical hole with defined diameter and depth is drilled. During the installation of screw anchors, the applied torque is limited to a value beyond which the capacity of the installed anchor could be compromised. Exceeding the specified torque could lead to failure by shearing of either the steel anchor or the concrete [47].

In addition to its ease of installation, screw anchors can be used in cracked concrete, as the threads have a capability of crossing cracks, and also to be easily uninstalled. This makes screw anchors excellent for temporary application. The amount of undercut (difference between the outer diameter of the thread and drilled-hole diameter) influences the load carrying capacity of the screw anchor as well as the failure mode [15]. However, a higher level of undercut increases the difficulty of installation of the anchor. Also, for deeply embedded anchors with shallow undercuts, pullout in tension is dominant, while concrete breakout over the entire depth of embedment is predominant for shallow embedded anchors with deep undercuts A proper balance is therefore required between the anchor capacity and ease of installation. This results usually in a mixed failure mode where the lower portion of the anchor pulls out with a concrete cone breakout towards the surface of embedment [15]. Fig. 2.5 shows the different types of screw anchors employed in design.

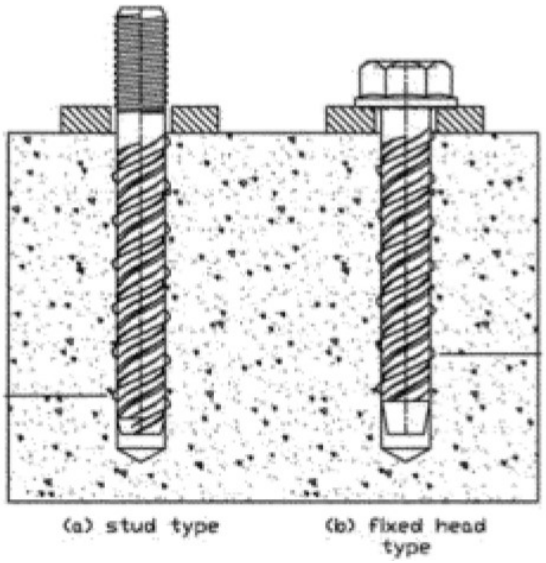

Fig. 2.5: Screw Anchors Types in Concrete [33]

Though the design of screw anchors follow the provisions of CCD method [5], tests carried out by Kuenzlen and Sippel [47] showed that the use of the CCD Method would not be appropriate without making some modifications to the design equations. Kuenzlen [48] proposed modifications to the calculation of the effective embedment depth in order to use the CCD method for screw anchors. Olsen et al. [15] observed that the modified CCD equation proposed by Kuenzlen accurately estimated the tensile capacity of screw anchors and proposed additional limits for nominal effective depth and anchor spacing. Mohyeddin et al. [49] observed a direct correlation between the compressive strength of concrete and the ultimate tensile capacity of screw anchors embedded in concrete aged 24 hours to 28 days. This observation agrees with the formulation of the CCD method where the anchor capacity in tension is directly related to the square-root of the concrete compressive strength.

2.3 Anchor Mode of Failure and Capacity

2.3.1 Failure Modes

2.3.1.1 Failure Modes in Tension

Eligehausen [44] identified four main failure modes associated with anchors subjected to tensile loads and located far away from edges of the substrate material. The failure modes are pull-out of metal anchor without significant damage to concrete, concrete cone breakout, splitting of concrete beam, and fracture of metal anchor. Concrete cone failure occurs with little or no warning and is a less desirable mode of failure. Ductile steel failure on the other hand provides adequate deformation during the loading process prior to failure and is a more desirable mode of failure of anchors. Failure in brittle cone breakout or steel yielding depends on the depth of embedment of the anchor. At a critical depth of embedment, failure of anchors transition from concrete breakout to steel yielding and fracture. This critical embedment depth of expansion anchors depends on the expansion mechanism and is determined in the anchor pre-qualification test [5] as stated in ACI 355.2 [32].

Pull-out failure is associated with all types of post-installed anchors where the entire anchor slides out of the drilled hole under tensile loading. For bonded anchors, pull-out failure is a result of bond failure at either between the anchor-bonding agent interface or bonding agent-concrete interface [25].

For screw anchors, pull-out is a result of the shearing of concrete along the embedment depth [15]. Pull-out failure in undercut anchors and headed studs result from inadequate mechanical interlock between anchor and concrete substrate [26]. For displacement-controlled expansion anchors, pull-out failure occurs when the expansion forces generated

during installation is insufficient to hold the anchor at the installed embedment depth for loads corresponding to concrete cone failure [26]. In torque-controlled expansion anchors, pull-through failure, which involves the sliding out of the anchor shank from the expansion sleeve is possible in addition to pull-out failure. Pull-out/pull-through failure depends on the deformability of the substrate material, geometry of drilled hole, and design of expansion mechanism [5]. The pull-out resistance also depends on friction between the outer face of the expansion sleeve and the walls of the concrete while the pull-through resistance depends on the friction between the expansion cone of the anchor and the inner face of the expansion sleeve [50]. Pull-through failure is the desired mode of failure for torque controlled anchors rather than a pull-out failure mode [26]. The desirability of pull-through over pull-out failure in torque-controlled expansion anchors is as a result of follow-up expansion, a phenomenon unique to that anchor type.

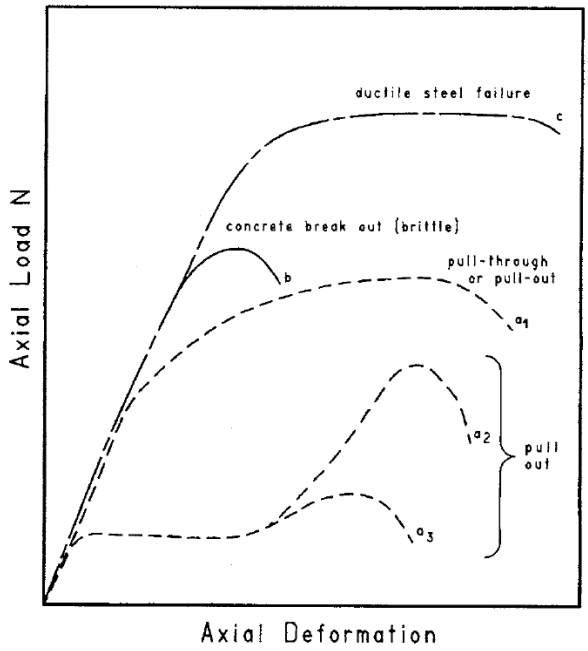

Fig. 2.6: Idealized Load-Deformation Curves for Anchor Failure Modes [5]

Fig. 2.6 shows an idealized load-deformation behavior for the various anchor failure modes. Curve a_1 represents the pull-out behavior of headed studs and undercut anchors as well as the pull-through behavior of torque-controlled expansion anchors. In curves a_2 and a_3 anchor pull-out begins once the preload is exceeded by the applied force in torque-controlled anchors. The pull-out leads to excessive axial displacement until the anchor establish contact with the walls of the concrete again. In curve a_2, the development of follow-up expansion leads to additional capacity to resist more load until failure. The amount of capacity developed after the onset of follow-up expansion in curve a_2 however is greatly affected by the embedment depth at which it develops. In curve a_3, very little follow-up expansion develops after anchor re-establishes contact, leading to failure at a much lower load. Pull-out failure in torque-controlled expansion anchors signify improper and inconsistent development of follow-up expansion as seen in curves a_2 and a_3, which makes pull-out failure much less predictable (in terms of anchor capacity) and an undesired mode of failure in those types of anchors

When mechanical expansion anchors develop sufficient expansion forces, or when undercut anchors or headed studs have enough bearing surfaces, cone breakout failure will occur so long as the steel capacity is not exceeded or there is no pull-through failure [26]. The concrete cone failure mode results from the utilization of the tensile capacity of concrete, leading to the formation of a cone-shaped fracture surface. The load-displacement behavior of anchors failing in concrete cone breakout is indicated by curve *b* in Fig. 2.6. The curve shows a relatively non-ductile behavior. While displacement-controlled anchors exhibit limited displacement before failure due to high slip-resistance as a result of high expansion forces, the presence of follow-up expansion in torque-controlled anchors allow

further deformation at service load levels through to failure of the anchor as further slip can occur. When headed studs or undercut anchors are located close to substrate edges, the break-out cone may involve local blow-out of the edge due to the expansion forces induced in the concrete. The load-displacement behavior utilizes the tensile capacity of concrete and follows the trend of curve *b*. However, a reduction in the peak load as a function of the edge distance needed to produce a full concrete cone is observed. The minimum edge distance required to avoid a side blow-up is known as the critical edge distance. For anchor groups, the minimum spacing required to avoid the intersection of failure cones of adjacent anchors is known as the critical spacing.

For screw anchors, a mixed failure mode involving pullout of the lower installed part of the anchor with a concrete breakout cone towards the surface is possible as the threads may not be too deep to result in full concrete cone breakout or too shallow to result in pull-out failure [15].

When the thickness of the substrate material (beam, slab, etc.) is not enough, splitting failure of the substrate may occur. Splitting failure may also result if the anchor is installed close to edges, or when a line of anchors are installed close to each other [5], [26]. Splitting failure utilizes the tensile strength of concrete, with a load-displacement behavior similar to the that of concrete breakout failure shown by curve *b*. However, since the full concrete breakout capacity is not achieved, the splitting capacity of an anchor system or a group is lower than the ultimate concrete breakout capacity.

Steel failure represents the highest limit achievable for the load-carrying capacity of an anchor. When a ductile steel is used, and there is sufficient length for elongation of the anchor, ductile behavior of type shown by curve *c* is observed for the load-displacement

relationship of the anchor. Fig. 2.7 shows the failure modes of anchors subjected to tensile loading.

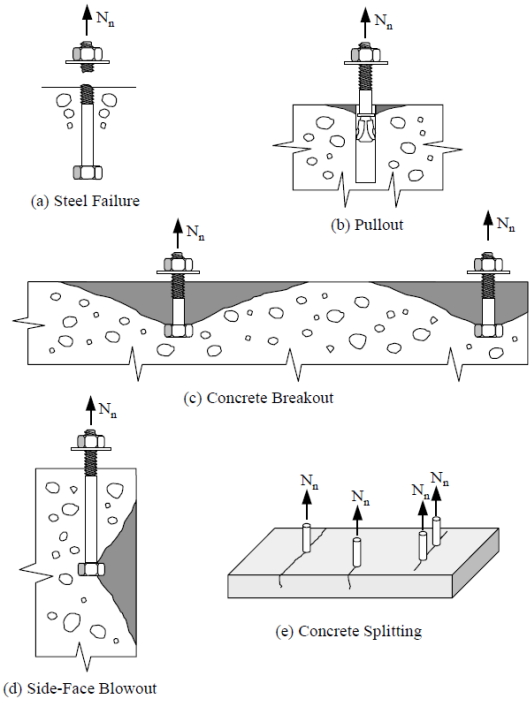

Fig. 2.7: Failure Modes under Tensile Loading [2]

2.3.1.2 Failure Modes under Shear Loading

Fig. 2.8 shows a typical load-displacement behavior of an expansion anchor subjected to shear loading while Fig. 2.9 illustrates the various failure modes of anchor systems subjected to shear loading. At the start of loading, load is transfered between baseplate and concrete through friction as a result of the initial preload on the acnhor. After the external shear force exceeds the friction resistance, the baseplate slips in order to engage the anchor. Once the baseplate engages the anchor, the anchor begins to bear on the plate, initiating a catenary action resulting in a tensile force in the anchor bolt [26].

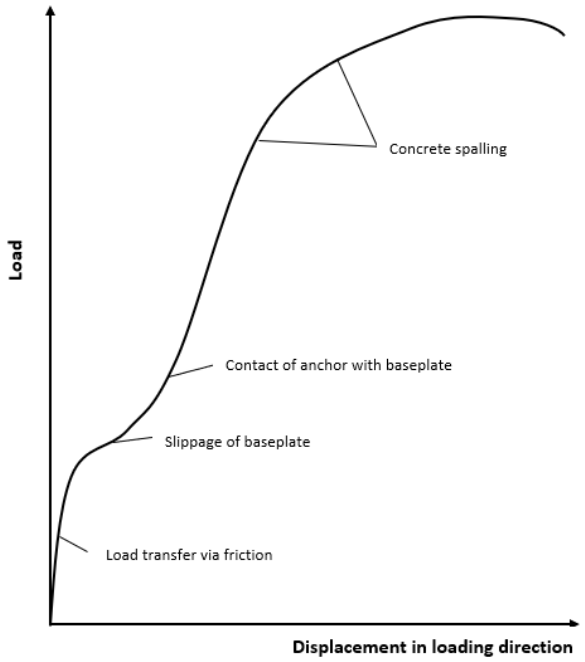

Fig. 2.8: Typical Load-Displacement Behavior of Expansion Anchor in Shear [26]

Increasing the applied shear force increases the bearing stress on the concrete at the surface, once this stress exceeds the compressive stress of concrete, the surface concrete begins to crush and fall off. This effect of concrete spalling is increasing moment arm and any associated flexural stress as the bearing resultant force is transferred deeper into the substrate material. If there is sufficient embedment, the anchor may resist additional load until failure in shear of the steel anchor.

In general, total displacement of anchors at ultimate load levels under shear are markedly greater than under tension due to the combined effect of spalling of concrete and the bending deformation of the anchor [26]. When expansion anchors are installed at shallow depths and located far away from edges, the anchor may pull out of the hole if sufficient friction is not developed to accommodate the catenary tensile force generated due to the lateral deformation.

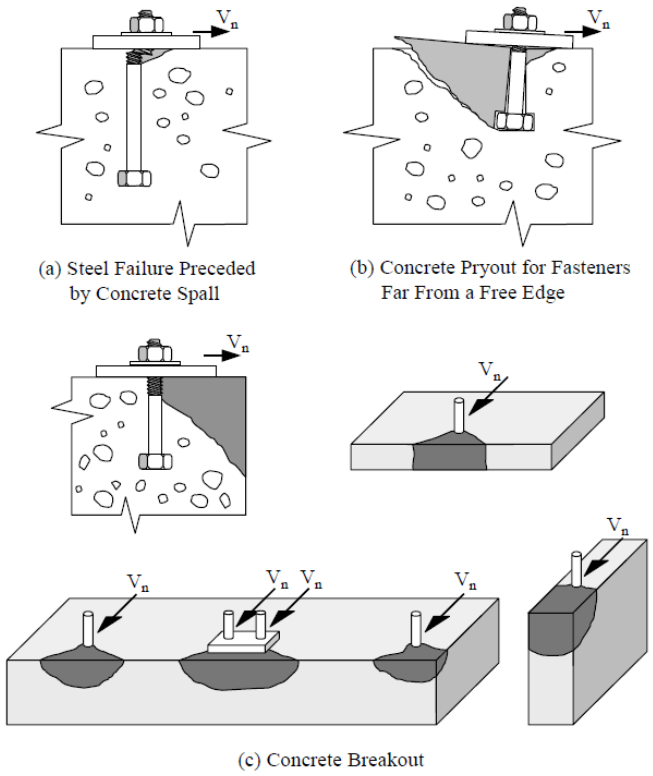

Fig. 2.9: Failure Modes for Anchors Loaded in Shear [2]

When anchors are located close to edges of the concrete substrate and are loaded in the direction perpendicular to the closest edge, a semi-conical concrete breakout may occur. The fracture surface of the concrete would radiate from the point of bearing of the anchor towards the free edge [5], [26]. This failure mode is known as concrete edge failure.

When anchors are located far away enough from free edges to preclude edge breakout failure and are installed at shallow depths (low depth to anchor diameter ratio), another failure mode known as pry-out failure may occur. Pry-out failure occurs when anchors with sufficient stiffness under shear loading exhibit enough rotation to fracture a cone of concrete at the side opposite to the direction of the shear force.

Several researchers have conducted studies on anchors under static shear loading. Ollgaard et al. [51] conducted pushoff tests on 48 two-slab shear connectors in normal and light-

weight concrete samples and proposed an empirical equation based on the stud area, the elastic modulus of concrete and the compressive strength of concrete to calculate shear capacity. Though the empirical equation correlated well with the test data, the authors simplified it through a linearized multiple regression analysis and rounding of exponents to arrive at a satisfactory design equation. The empirical equation was later modified by Shaikh and Yi [52] by eliminating the elastic modulus term and replacing it with equations from the ACI Code [3]. The authrs also introduced unit weight factor for concrete. Shaikh and Li [52] also ensured that in the modification of the Ollgaard equation, the coefficient were changed to correlate with lower bound of data from tests reviewed in their study. Anderson and Meinheit [53] conducted analysis on a database of previous pushoff tests in addition to new experimental tests and proposed an equation based on effective embedment depth, concrete compressive stregth and anchor stud diameter to calculate the pryout capacity of anchors in shear. Finally, Jebara et al. [17] used experimental results of single anchor under pure shear to propose an equation for pryout capacity of anchors. The proposed equation was compared with current design equations and was observed to be adequate, particularly for stiff anchors where pryout is likely.

2.3.2 Tensile and Shear Capacity of Concrete Anchors

2.3.2.1 Tensile Capacity

Since a ductile mode of failure is preferred to the brittle mode of failure, the capacity of anchors in tension is generally based on limits on the embedment depth to prevent brittle failure [5].

The generalized empirical equation based on many pull-out tests of headed studs under axial tensile loading in uncracked concrete is presented in Equation 1 [54]:

$$\boldsymbol{N_u = a \cdot (f'_c)^b \cdot (h_{ef})^c} \quad \textbf{[1]}$$

Where, $f'_c =$ cylinder concrete compressive strength, N/mm^2

$h_{ef} =$ embedment depth, mm

$a =$ constant for load calibration and dimensional consistency

$b =$ is the influence of compressive strength of concrete

$c =$ is the influence of embedment depth.

The first radical represents the tensile strength of concrete, with *b = 0.5* assumed. The value of *c* has been the major point of deviation between the various methods used for calculating the concrete breakout strength.

Earlier editions of ACI Committee 349 (ACI 349-85) report proposed *c = 2.0* following from their guiding principle in breakout capacity calculation. The guiding principle in the design approach was that the concrete breakout strength be based on a constant tensile stress over the projected area of an inverted cone truncated by the head of the anchor with circumferential base at the surface of the substrate [5]. The inclination of the failure plane of the truncated cone to the surface of the concrete was assumed to be 45^o, and thus would result in a base diameter equal to the sum of twice the effective embedment and the anchor head diameter.

Since the stress is assumed to be uniform, the anchor capacity becomes the product of the stress and the projected area consequently leading to the assigned value of *c*. The equation for the concrete breakout capacity of concrete based on ACI 349-85 is given in Equation 2 and Equation 3 in US customary and SI units, respectively.

$$N_u = 4 \cdot \sqrt{f'_c} \cdot \pi \cdot h_{ef}^2 \cdot \left(1 + \frac{d_h}{h_{ef}}\right) \quad [2]$$

$$N_u = 0.96 \cdot \sqrt{f'_{cc}} \cdot h_{ef}^2 \cdot \left(1 + \frac{d_h}{h_{ef}}\right) = 1.04 \cdot \sqrt{f'_c} \cdot h_{ef}^2 \cdot \left(1 + \frac{d_h}{h_{ef}}\right) \quad [3]$$

Where f'_{cc} is the compressive capacity of a 200-mm concrete cube and $f'_c = 0.85 f'_{cc}$.

The CCD method [5] is a newer and widely accepted method for calculating the breakout capacity and has been adopted in both the American and Canadian Codes [2], [3]. Transition from the ACI approach to the CCD method was as a result of research carried out by several researchers, including Eligehausen and Ozbolt [55] where numerical analyses of pull-out tests showed that the size effect law, presented by Bazant et al. [56] and given in Equation 4, applied in the pull-out capacity of headed studs.

$$N_u = N_{u1} \cdot B \cdot \left(1 + \frac{h_{ef}}{d_o}\right)^{-\frac{1}{2}} \quad [4]$$

$$N_{u1} = a \cdot (f'_c)^{0.5} \cdot \left(h_{ef}\right)^2$$

N_u and N_{u1} represent the capacities including and excluding size effects respectively and B and d_o are constants determined from regression analysis. N_{u1} is of the form of Equation 1 where a remains the calibration constant and b and c are *0.5* and *2.0* respectively.

Eligehausen and Sawade [57] observed that the circumferential crack that results from the cone breakout of anchors subjected to tensile loading propagated in a mixed mode, rather than uniformly with the tensile strength of concrete over the projected area. They reported that the behavior of concrete and the growth of cracks depend on the specific fracture energy required for crack propagation. A formulation based on linear-elastic fracture

mechanics for the concrete breakout capacity and depending on the fracture energy and embedment depth was proposed (Equation 5).

$$N_u = 2.1 \cdot \sqrt{(E \cdot G_f)} \cdot h_{ef}^{\frac{3}{2}} \quad [5]$$

G_f is total specific fracture energy

E is modulus of elasticity of concrete

Eligehausen and Ozbolt [58] simulated the behavior of headed studs considering several design factors and compared with previous experimental data and concluded that failure load based on the circumferential crack propagation depends on the fracture energy. The average angle for the circumferential cracks was found to be about 35^o, and radial cracking developed at much higher loads at the surface of the concrete. They also reported that contrary to the ACI 349-85 approach, the cone breakout capacity did not depend on the square of the embedment depth. Thus, the non-size effect expression used in the ACI method would underestimate the capacity of shallow anchors and overestimate the capacity of deeper anchors.

Breakout capacity calculated using the size effect law [55], [56] was in agreement with the equation proposed by Eligehausen and Sawade [57] (Equation 4) and thus rather than the square of the effective embedment depth assumed in the non-size effect ACI relationship, the breakout capacity of the anchor is proportional to the three-second power of the embedment depth. Fuchs et al. [5] maintained the size effect provision in formulating the CCD method and coupled with the κ-factor approach formulated an expression for concrete breakout capacity of a single headed anchor without edge effect as given in Equation 6.

$$\boldsymbol{N_u = k_1 \cdot \sqrt{f'_c} \cdot h_{ef}^2 \cdot k_2 \cdot \frac{k_3}{\sqrt{h_{ef}}}} \quad [6]$$

Where $\boldsymbol{k_1, k_2, k_3}$, are calibration factors that can be combined into $\boldsymbol{k_n}$.

$k_1 . \sqrt{f'_c}$ expresses the effect of tensile capacity of the concrete.

$k_2 . h_{ef}^2$ expresses the effect of the area of the failure surface.

$\frac{k_3}{\sqrt{h_{ef}}}$ expresses the size effect term.

Combining the k-factors, Equation 6 can be rewritten as:

$$\boldsymbol{N_u = k_n \cdot \sqrt{f'_c} \cdot h_{ef}^{1.5}} \quad [7]$$

where

k_n = 16.8 for cast-in-place anchors

k_n = 14.7 for post-installed anchors.

Note that if the cube of the compressive strength of concrete is used in Equation 7, the values of k_n become 15.5 and 13.5 respectively for cast-in-place anchors and post-installed anchors.

Additionally, the CCD method assumed an inverted pyramid with square base as projected area for analysis and design.

The CCD method however does not yield accurate anchor capacity results for screw anchors and must be modified as proposed by Eligehausen and Sippel [47] and captured by Olsen et al. [15]. The modification involves changes to the determination of the effective embedment depth as proposed by Kuenzlen [48]. The modified effective embedment depth is calculated using Equation 8. Fig. 2.10 shows the various parameters taken into consideration for modifying the effective embedment depth of screw anchor.

$$h_{ef} = 0.85 \cdot (h_{nom} - 0.5h_t - h_s) \quad [8]$$

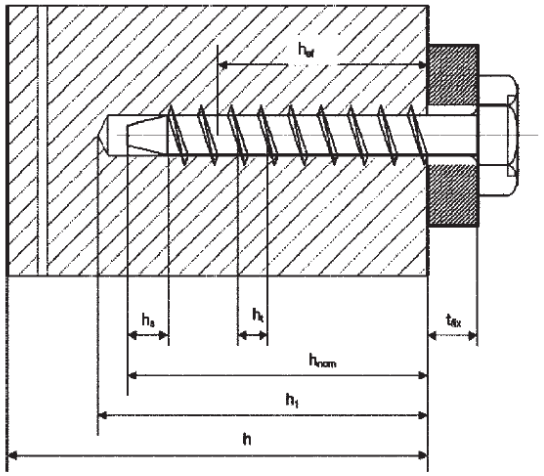

Fig. 2.10: Typical factors affecting embedment depth of screw anchors [33]

For bonded anchors, the uniform bond model proposed by Cook et al. [59] and presented by Cook and Kunz [37] may be used to predict the tensile capacity of unheaded bonded anchors of all ranges of embedment depth as well as headed bonded anchors of shallow embedment depth. The tensile capacity of the anchors based on the uniform bond model is illustrated in Equation 9. Gesoglu et al. [12] observed that the uniform bond model appears to more appropriately describe the behavior of bonded anchors of both shallow and deep embedment subject to concrete cone failure mode. As observed by Olsen et al. [15], for the same mechanical screw anchor, a uniform bond stress derived from the uniform bond model would not apply to different embedment depths of the same anchor.

$$N_u = \tau_k \cdot \pi \cdot d \cdot h_{ef} \quad [9]$$

Where τ_k is the characteristic bond strength of the bonding agent determined from test, d is the diameter of the anchor shank.

As stated earlier, design of anchorage is based on the CCD method both in the ACI and Canadian codes of practice. However, nominal anchor capacities are based on 5% fractile

with 90% confidence, thus modifications to the design model are made. Again, as the design codes are based on uncracked concrete, modification factors, as well as material resistance factors are employed to assure safe designs. Factors that necessitates modification in addition to the presence of cracks include the eccentricity of loading, spacing and edge distances, the concrete type (normal or light-weight) and the embedment depth. For headed studs and headed bolts with embedment depths between 275 mm and 625 mm, Equation 10 is used instead of Equation 7 based on the provisions of the design codes [2], [3].

$$N_u = k_n \cdot \sqrt{f'_c} \cdot h_{ef}^{\frac{5}{3}} \qquad [10]$$

Where $k_n = 6.59$

2.3.2.2 Shear Capacity

When anchors are subjected to shear loading, internal bearing pressures develop near the concrete surface at the face of the anchor in the direction of the shear load and at the end of the anchor in a direction opposite to the shear loading due to restraint to rotation [53]. These stresses may result in varied failure modes depending on the distance of the anchor from the edge and the embedment of the anchor relative to the critical edge distance, as well as the stiffness of the anchor (defined by the depth to diameter ratio). For deeply embedded anchors at a distance less than the critical edge distance, breakout of a concrete (Fig. 2.11) in the direction of the shear force is observed. On the other hand, when a stiff anchor (depth to diameter ratio of less than 4.2 [17]) is located far enough from the edge of the concrete, pryout failure (Fig. 2.12) is observed. For deeper embedment where the concrete breakout force exceeds the force required to fracture the steel, the anchor tends to fail by steel fracture (Fig. 2.12).

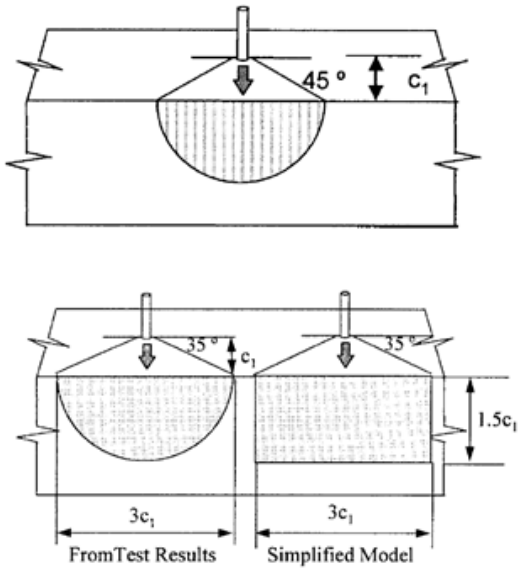

Fig. 2.11: Idealized Concrete Breakout Cone Models for Shear Loaded Anchors – ACI 349-85 (Top), CCD Method (Bottom) [60]

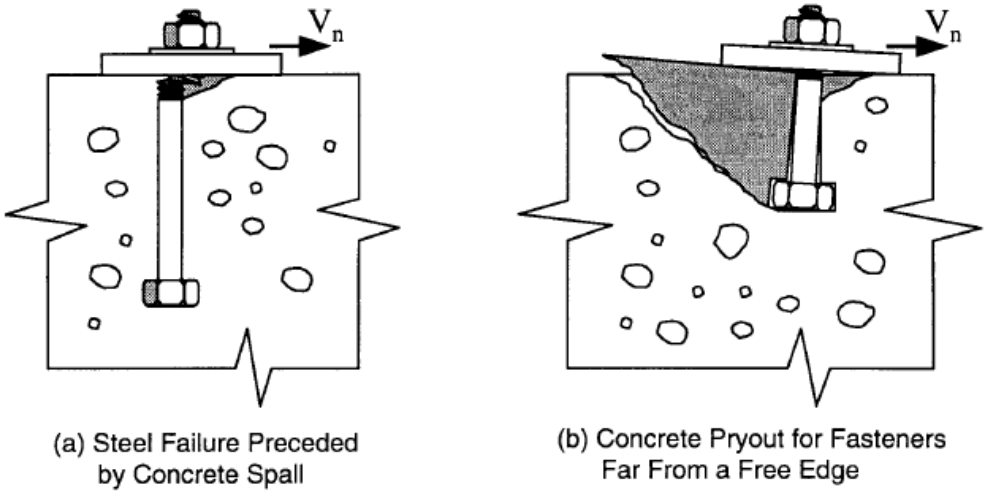

Fig. 2.12: Typical Steel and Concrete Pryout Failure Modes for Anchors in Shear [61]

The capacity of an anchor in concrete breakout failure due to limited edge distance is similar to the concrete breakout failure in tension. Similar to the tension design, earlier editions of ACI Committee 349 report based the shear capacity on a 45° cone breakout and calculated using Equation 11 [5], [60]. Similar to the tensile breakout capacity, the shear

capacity varies directly with the square of the edge distance, obviously neglecting the size effect.

Based on the size-effect provisions however, the CCD method [5], proposed Equation 12 that has been widely adopted by recent Canadian and American Design Codes. In addition to the size effect provisions, the CCD method takes into consideration the stiffness of the anchor which depends on its diameter, d and the activated load-bearing length, l . The activated load-bearing length must not be more than eight times the anchor diameter [2]. A 35° cone model from test results was simplified to a 35° pyramid as illustrated in Fig. 2.11.

Muratli et al. [60] developed a modified form of the CCD method (Equation 13) based on regression analysis of data from various tests on the breakout capacity of anchors in concrete.

$$\boldsymbol{V_u = 0.52 \cdot \sqrt{f'_c} c_1^2} \qquad \textbf{[11]}$$

$$\boldsymbol{V_u = 1.08 \cdot \left(\frac{l}{d}\right)^{0.2} \cdot \sqrt{d f'_c} \cdot c_1^{1.5}} \qquad \textbf{[12]}$$

$$\boldsymbol{V_u = 2.93 \cdot l^{0.1} \cdot d^{0.3} \cdot \sqrt{f'_c} . c_1^{1.4}} \qquad \textbf{[13]}$$

c_1 is the distance from the anchor to the edge of the concrete in mm.

When anchors are far enough away from edges to preclude concrete breakout and pryout failure, deep embedded anchors would fail in steel fracture. The capacity of the anchor is consequently given by Equation 14 [62] as the product of the effective shear area (A_{sv}) of the anchor and the ultimate stress in shear (f_{uv}) of the steel material.

$$V_u = A_{sv} \cdot f_{uv} \quad [14]$$

For shallow embedded stocky anchors far away from the edges of concrete, pryout failure governs. Pryout failure of anchors under shear loading has been investigated by several researchers including Jebara et al. [17], [63], Jebara [64], Anderson and Meinheit [53][62], Ollgaard et al. [51], Zhao [65], Hofmann et al. [66] and Hawkins [67] where the behavior of stud anchors under shear loading were tested and design equations formulated. Work done by Ollgaard et al. [51] became the basis for the calculation of the pryout capacity of stud anchors by the American Institute of Steel Construction (AISC). The nominal anchor capacity (Equation 15) proposed by the authors was consistent both for failure in steel anchor and concrete for values of effective depth to stud diameter ratio of 3.26. The capacity obtained was a function of the elastic modulus of concrete, the compressive strength of concrete and the cross-sectional area of the anchor. A simplification of Equation 15 to Equation 16 was obtained by Shaikh and Li [52], through a research under the auspices of the Prestressed Concrete Institute (PCI) Connection Details Committee and was adopted into the PCI Design Handbook.

$$V_u = 0.5 \cdot A_{sv} \cdot \sqrt{(E_c \cdot f'_c)} \quad [15]$$

$$V_u = 66.42 \cdot \lambda \cdot A_{sv} \cdot \sqrt{f_c} \quad [16]$$

λ represents the concrete unit weight factor.

It was however observed that none of the above equations considered the effect of the embedment depth on the pryout capacity of the anchor. Hawkins [67] observed that for anchors with effective depth to diameter ratio less than or equal to 4 and embedded far

away from the edge, Equation 17, derived from statistical analysis of test results is adequate to predict the pryout capacity of the anchor. Zhao [65], however reported that for single and four anchors in a group with effective depth to diameter ratio less than or equal to 4.1, the pryout capacity is a function of the cone breakout capacity in tension (Equation 7 or Equation 9). The predicted capacity by Zhao has been adopted by the ACI and Canadian codes for the calculation of the pryout capacity of anchors. Equation 18 shows Zhao's equation as it applies in the Appendix D of the Canadian Code [2].

$$\boldsymbol{V_u = 13 \cdot \sqrt{f'_c} \cdot d^{\frac{1}{3}} \cdot \left(381 + 1.1 h_{ef} + d_w\right)} \quad \textbf{[17]}$$

d_w is the washer diameter in mm

$$\boldsymbol{V_u = k_{np} \cdot N_u} \quad \textbf{[18]}$$

k_{np} = 1 for effective depth less than or equal to 65 mm, and k_{np} = 2 otherwise.

Anderson and Meinheit [53] proposed a modified pryout capacity formula from analysis of data from several pushoff tests for embedment depth to diameter ratio less than or equal to 4.5, including Zhao and Hawkins's results. They included the contribution of the effective embedment depth and anchor diameter and by using a linear multi-variable regression analysis obtained Equation 19. Jebara et al. [17] observed that the modified pryout capacity proposed by Anderson and Meinheit [53], Ollgaard et al. [51] and Shaikh and Li's [52] were conservative, while the formulation proposed by Zhao [65] was unconservative in estimating the pryout capacity of stocky stud anchors. They therefore proposed a pryout capacity of a single anchor under pure shear loading in the form of

Anderson and Meinheit equation based on experimental results and regression analysis of test results. Their proposed equation is herein presented as Equation 20.

$$V_u = 26.4 \cdot \lambda \cdot d^{1.5} \cdot \sqrt{\left(f_c^{'} \cdot h_{ef}\right)} \quad [19]$$

$$V_u = 6.52 \cdot h_{ef}^{1.5} \cdot f_c^{'0.5} \cdot d^{0.5} \quad [20]$$

2.3.3 Anchor Behavior under High Strain-Rate Loading

Under high loading rates, the capacities of both steel and concrete have been observed to increase. This phenomenon has been adequately studied and confirmed by researchers including Malvar and Crawford [23], [24], who conducted extensive literature review on the subject to characterize the compressive and tensile strength of concrete and the strength of steel reinforcement (yield and ultimate) at high rates of loading. For High Specific Strength Steel (HSSS), Wei et al. [68] observed that both the yield stress and ultimate stress increase with increasing strain rate as testing was carried out at rates ranging from 0.0006 /s to 56 /s. In investigating the effects of strain rate on yield stress of three structural steel types (ASTM A36, ASTM A441 and Quenched and Tempered (Q-T)) Nagaraja et al. [69] observed that though the ratio of the dynamic yield to static yield stress increased with increasing loading rates, the degree of increase was lower as the yield strength of the steel increased. Bischoff and Perry [21] report up to 85% increase in plain concrete compressive strength under strain rate of up to 10 /s while Fu et al.[70] reported up to 70% increase in the tensile strength of concrete at increased strain rates. Consequently, it is expected that under dynamic loading conditions, concrete anchors are expected to develop higher ultimate loads compared to loading under static conditions.

The behavior of anchors under high loading rates in tension and shear have however not been adequately investigated, with many tests carried out on simulated earthquake conditions. ACI 355.2 [32], the basis for post-installed anchor qualification for use in both the USA and Canada only prescribes load cycle of moderate testing conditions [71]. It is however expected that anchors may be exposed to more severe conditions under dynamic loading. Mahrenholtz and Eligehausen [71] subjected undercut anchors to high frequency loading and crack cycling to simulate seismic loading conditions. They observed that there was significant decrease in anchor displacement as well as increase in initial stiffness during the tests, contrary to their expectation (based on beneficial effects of high frequency loading on materials). They consequently concluded that design displacements under quasi-static loading conditions should not be reduced for seismic applications. Rodriguez [30] and Rodriguez et al. [8] conducted experimental tests on the static and dynamic behavior of grouted and mechanical expansion anchors under the auspices of the US Nuclear Regulatory Commission to simulate loading under seismic conditions. They observed that the tensile capacity of anchors under dynamic loading was adequately defined by the CCD method, in general, and only required the static capacity to be multiplied by a DIF to yield the dynamic capacity. Rodriguez et al. observed a deteriorating internal and external friction condition for wedge-type expansion anchors, leading to lower dynamic capacities when failure mode is anchor pull-through. For grouted and undercut anchors, concrete breakout failure was observed for both static and dynamic conditions, with of the dynamic breakout strength having a DIF of 1.24. They recommend a DIF of 1.15 when steel failure mode is observed.

Consistent with Rodriguez [30], Mahrenholtz [72] observed that wedge-type expansion anchors predominantly failed in anchor pull-through and anchor pullout failure mode under loading rates of up to 1000 kN/s in cracked concrete. Pull-out failure was reported to occur when crack width was large enough to prevent full expansion of the sleeve. The author observed a general trend of increased tensile capacity of anchors with increasing loading rate, irrespective of the failure mode. After conducting further tests to study effects of increasing loading rates on the frictional resistance of the expansion anchors, Mahrenholtz [72] observed no definite relationship between the loading rate and external friction, but a general trend of reduced internal friction with increased loading rates. The increased tensile capacity observed under pull-out and pull-through failure was therefore attributed to the beneficial effects of the indentation resistance provided by the walls of the concrete to the expansion of the anchor sleeve.

Solomos and Berra [28] employed a Split-Hopkinson Pressure Bar (SHPB) to conduct dynamic pull-out tests on cast-in-place and post-installed anchors (bonded and undercut anchors) and observed comparable anchor capacities under similar embedment depths. They also observed that anchor capacities under dynamic conditions were higher than those under static conditions and recorded DIF values of up to 1.67 from the tests, consistent with the DIF of up to 1.6 obtained by Ahmed and Braimah [27] when a numerical analysis of undercut anchors subjected to loading of up to 10^3 /s was carried out. Braimah et al. [25] recommended DIF of 1.2 for adhesive anchors installed at 90^o and a DIF of 3.3 for adhesive anchors installed at 45^o to the concrete surface. Fujikake et al. [31] observed that the ultimate cone resistance of headed studs and bond resistance of bonded anchors increased with increasing loading rates. They reported that the dynamic cone resistance is closely

related to the dynamic tensile strength of concrete. The authors proposed an empirical equation for calculating both the dynamic bond and cone resistances. Equation 21 was adapted by the authors from the form of the nominal anchor capacity based on the CCD method.

$$\boldsymbol{P_{cd} = A_e \cdot f_{td} \cdot \frac{\alpha}{\sqrt{h_{ef}}}} \qquad \textbf{[21]}$$

Where A_e represents the projected area of a conical concrete breakout, f_{td} represents the dynamic tensile strength of concrete and $\frac{\alpha}{\sqrt{h_{ef}}}$ represents the size effect term. The α in the size effect term was determined by the authors to be 3.48 x 10^{-3}. The dynamic tensile capacity of concrete was related to the static tensile strength proposed by Ross et al. [29] and given in Equation 22.

$$\boldsymbol{f_{td} = f_t \cdot exp\left[0.00126 \cdot \left(\log_{10}\frac{\dot{\varepsilon}}{\dot{\varepsilon}_s}\right)^{3.373}\right]} \qquad \textbf{[22]}$$

The static and dynamic strain rates are represented by $\dot{\varepsilon}_s$ and $\dot{\varepsilon}$ respectively. Ross et al. [29] proposed the static strain rate to be 10^{-7} /s. f_t represents the static tensile strength of concrete.

2.4 Summary

The flexibility of application of post-installed anchors makes them prime candidates for use in both structural and non-structural attachments. Their behavior under static and extreme loading conditions, just like all other engineering materials, needs to be fully understood to ensure their use in both safe and economic ways. Behavior of post-installed anchors under general static loading conditions have been investigated and documented by many researchers. However, under extreme loading conditions such as impact and blast,

not much has been found in literature. Under dynamic conditions, many engineering materials experience increased ultimate capacities. These beneficial effects would however need to be confirmed in order that they can be used in design.

This chapter reviewed the available literature on anchors, their classification, and their response to loading, both with respect to failure modes and ultimate capacities. Literature on anchor behavior under dynamic loading mostly concentrated on anchor response to earthquake loading. In fact, the standard document in use in the USA and Canada for qualification of post-installed anchors only prescribes load cycling of low frequencies as part of qualification for seismic loading. Other research found only dealt with the dynamic load effects on cast-in-place and bonded anchors with only few tests exclusively on post-installed mechanical anchors.

The proposed research in this thesis aims to add to the knowledgebase on the effects of high-strain rate loading on post-installed mechanical anchors. The research comprises two types of torque-controlled expansion anchors and one type of screw anchor manufactured by Simpson Inc.

3 Chapter: Experimental Program

3.1 General

The experimental program was designed to subject steel mechanical anchors embedded in concrete to both impact load in a drop-mass test frame and under quasi-static loading in a hydraulic actuated loading frame. Concrete beams were sized to preclude the influence of edge effects on the capacity of the singly tested anchors. Three samples of each diameter of each anchor type was tested in either tension or shear. In all, about 96 anchors were tested in the research program.

Displacement measurements were achieved by using calibrated String Potentiometers ("String-Pot") and Linear Vertical Displacement Transducers (LVDT) while strain measurement on at least one anchor from each group in tension was achieved through 350-ohm strain gauges.

This chapter outlines the testing procedures for both static and impact test of anchors including the preparatory procedures, test setup, and data acquisition. The procedures used for casting and curing concrete as well as material testing of concrete and steel anchors are also presented in this chapter.

3.2 Concrete Beams

Eighteen (18) Plain concrete beams with cross-section of 300×300 mm and length of 2280 mm were cast and used as substrates for installing the mechanical anchors for testing. The concrete mix was designed and supplied by a local producer. A concrete compressive strength of 35 MPa was specified and supplied in two batches for casting of the beams. The concrete beams were cured and stored in the Civil Engineering Laboratory for four months before testing of anchors started.

3.2.1 Concrete Beam Formwork

Fig. 3.1 shows the formwork used for the casting of the concrete beams. Three (3) wooden formwork combos for casting three beams each were constructed in the Civil Engineering Laboratory Wood Workshop. Each formwork combo was made from 1200×2400 mm, 19-mm thick plywood base, partitioned into three compartments of 300 mm widths using 300 mm wide 19-mm thick plywood. The 300 mm wide boards were placed vertically to form the side faces of the formwork. To ensure the sides of the formwork would not bulge out during the casting of concrete, pieces of 38×63-mm wooden planks were nailed to the top and bottom edges of the combo. The top planks also served as attachment points for top bracings for integrity.

Fig. 3.1: Formwork for Casting Concrete

3.2.2 Casting and Curing of Concrete

Concrete was cast once the order arrived. Slump test was carried out on concrete samples to confirm good workability in accordance with ASTM C143/143M – 15 [73]. The measured slump of the concrete was 150±10 mm. The concrete was poured in three layers and compacted with a poker vibrator to eliminate voids. The surface of the concrete was smoothened with a metal trowel, and steel reinforcement hooks (lifting lugs) fixed at the end to enable lifting and movement of cured concrete beams. The concrete beams were covered with wet hessian fabric eight (8) hours after casting and moist cured for about three (3) days before formwork was removed. Fig. 3.2 shows the sketch of the cast concrete.

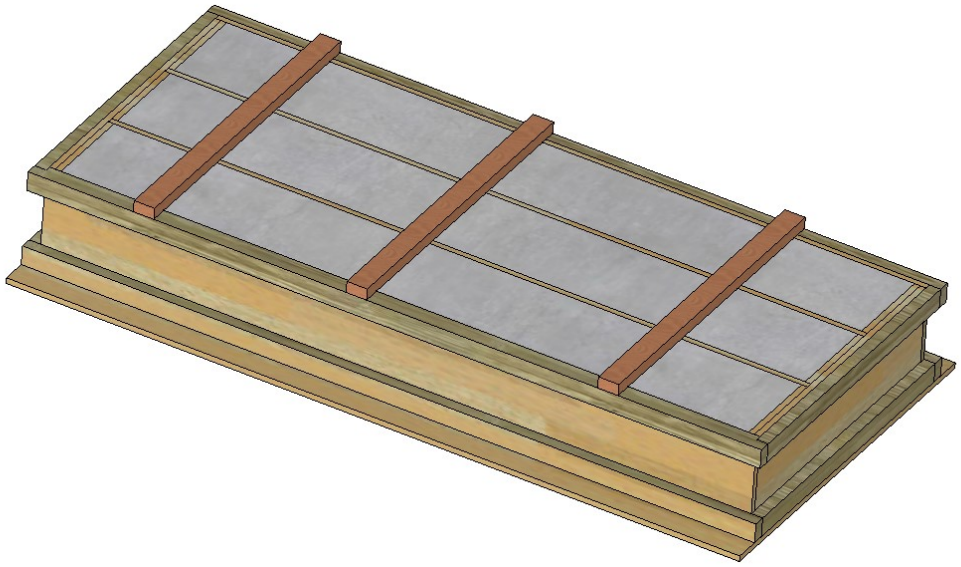

Fig. 3.2: Cast Concrete Beams

3.2.3 Concrete Cylinders Compressive Strength Test

To determine the compressive strength of the cast concrete, twenty (20) 100×200 mm concrete cylinders were cast together with the concrete beams and cured under similar conditions. Ten (10) of the cylinders (Fig. 3.3) were capped and tested using a Tinius Olsen compression machine (model 300H3) connected to an MTS 458 controller for data acquisition and storage. The tests were conducted in accordance with ASTM C39 [74].

Fig. 3.3: Concrete Cylinder Showing LVDT Compressometer

Table 3.1 presents the results of the compressive strength and elastic modulus obtained from testing five samples of each batch of concrete. The stress was obtained by dividing the compressive force by the cross-sectional area of the cylinder, while the strains were obtained by dividing the compressive deformation by the original length of the cylinder. The elastic modulus was calculated using the secant modulus approach as per ASTM C469/C469M – 14 [75]. The secant modulus is determined as the slope of a straight line joining the origin and the point on the stress-strain curve corresponding to 40% of the ultimate cylinder crushing stress.

Table 3.1: Concrete Properties from Cylinder Crushing Test

Batch	Average Compressive Strength (MPa)	Average Elastic Modulus (MPa)
1	44.6±2	25540±4000
2	33.7±2	23372±3000

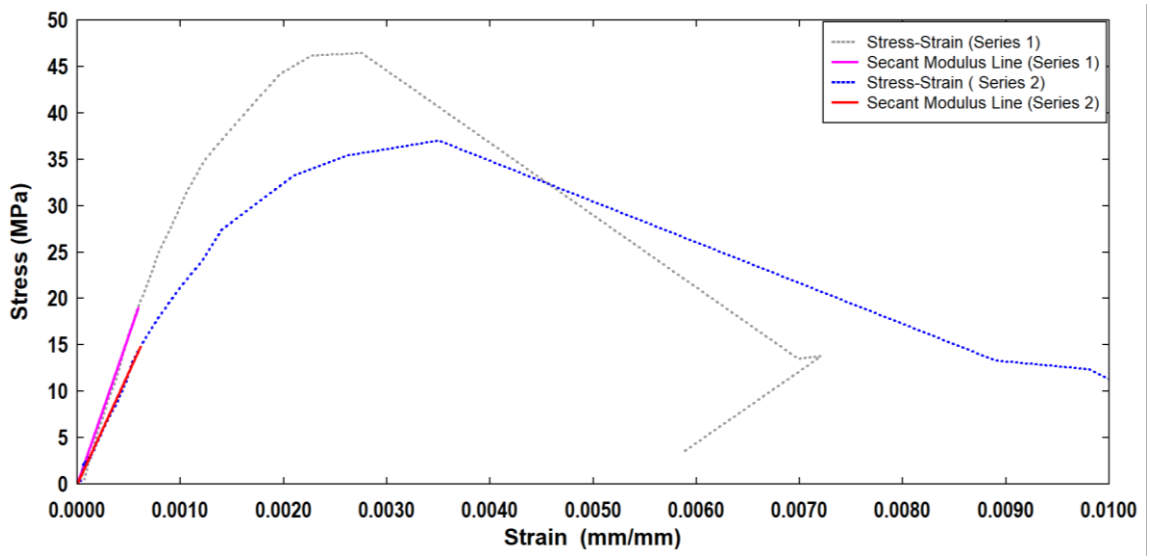

Fig. 3.4: Typical Stress-Strain Relationship for Concrete

A typical stress-strain relationship of the concrete is shown in Fig. 3.4. The average compressive strength of the first and second batches of concrete was 44.6 ±2 MPa and 33.7 ±2 MPa respectively tested 10 months of casting. The average elastic moduli as well were 25540 ±4000 MPa and 23372 ±3000MPa for the first and second batches respectively. The first batch of concrete beams were used for the shear tests while the second batch used for the tension test of the anchors.

3.3 Anchors

3.3.1 Anchor Specification and Installation

3.3.1.1 Strong-Bolt® 2

Strong-Bolt 2 anchors are torque-controlled expansion anchors consisting of an anchor body, expansion clip (sleeve), nut, and a washer [76]. A typical anchor of this type is shown in Fig. 3.5(a). The anchor body has a tapered mandrel (cone) formed on the installed end of the anchor and a threaded section at the opposite end. The taper of the mandrel increases in diameter towards the installed end of the anchor. The three-segment expansion clip wraps around the tapered mandrel. The expansion clip is free to rotate about the mandrel

before the anchor is installed. When a pre-determined torque is applied to the hex nut during installation, the mandrel is drawn into and expanding the expansion clip. Thereby engaging the drilled hole to transfer the applied load. The mandrel for the Strong-Bolt 2 is tapered at an angle of 12.3^{o} with clip lengths of 7.3 mm, 16.7 mm and 22.3 mm for the 6.4-mm, 9.5-mm, and 12.7-mm diameter anchors respectively. Pertinent information regarding installation can be found in Table 3.2 and Table 3.3.

3.3.1.2 Wedge-All®

The Wedge-All anchors are also torque-controlled expansion anchors. They also consist of an anchor body, an expansion clip, nut and a washer. The mandrel is tapered at an angle of 6.3^{o} with expansion clip length of 11.5 mm and 15.9 mm for the 9.5-mm and 12.7-mm diameter anchors tested. The Wedge-All® has a one-piece clip [77] instead of the three-segment clip in the Strong-Bolt® 2 anchor. During installation, the mandrel is pulled into the expansion clip at a predetermined torque applied to the hex nut. The mandrel expands clip and transfers the expansion forces to the walls of the concrete hole to resist applied loads. A typical Wedge-All anchor is shown in Fig. 3.5 (b). Installation information can also be found in Table 3.2 and Table 3.3.

3.3.1.3 Titen HD®

Titen HD® is a threaded screw anchor with hex-washer head (Fig. 3.5 (c)). Anchor diameters of 6.4 mm, 9.5 mm and 12.7 mm were tested in the experimental program. The anchors were installed into predrilled holes of matching diameters by tightening until a preset torque was met. The anchors come with threads with a pitch of 1.9 mm, 7.2 mm and 7.4 mm for the 6.4-mm, 9.5-mm and 12.7-mm diameter anchors. The first three lines of

the threads are designed in saw-like manner to cut into the concrete walls while the subsequent threads are smooth. The installation information can be found in Table 3.2 and Table 3.3.

Table 3.2: Basic Design Information for Tested Anchors

Anchor Type	Diameter (mm)	h_{nom} (mm)	h_{ef} (mm)	l (mm)	C_{ac}* (mm)	A_{se}** (mm)	f_{ut} (MPa)
Strong-Bolt® 2	6.4	44.5	38.1	38.1	63.5	20.5	483
Strong-Bolt® 2	9.5	73.0	63.5	63.5	150.0	33.2	793
Strong-Bolt® 2	12.7	98.4	85.7	85.7	187.5	67.7	793
Wedge-All®	9.5	73.0	67.0	67.0	95.0	33.2	793
Wedge-All®	12.7	98.4	86.0	86.0	127.0	67.7	793
Titen HD®	6.4	63.5	49.3	49.3	150.0	27.1	860
Titen HD®	9.5	82.6	61.0	61.0	92.1	63.9	758
Titen HD®	12.7	101.6	75.9	75.9	114.3	118.1	758

*Critical edge distance for shear application
** Minimum tensile and shear areas reported on anchor design documentation

3.3.1.4 Design and Installation

Basic anchor design parameters are shown in Fig. 3.6 for expansion anchors and Fig. 2.10 for the screw anchors. The design parameters include the hole depth, the nominal embedment depth, the effective embedment depth, the nominal diameter of anchor and the overall anchor length. These parameters are important in order to ensure that installed anchors develop the required strength.

The anchor installation followed the manufacturer prescribed installation sequence in all cases. The installation sequence for the torque-controlled anchors is illustrated in Fig. 3.7 and is as follows:

- Use a hammer drill with carbide drill bit to drill a hole to the prescribed depth. The appropriate drill bit diameters for the various anchor diameters are shown on Table 3.3.

- Clean the hole by brushing the sides with a stiff brush and using compressed air to flush out the dust and debris in the drilled hole
- Place the anchor in hole and install nut to flush with the surface of the anchor plate and hit with a hammer until anchor seats well into the bottom of the hole.
- Apply torque to anchor until prescribed torque is reached.
- For the Titen HD® screw anchor, after hole is drilled, insert anchor into the hole and torque to the prescribed installation torque.

Edge distance in the experimental program was 150 mm, which was enough to preclude edge effects for all anchors, except for the 12.7 mm diameter Strong-Bolt® 2 anchors. Though anchors were not tested in groups, spacing for subsequent anchors tested on the same concrete beam were chosen to meet the minimum spacing required by the manufacturer. For anchors that failed in concrete breakout, subsequent holes were drilled far enough away from the damaged area to avoid interaction of the failure surfaces. Table 3.3 shows the manufacturer recommended installation parameters for the tested anchors.

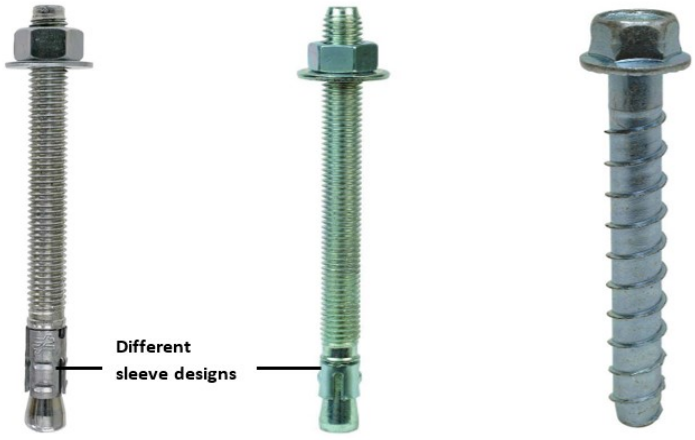

(a) (b) (c)

Fig. 3.5: Tested Anchors: (a) Strong-Bolt® 2, (b) Wedge-All®, (c) Titen HD® [78]

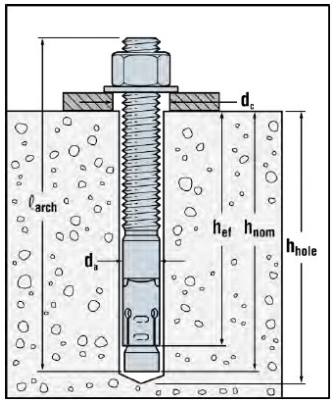

Fig. 3.6: Design Information for Expansion Anchors [78]

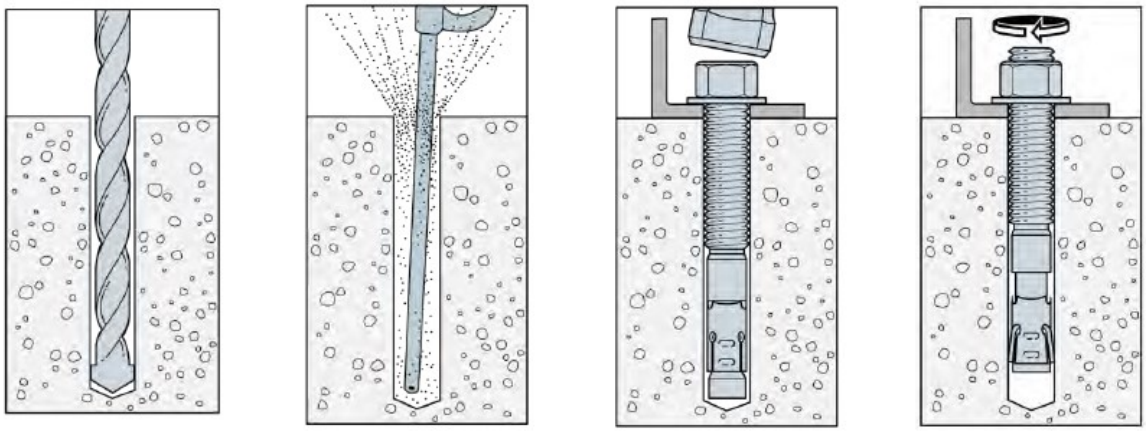

Fig. 3.7: Manufacturer Prescribed Installation Sequence for Torque-Controlled Expansion Anchors

[78]

Table 3.3: Installation Data of Anchors

Anchor Type	Diameter (mm)	Drill bit diameter (mm)	Hole depth (mm)	Installation Torque (N-m)
Strong-Bolt® 2	6.4	6.4	48.0	5.42
	9.5	9.5	76.0	40.7
	12.7	12.7	105.0	81.4
Wedge-All®	9.5	9.5	76.0	40.7
	12.7	12.7	105.0	81.4
Titen HD®	6.4	6.4	67.0	32.5
	9.5	9.5	88.9	67.8
	12.7	12.7	114.3	88.1

3.3.2 Anchor Mechanical Properties

The mechanical properties of the anchors under quasi-static loading rates were obtained by carrying out tension tests on anchor samples in an Instron Load Frame (Fig. 3.8) in accordance with ASTM E8/E8M-13 [79]. The test frame was equipped with an extensometer capable of measuring strain directly. Before testing, the installed parts of the expansion anchors which included the mandrel and expansion clips were cut off, allowing test on the threaded part of the anchors. For the screw anchors, the hex heads were cut off and portions of the threads to the installed side of the anchor were ground off to allow for firm grip in the test machine. The anchors were tested in displacement-controlled mode at a loading rate of 0.04 mm/s.

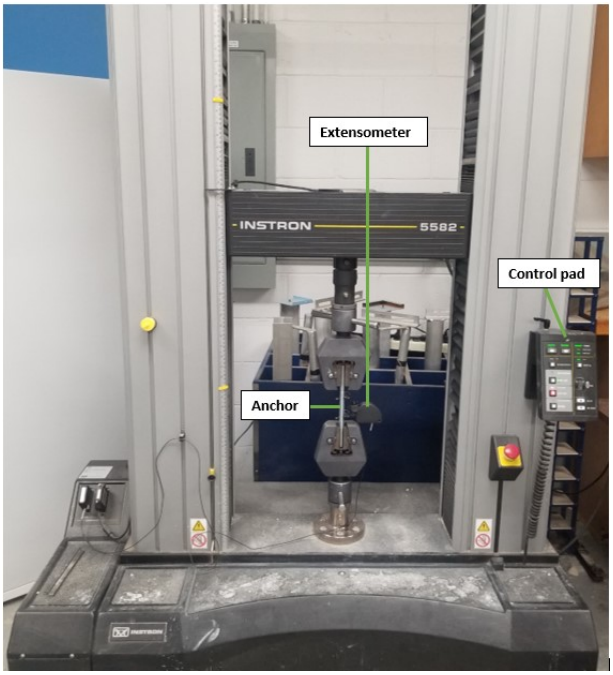

Fig. 3.8: Instron 5582 Test Frame

A set of supplementary tests were then carried out using an MTS 810 Material Tester (Fig. 3.9)also in displacement-controlled mode. However, tests were carried out at higher loading rates to obtain the behavior of the bare steel anchor at increased loading rates. The anchors were loaded in displacement-controlled rates ranging from 15 to 36 mm/s which

resulted in strain rates of up to 0.05 /s. The mechanical properties of the bare steel anchor assessed under the primary tension and supplementary high-rate tension tests were the ultimate capacity, stress and strain corresponding to the yield and ultimate loads and the modulus of elasticity. The strain rate was obtained by dividing the yield strain by the time to yield strain as per UFC-340-02 [80]. The yield stress was obtained using the 0.2% offset strain method stipulated in ASTM E8/E8M-13 [79] while the elastic modulus was obtained by finding the slope of the initial straight part of the stress-strain curve up to at least 50% of the average stress of the plateau. Three samples of each anchor type were tested at each loading rate in both the primary and supplementary tension tests.

Fig. 3.9: Setup for High-rate Test for Bare Anchors

3.3.3 Strong Bolt® 2 Anchors

In addition to the primary tensile test of the bare anchor at 0.04 mm/s, the 6.4-mm diameter anchors were tested at supplementary rates of 15 and 30 mm/s. The stress-strain curves (Fig. 3.10) obtained for the tests showed an increase in average ultimate loads as well as the ultimate stresses while the loading rate increased. The average ultimate loads increased

from 9.3 to 10.2 and then 10.4 kN as the loading rate increased from 0.04 mm/s to 15 mm/s and then 30 mm/s while the ultimate stress increase from 476 to 518 and then 526 MPa, respectively.

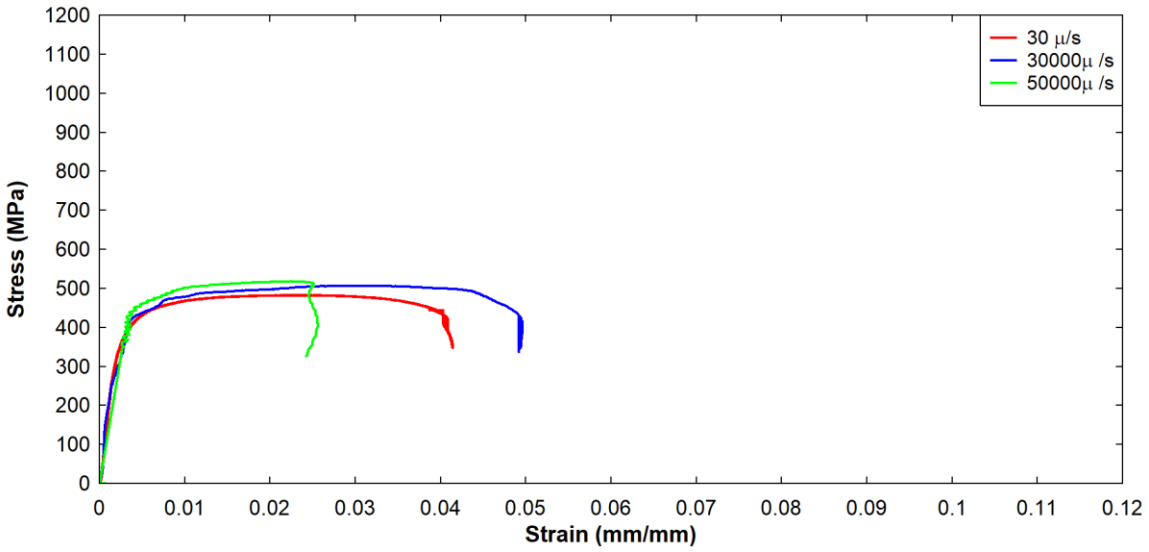

Fig. 3.10: Typical Stress-Strain Curve for 6.4-mm Diameter Strong-Bolt® 2 Bare Anchor

Table 3.4: Tensile Test Data for 6.4-mm Diameter Strong Bolt® 2 Bare Anchors

6.4-mm Diameter Strong Bolt 2						
Test	Peak Load [kN]	Yield		Ultimate		Elastic Modulus
		Stress [MPa]	Strain	Stress [MPa]	Strain	[GPa]
Strain Rate: 0.00003 /s (0.04 mm/s)						
1	9.5	422	0.004	485	0.034	181
2	9.5	416	0.004	484	0.023	185
3	9.0	399	0.004	459	0.022	210
Average	**9.3**	**412**	**0.004**	**476**	**0.026**	**192**
Strain Rate: 0.03 /s (15 mm/s)						
1	10.3	425	0.004	523	0.024	205
2	10.3	426	0.004	524	0.024	199
3	10.0	428	0.004	507	0.025	200
Average	**10.2**	**426**	**0.004**	**518**	**0.024**	**201**
Strain Rate: 0.05 /s (30 mm/s)						
1	10.2	430	0.004	518	0.022	202
2	10.4	429	0.004	528	0.023	212
3	10.5	431	0.004	532	0.022	200
Average	**10.4**	**430**	**0.004**	**526**	**0.022**	**205**

The average ultimate stress increased by 8.8% and 10.5% (resulting in DIF of 1.09 and 1.11 respectively) as the loading rate increased to 15 mm/s and 30 mm/s from the quasi-static rates. However, doubling of the loading rate from 15 mm/s to 30 mm/s only resulted in 1.5% increase in the peak load and ultimate stress.

On the other hand, the yield stresses increased by 3.4% and 4.4% (DIFs of 1.03 and 1.04 respectively) of the quasi-static yield stress as the loading rate increased to 15 mm/s and 30 mm/s, these were however lower than the increases related to the ultimate conditions contrary to the findings of Malvar and Crawford [24] even though the yield strength of the anchor steel was within the range investigated by Malvar and Crawford. The elastic modulus increased by 4.9% and 6.6% from the quasi-static values as the loading rates increased to 15 and 30 mm/s.

The average strain rates from the tests corresponded to 30 $\times 10^{-6}$ /s, 30,000 $\times 10^{-6}$ /s and 50,000 $\times 10^{-6}$ /s for loading rates of 0.04 mm/s, 15 mm/s and 30 mm/s. Though the yield strains were about the same, the ultimate strains reduced with increasing loading rates. Table 3.4 provides a summary of the mechanical properties obtained for all the samples.

The results for the 9.5-mm diameter anchors presented in Fig. 3.11 and Table 3.5 were tested at 17 mm/s and 34 mm/s in addition to the primary tensile test at 0.04 mm/s. Except for the second sample tested at a rate of 17 mm/s (Table 3.5), the rest of the tests showed a general increase in yield stress and ultimate stress as the loading rate increases. The average ultimate load increased from 34.5 kN to 36.7 kN and then to 37.2 kN when the loading rate increased from 0.04 mm/s to 17 mm/s and then 34 mm/s.

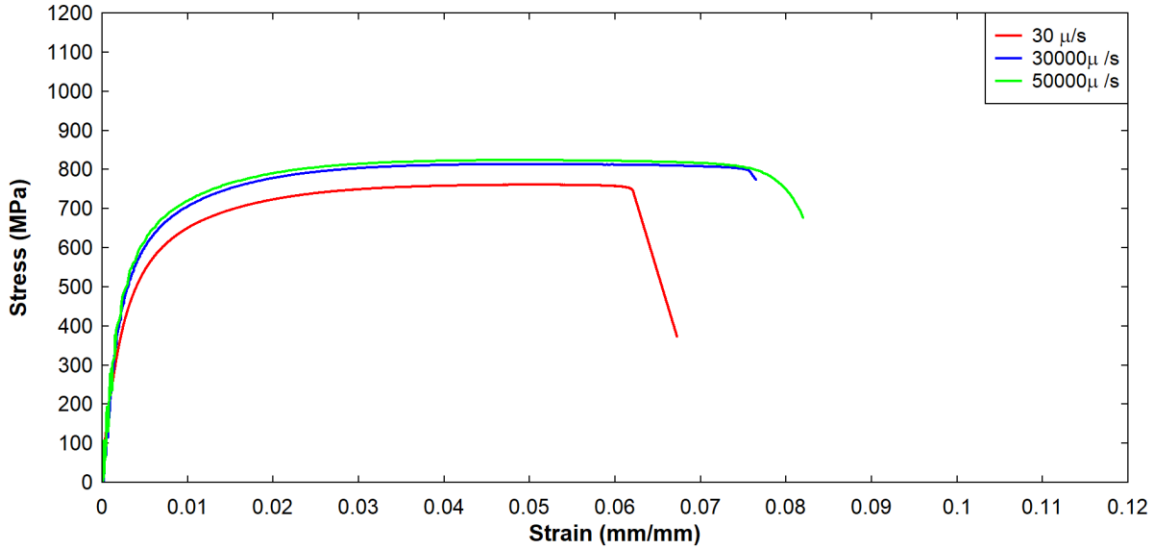

Fig. 3.11: Typical Stress-Strain Curves for 9.5-mm Diameter Strong-Bolt® 2 Bare Anchor

Table 3.5: Tensile Test Data for 9.5-mm Diameter Strong Bolt® 2 Bare Anchors

9.5-mm Diameter Strong Bolt 2						
Test	**Peak Load [kN]**	**Yield**		**Ultimate**		**Elastic Modulus**
		Stress [MPa]	**Strain**	**Stress [MPa]**	**Strain**	**[GPa]**
Strain Rate: 0.00003 /s (0.04 mm/s)						
1	34.5	532	0.0047	761	0.051	202
2	34.5	540	0.0049	761	0.056	198
3	34.5	545	0.0047	761	0.053	203
Average	**34.5**	**539**	**0.0048**	**761**	**0.053**	**201**
Strain Rate: 0.03 /s (17 mm/s)						
1	36.9	593	0.0047	814	0.052	201
2*	48.9	835	0.0058	1078	0.052	197
3	36.5	570	0.0046	804	0.049	191
Average	**36.7**	**582**	**0.0047**	**809**	**0.051**	**196**
Strain Rate: 0.05 /s (34 mm/s)						
1	37.4	598	0.0044	824	0.047	228
2	37.3	596	0.0049	823	0.051	181
3	36.8	578	0.0047	811	0.053	194
Average	**37.2**	**591**	**0.0047**	**819**	**0.050**	**201**

*Not considered in calculating the averages

The average ultimate stress also increased from of 761 MPa to 809 MPa and then to 819 MPa as the loading rate increased from 0.04 mm/s to 17 mm/s and 34 mm/s respectively. The increased loading rate resulted in 6.3%, and 7.6% (DIFs of 1.06 and 1.08 respectively)

increase in the ultimate stress for the 17 mm/s and 34 mm/s. However, only 1.2% of increase was observed for doubling the loading rate from 17 mm/s to 34 mm/s.

For the yield stress, increasing the loading rate to 17 mm/s resulted in an increase of 8.0% while an increase to 34 mm/s resulted in an increase of 9.6% (leading to DIFs of 1.08 and 1.1 respectively). These results are in contrast to the results obtained for the 6.4-mm diameter anchors but in agreement with Malvar and Crawford [24].

Though the yield strain did not change for the high loading rates, the ultimate strains reduced from 0.053 to 0.051 and then to 0.050 as the loading rate increased from 0.04 mm/s to 17 mm/s and 34 mm/s respectively. The average elastic modulus decreased by 2.5% as the loading rate increased from 0.04 mm/s to 17 mm/s and did not change much from the quasi-static value at loading rate of 34 mm/s. The resulting strain rates obtained from the loading rates were 30 $\times 10^{-6}$ /s , 30,000 $\times 10^{-6}$ /s and 50,000 $\times 10^{-6}$ /s .

The 12.7-mm diameter anchors were tested at rates of 18 mm/s and 36 mm/s in addition to the primary rate of 0.04 mm/s (Fig. 3.12) and Table 3.6). The results of these tests show a similar behavior to the 9.5-mm diameter anchors. In general, an increase in the ultimate load and yield stress as the loading rate increased was observed. The ultimate load increased from an average of 63.5 kN to 67.6 kN as the loading rate increased from 0.04 mm/s to 18 mm/s, and then reduced to 67.3 kN at a loading rate of 36 mm/s. The ultimate stress similarly increased from 776 MPa to 827 MPa and then 824 MPa, representing increases of 6.7% and 6.2% (DIF of 1.07 and 1.06 respectively) from the quasi-static values. The yield stresses also increased from 576 MPa to 630 MPa and reduced to 624 MPa as the loading rate increased from 0.04 to 18 and then 36 mm/s. This represented a 9.4% and 8.3% increase (DIFs of 1.09 and 1.08 respectively) at loading rates of 18 mm/s

and 36 mm/s, higher than the increase in the ultimate stresses and consistent with the results obtained for the 9.5-mm diameter anchors.

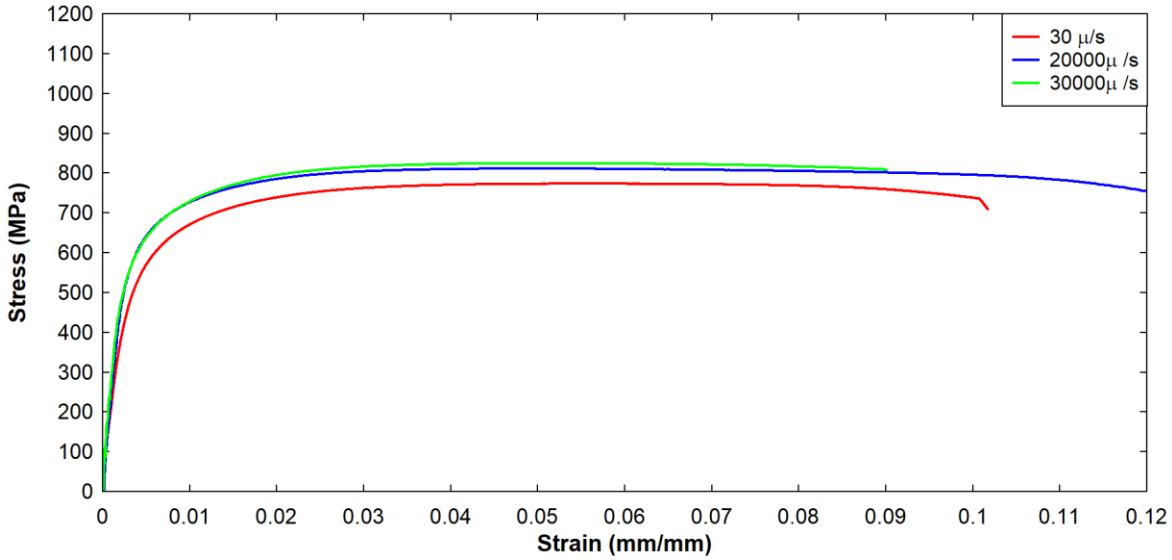

Fig. 3.12: Typical Stress-Strain Curves for 12.7-mm Diameter Strong-Bolt® 2 Bare Anchor

Table 3.6: Tensile Test Data for 12.7-mm Diameter Strong Bolt® 2 Bare Anchors

12.7-mm Diameter Strong Bolt 2						
Test	**Peak Load [kN]**	**Yield**		**Ultimate**		**Elastic Modulus**
		Stress [MPa]	**Strain**	**Stress [MPa]**	**Strain**	**[GPa]**
Strain Rate: 0.00003 /s (0.04 mm/s)						
1	63.7	580	0.0051	780	0.054	196
2	63.2	575	0.0051	773	0.054	202
3	63.4	573	0.0049	776	0.055	210
Average	**63.5**	**576**	**0.0050**	**776**	**0.054**	**203**
Strain Rate: 0.02 /s (18 mm/s)						
1	67.6	630	0.0047	828	0.049	234
2	66.3	630	0.0046	811	0.049	230
3	68.8	631	0.0049	842	0.049	216
Average	**67.6**	**630**	**0.0047**	**827**	**0.049**	**226**
Strain Rate: 0.03 /s (36 mm/s)						
1	67.2	627	0.0047	823	0.049	281
2	67.4	629	0.0045	825	0.047	265
3	67.4	616	0.0043	825	0.005	258
Average	**67.3**	**624**	**0.0045**	**824**	**0.034**	**268**

The general decrease in the yield strains resulted in stiffer anchors as the loading rate increased. This resulted in increased modulus of elasticity as the loading rate increased. The increased loading rate increased the elastic modulus by 11.8% and 32.5% for loading rates of 18 mm/s and 36 mm/s. However, between the higher loading rates, an increase of 18.5% was observed as the loading rate was doubled, even though there was a slight reduction in the peak load at the higher loading rate.

3.3.4 Wedge-All® Anchors

The 9.5-mm diameter anchors were subjected rates of 17 mm/s and 34 mm/s after the quasi-static bare anchor tests. The results presented on Fig. 3.13 and Table 3.7 show a general increase in yield stress as well as ultimate load and stresses as the loading rate increased. The average ultimate loads increased from 28.0 kN to 29.9 kN as the loading rate increased from the quasi-static level to 17 mm/s and then to 30.2 kN at 34 mm/s. The yield stress increased by 13.1% (DIF of 1.13)from the quasi-static value at a loading rate of 17 mm/s, and then by 14.5% (DIF of 1.15) at 34 mm/s. Between 17 mm/s and 34 mm/s of loading, the yield stress increased by only 1.2%. However, the yield strains decreased from 0.0046 to 0.0045 at 17 mm/s, and then to 0.0044. This resulted in an increase in the elastic modulus by 13.9% of the quasi-static values at 17 mm/s, and then by 18.1% at a loading rate of 34 mm/s. By doubling the loading rate, the elastic modulus increased by 3.7%.

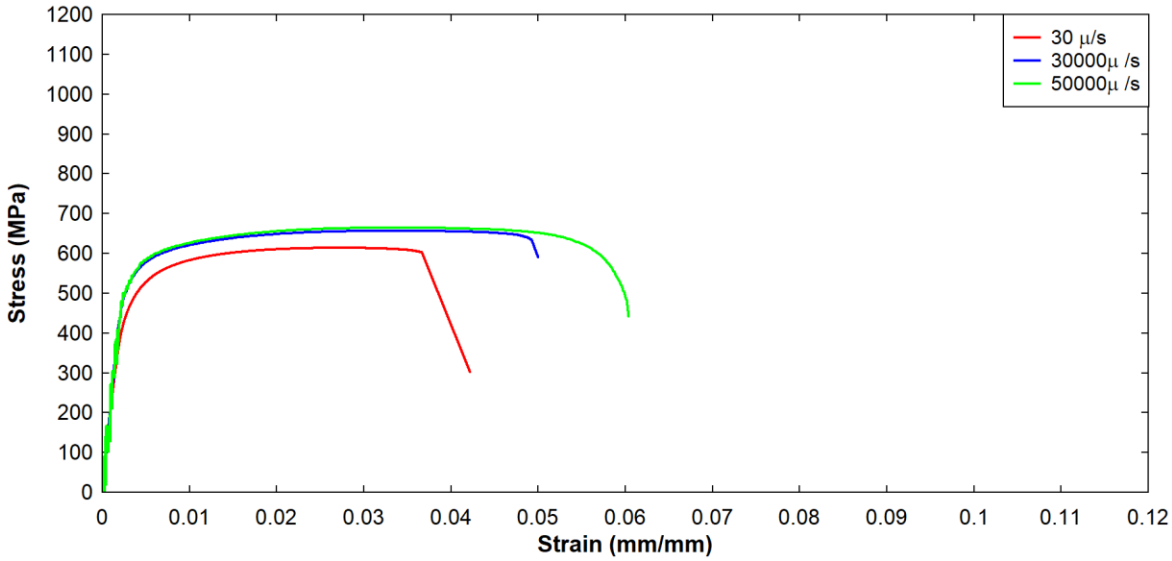

Fig. 3.13: Typical Stress-Strain Curve for 9.5-mm Diameter Wedge-All® Bare Anchor

Table 3.7: Tensile Test Data For 9.5-mm Diameter Wedge-All® Bare Anchors

9.5-mm Diameter Wedge-All						
Test	**Peak Load [kN]**	**Yield**		**Ultimate**		**Elastic Modulus**
		Stress [MPa]	**Strain**	**Stress [MPa]**	**Strain**	**[GPa]**
Strain Rate: 0.00003 /s (0.04 mm/s)						
1	28.0	490	0.0047	616	0.029	198
2	27.9	518	0.0045	614	0.027	210
3*	26.2	530	0.0046	610	0.020	205
Average	**28.0**	**504**	**0.0046**	**615**	**0.028**	**204**
Strain Rate: 0.03 /s (17 mm/s)						
1	30.7	586	0.0046	676	0.036	240
2	29.8	570	0.0045	657	0.033	229
3	29.1	555	0.0044	642	0.034	228
Average	**29.9**	**570**	**0.0045**	**658**	**0.034**	**232**
Strain Rate: 0.05 /s (34 mm/s)						
1	30.2	576	0.0045	665	0.034	241
2	30.5	579	0.0045	672	0.040	223
3	30.0	575	0.0043	661	0.035	258
Average	**30.2**	**577**	**0.0044**	**666**	**0.036**	**241**

*Not considered in calculating the averages

The ultimate stresses also increased by 7.0% (DIF of 1.07) as the loading rate was increased to 17 mm/s, and then by 8.3% (DIF of 1.08) at a loading rate of 34 mm/s. The ultimate stress only increased by 1.1% as the loading rate was doubled.

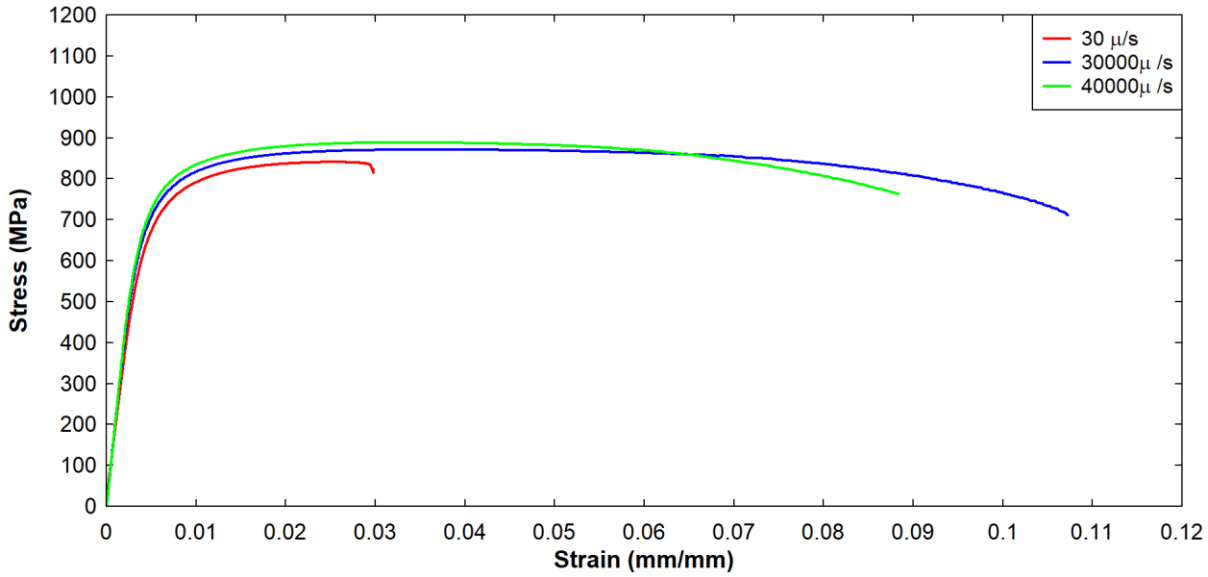

Fig. 3.14: Typical Stress-Strain Curve For 12.7-Mm Diameter Wedge-All® Bare Anchor

Table 3.8: Tensile Test Data For 12.7-mm Diameter Wedge-All® Bare Anchors

12.7-mm Diameter Wedge-All						
Test	**Peak Load [kN]**	**Yield**		**Ultimate**		**Elastic Modulus**
		Stress [MPa]	**Strain**	**Stress [MPa]**	**Strain**	**[GPa]**
Strain Rate: 0.00003 /s (0.04 mm/s)						
1	68.7	714	0.0059	841	0.025	189
2	67.5	692	0.0059	826	0.029	184
3	69.1	704	0.0057	846	0.028	198
Average	**68.4**	**703**	**0.0058**	**838**	**0.027**	**190**
Strain Rate: 0.03 /s (18 mm/s)						
1	71.2	734	0.0056	871	0.036	201
2	72.3	749	0.0057	885	0.035	202
3	72.1	746	0.0057	883	0.036	201
Average	**71.9**	**743**	**0.0057**	**880**	**0.036**	**201**
Strain Rate: 0.04 /s (36 mm/s)						
1	72.6	755	0.0057	889	0.033	209
2	73.3	753	0.0055	897	0.034	218
3	72.9	744	0.0055	892	0.034	205
Average	**72.9**	**751**	**0.0056**	**893**	**0.034**	**211**

For the 12.7-mm diameter anchors, the supplementary testing was done at 18 mm/s and 36 mm/s in addition to the primary test at 0.004 mm/s. The stress-strain behavior (Fig. 3.14)

and the summary of the data (Table 3.8) shows a general increase in ultimate load, yield stress and ultimate stress as the loading rate increased.

The ultimate load increased from an average of 68.4 kN to 71.9 kN when loading rate increased to 18 mm/s and then to 72.9 kN at a loading rate of 36 mm/s. The yield stress increased by 5.7% (DIF of 1.06) of the quasi-static value at loading rate of 18 mm/s, and then by 6.8% (DIF of 1.07) at 36 mm/s. Similar to the 9.5-mm diameter anchors, doubling the loading rate increased the yield stress by 1.1%.

Reduction in the yield strains from 0.0058 to 0.0056 as the loading rates increased resulted in a 5.7% and 10.8% increase in the elastic modulus of the anchors at the supplementary loading rates of 18 mm/s and 36 mm/s.

The ultimate stress increased by 5.0% (DIF of 1.05) of the quasi-static value when the loading rate was increased to 18 mm/s, and then 6.6% at the loading rate of 36 mm/s. The increase in ultimate stress after doubling the loading rate was about 1.5% (DIF of 1.02). The ultimate strains on the other hand increased from 0.027 to 0.036 after the loading rate was increased from the quasi-static rate of 0.04 to 18 mm/s, before reducing slightly to 0.034 at 36 mm/s.

3.3.5 Titen HD Anchors

The 6.4-mm diameter anchors were tested at supplementary rates of 15 mm/s and 30 mm/s in addition to the quasi-static rate of 0.04 mm/s. The stress-strain plots (Fig. 3.15) and summary of the test data (Table 3.9) confirmed the general trend of increase in ultimate load, yield stress and ultimate stress as loading rates increased. The yield and ultimate strains also showed a general increase as the loading rate was increased.

The ultimate load and stress increased by about 2.5% (DIF of 1.03) as the loading rate increased from 0.04 mm/s to 15 mm/s and 30 mm/s. There was no change in the ultimate stress as the loading rate was doubled. The yield stress however showed a higher magnitude of change as the loading rate increased.

The yield stress increased by 3.5% and 4.0% (DIF of 1.04 for both) as the loading rate increased from 0.04 mm/s to 15 mm/s and 30 mm/s. The yield strains did not change much as the loading rate increased, while the ultimate strains increased from 0.026 at the quasi-static loading rate of 0.04 mm/s to 0.033 at 15 mm/s, and then reducing to 0.029 at 30 mm/s. The elastic modulus remained fairly constant in the region of 210 GPa as the loading rate increased from the 0.04 mm/s to 30 mm/s. The strain rates calculated for the loading rates were 30 $\times 10^{-6}$ /s, 20,000 $\times 10^{-6}$ /s and 30,000 $\times 10^{-6}$ /s.

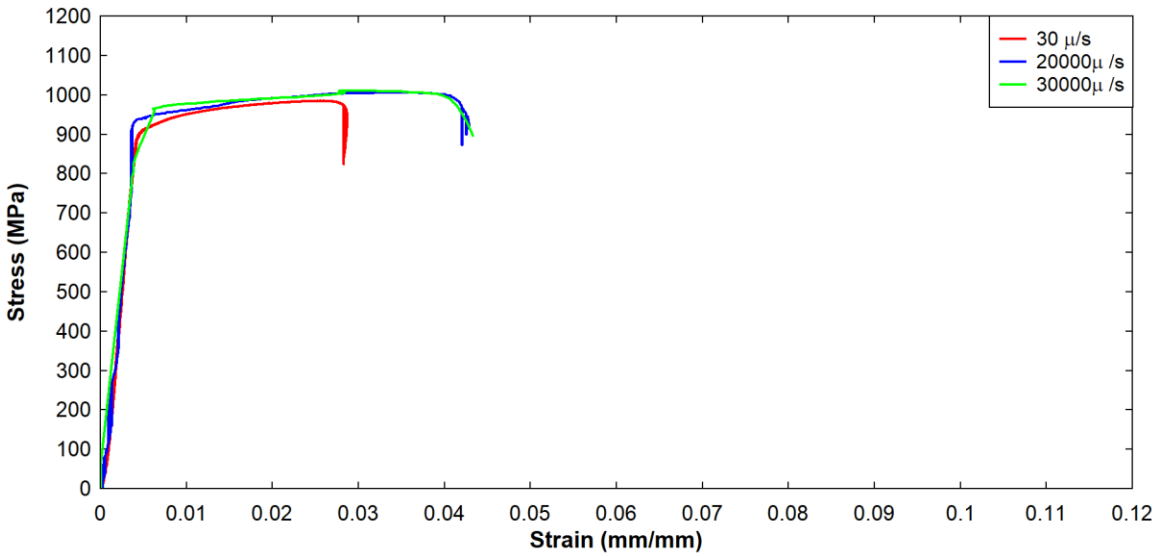

Fig. 3.15: Typical Stress-Strain Curve For 6.4-Mm Diameter Titen HD® Bare Anchor

The average yield stress increased by 2.5% as the loading rate increased to 17 mm/s, and then by 2.9% at a loading rate of 34 mm/s. The yield strains however decreased as the loading rate increased, leading to a general increase in the elastic modulus at higher loading rates. There was an increase of 4.4% in the elastic modulus at loading rate of 17 mm/s, and

7.7% at loading rate of 34 mm/s. Between 17 mm/s and 34 mm/s, loading rates, the elastic modulus increased by 3.3% while the average yield stress did not change much.

Similarly to the yield stresses, the ultimate stresses increased by an average amount of 4.2% at loading rate of 17 mm/s, and 4.4% at 34 mm/s. Though there was little variation in the values of ultimate stress and strains at the supplementary loading rates, the ultimate strain increased by almost 70% of the quasi-static ultimate strains.

Table 3.9: Tensile Test Data For 6.4-mm Diameter Titen HD® Bare Anchors

6.4-mm Diameter Titen HD						
Test	**Peak Load [kN]**	**Yield**		**Ultimate**		**Elastic Modulus**
		Stress [MPa]	**Strain**	**Stress [MPa]**	**Strain**	**[GPa]**
Strain Rate: 0.00003 /s (0.04 mm/s)						
1	28.8	926	0.0064	986	0.023	210
2	27.7	922	0.0068	974	0.025	190
3	28.3	907	0.0060	970	0.030	227
Average	**28.3**	**918**	**0.0064**	**977**	**0.026**	**209**
Strain Rate: 0.02 /s (15 mm/s)						
1	29.4	951	0.0065	1006	0.033	210
2	29.1	950	0.0066	995	0.040	212
3	28.4	948	0.0065	989	0.026	210
Average	**29.0**	**950**	**0.0065**	**997**	**0.033**	**211**
Strain Rate: 0.03 /s (30 mm/s)						
1	29.5	967	0.0064	1011	0.028	206
2	28.5	939	0.0067	976	0.030	201
3	29.3	960	0.0065	1003	0.030	211
Average	**29.1**	**955**	**0.0065**	**997**	**0.029**	**206**

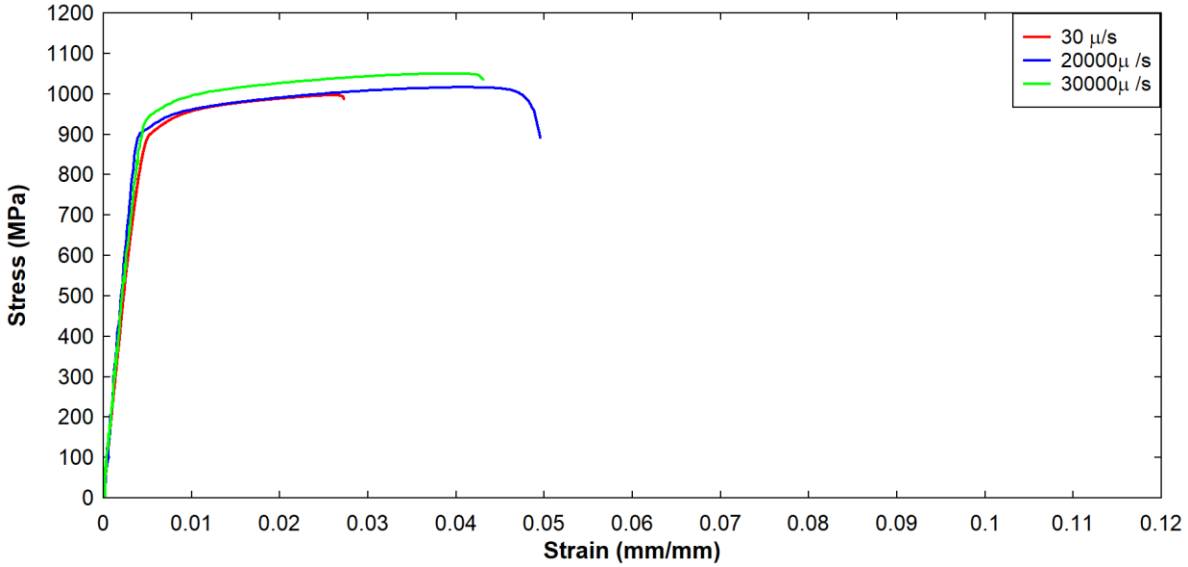

Fig. 3.16: Typical Stress-Strain Curve for 9.5-Mm Diameter Titen HD® Bare Anchor

Table 3.10: Tensile Test Data for 9.5-mm Diameter Titen HD® Bare Anchors

9.5-mm Diameter Titen HD						
Test	**Peak Load [kN]**	**Yield**		**Ultimate**		**Elastic Modulus**
		Stress [MPa]	**Strain**	**Stress [MPa]**	**Strain**	**[GPa]**
Strain Rate: 0.00003 /s (0.04 mm/s)						
1	63.9	928	0.0066	983	0.024	208
2	63.4	900	0.0056	975	0.022	253
3	64.8	922	0.0065	997	0.026	203
Average	**64.0**	**917**	**0.0062**	**985**	**0.024**	**222**
Strain Rate: 0.02 /s (17 mm/s)						
1	64.4	920	0.0063	990	0.034	215
2	68.3	949	0.0056	1050	0.045	263
3	67.5	950	0.0064	1039	0.040	216
Average	**66.7**	**940**	**0.0061**	**1026**	**0.040**	**231**
Strain Rate: 0.03 /s (34 mm/s)						
1	66.0	929	0.0059	1016	0.041	236
2	66.2	944	0.0057	1019	0.043	254
3	68.3	960	0.0062	1050	0.039	228
Average	**66.8**	**944**	**0.0059**	**1028**	**0.041**	**237**

For the 12.7-mm diameter anchors, the supplementary loading rates were 18 mm/s and 36 mm/s which resulted in strain rates of 20,000 $\times 10^{-6}$ /s and 40,000 $\times 10^{-6}$ /s . For tests at the 0.04 mm/s and 36 mm/s loading rates, the anchors fractured without showing any yield

plateau (Fig. 3.17 and Table 3.11). However, the testing at 18 mm/s loading rate produced consistent yield plateaus for all three anchor samples.

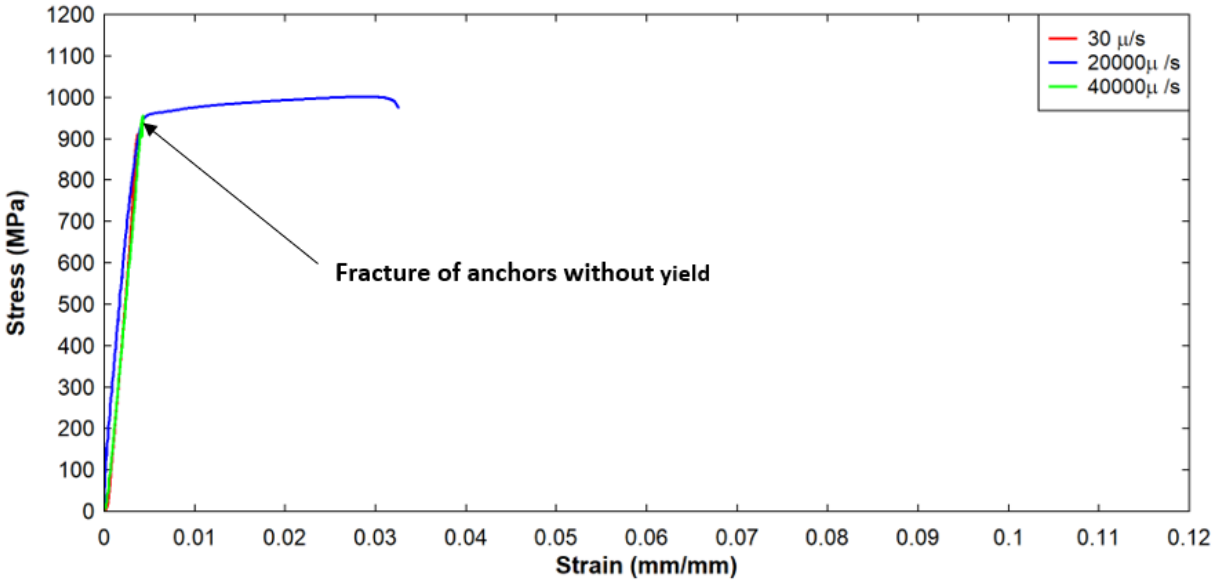

Fig. 3.17: Typical Stress-Strain Curve for 12.7-mm Titen HD® Bare Anchor

Table 3.11: Tensile Test Data for 12.7-mm Diameter Titen HD® Bare Anchors

12.7-mm Diameter Titen HD						
Test	**Peak Load [kN]**	**Yield**		**Ultimate**		**Elastic Modulus**
		Stress [MPa]	**Strain**	**Stress [MPa]**	**Strain**	**[GPa]**
Strain Rate: 0.00003 /s (0.04 mm/s)						
1	105.0	No Discernible Yield Point		882	0.004	204
2	105.6			887	0.004	209
3	108.8			914	0.004	236
Average	**106.5**			**894**	**0.004**	**216**
Strain Rate: 0.02 /s (18 mm/s)						
1	118.2	947	0.0056	993	0.036	264
2	119.1	963	0.0059	1001	0.029	247
3	122.0	982	0.0061	1025	0.030	248
Average	**119.8**	**964**	**0.0059**	**1006**	**0.032**	**253**
Strain Rate: 0.04 /s (36 mm/s)						
1	113.6	No Discernible Yield Point		955	0.004	230
2	101.6			854	0.004	233
3	106.5			895	0.004	223
Average	**107.3**			**901**	**0.004**	**229**

The ultimate load and stress increased from an average of 106.5 kN and 894 MPa at the quasi-static loading rate to 119.8 kN and 1006 MPa (DIF of 1.13)) at loading rate of 18 mm/s before decreasing to 107.3 kN and 901 MPa (1.01) at loading rate of 36 mm/s. Similarly, the elastic modulus increased by 16.9% at 18 mm/s, and just by 6% at loading rate of 36 mm/s. While the anchors failed at a strain of 0.004 for the 0.04 mm/s and 36 mm/s loading rates, they failed at an average strain of 0.032 at 18 mm/s. The lower ultimate loads associated with the 36 mm/s loading rate is attributed to the fact that failure at this rate occurred within the grips of the testing machine where the anchor diameter was slightly smaller.

3.4 General Test Setup (Static and Dynamic Test)

The test setup for the mechanical anchor systems was designed to meet the requirement of ASTM E488/488M–15 [35]. Instead of a loading ring, restraining bars, spaced at 500 mm, were used to restrain the concrete beam to the floor. The spacing of the restraining bars was chosen to meet the minimum spacing requirement for anchors to avoid interaction with the failure cones. Except for the test frames and the data acquisition systems, the concrete beam restraints were the same for both static and dynamic (drop mass) tests. Both tension and shear tests were conducted with a pull-action from the force-imparting mechanism (hydraulic actuator and first-class lever system for the static and drop-mass tests respectively) through a one-meter long 25-mm diameter threaded rod (pull rod) and a coupling system to the anchors.

Fig. 3.18 shows the arrangement of the coupling system for tension test. The coupling system differed slightly between the expansion and the screw anchors. For the expansion anchors, two couplers were used to connect the anchor to the pull rod. The first coupler,

referred to as “coupler 1” was a 25-mm diameter threaded rod (50 mm in length) with internal threads cut to match with the threads of the anchors to be tested. The second coupler, referred to as “coupler 2” was 50-mm diameter bar (80-mm long) with a 25-mm diameter thread cut internally through to accommodate both the pull rod and coupler 1. For the screw anchor, a variation of coupler 2 with internal threads cut in the upper half to accommodate the pull rod was used. The bottom half was modified to allow the anchor hex- head to be slotted and held in place during the tests.

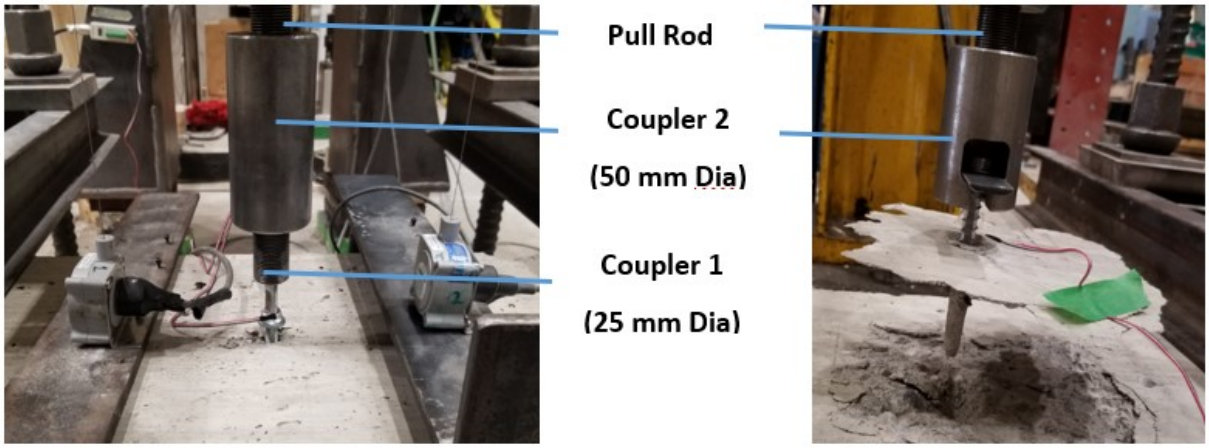

Fig. 3.18: Coupling Arrangement with Anchor for Tension Test

The setup arrangement for the shear test was the same for both static and dynamic tests. Fig. 3.19 shows the arrangement at the vicinity of the anchor for the shear test. Shear loading plates of dimensions meeting the requirements of ASTM E488/488M[35] were used. Plate thickness of 9 mm and hole diameter of 11 mm were used for the 6.4-mm and 9.5-mm diameter anchors while plate thickness of 12 mm and hole diameter of 15 mm was used for the 12.7-mm anchors. Two sheets of polytetrafluoroethylene (PTFE) were inserted between the concrete and loading plate to reduce friction during shear testing. The first sheet was fixed on the contact face of the shear plate, while the second sheet was fixed to the face of the concrete beam prior to every test. The loading plate was connected to the pull rod through coupler 2.

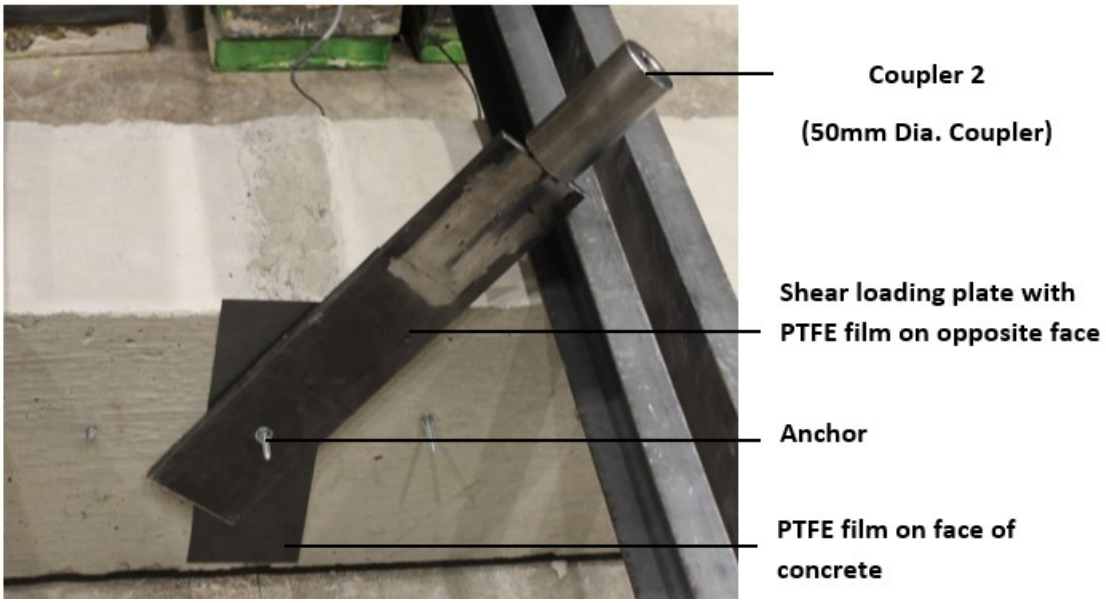

Fig. 3.19: Coupling Arrangement with Anchor for Shear Test

Fig. 3.20 shows the holding down restraint system. It comprised a pair of back-to-back channel sections and two pairs of dywidag bars bolted to the laboratory floor and the back-to-back channel sections.

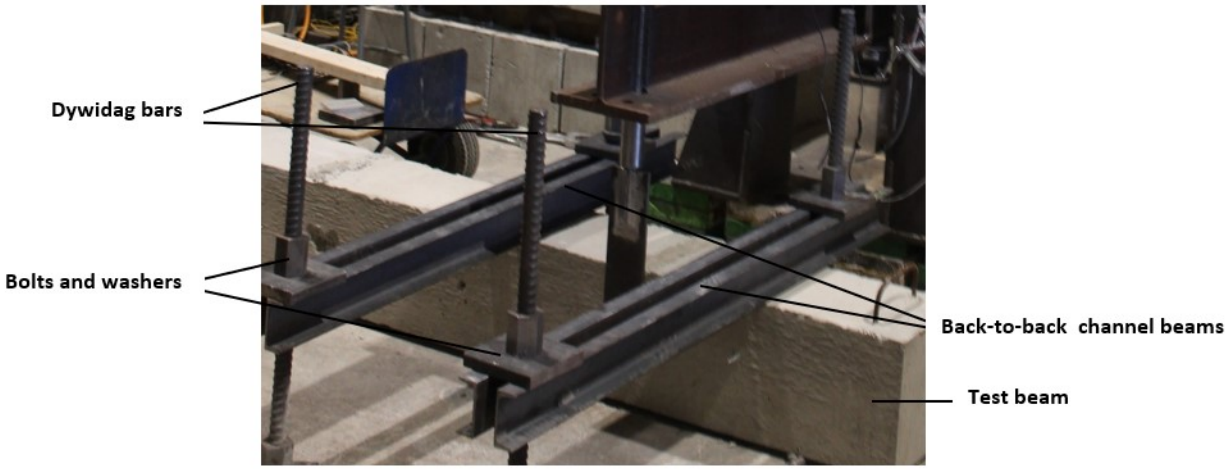

Fig. 3.20: Holding Down system

Two different displacement measurement instruments were used in the course of the experimental program. A pair of LVDTS were initially used during the dynamic drop-mass testing and were later replaced with a pair of string-pots. The LVDTs were replaced because their position of installation relative to the steel beam exposed them to rebound

impact during the dynamic tests. Fig. 3.21 and Fig. 3.22 shows the installed LVDTS and string-pots respectively. The string-pot assembly consisted an outrigger system attached to the pull-rod so the extended string can be attached to it. The string-pots are screwed to a steel plate which in turn is secured to the sides of the concrete beam.

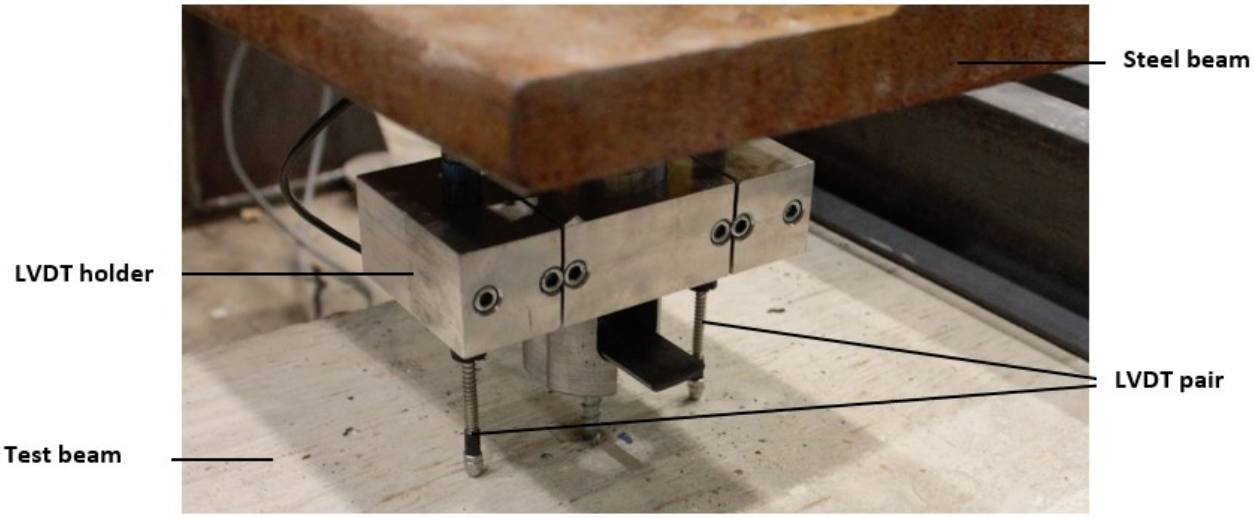

Fig. 3.21: LVDT Setup for Displacement Measurement

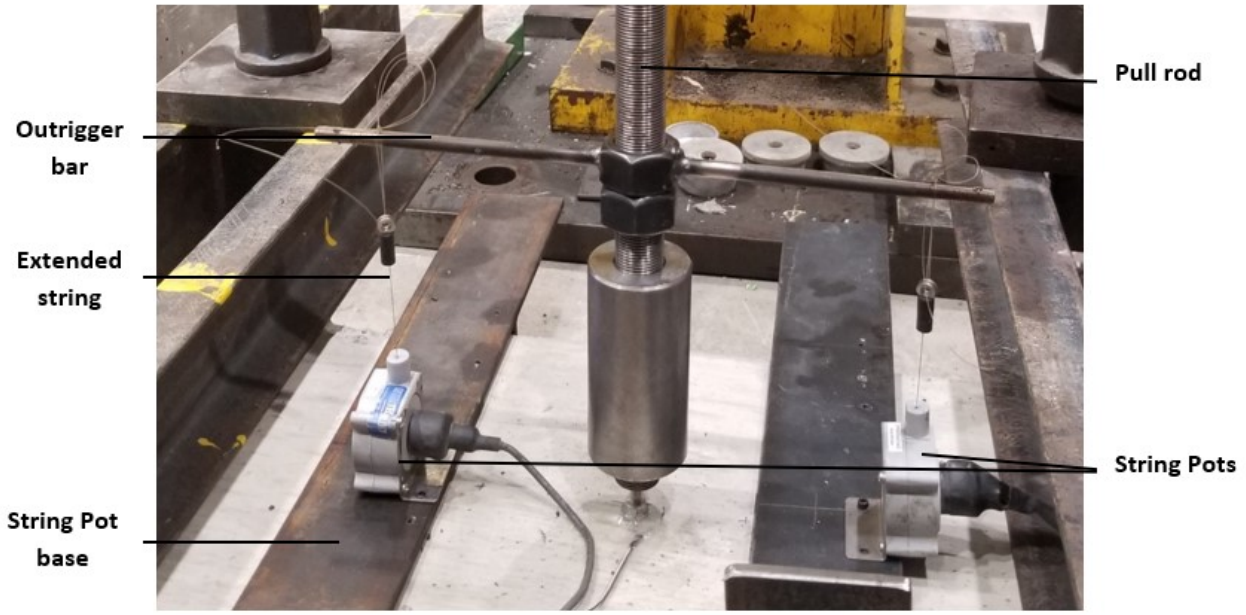

Fig. 3.22: String Pot Setup for Displacement Measurement

3.5 Static Test

3.5.1 Static Test Setup

Fig. 3.23 and Fig. 3.24 illustrate the static test frame and detailed arrangement during the static test. The setup comprises a 55-kip double-acting MTS actuator mounted on a steel frame with back-to-back MC460×86 cross-beam framing into two W310×158 columns. The actuator is mounted on a steel plate pad at mid-span of the cross-beam and controlled by an MTS 458.10 control system. Steel anchor displacements were measured with two calibrated String-Pots connected to an outrigger attached to the pull-rod. The pull-rod was connected to the MTS actuator through a 25-mm thick steel plate at its upper end.

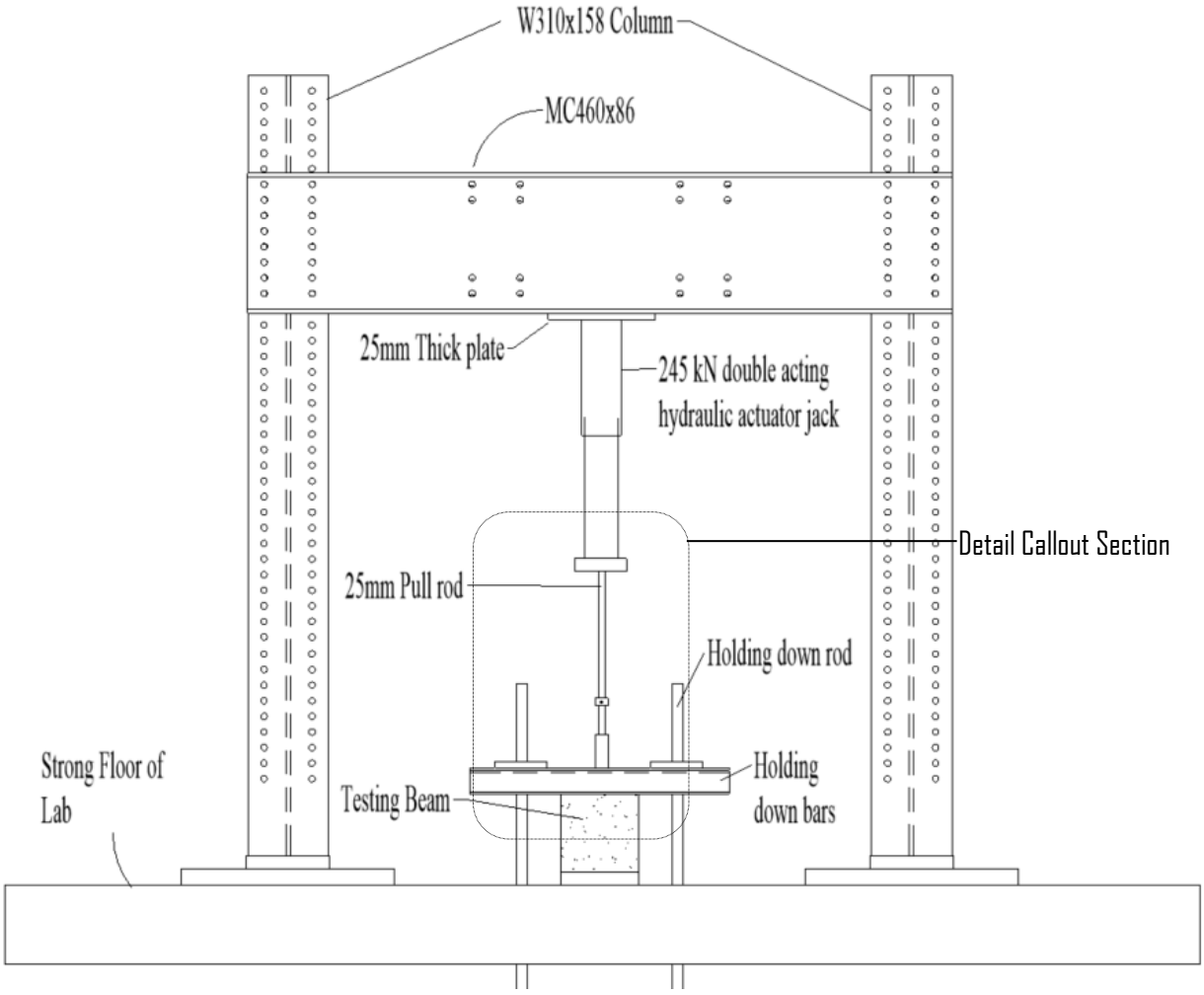

Fig. 3.23: Test Frame for Static Test of Anchors

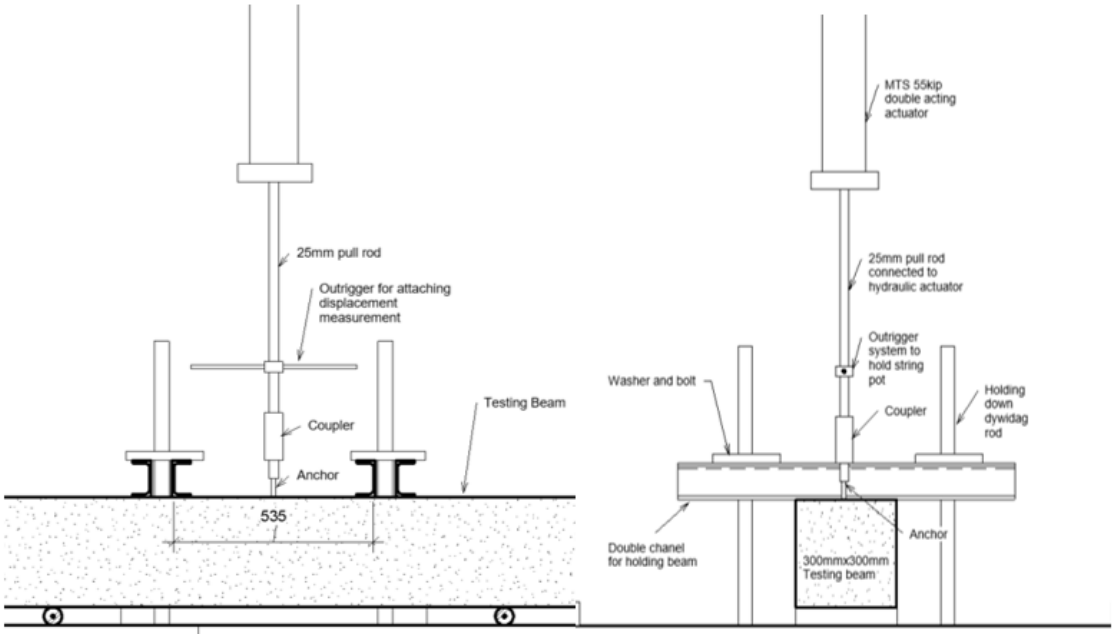

Fig. 3.24: Details of Static Test Setup

The data acquisition system for the static test includes an acquisition computer, the MTS 458.10 Control system and a cDAQ 9178 data acquisition module from National Instruments. The acquisition computer integrates and displays data acquired from the cDAQ 9178 module where the strain gauges and the String Pots are connected to through junction bridges. Movement of the hydraulic actuator can be controlled both manually by a toggle on the MTS Control or remotely through the acquisition computer in either a displacement-controlled or load-controlled mode. Fig. 3.25 shows the components of the data acquisition system for the static test.

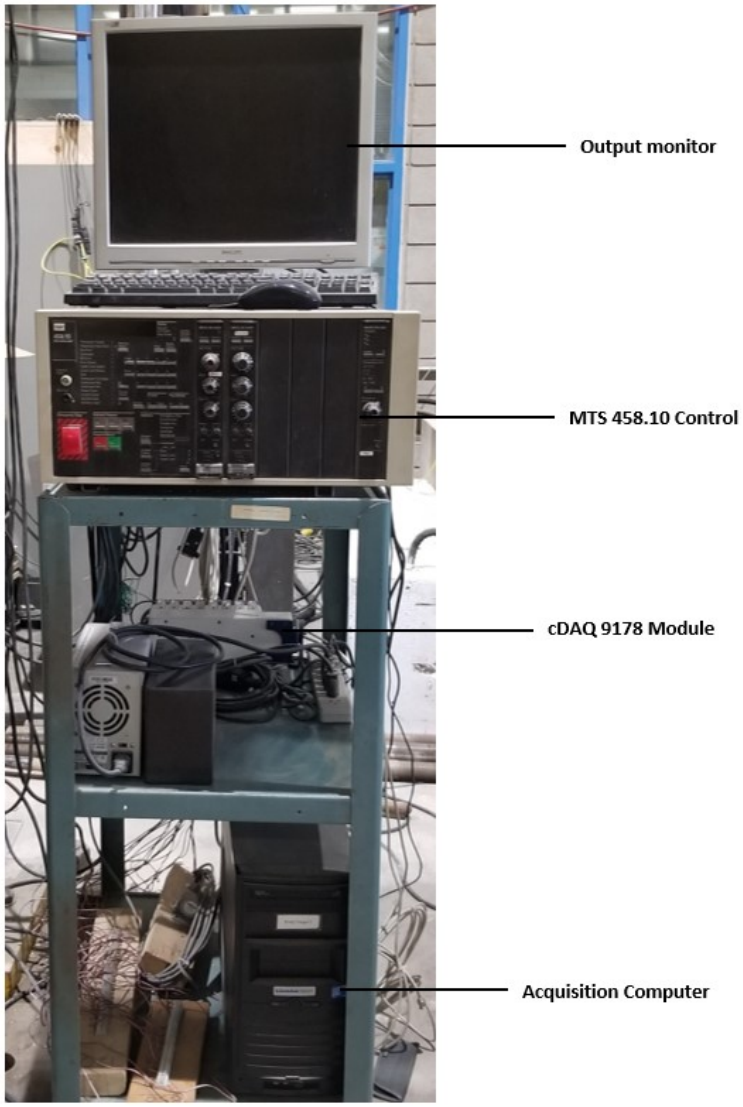

Fig. 3.25: Data Acquisition System for Static Test

3.5.2 Static Test Procedure

Tension and shear loading under static testing were carried out in accordance with the provisions of ASTM E488/E488M-15 [35]. Loading was carried out under displacement-controlled mode with the loading rate selected to ensure that failure of the anchor occurred between one (1) and three (3) minutes from the start of loading. To accommodate for the change in position of the anchor, the actuator pad was slightly moved on the test frame

beam in order to align with the pull rod assembly to the side of the beam. The following sequence was followed during the testing.

- The anchor was installed on the concrete beams following the manufacturer recommended procedure outlined earlier and the beam was positioned directly beneath the hydraulic actuator and pull-rod assembly.
- For tension test, couplers (Coupler 1 and Coupler 2) were connected to anchor. The hydraulic actuator was adjusted to align with the pull-rod and connected to the anchor and coupler assembly with Coupler 2 . For shear test, the PTFE film was installed on the side of the beam before installing the shear loading plate. The shear loading plate was then connected to Coupler 2 before connection with the pull-rod.
- The back-to-back channel restrained system was used to restrain the concrete beam to the laboratory strong floor.
- The String-Pots were attached to the beams and connected to the pull rod.
- The String-Pot, strain gauges (if applicable), load cells were checked and connected to the data acquisition system and then the axial load was applied to the anchor until failure.

3.6 Dynamic (Impact) Test

3.6.1 Drop Test Setup

The loading apparatus consisted of the drop-mass test frame, a lever system and data acquisition system. Fig. 3.26 shows the drop-mass test frame and first-class lever system. The drop-mass test frame consisted of a 235-kg mass installed on two circular steel guides. The 235-kg mass can be raised up the guides with a pneumatic lifting system, to a maximum height of 2.0 m. For each test the drop-mass was raised to a predetermined height

and then released to free-fall onto one end of the first-class lever beam. The tup of the drop-mass was strain-gauged to measure the impact force. A set of photo-emitters were installed on the drop-mass frame While a photo-interruptor consisting of a steel bar was attached to the drop mass, which would interrupt the light emitted by the photo-emitters when it travelled pass it. The photo interrupter was used to trigger the data acquisition system.

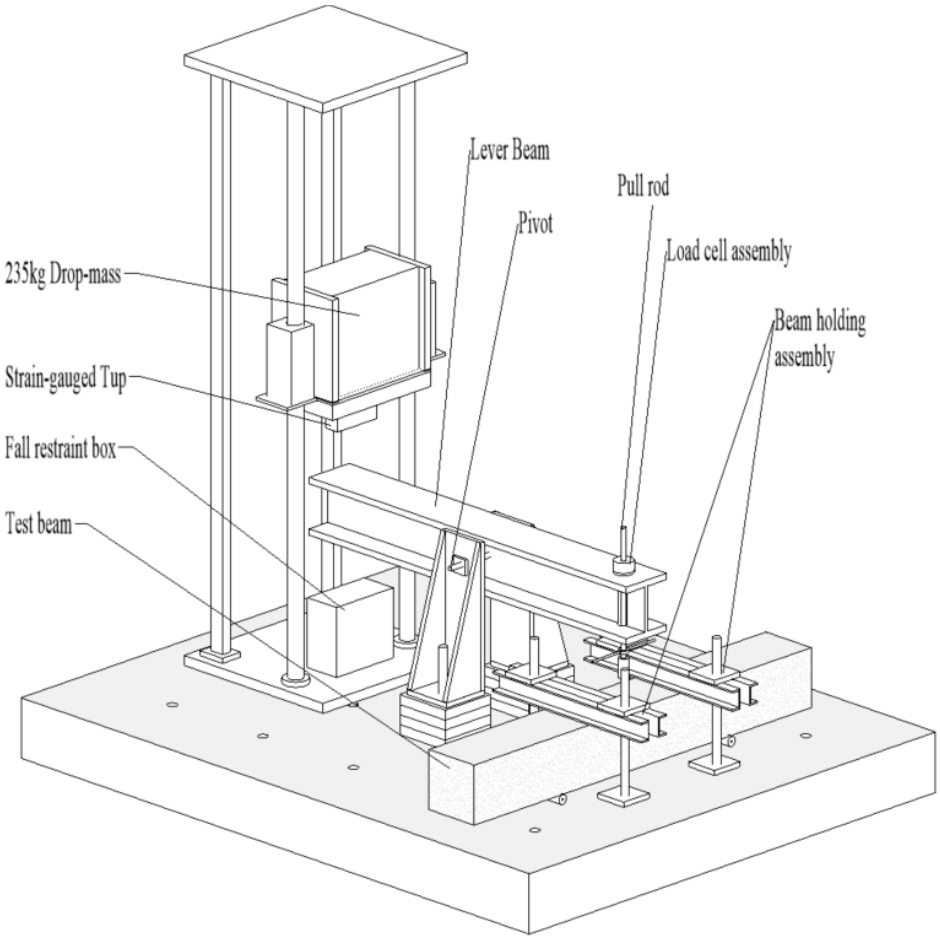

Fig. 3.26: Impact Test Setup

The lever system consists of a 2.10-m W250×167 steel beam pivoted with two welded steel frames to form a first-class lever. The pivot of the lever system was positioned to yield a mechanical advantage of 1.0. The rear end of the lever system was aligned to match with the tup of the drop-mass to provide the effort of the system. The loads measured through the strain-gauged tup is referred to as the “Compression Load”. At the opposite end, the

tested anchor was attached to and loaded by the downward movement of the compression end of the lever.

The upward movement of the front end of the lever applied a tensile (or shear) load on the anchor through the pull-rod. To measure the tensile or shear load on the anchor, a PicoCoulomB (PCB) piezoelectric load cell was placed on top of the steel beam and tightened to the pull-rod. A spherical self-centering washer set was installed on top of the load cell to align the pull-rod and eliminate bending of the rod when connected to test anchors. At the effort end of the lever, a restraint box was placed to prevent the drop-mass from driving the lever to the floor during test.

Data Acquisition and Calibration

A Yokogawa DL750P ScopeCorder data acquisition system (Fig. 3.27) capable of measuring up to one million samples per second was employed for data acquisition, display and storage during the drop-mass testing. Similarly to the static test, the anchor displacement was measured with either two LVDTs or two String-Pots connected to outriggers on either side of the anchor. Additionally, a strain gauge was installed on one anchor from each group of test specimen to determine the stress-strain behavior as well as the strain rate during the tests. The data acquired during the test were as follows:

- Tup strain gauge load
- PCB load cell load
- Two displacement measurements
- 350-Ohm strain measurement
- Photo-interruptor voltage measurement

Fig. 3.27: Yokogawa DL750P ScopeCorder for Data Acquisition

Tup Strain Gauge

The tup of the 235-kg drop-mass was strain gauged in a full-bridge to measure the impact load during the test. Prior to the anchor testing the tub was calibrated by applying known loads and measuring the corresponding voltage from the full-bridge strain gauge. Fig. 3.28 presents the calibration plot for the strain gauge. The linear equation of fit with the correlation coefficient of 0.999 are presented on the graph.

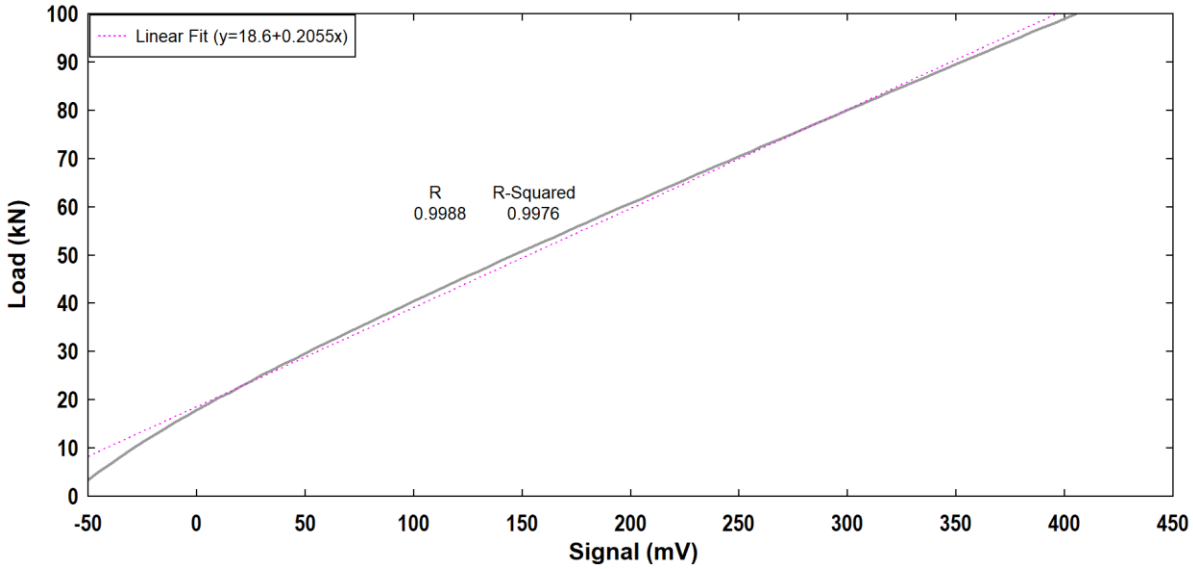

Fig. 3.28: Tup Strain-Gauge Calibration Plot

PCB Piezoelectric Load Cell

A PCB Piezoelectric Load Cell, ICP® Quartz Model 207C Load Ring (Fig. 3.29), was used to acquire the load on the pull-rod and test anchor. The load cell has a maximum range of 450 kN with a resolution of 8.9 N. Its sensitivity of 0.011 mV/N specified by the manufacturer was setup in the ScopeCorder to save and display anchor force readings during the test. The load cell was powered by a PCB model 482A22 signal conditioner to a working voltage.

Initial calibration of the test setup was carried out on a 25-mm threaded bar to obtain load duration as well as derive a relationship between the peak load on the anchor and the drop height. Fig. 3.30 shows the calibrated anchor load "Tension Load" and impact load "Compression Load" at heights of 50 mm, 100 mm and 150 mm. A calibration plot for the peak loads against the drop heights are also presented in Fig. 3.31.

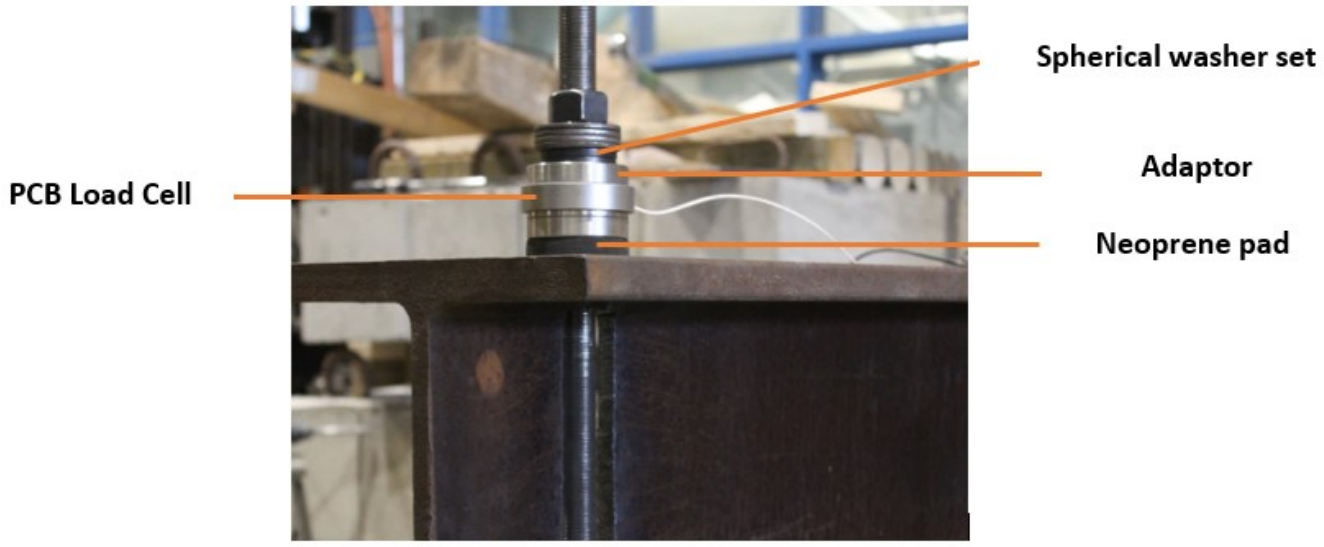

Fig. 3.29: Load Cell, Adaptors and Spherical Washers

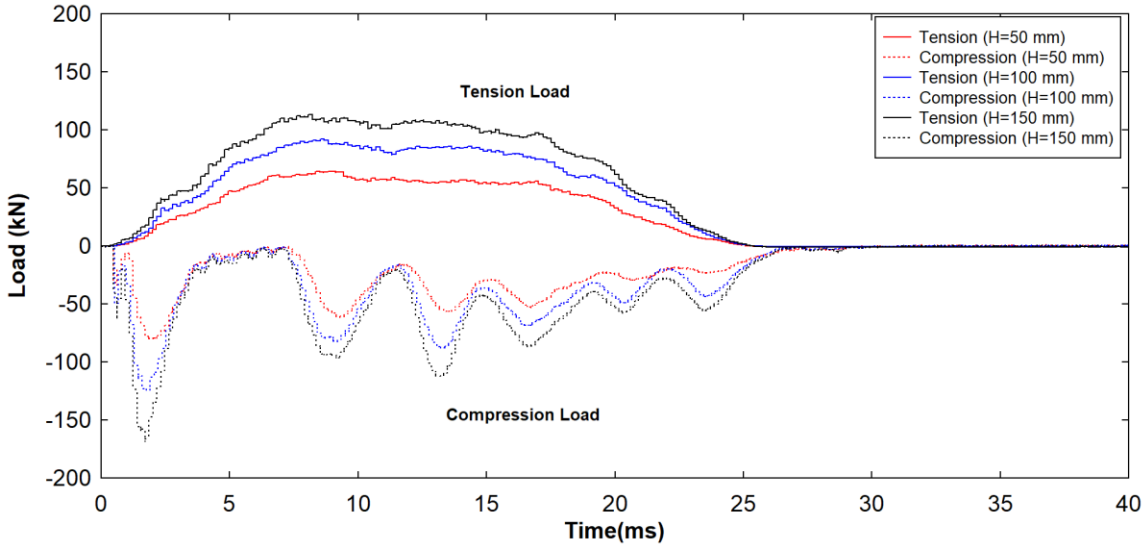

Fig. 3.30: Typical Load Versus Time Plot for Tension and Compression Loads

The mass was dropped on to a 25.4-mm neoprene pad while a 12.7-mm neoprene pad was sandwiched between the PCB piezoelectric load cell and the W250 lever to lengthen the duration of the impact load on the anchorage system to meet with the 30-ms duration requirement of ASTM E488/E488M-15 for shock test. The neoprene pads had a hardness of 50 on the durometer scale.

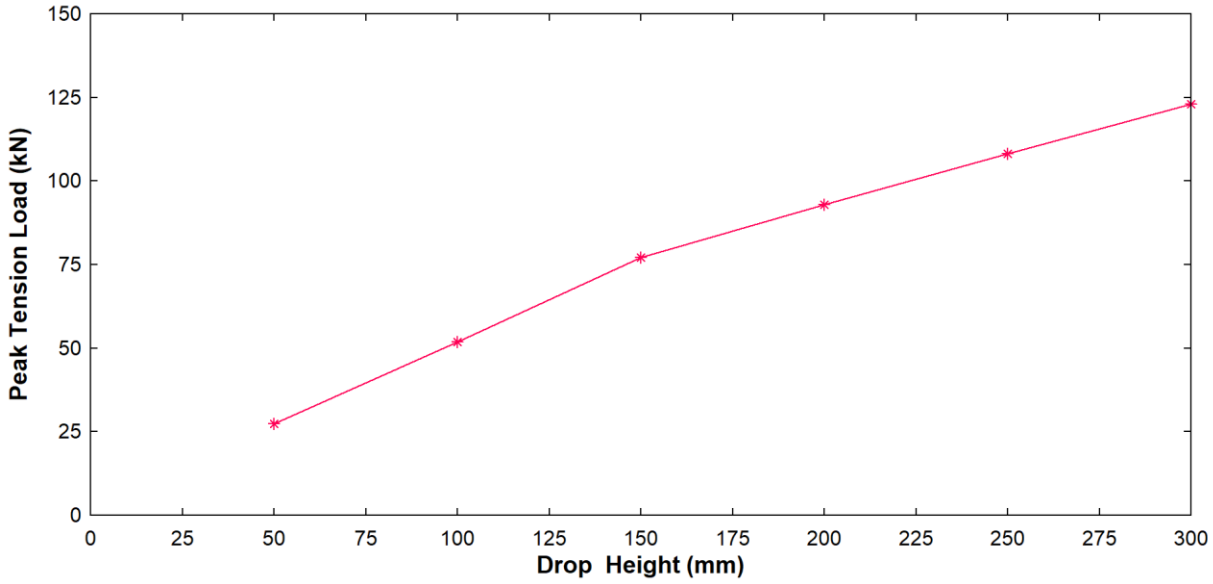

Fig. 3.31: Calibration Plot of Peak Load Vs Drop Height

String Potentiometers

Two SP1-4 String Potentiometers (String-Pots) from Intertechnology® were used for displacement measurements after it was observed that the LVDTs, initially used to measure anchor displacements, were susceptible to damage from impact of the lever beam. The String-Pots had a range of 120 mm and were mounted on steel supports on steel brackets attached to the concrete test beam. The String-Pots were calibrated to obtain calibration factor to input into the ScopeCorder. Fig. 3.32 and Fig. 3.33 show the calibrated plots and input equations used. Both linear fit lines had correlation coefficient of 0.9999.

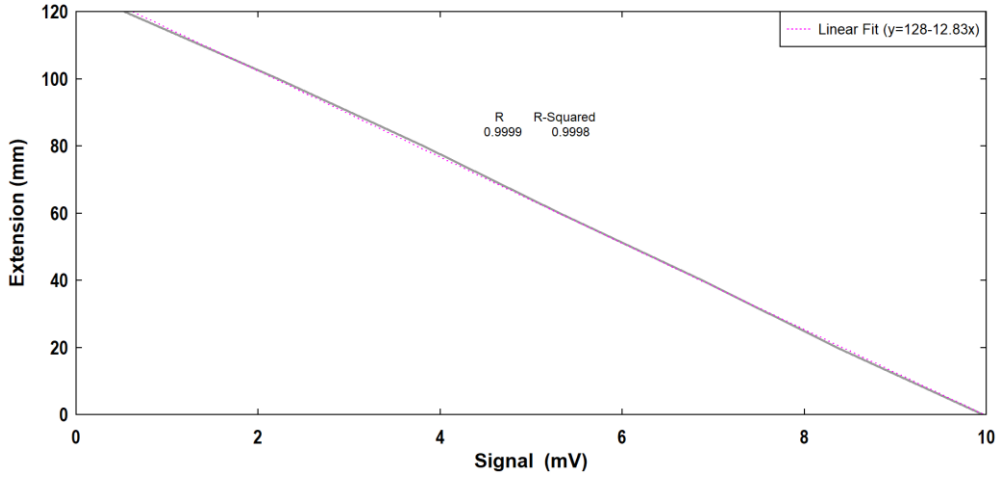

Fig. 3.32: String Potentiometer 1 Calibration Plot

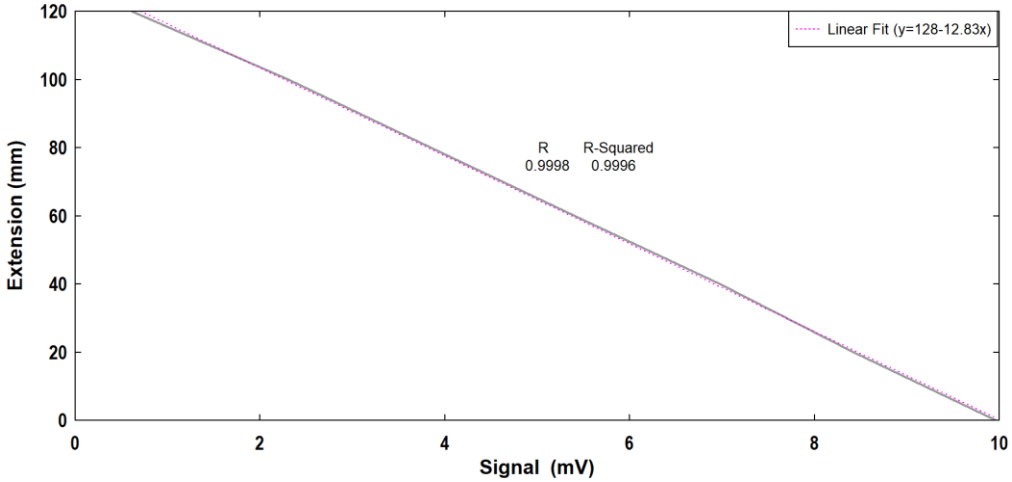

Fig. 3.33: String Potentiometer 2 Calibration Plot

Strain Gauge

A 350-Ohm strain gauge attached to the anchor was also connected the ScopeCorder through a Yokogawa Model 701956 NDIS-350 Ohm Enhanced Shield bridge head. At least one anchor from each size tested in tension was strain-gauged to determine the stress-strain behavior of the anchor under tension loading as well as enable the estimation of the rate of strain on the steel anchor.

Photo-Interruptor

Fig. 3.34 shows the Photo-emitter and Photo-interruptor assembly on the drop-mass test frame. In normal condition, the emitter gives an output voltage of 5 mV through the ScopeCorder. However, when the interruptor passes through the emitter, cutting the beam of light, a voltage reading of 0 mV is recorded. This arrangement was used to trigger data acquisition of the ScopeCorder to maximize sampling rate on the available disk space. A trigger buffer length of either 10 ms or 20 ms was set during the test depending on how fast the drop-mass moved to ensure the entire data range was captured for each test.

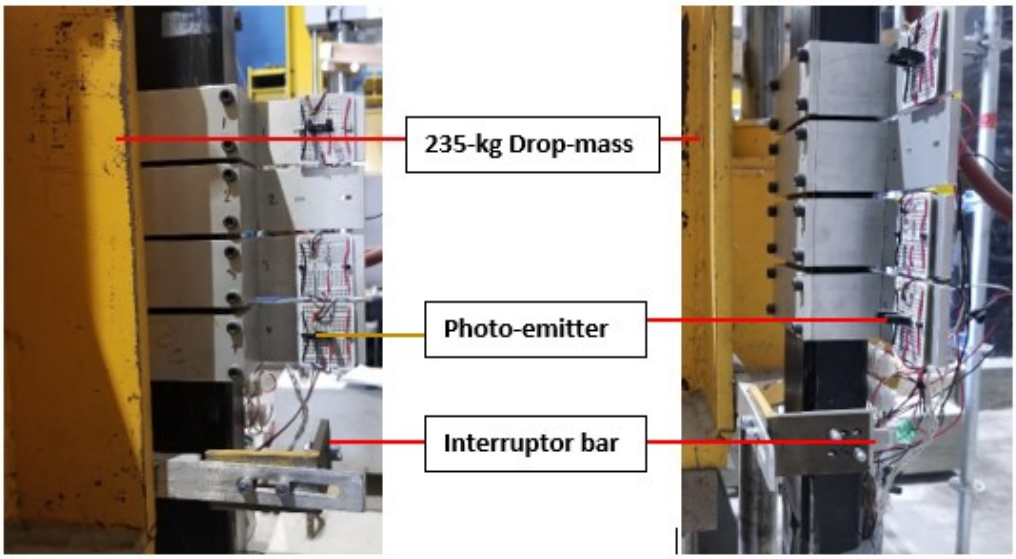

Fig. 3.34: Photo-emitter and Interruptor at the back of the drop-mass frame

3.6.2 Test Procedure

The test procedure adopted for the drop-mass tests was similar for both tension and shear tests. The difference however was that in the shear test, a shear loading plate with a PTFE film connects the anchor to the coupler instead of the threaded rod coupler used in the tension test. Fig. 3.18 and Fig. 3.19 shows the setup at the anchor end of the beam for tension and shear testing. The general sequence during the test was as follows:

- Drop mass was raised to a predetermined height and supported off the first-class lever beam to allow for alignment of the assembled test anchorage system
- Coupler 1 was connected to the test anchor, and then to Coupler 2 for tension test. For the shear test a PTFE sheets were installed, and the shear loading plate placed and screw into coupler.
- The beam restraint system was assembled and connected to the strong laboratory floor.
- String-Pots or LVDTs and strain-gauges (if applicable) were connected to the ScopeCorder.
- The drop-mass was then raised to a predetermined height and released for free-fall onto the first-class lever.
- Data acquisition was automatically triggered once the interruptor bar travelled passed the photo-emitter.
- Data was saved, observations recorded.
- The drop-mass test was repeated at subsequently predetermined heights if the anchor does not fail.

Initial drop height for each test was based on the height corresponding to failure load under static test conditions. In most cases, anchors did not fail at first impact, and further drops were required to check the residual capacity of the anchors. The specific drop heights and anchor behavior during the tests are presented and discussed in the experimental results chapter.

Since the two concrete batches showed different strengths, the tensile and shear tests were carried out with different batches in order to maintain consistency in material properties. The first batch of concrete was used for the shear testing while the second batch was used for the tensile test.

4 Chapter: Experimental Results

4.1 General

This chapter presents and discusses the results of the experimental investigation. The experimental static test results are compared with predictions made with the CCD design method for mechanical anchors. The second part presents the results of the dynamic tests and their comparison with the static failure loads to establish a Dynamic Load Ratio (DLR). The DLR is defined as ratio of the peak impact load to the average static failure load for each anchor series.

The nomenclature used in the experimental program include the loading regime: static tension or shear (ST or SS) or dynamic tension or shear (DT or DS); the anchor type: Strong-Bolt 2 (STB), Wedge-All® (WA), and Titen HD® (TTH); the anchor diameter: quarter inch (QI), three-eighths inch (TE), and half inch (HL), followed by a double-digit number for the static test or two set of double-digit numbers separated by a hyphen for the dynamic test. The first double-digit number indicated the nth anchor tested in the anchor group, while the second double digit number indicated the *j*-th drop test on the n-th anchor for the dynamic test. For example, ST-STB-QI-03 is a static tension test (ST) sample of a Strong-Bolt® 2 anchor (STB) with diameter of 6.4 mm (QI) and is the third anchor tested (03). Similarly, DT-STB-QI-03-02 is a dynamic tension test (DT) sample of a Strong-Bolt® 2 anchor (STB) with diameter of 6.4 mm (QI) and is the third anchor in the series (03) and under the second drop test (02).

Concrete Batch 2 was used for the tensile test while Batch 1 was used for the shear testing in both static and impact testing.

4.2 Static Tests

The result presented for the static tests include failure loads and modes of failure and their comparison with predictions from the CCD design method; as per the Canadian and the American Codes of design [2], [3].

4.2.1 Tension Test

In general, five anchor failure modes were observed in the test program:

- Steel fracture failure (SF)
- Concrete cone breakout failure (CC)
- Mixed pull-out and concrete breakout failure (PO-CC)
- Pull-through failure (PT)
- Splitting of Beam (SB)

The anchors were tested as described in Section 3.5.2 for both tension and shear.

Table 4.1: Predicted and Experimental Capacity of Anchors in Tension

Anchor Data				Anchor Capacity						
				Steel (kN)	Conc. (kN)	Pull-out (kN)	Predicted Failure		Experimental Failure	
Anchor Type	ϕ (mm)	h_{ef} (mm)	f_{ut} (MPa)				Load (kN)	Mode	Load (kN)	Mode
Strong Bolt 2	6.4	38.1	487.0	9.3	20.1	-	9.3	SF	8.9	SF
	9.5	63.5	761.0	34.5	43.2	20.8	20.8	PO	29.3	SF
	12.7	85.7	776.0	63.5	67.7	32.7	32.7	PO	46.9	CC
Wedge All	9.5	67.0	613.0	27.3	46.8	-	27.3	SF	27.1	SF
	12.7	86.0	838.0	68.4	68.1	-	68.1	CC	48.7	PT
Titen HD	6.4	49.3	853.0	28.3	29.5	-	28.3	SF	21.4	PO-CC
	9.5	61.0	773.0	64.0	40.6	-	40.6	CC	42.4	PO-CC
	12.7	75.9	758.4	106.5	56.5	-	56.5	CC	62.4	PO-CC

A summary of the predicted anchor capacities compared with the average experimental failure loads and predominant failure modes are presented on Table 4.1. The concrete breakout capacity based on the CCD method was calculated using Equation 7, with an

effectiveness factor (k_n) of 14.7 and concrete compressive strength of 33.7 MPa. The predicted steel failure loads were based on the average tensile failure loads from the material testing of the steel anchors presented in this thesis. CSA A23.3-14 [2] recommends the pull-out capacity of post-installed anchors based on 5% fractile of test results conducted in accordance with ACI 355.2 [32]. As the codes do not give guidance to the calculation of pull-out strength of post-installed anchors in tension, the pull-out capacities reported in Table 4.1 are based on manufacturer design guidance [81] where applicable. Stress-strain behavior of the anchors were provided in comparison with the bare anchor. The elastic modulus for each test was obtained as the average slope of the straight part of the curve.

4.2.1.1 Strong-Bolt® 2

Data for all the post-installed Strong-Bolt 2 anchors tested under static tension conditions are given on Table 4.2. As per ASTM E488/E488M-15 [35], the anchors were loaded at 0.04 mm/s, 0.05 mm/s and 0.08 mm/s for the 6.4-mm, 9.5-mm, and 12.7-mm diameter respectively in displacement-controlled mode to ensure failure occurred between 1 and 3 minutes of loading.

Table 4.2: Static Tension Test Data for Strong Bolt® 2 Anchors

Sample	ϕ	Failure Load		Failure Mode		Average Experimental. Failure Load	Initial Stiffness
		Predicted	Experimental				
	(mm)	(kN)	(kN)	Predicted	Actual	(kN)	kN/mm
ST-STB-QI-01	6.4	9.3	8.7	SF	SF	8.9	4.8
ST-STB-QI-02	6.4	9.3	8.7	SF	SF		85
ST-STB-QI-03	6.4	9.3	9.2	SF	SF		4.8
ST-STB-TE-01	9.5	20.8	29.9	PO	SF	29.3	53.5
ST-STB-TE-02	9.5	20.8	28.5	PO	SF		52.0
ST-STB-TE-03	9.5	20.8	29.5	PO	SF		22.0
ST-STB-HL-01	12.7	32.7	49.1	PO	CC	46.9	19.4
ST-STB-HL-02	12.7	32.7	47.9	PO	SB		19.4
ST-STB-HL-03	12.7	32.7	43.8	PO	CC		10.0

The table shows that all tested 6.4-mm diameter anchors failed in steel fracture mode (Fig. 4.1) with failure loads about 95% of the steel fracture load of 9.3 kN obtained under the bare anchor tests (Table 3.4). The 9.5-mm diameter anchors were predicted to fail in pull-out mode, however all three anchors tested failed in steel fracture failure mode (Fig. 4.2). The average failure load was about 41% more than the predicted pull-out load but only about 85% of the ultimate load under the bare anchor tests (34.5 kN).

The 12.7-mm diameter anchors were also predicted to fail in pull-out mode, however, they failed predominantly in concrete breakout mode. Two test samples failed in concrete breakout mode (Fig. 4.3) while one failed in concrete beam splitting (Fig. 4.4). The average breakout capacity of the two anchors (46.5 kN) was about 42% more than the predicted pull-out capacity, and about 31% lower than the predicted concrete breakout capacity of 67.7 kN (Table 4.1). It is however noted that, the breakout capacity of 46.5 kN (excluding the splitting failure capacity) observed matched with the breakout capacity of 46.8 kN calculated using the CCD method and the average measured breakout depth of 66 mm (Table 4.3). The breakout cone properties for the 12.7-mm diameter anchors summarized on Table 4.3 gives and average cone breakout angle of 23.5°, which is less than the 35° proposed by the CCD method.

Table 4.3: Failure Cone Features for 12.7-mm Diameter Strong-Bolt® 2 Anchorage System

Sample	Cone Properties		
	Depth	Diameter (mm)	Angle (Deg)
ST-STB-HL-01	65	315	23
ST-STB-HL-03	67	315	24
Average	66	315	23.5

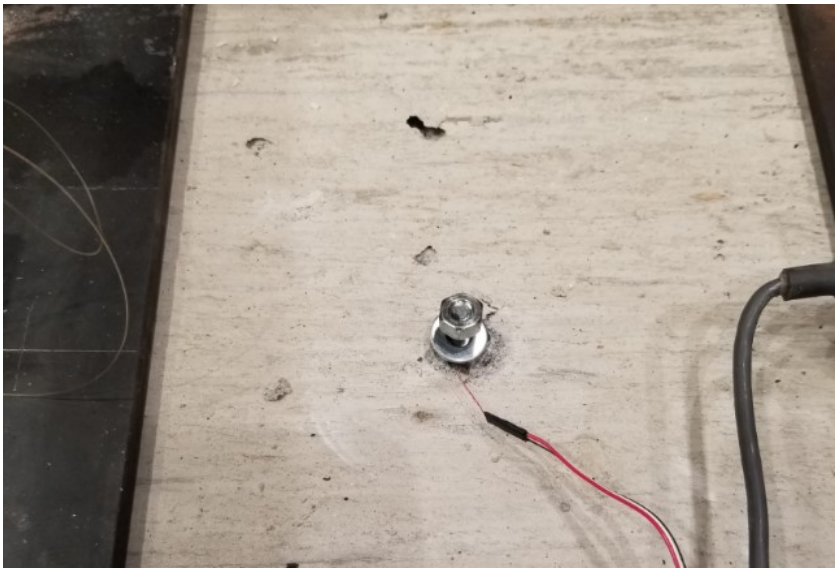

Fig. 4.1: Typical Steel Failure for 6.4-mm Diameter Anchor System in Tension (STB)

Fig. 4.2: Typical Steel Failure for 9.5-mm Diameter Anchor System in Tension (STB)

Fig. 4.3: Typical Concrete Break Failure for 12.7-mm Diameter Anchor System in Tension (STB)

Fig. 4.4: Beam Splitting Failure in 12.7-mm Diameter Anchor System in Tension (STB)

4.2.1.1.1 Load Displacement Behavior

The load-displacement behavior of the anchors is discussed in this section. To estimate the effects of embedment on the anchor behavior, the average bare anchor load-displacement curve is plotted together with the three anchor samples.

The load-displacement behavior for the 6.4-mm diameter anchors is shown in Fig. 4.5. Except for ST-STB-QI-02, all the tested anchor systems exhibited lower initial axial stiffness than the bare anchor test. The bare anchor exhibited an average initial axial stiffness of 15.1 kN/mm while samples ST-STB-QI-01 and ST-STB-QI-03 had initial axial stiffnesses of about 4.8 kN/mm. Sample ST-STB-QI-02 on the other hand had an initial axial stiffness of about 85 kN/mm. Also, except ST-STB-QI-03, the tested anchor systems exhibited displacements corresponding to ultimate load comparable to the bare anchor. The displacements corresponding to the ultimate load at 5 mm, 4 mm and 8 mm for ST-STB-QI-01, ST-STB-QI-02 and ST-STB-QI-03 respectively while the displacement corresponding to ultimate load for the bare anchor was 5 mm.

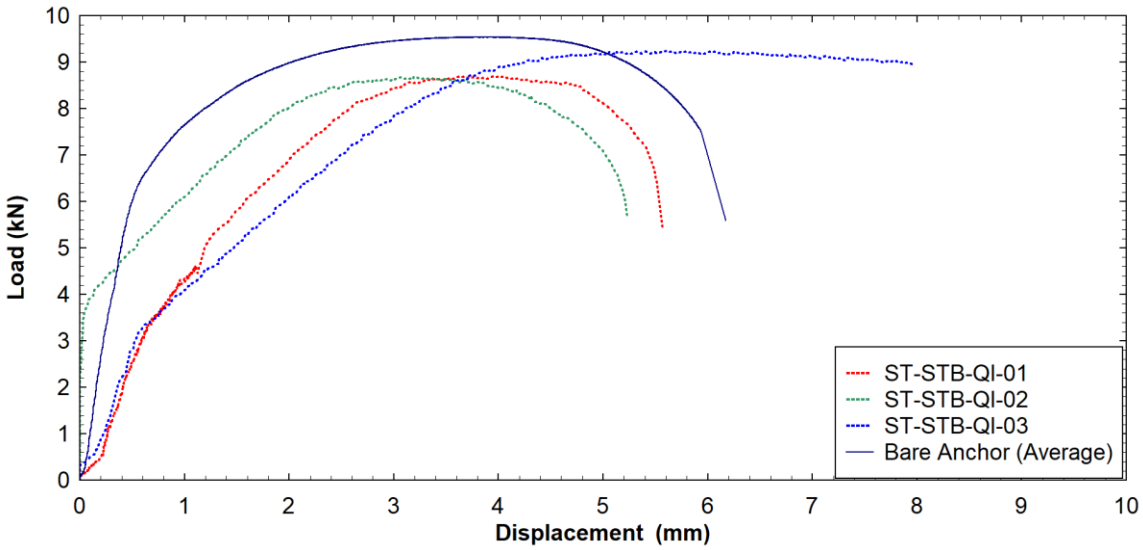

Fig. 4.5: Load-Displacement Curves for 6.4-mm Diameter Anchor System in Tension (STB)

Fig. 4.6 shows the load-displacement behavior of the three tested 9.5-mm diameter anchors together with a typical bare anchor behavior. In contrast to the behavior of the 6.4-mm diameter anchors, all the tested anchors exhibited higher initial axial stiffness than the bare anchor. The average initial axial stiffness of the anchor systems was 43 kN/mm while the bare anchor exhibited an initial axial stiffness of 16 kN/mm. The anchor systems and bare

anchor show a reduction in the stiffness until a zero stiffness at the peak axial load. This is followed by a negative stiffness until failure.

The ultimate loads and corresponding displacements of the anchor systems were consistently lower than the those for the bare anchor. The bare anchor failed within the threaded length because of the location of the grips while failure of the anchor systems failed below the threaded length (in the installed part of the anchor) as can be seen in Fig. 4.2. The anchor systems attained an average ultimate load of 29.3 kN while the bare anchors reached an average ultimate load of 34.5 kN. The bare anchor reached an average displacement of 8 mm at ultimate load while the anchor systems reached an average displacement of 5.7 mm at ultimate loads.

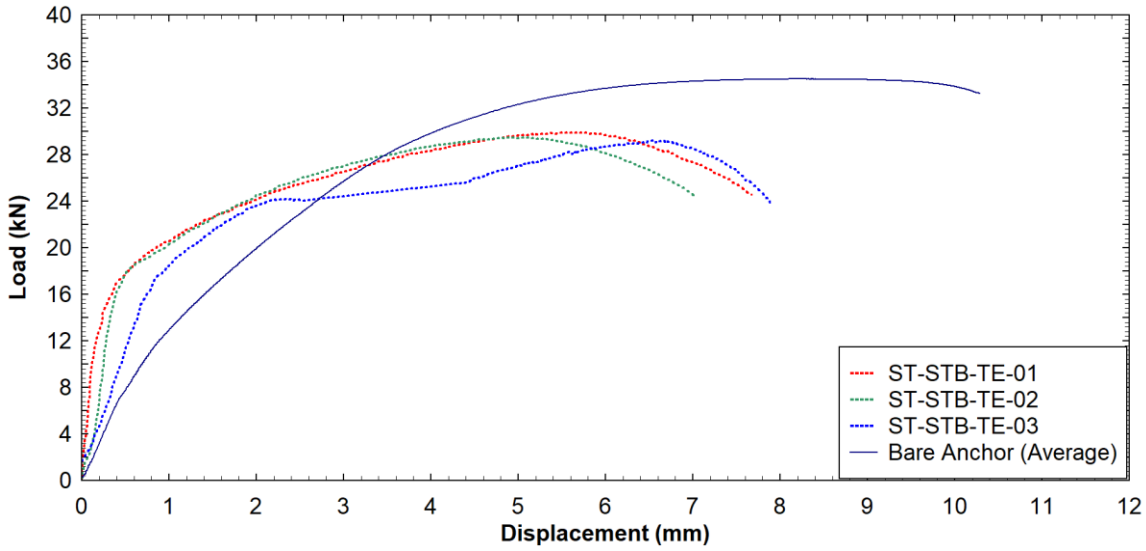

Fig. 4.6: Load-Displacement Curves for 9.5-mm Diameter Anchor System in Tension (STB)

The load-displacement behavior of the 12.7-mm diameter anchors together with a typical bare anchor behavior are shown in Fig. 4.7. ST-STB-HL-01 and ST-STB-HL-02 exhibited initial axial stiffness of 18 kN/mm, similar to the axial stiffness of the bare anchor. ST-STB-HL-03 on the other hand exhibited a lower initial axial stiffness of 4 kN/mm. At about

40 kN and displacement of 8.5 mm, ST-STB-HL-01 slipped before re-establishing contact with the concrete walls at a displacement of about 15 mm.

All three anchor systems failed at higher ultimate displacements then the bare anchor however the ultimate loads were lower. The difference in ultimate load is attributed to the difference in failure mode - steel fracture for the bare anchor and concrete cone breakout failure for the anchor system. Even though ST-STB-HL-02 failed in beam splitting mode, the ultimate load was similar to ST-STB-HL-01 which failed in concrete cone breakout mode. The anchor systems reached ultimate load at an average displacement of 21 mm while the bare anchor reached ultimate load at a displacement of 13.5 mm.

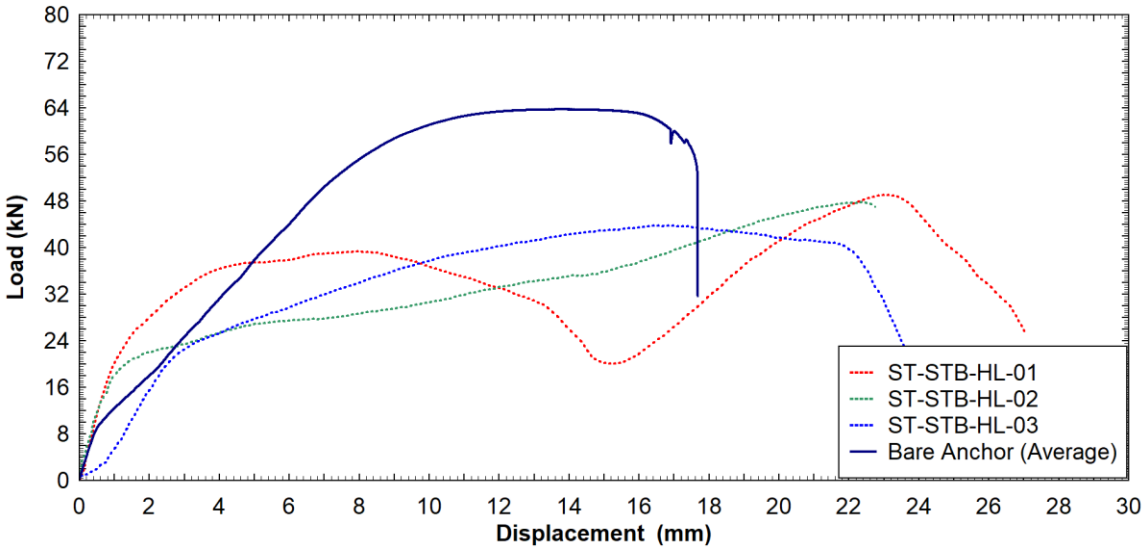

Fig. 4.7: Load-Displacement Curves for 12.7-mm Diameter Anchor System in Tension (STB)

4.2.1.1.2 Stress-Strain Behavior

The stress-strain behavior of the Strong-Bolt 2 anchor systems was compared with typical bare anchor stress-strain behavior. For the 6.4-mm diameter anchors, the stress-strain behavior for the anchor systems (Fig. 4.8) were similar to that of the bare anchor. This is expected as all the anchors failed in steel fracture failure modes. The ultimate strain values were not recorded as the strain gauges failed at various stages during the static testing

before anchor failure was reached. The lower stresses attained at a given strain value, particularly for ST-STB-QI-01 and ST-STB-QI-02, can be attributed to the failure of the anchors at the location of the installed strain gauge where the threads were filed off to yield a smooth surface for strain gauge application. The same reason can account for the lower elastic modulus of all three anchor samples as the same area was used in calculating the stress for bare anchor tests and anchor system tests. ST-STB-QI-01 and ST-STB-QI-02 had elastic modulus of 152 GPa while ST-STB-QI-03 had an elastic modulus of 130 GPa. The elastic modulus of the bare anchor is about 200 GPa.

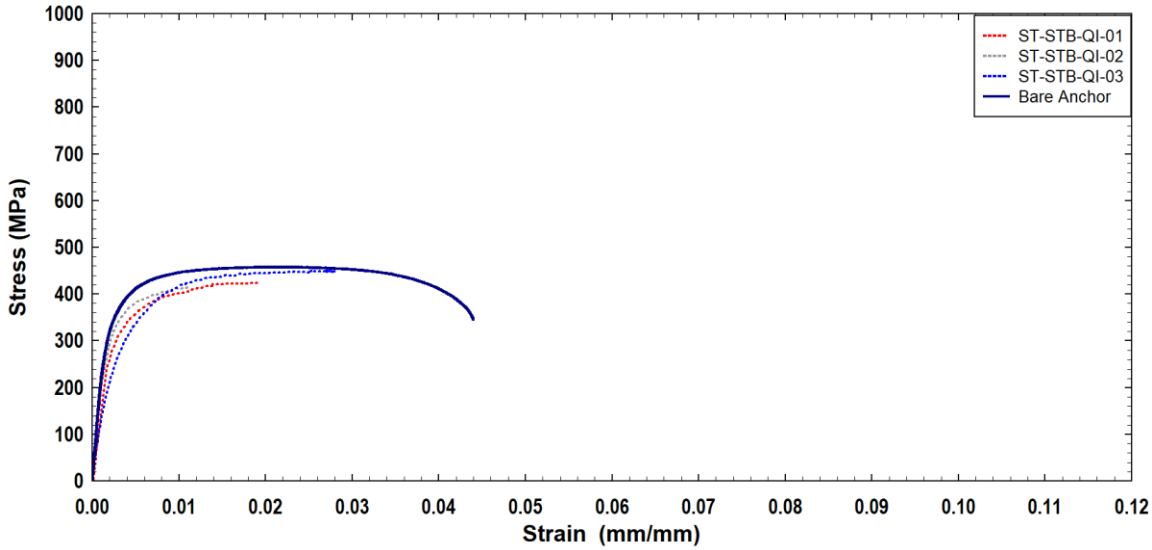

Fig. 4.8: Stress-Strain Curves for 6.4-mm Diameter Anchor System Test in Tension (STB)

For the 9.5-mm diameter anchors, only two samples returned valid strain data (Fig. 4.9). While ST-STB-TE-02 behaved similarly with the bare anchor with an elastic modulus of 197 GPa, ST-STB-TE-01 exhibited a higher elastic modulus of about 250 GPa. Similarly to the 6.4-mm diameter anchors, the strain gauges failed during the loading process and thus the ultimate strains were not recorded.

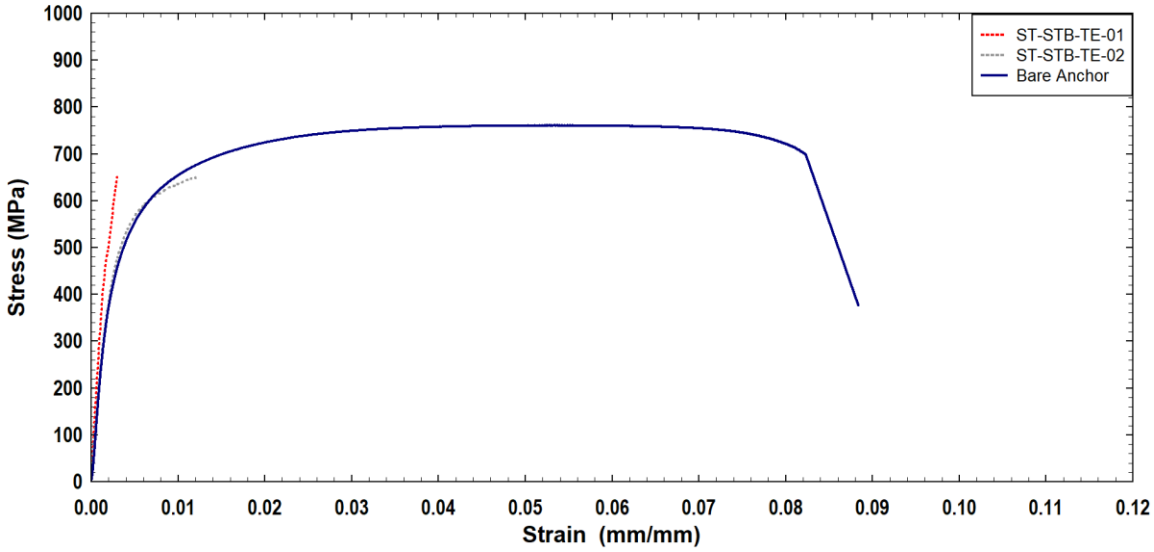

Fig. 4.9: Stress-Strain Curves for 9.5-mm Diameter Anchor System Test in Tension (STB)

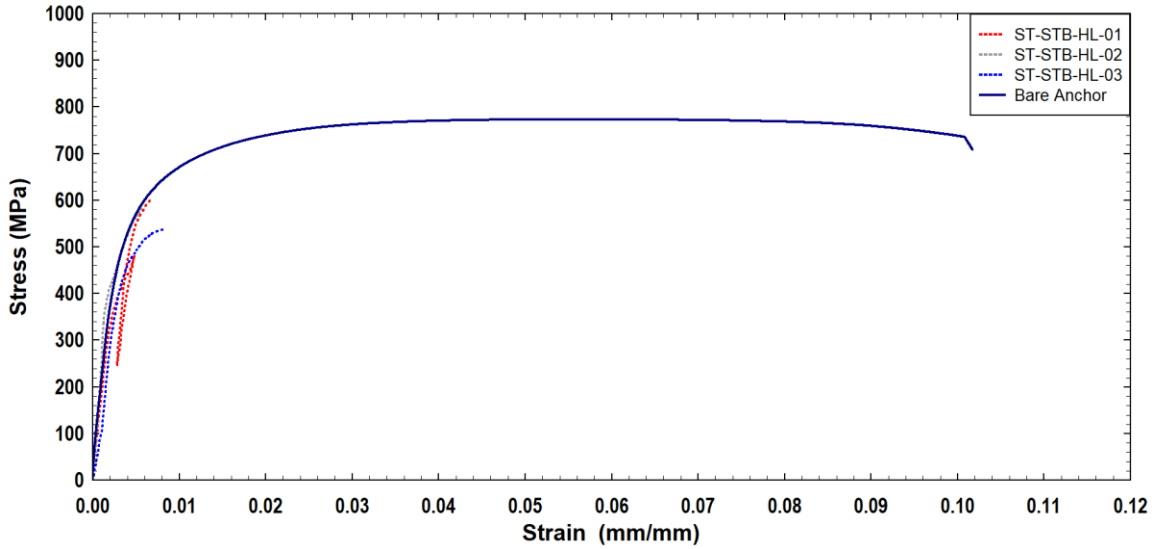

Fig. 4.10: Stress-Strain Curves for 12.7-mm Diameter Anchor System Test in Tension (STB)

The stress-strain behavior of the 12.7-mm diameter anchor systems is shown in Fig. 4.10. The slip and subsequent re-establishment of contact of ST-STB-HL-01 can be seen in the behavior of the stress-strain curve. Similarly the failure of strain gauges before the failure of the anchors made it impossible to record the ultimate strain anchor systems. All anchor systems however exhibited comparable elastic modulus of about 190 GPa to the bare anchor.

4.2.1.1.3 Summary and Discussion of Static Tension Test Results for Strong Bolt® 2

The static tension test results showed that only the 6.4-mm diameter anchors failed in the same failure mode experimentally and as predicted. While the 9.5-mm and 12.7-mm diameter Strong-Bolt 2 anchors were predicted to fail in pull-out mode, the 9.5-mm diameter anchor failed in steel fracture and the 12.7-mm diameter anchor failed in concrete breakout failure mode in the experimental test. Moreover, the 9.5-mm and 12.7-mm diameter anchor systems failed experimentally at higher loads than the predicted failure loads. Due to filing off of threads to install strain gauges, the steel fracture failure loads were affected when the failure occurred in the vicinity of the reduced cross-sectional area. This was particularly evident for the 6.4-mm diameter anchors.

The initial axial stiffness and the load-displacement behavior of the anchors showed some variability, with the initial axial stiffness of the 6.4-mm diameter anchors ranging from 4.8 kN/mm to 85 kN/mm. This difference may be attributed to the quality of installation of these anchors.

Similarly to the initial axial stiffness of the anchors, the elastic modulus of the anchor systems was variable. The strain gauges failed during the loading process, before failure of the anchor and this made it difficult to obtain the stress-strain parameters at fracture of the anchors that failed in steel fracture. This limitation could also be result of variability and quality of the installation.

4.2.1.2 Wedge-All®

Table 4.4 provides a summary of the experimental results compared with predictions for the Wedge-All anchors. Both the failure load and failure mode agreed with predictions for

the 9.5-mm diameter anchors where the failure mode is by steel fracture (Fig. 4.11). The average experimental failure load of the 9.5-mm diameter anchors was 27.1 kN, compared to the predicted value of 27.3 kN.

Table 4.4: Static Tension Test Data for Wedge All Anchors

Sampler	ϕ	Failure Load		Failure Mode		Average Experimental Failure Load	Initial Stiffness
		Predicted	Experimental				
	(mm)	(kN)	(kN)	Predicted	Experimental	(kN)	(kN/mm)
ST-WA-TE-01	9.5	27.3	26.5	SF	SF	27.1	32
ST-WA-TE-02	9.5	27.3	27.9	SF	SF		24
ST-WA-TE-03	9.5	27.3	27.0	SF	SF		31
ST-WA-HL-01	12.7	68.1	47.0	CC	PT	48.7	42
ST-WA-HL-02	12.7	68.1	50.3	CC	PT		35
ST-WA-HL-03	12.7	68.1	48.4	CC	PT		26

Fig. 4.11: Steel Fracture Failure for ST-WA-TE-01

Fig. 4.12: Pull-through Failure for ST-WA-HL-01

For the 12.7-mm diameter anchors, the failure mode observed was pull-through (Fig. 4.12) as opposed to the predicted concrete breakout failure mode. The average experimental failure load was 48.7 kN, about 71.5% of the predicted concrete breakout capacity of 68. kN. The anchors were tested in displacement control mode at 0.05 mm/s and 0.08 mm/s for the 9.5-mm and 12.7-mm diameter anchors respectively to ensure failure occurred between one (1) and three (3) minutes as per ASTM E488/E488M-15 [35].

4.2.1.2.1 Load-Displacement Behavior

The load-displacement curves for the 9.5-mm diameter anchors, including the average response of the bare anchor is given in Fig. 4.13. The tests show stiffer anchor systems than the bare anchor. The bare anchor exhibited initial axial stiffness of 16 kN/mm followed by reducing stiffness until zero stiffness at the peak axial load. The initial stiffness of ST-WA-TE-01, ST-WA-TE-02 and ST-WA-TE-03 were about 32 kN/mm, 24 kN/mm

and 31 kN/mm respectively. Except for the values of the ultimate loads, both the bare anchor and anchorage system exhibited similar post yield behavior. This behavior was expected since their failure modes were the same; steel fracture failure.

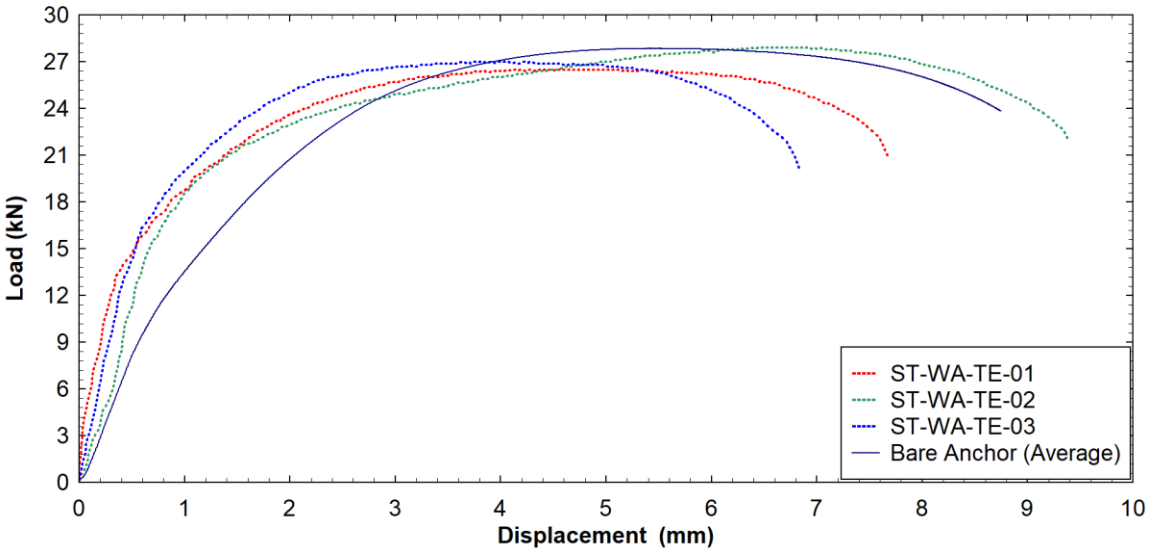

Fig. 4.13: Load-Displacement Curves for 9.5-mm Diameter Anchor System in Tension (WA)

For the 12.7-mm diameter anchors, the difference in the failure modes was shown in the load-displacement relationships of the anchor systems and the bare anchors (Fig. 4.14). The anchorage systems exhibited different initial axial stiffness at the onset of loading. The response was however same after a load of 20 kN. The difference in the initial behavior may be due to variations in the installation process (quality of installation).

While ST-WA-HL-01 and ST-WA-HL-03 exhibited almost no displacement until axial loads of 8 and 12.6 kN respectively, resulting in initial axial stiffness of 42 kN/mm and 26 kN/mm respectively, ST-WA-HL-02 experienced displacement at the onset of loading with a stiffness of 40 kN/mm. The bare anchor on the other hand displayed an initial axial stiffness of 17.5 kN/mm up to 7 kN and then reduced to 6 kN/mm. The change in stiffness observed in the bare anchors tested could be due to slip of the cross-heads during the testing as it was not evident in the stress-strain curve (Fig. 4.16).

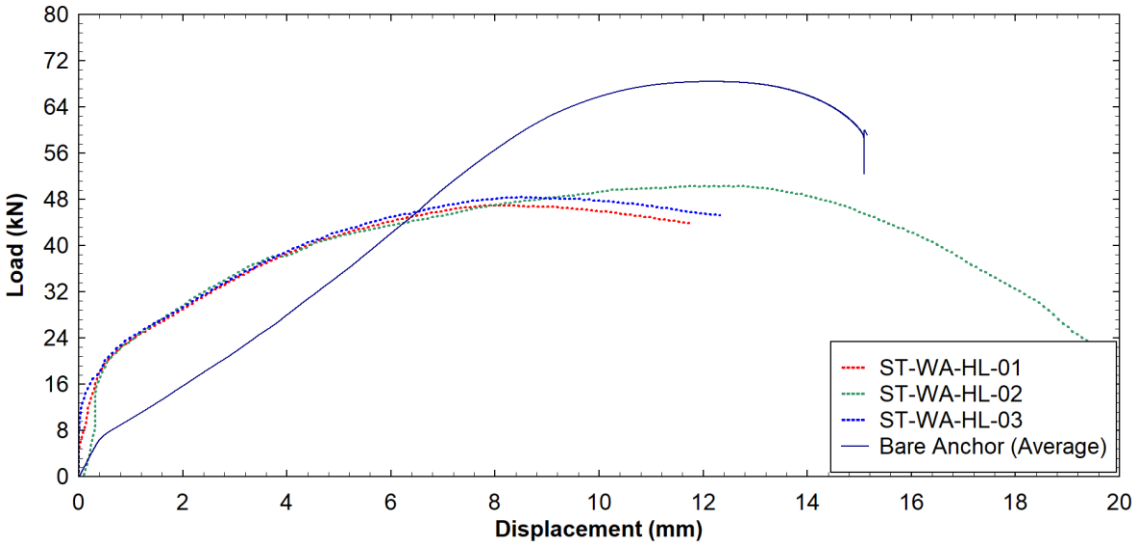

Fig. 4.14: Load-Displacement Curves for 12.7-mm Diameter Anchor System in Tension (WA)

4.2.1.2.2 Stress-Strain Behavior

Only one sample each of the 9.5-mm and 12.7-mm diameter anchor systems had the strain gauge survive the testing. Thus, only the stress-strain behavior of these anchor is presented and discussed. For the 9.5-mm diameter anchors, ST-WA-TE-02 had a stress-strain curve matching the relationship for the bare anchor (Fig. 4.15) even though the strain gauge did not survive until to the ultimate load.

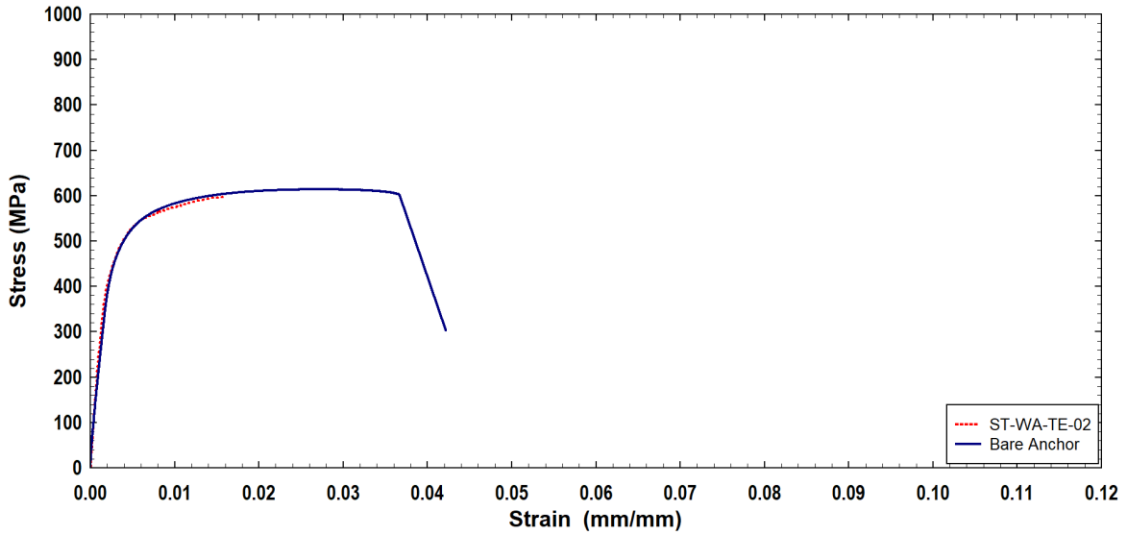

Fig. 4.15: Stress-Strain Curves for 9.5-mm Diameter Anchor System Test in Tension (WA)

The 12.7-mm diameter anchor systems exhibited a higher elastic modulus of the anchor system of 220 GPa compared to 190 GPa for the bare anchor (Fig. 4.16).

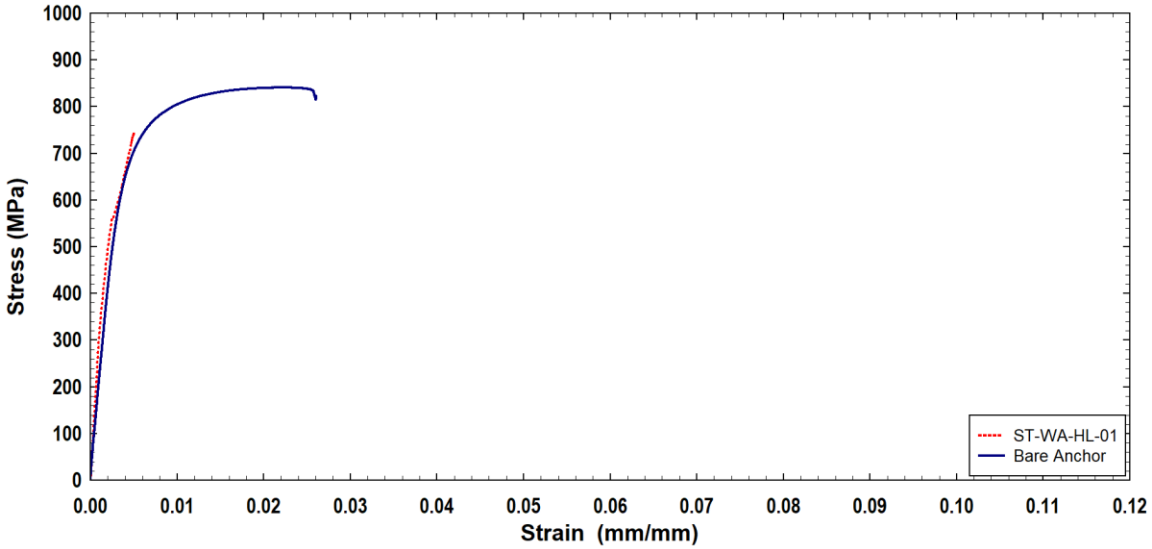

Fig. 4.16: Stress-Strain Curves for 12.7-mm Diameter Anchor System Test in Tension (WA)

4.2.1.2.3 Summary and Discussion of Tension Test Results for Wedge-All® Anchors

For the Wedge-All anchors, only the 12.7-mm diameter anchors had a different failure mode than the predicted. The predicted failure mode of concrete breakout and pull-through for the experimental resulted in decreased anchor capacity of about 28%. For the 9.5-mm diameter anchors, the experimental and predicted failure modes were steel fracture and thus the failure load was the similar. The prediction failure load was 27.3 kN, while the average experimental failure load was 27.1 kN.

For of the Wedge-All anchor, the load-displacement behavior was quite consistent with each other. The anchors exhibited similar initial stiffness as well as general behavior during loading. The load displacement behavior for the 12.7-mm bare anchor however showed a region of reduced stiffness that could be attributed to slippage in the grips.

Similarly to the Strong Bolt 2, not all the strain gauges survived the static testing up to anchor failure. Thus, the ultimate strain of the anchors was not recorded. For that matter, the post-yield behavior for the anchor systems were not assessed.

4.2.1.3 Titen HD®

Table 4.5 provides the summary of the Titen HD anchors tested under static tension conditions. The table shows that all of the anchors failed in a mixed mode of anchor pull-out and concrete breakout as shown in Fig. 4.17. The predicted failure mode for the 6.4-mm diameter anchor was steel fracture mode while that for the 9.5-mm and 12.7-mm diameter anchors was concrete breakout mode.

The table shows that the predicted failure load was unconservative for the 6.4-mm diameter anchor as they failed at loads much less than predicted. The corresponding concrete breakout capacity presented on Table 4.1 of 29.5 kN is about 38% higher than the average experimental failure load.

Table 4.5: Static Tension Test Data for Titen HD® Anchors

Sample Number	ϕ	h_{ef}	Failure Load		Failure Mode		Average Experimental Failure Load	Initial Stiffness
			Predicted	Experimental				
	(mm)	(mm)	(kN)	(kN)	Predicted	Experimental	(kN)	(kN/mm)
ST-TTH-QI-01	6.4	49.3	28.3	20.4	SF	PO-CC	21.4	1.0
ST-TTH-QI-02	6.4	49.3	28.3	21.6	SF	PO-CC		2.5
ST-TTH-QI-03	6.4	49.3	28.3	22.2	SF	PO-CC		2.5
ST-TTH-TE-01	9.5	61.0	40.6	42.9	CC	PO-CC	42.4	3.0
ST-TTH-TE-02	9.5	61.0	40.6	42.3	CC	PO-CC		3.0
ST-TTH-TE-03	9.5	61.0	40.6	42.1	CC	PO-CC		3.0
ST-TTH-HL-01	12.7	75.9	56.5	58.6	CC	PO-CC	62.4	9.0
ST-TTH-HL-02	12.7	75.9	56.5	64.0	CC	PO-CC		9.0
ST-TTH-HL-03	12.7	75.9	56.5	64.6	CC	PO-CC		11.0

For the 9.5-mm and 12.7-mm diameter anchors, the experimental failure loads were, 42.4 kN and 62.4 kN, 4.4% and 10.4% higher than the predicted failure loads, respectively. The

properties of the concrete breakout plugs (cones) for each anchor diameter (Table 4.6, Table 4.7 and Table 4.8) obtained from measured average breakout diameter and concrete breakout depths show an average concrete cone failure angle of 33°, 25°, and 18° for the 6.4-mm, 9.5-mm, and 12.7-mm diameter anchors respectively. All these angles are less than the proposed 35° in the CCD method.

Fig. 4.17: Typical Mixed Pull-out and Concrete Breakout Failure for Anchor System in Tension (TTH)

The anchors were tested at 0.04 mm/s, 0.05 mm/s and 0.07 mm/s in a displacement control mode. The pull-out depth and concrete breakout cone depth varied with the anchor diameter. For the 6.4-mm and 9.5-mm diameter anchors, the average pull-out depths were about 79% and 69% of the average concrete breakout depths, and about 220% for the 12.7-mm diameter anchors (Table 4.6, Table 4.7, and Table 4.8). Though the failure modes of all three diameter groups were mixed pullout and concrete breakout, the concrete breakout was dominant in the 6.4-mm and 9.5-mm diameter anchors as the breakout depth was more

than the pullout depth in contrast to the 12.7-mm diameter anchors where the pullout failure dominated with a larger depth than the concrete breakout depth.

Table 4.6: Mixed Failure Properties of 6.4-mm Diameter Anchors System (TTH)

Sample	Depth (mm)		Cone Properties	
	Pull-out	Concrete	Diameter (mm)	Av. Angle (Deg)
ST-TTH-QI-01	20	30	119	28
ST-TTH-QI-02	20	30	71	43
ST-TTH-QI-03	27	23	98	27
Average	**22**	**28**	**96**	**33**

Table 4.7: Mixed Failure Properties of 9.5-mm Diameter Anchors System (TTH)

Sample	Depth (mm)		Cone Properties	
	Pull-out	Concrete	Diameter (mm)	Av. Angle (Deg)
ST-TTH-TE-01	32	29	147	23
ST-TTH-TE-02	10	51	205	28
ST-TTH-TE-03	33	28	133	24
Average	**25**	**36**	**162**	**25**

Table 4.8: Failure Propertied of 12.7-mm Diameter Anchor System (Titen HD®)

Sample	Depth (mm)		Cone Properties	
	Pull-out	Concrete	Diameter (mm)	Av. Angle (Deg)
ST-TTH-HL-01	42	35	161	25
ST-TTH-HL-02	56	21	155	16
ST-TTH-HL-03	61	16	140	14
Average	**53**	**24**	**152**	**18**

4.2.1.3.1 Load-Displacement Behavior

The load-displacement behavior of the Titen HD anchors are presented in Fig. 4.18, Fig. 4.19, and Fig. 4.20 for the 6.4-mm, 9.5-mm and 12.7-mm diameter anchors respectively. The average load-displacement behavior of the bare anchor is also plotted for comparison.

For the 6.4-mm and 9.5-mm diameter anchor systems, there are two distinct response (behavior).

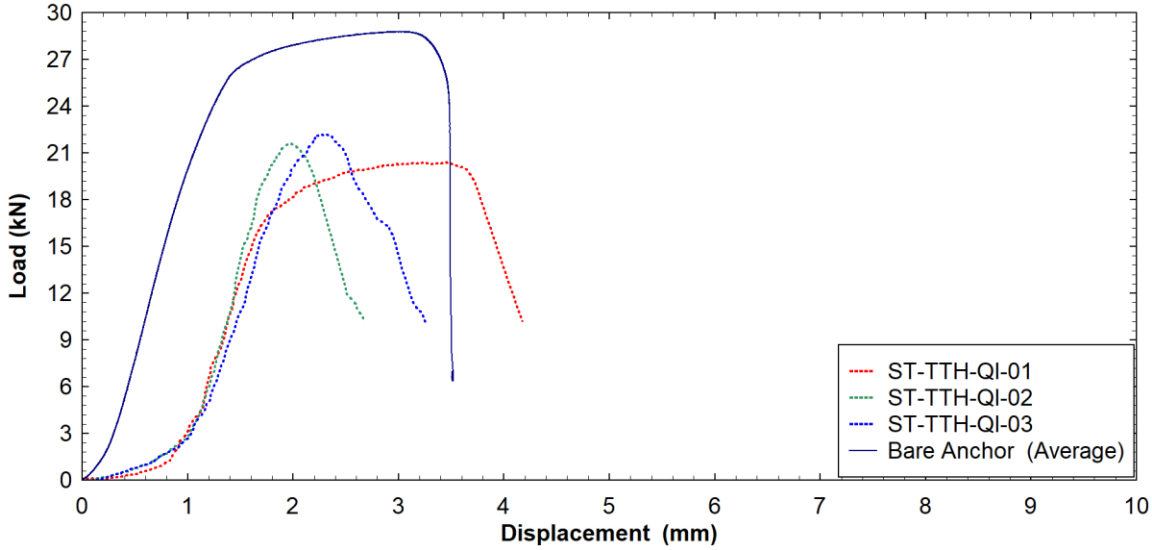

Fig. 4.18: Load-Displacement behavior of 6.4-mm Diameter Anchor System in Tension (TTH)

The first region was characterized by low resistance to displacement (low stiffness) while the second region was characterized by an increased resistance to displacement (stiffness) similar to that of the bare anchor. The average stiffness for the low resistance region for the 6.4-mm diameter anchor system was about 2 kN/mm while the average stiffness for the high stiffness region was about 22 kN/mm. For the 9.5-mm diameter anchor system, the average stiffness of the low resistance region was about 3 kN/mm while that for the high resistance region was about 28 kN/mm.

The low resistance region is characterized by seating of the anchor threads into the groves cut into concrete during installation. Once the seating is complete, the anchor resistance to pull-out increases.

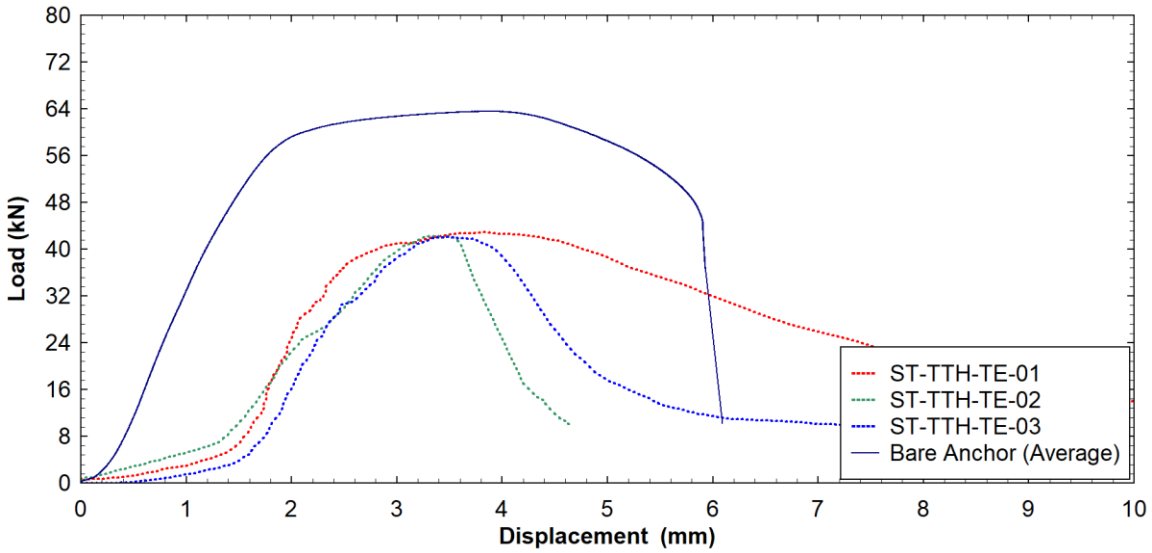

Fig. 4.19: Load-Displacement behavior of 9.5-mm Diameter Anchor System in Tension (TTH)

The axial stiffness of the bare anchors was similar to the stiffness in the high resistance region for both the 6.4-mm and 9.5-mm diameter anchors. For the 6.4-mm diameter anchors, ST-TTH-QI-02 and ST-TTH-QI-03 failed suddenly after reaching the peak load (consistent with concrete breakout failure) while ST-TTH-QI-01 displayed a reduced stiffness, post peak up to failure. Similarly for the 9.5-mm diameter anchors, while ST-TTH-TE-02 and ST-TTH-TE-03 failed immediately after reaching peak load, ST-TTH-TE-01 had an extended displacement of about 1 mm at a reduced stiffness of -3 kN/mm prior to failure.

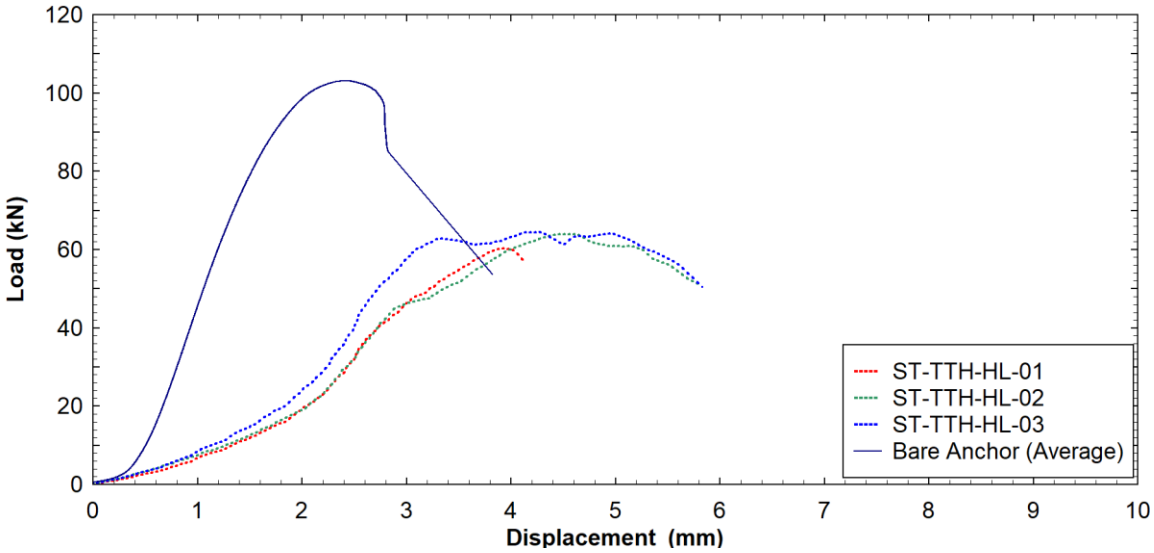

Fig. 4.20: Load-Displacement behavior of 12.7-mm Diameter Anchor System in Tension (TTH)

The 12.7-mm diameter anchor systems behaved quite differently from the bare anchor test and the 6.4-mm and 9.5-mm diameter anchor systems tests. While the bare anchor reached an ultimate load at a total displacement of 2.5 mm, the average displacement corresponding to the ultimate loads of the 12.7-mm diameter anchor systems was 4 mm. ST-TTH-HL-01 and ST-TTH-HL-02 had an initial axial stiffness of 9 kN/mm and increasing to about 33 kN/mm before failure, while the initial stiffness of ST-TTH-HL-03 was about 11 kN/mm before increasing to 40 kN/mm. The average bare anchor stiffness was 67 kN/mm.

4.2.1.3.2 Stress-Strain Behavior

The stress-strain relationship for anchor systems in comparison with the associated bare anchors are shown in Fig. 4.21, Fig. 4.22, and Fig. 4.23 respectively for the 6.4-mm, 9.5-mm, and 12.7-mm diameter anchors. The strain gauges on only ST-TTH-QI-02 and ST-TTH-QI-03 were functional for the 6.4-mm diameter anchor while strain gauges on all the 9.5-mm diameter anchors were functional for the duration of the static tension testing.

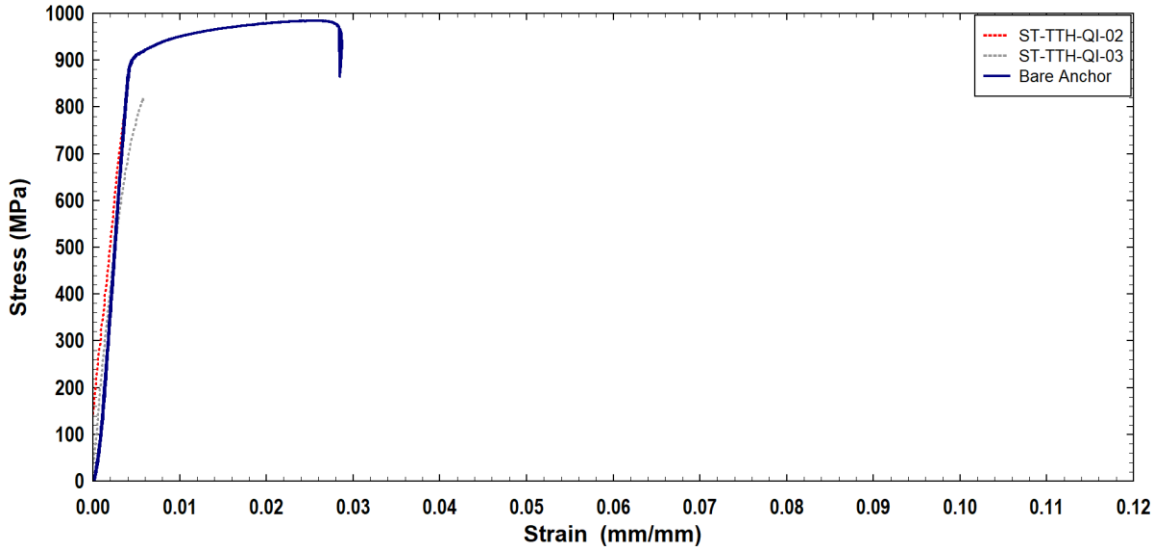

Fig. 4.21: Stress-Strain Curves for 6.4-mm Diameter Anchor System (TTH)

The elastic modulus for the anchor systems were 180 GPa and 160 GPa for ST-TTH-QI-02 and ST-TTH-QI respectively, compared to the 209 GPa obtained for the bare anchor for the 6.4-mm diameter anchors. The strain rate of the 6.4-mm diameter anchor is in the order of 10^{-5} /s.

For the 9.5-mm diameter anchors, the elastic moduli for the anchor systems were 160 GPa, 100 GPa and 120 GPa for ST-TTH-TE-01, ST-TTH-TE-02, and ST-TTH-TE-03 respectively while the that for the bare anchor was 220 GPa. The average strain rate obtained for the 9.5-mm diameter anchors was also in the order of 10^{-5} /s. For the 12.7-mm diameter anchors, the anchor systems displayed varied stress-strain behavior. ST-TTH-HL-02 and ST-TTH-HL-03 exhibited elastic modulus of 33 GPa and 60 GPa respectively. The elastic modulus for the bare anchor test was 216 GPa (Fig. 4.23). Also, strain rate in the order of 10^{-5} /s was obtained for the 12.7-mm diameter anchors.

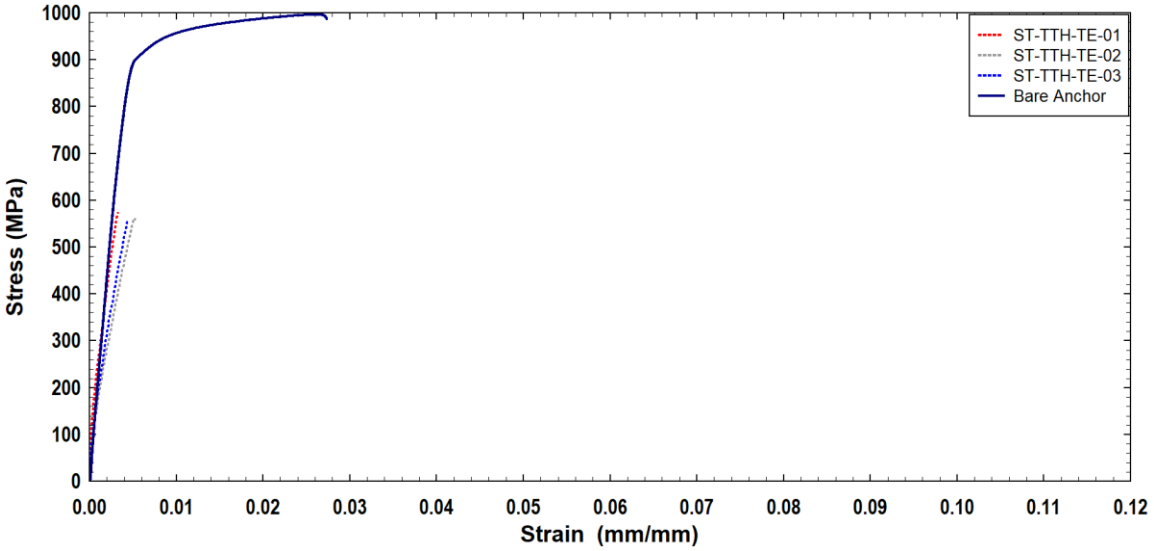

Fig. 4.22: Stress-Strain Curves for 9.5-mm Diameter Anchor System (TTH)

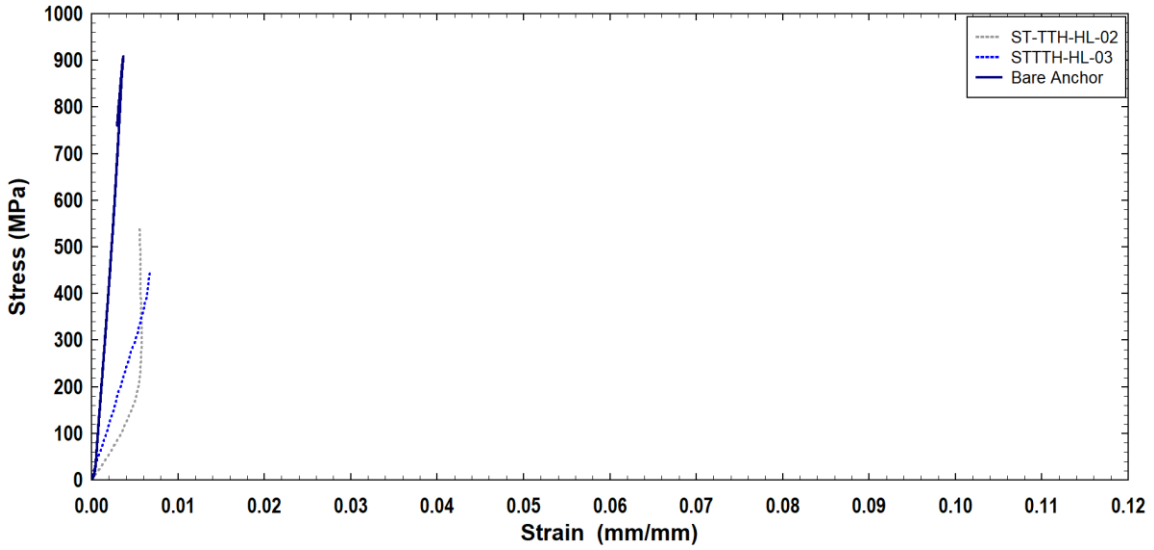

Fig. 4.23: Stress-Strain Curves for 12.7-mm Diameter Anchor System (TTH)

4.2.1.3.3 Summary and Discussion of Tension Test Result for Titen HD®

The Titen HD anchor systems failed in a similar mode for all three anchor diameters. However, while the 6.4-mm diameter anchors were predicted to fail in steel fracture mode at 28.3 kN, the average experimental failure load was 21.4 kN (76% of the predicted). The 9.5-mm diameter anchors failed at a slightly higher load than predicted (4% higher than

predicted) while the 12.7-mm diameter anchors failed at 62.4 kN, 10% higher than the predicted failure load.

The load-displacement behavior for the anchor systems generally showed two regions of behavior for the 6.4-mm and 9.5-mm diameter anchors. The low resistance (stiffness) region occurs at a displacement of about 1 mm and 1.5 mm. The high resistance regions exhibited stiffness similar to the bare anchors. The 12.7-mm diameters however showed lower stiffness compared to the bare anchor stiffness.

The concrete breakout angles reported in Table 4.6 to Table 4.8 were based on the breakout concrete depth and the diameter measured on the surface of the test beams. However, it can be seen in Fig. 4.17 that the breakout cone did not follow one angle, a steeper angle can be seen from the anchor tip until close to the surface where the slope changed. This could account for the average shallow angles obtained.

Table 4.9: Recalculated Failure Parameters for Titen HD Anchors in Tension

Anchor	Measured			Cone Properties			Calculated Capacity (kN)		Exp. Capacity (kN)	Recalculated	
	Depth (mm)	Dia. (mm)	Angle (Deg.)	Slant length (mm)	Surface Area (mm^2)	Projected Area (mm^2)	Based on Surface Area	Based on Proj. Area		Dia. (mm)	Angle (Deg.)
TTH-QI-01	30.0	119	28	66.6	12456	11122	72.3	64.6	20.4	54.8	51
TTH-QI-02	30.0	71	43	46.5	5184	3959	30.1	23.0	21.6	57.1	50
TTH-QI-03	23.0	98	27	54.1	8333	7543	48.4	43.8	22.2	63.3	39
TTH-TE-01	29.0	147	23	79.0	18245	16972	105.9	98.5	42.9	90.1	36
TTH-TE-02	51.0	205	28	114.5	36866	33006	214.0	191.6	42.3	72.6	58
TTH-TE-03	28.0	133	24	72.2	15074	13893	87.5	80.7	42.1	89.7	35
TTH-HL-01	35.0	161	25	87.8	22199	20358	128.9	118.2	58.6	104.8	37
TTH-HL-02	21.0	155	16	80.3	19550	18869	113.5	109.5	64.0	117.7	22
TTH-HL-03	16.0	140	14	71.8	15791	15394	91.7	89.4	64.6	120.1	17

From Table 4.9, it can be seen that except for TTH-QI-02, anchor capacity based on the CCD method and concrete breakout failure mode is significantly higher than the experimental. The observed failure mode for the Titen HD anchors was mixed anchor

pullout and concrete breakout mode with the anchor breakout depth significantly less than the modified effective embedment length. The anchor capacities were recalculated based on both the surface area of the breakout cone and projected area calculated with the measured concrete breakout depth and diameter and the capacities far in excess of the experimental capacities. It is therefore concluded that as observed from Fig. 4.17, both the actual cone surface and projected areas would be much smaller than the values obtained from the experimentally measured diameter. Recalculated diameters based on the experimental anchor capacities resulted in much steeper breakout angles, with average of 47°, 43° and 25° for the 6.4-, 9.5 and 12.7-mm diameter anchors respectively. These angles must be confirmed with further testing of the Titen HD anchors.

4.2.2 Shear Test

The static shear test of the anchors was conducted as described in Section 3.5.2. Three anchors from each group of anchor type and anchor diameter was tested in displacement-control mode at rates between 0.05 mm/s to 0.2 mm/s to achieve failure within 1 to 3 minutes as per ASTM E488/E488M–15 [35]. All the anchor systems tested failed by the steel fracture mode as the edge distances were greater than the minimum required by manufacturer to preclude concrete breakout [81]. The load-displacement behavior for each anchor type are discussed separately, however, Table 4.10 summarizes the data from the experimental tests and compared with the predictions from the code design equations. The experimental failure loads in all cases except for the 9.5-mm diameter Titen HD® anchor system was higher than the predicted failure loads in shear.

Table 4.10: Predicted and Experimental Capacity of Anchors in Shear

Anchor Data				k_{np}	Anchor Capacity						
					Pryout (kN)	Steel (kN)	Conc. Breakout (kN)	Predicted Failure		Experimental Failure	
Anchor Type	ϕ (mm)	l_e (mm)	f_{ut} (MPa)					Load (kN)	Mode	Load (kN)	Mode
Strong Bolt 2	6.4	38.1	487.0	1	22.9	5.9	47.6	5.9	SF	7.4	SF
	9.5	63.5	761.0	1	49.3	20.7	59.3	20.7	SF	24.8	SF
	12.7	85.7	776.0	2	154.7	38.0	68.7	38.0	SF	42.5	SF
Wedge All	9.5	67.0	613.0	2	107.0	16.7	60.0	16.7	SF	20.8	SF
	12.7	86.0	838.0	2	155.5	41.1	68.8	41.1	SF	51.5	SF
Titen HD	6.4	49.3	977.0	1	33.7	17.1	50.1	17.1	SF	18.1	SF
	9.5	61.0	985.0	1	46.4	38.0	58.8	38.0	SF	37.4	SF
	12.7	75.9	894.0	2	129.1	65.8	62.1	62.1	SF	73.4	SF

The pryout capacity and corresponding modification factors were calculated based on Equation 18. The shear resistance based on this equation is the tension capacity of an equivalent anchor whose effective embedment length is equal to the load-bearing length of the anchor in shear. The tension capacity of the anchor in tension is thus multiplied by a

pryout modification factor depending on the load bearing length to obtain the pryout resistance of the anchor in shear. The concrete strength used was 44 MPa.

The steel breakout capacity is based on Appendix D of CSA A23.3-14 [2] using ultimate capacity of steel obtained from tensile test of bare steel anchors. The concrete breakout capacities were calculated using Equation 12. A typical shear failure of the anchors is shown on Fig. 4.24. The failure is characterized by crushed concrete in the direction of the applied shear load indicated in the figure.

Fig. 4.24: Typical Shear failure in Anchor System

4.2.2.1 Strong-Bolt® 2

Data for the Strong-Bolt 2 anchors tested under static shear loading conditions are presented on Table 4.11. As discussed, previously, all the anchors failed in steel fracture mode, with experimental failure loads consistently higher than the predicted failure loads. The experimental failure loads for the 6.4-mm diameter anchor was about 25% more than the predicted failure load while those for the 9.5-mm and 12.7-mm diameter anchors were 20% and 12% more than the predicted failure loads.

Table 4.11: Static Shear Test Data for Strong Bolt® Anchors

Sample	ϕ	Failure Load		Failure Mode		Average Experimental Load
		Predicted	Experimental			
	(mm)	(kN)	(kN)	Predicted	Actual	(kN)
SS-STB-QI-01	6.4	5.9	7.4	SF	SF	7.4
SS-STB-QI-02	6.4	5.9	7.4	SF	SF	
SS-STB-QI-03	6.4	5.9	7.3	SF	SF	
SS-STB-TE-01	9.5	20.7	25.6	SF	SF	24.8
SS-STB-TE-02	9.5	20.7	24.5	SF	SF	
SS-STB-TE-03	9.5	20.7	24.2	SF	SF	
SS-STB-HL-01	12.7	38.0	40.4	SF	SF	42.5
SS-STB-HL-02	12.7	38.0	44.0	SF	SF	
SS-STB-HL-03	12.7	38.0	43.1	SF	SF	

4.2.2.1.1 Load Displacement Behavior

The load-displacement behavior for the 6.4-mm (Fig. 4.25), 9.5-mm (Fig. 4.26) and 12.7-mm (Fig. 4.27) diameter anchors are characterized by a distinct initial behavior of no displacement as applied loading increased. This behavior is an indication of the load transfer through friction due to the contact established by the initial torqueing of the anchors. In this range, the 6.4-mm diameter anchors resisted up to 2.5 kN of load before the start of displacement while the 9.5-mm and 12.7-mm diameter anchors resisted up to 8 kN of load before the start of displacement. SS-STB-TE-03 however behaved contrary to this general trend. SS-STB-TE-03 is characterized by immediate displacement on the onset of loading. This can be attributed to inadequate contact of the loading plate to the side of the concrete beam which resulted in transfer of load to the anchor without the resistance to contact friction.

The 6.4-mm diameter anchors behaved similarly in the post-friction transfer range, deforming with average stiffness of 13 kN/mm in the loading direction until ultimate load. The anchors reached an average ultimate load of 7.4 kN at an average displacement of 4.5

mm with individual displacements of 5.0 mm, 4.7 mm and 3.8 mm for SS-STB-QI-01, SS-STB-QI-02 and SS-STB-QI-03 respectively.

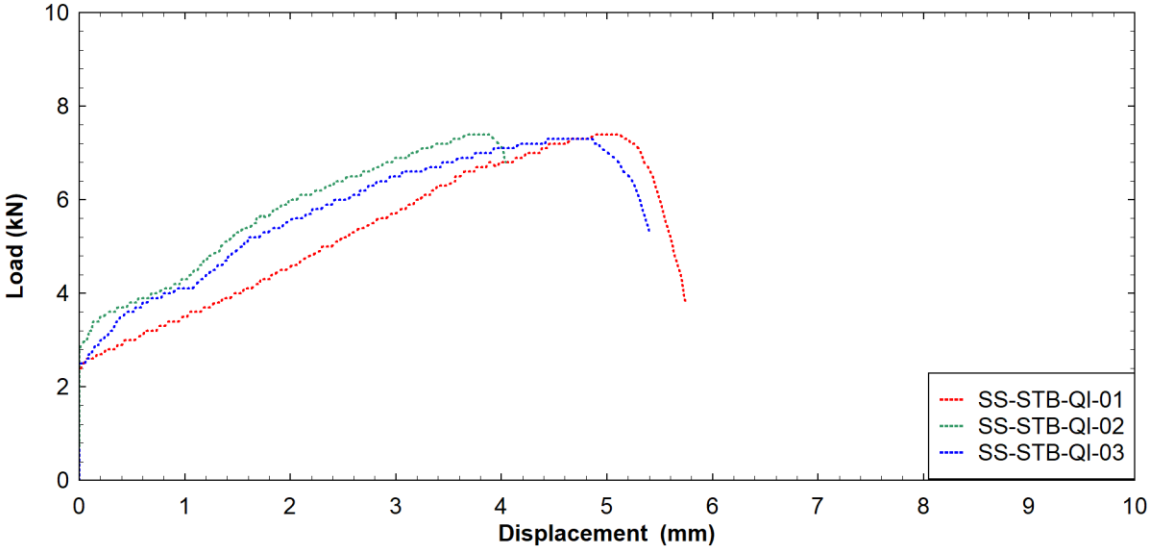

Fig. 4.25: Load-Displacement Curves for 6.4-mm Diameter Anchor System in Shear (STB)

The post contact friction behavior of the 9.5-mm diameter anchors (Fig. 4.26) was different from that of the 6.4-mm diameter anchors. All three 9.5-mm diameter anchors showed slip (displacement) of about 1 mm after the contact friction was overcome. SS-STB-TE-01 slipped with zero stiffness after the contact friction was overcome while for SS-STB-TE-02 and SS-STB-TE-03 the slip was gradual. Once the shear bearing plate made contact with the anchor the resistance increased with a stiffness of 2.4 kN/mm for SS-STB-TE-02 and SS-STB-TE-03 and 3 kN/mm for SS-STB-TE-01. Again, while SS-STB-TE-02 and SS-STB-TE-03 reached ultimate loads of 24.5 and 24.2 kN at 5.8 mm, SS-STB-TE-01 attained ultimate load of 25.6 kN at 6.6 mm of displacement.

For the 12.7-mm diameter anchors, the post contact friction behavior was similar for all anchors. SS-STB-HL-03 exhibited a stiffness of 6 kN/mm, similarly to the 6.4-mm diameter anchors, while SS-STB-HL-01 and SS-STB-HL-02 exhibited a stiffness to 3.2 kN/mm. The ultimate loads of SS-STB-HL-01, SS-STB-HL-02 and SS-STB-HL-03 were

40.4 kN, 44 kN and 43.1 kN respectively with corresponding displacements of 7.3, 8.4 and 7.6 mm respectively.

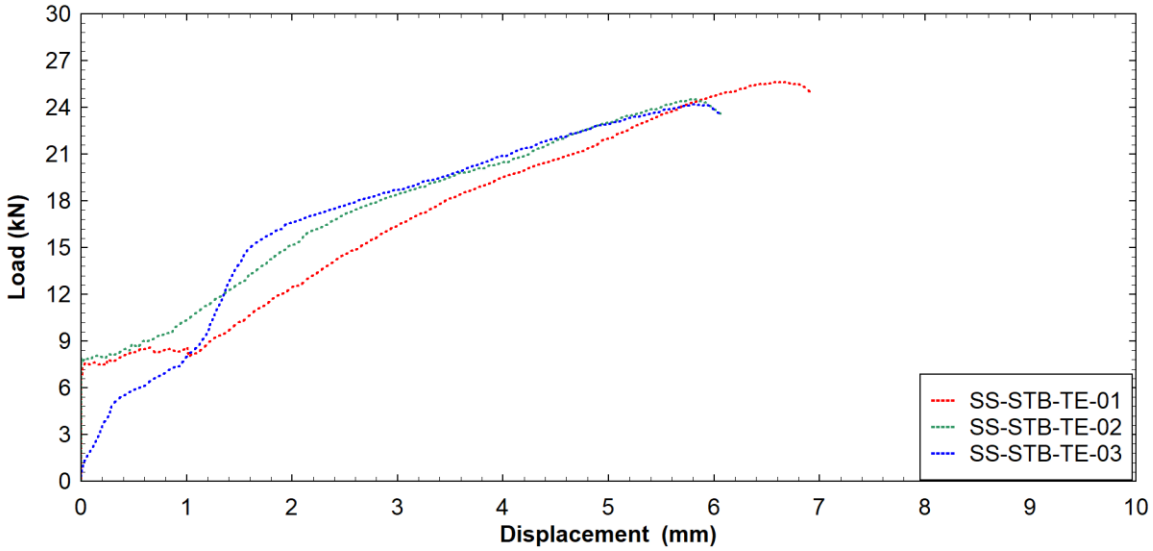

Fig. 4.26: Load-Displacement Curves for 9.5-mm Diameter Anchor System in Shear (STB)

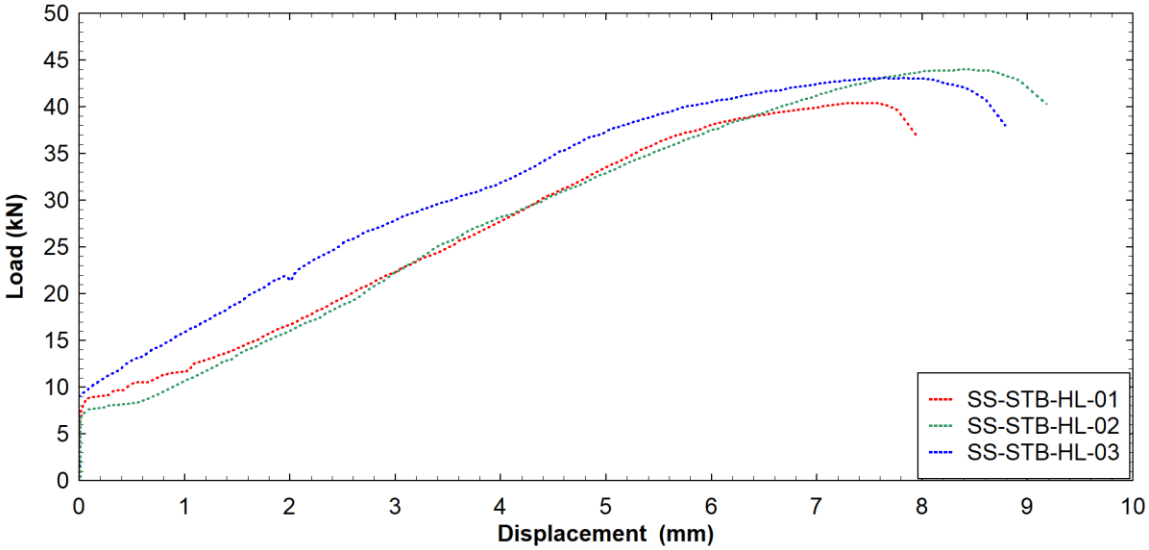

Fig. 4.27: Load-Displacement Curves for 12.7-mm Diameter Anchor System in Shear (STB)

4.2.2.2 Wedge-All®

Table 4.12 presents the experimental test results of the Wedge-All anchor systems in shear and its comparison with the predicted failure loads and failure modes. All the Wedge-All anchors failed in steel fracture failure mode at ultimate loads greater than the predicted

failure loads. For the two anchor diameters investigated (9.5 mm and 12.7 mm), the experimental failure loads were 25% higher than the static failure loads, even though the failure modes were the same as predicted. The failure of the anchors was generally preceded by spalling of crushed concrete in the loading direction as shown in Fig. 4.24.

Table 4.12: Static Shear Test Data for Wedge All® Anchors

Sample	ϕ	Failure Load		Failure Mode		Average Experimental Load
		Predicted	Experimental			
	(mm)	(kN)	(kN)	Predicted	Experimental	(kN)
SS-WA-TE-01	9.5	16.7	21.7	SF	SF	20.8
SS-WA-TE-02	9.5	16.7	20.0	SF	SF	
SS-WA-TE-03	9.5	16.7	20.7	SF	SF	
SS-WA-HL-01	12.7	41.1	52.9	SF	SF	51.5
SS-WA-HL-02	12.7	41.1	49.2	SF	SF	
SS-WA-HL-03	12.7	41.1	52.5	SF	SF	

4.2.2.2.1 Load-Displacement Behavior

The load-displacement behavior of the 9.5-mm and 12.7-mm diameter anchor systems are illustrated in Fig. 4.28 and Fig. 4.29 respectively. For the 9.5-mm diameter anchor system, the frictional resistance is overcome at different load level: 11 kN for SS-WA-TE-01 and 6 kN for SS-WA-TE-02 and SS-WA-TE-03. While SS-WA-TE-01 and SS-WA-TE-03 showed negligible base plate slip before bearing on anchors, SS-WA-TE-02 showed a base slip of about 0.7 mm before bearing on anchors. The post-friction range for SS-WA-TE-01 and SS-WA-TE-03 and post-slip behavior of SS-WA-TE-02 was characterized by bilinear stiffness ranges. The first range was characterized by high resistance and then followed by a low resistance region for the second range. Stiffnesses of 5.0 kN/mm, 4.0 kN/mm and 6.0 kN/mm were attained for the first range for SS-WA-TE-01, SS-WA-TE-02 and SS-WA-TE-03 respectively. For the second range, stiffnesses of 1.6 kN/mm and 2.3 kN/mm were attained for SS-WA-TE-01, and then SS-WA-TE-02 and SS-WA-TE-03

respectively. SS-WA-TE-01 attained ultimate load of 21.7 kN at a displacement of 5 mm while the SS-WA-TE-02 and SS-WA-TE-03 reached ultimate loads at 20.0 kN and 20.7 kN respectively at displacements of 5.6 mm and 5 mm.

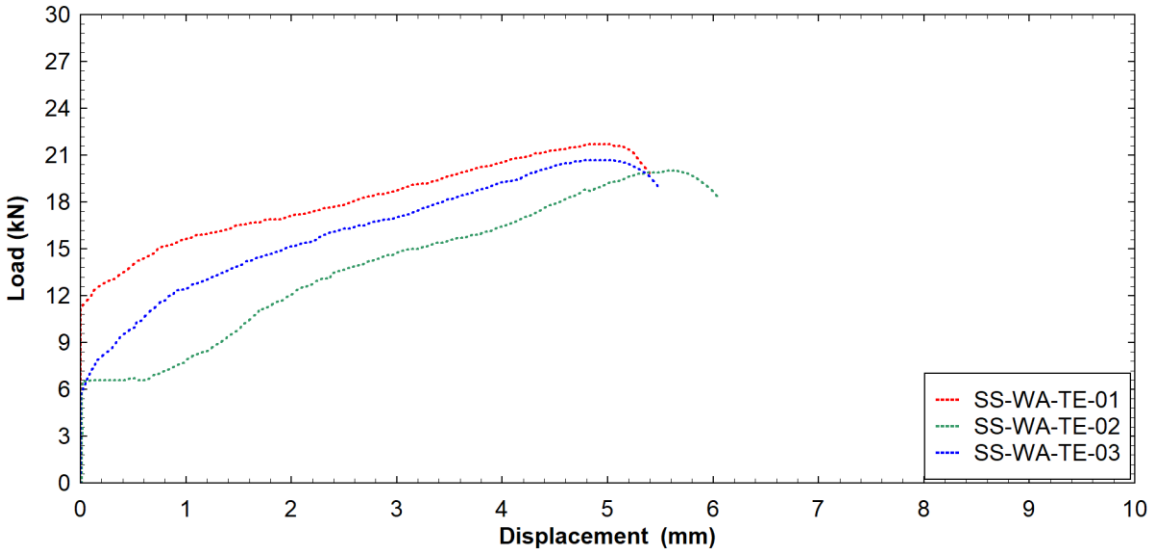

Fig. 4.28: Load-Displacement Curves for 9.5-mm Diameter Anchor System in Shear (Wedge-All®)

The behavior of all the 12.7-mm diameter Wedge-All anchors was consistent during the contact frictional resistance stage. All the anchors showed initial frictional resistance of 4 kN. The post-friction transfer range for these anchors also showed bilinear stiffnesses similarly to the 9.5-mm diameters. Stiffnesses of 12.7 kN/mm and 11.4 kN/mm were attained SS-WA-HL-01, and SS-WA-HL-02 and SS-WA-HL-03 respectively while for the second range, stiffnesses of 6.9 kN/mm, 4.6kN/mm and 5.9kN/mm were attained for SS-WA-HL-01, SS-WA-HL-02 and SS-WA-HL-03 respectively. While SS-WA-HL-01 plateaued for about 4 mm before reaching ultimate load of 52.9 kN at displacement of 9 mm, SS-WA-HL-02 and SS-WA-HL-03 achieved ultimate loads of 49.2 kN and 52.5 kN at displacements of 6.7 mm and 8 mm without significant plateau.

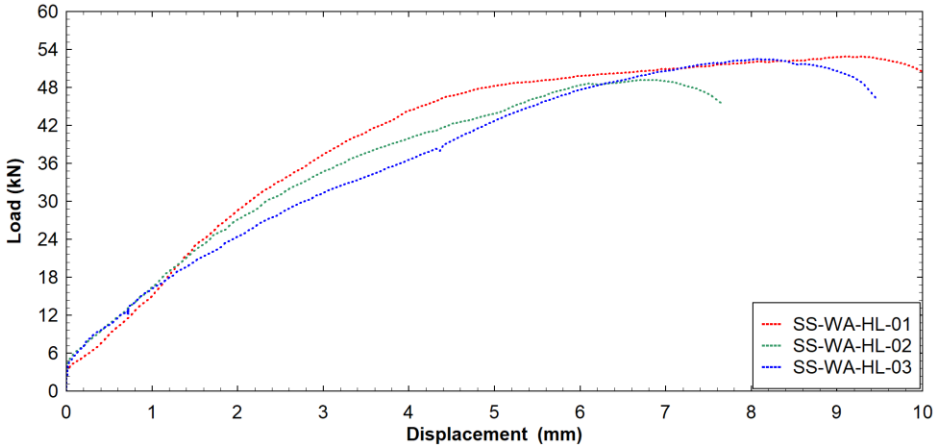

Fig. 4.29: Load-Displacement Curves for 12.7-mm Diameter Anchor System in Shear (Wedge-All®)

4.2.2.3 Titen HD®

The experimental test results presented on Table 4.13 show that except the 9.5-mm diameter Titen HD anchors, all the anchors failed at loads higher than the predicted loads. Similarly to the expansion anchors (Strong-Bolt 2 and Wedge-All), the Titen HD anchors all failed in steel fracture failure mode as predicted. While the experimental failure load for the 6.4-mm and 12.7-mm diameter anchors was 6% and 9% higher than the predicted failure loads, the experimental failure load for the 9.5-mm diameter anchor systems was 2% lower than the predicted failure load.

Table 4.13: Static Shear Test Data for Titen HD® Anchors

Sample	ϕ	Failure Load		Failure Mode		Average Experimental Load
		Predicted	Experimental			
	(mm)	(kN)	(kN)	Predicted	Actual	(kN)
SS-TTH-QI-01	6.4	17.1	19.6	SF	SF	18.1
SS-TTH-QI-02	6.4	17.1	15.1	SF	SF	
SS-TTH-QI-03	6.4	17.1	19.7	SF	SF	
SS-TTH-TE-01	9.5	38.0	34.9	SF	SF	37.4
SS-TTH-TE-02	9.5	38.0	40.5	SF	SF	
SS-TTH-TE-03	9.5	38.0	36.8	SF	SF	
SS-TTH-HL-01	12.7	65.8	74.9	SF	SF	73.4
SS-TTH-HL-02	12.7	65.8	77.9	SF	SF	
SS-TTH-HL-03	12.7	65.8	67.4	SF	SF	

4.2.2.3.1 Load-Displacement Behavior

The load-displacement behavior for the 6.4-mm diameter Titen HD anchor system (Fig. 4.30) shows a negligible frictional resistance of 0.7 kN. The post-friction behavior of the anchors is characterized by varied increased and decreased ranges of stiffness for all three anchors prior to reaching ultimate load. The average stiffness exhibited by the various anchor systems are 2.2 kN/mm, 2.4 kN/mm and 2.6 kN/mm SS-TTH-QI-01 SS-TTH-QI-02 and SS-TTH-QI-03 respectively. SS-TTH-QI-02 shows 2 mm plateau before reaching ultimate load. The anchor systems reach ultimate loads at displacements of 8 mm, 6.6 mm and 7 mm for SS-TTH-QI-01, SS-TTH-QI-02 and SS-TTH-QI-03 respectively.

For the 9.5-mm diameter anchors, the frictional resistance is 7.5 kN for SS-TTH-TE-01 and SS-TTH-TE-03 and 5.5 kN for SS-TTH-QI-02 (Fig. 4.31). The behavior of the anchor systems post contact-friction range is bilinear similar to the Wedge-All anchors. The behavior in the first range is uniform for all three anchors systems, with stiffness of 10 kN/mm. For the second range prior to ultimate loads, SS-TTH-TE-01 shows stiffness of 4 kN/mm before showing a plateau. SS-TTH-TE-02 and SS-TTH-TE-03 has stiffnesses of 3.1 kN/mm and 2.3 kN/mm respectively. SS-TTH-TE-01 reach ultimate load of 34.9 kN at displacement of 6 mm while SS-TTH-TE-02 and SS-TTH-TE-03 reach ultimate loads of 40.5 kN and 36.8 kN at displacements of 8.5 mm and 7.1 mm respectively.

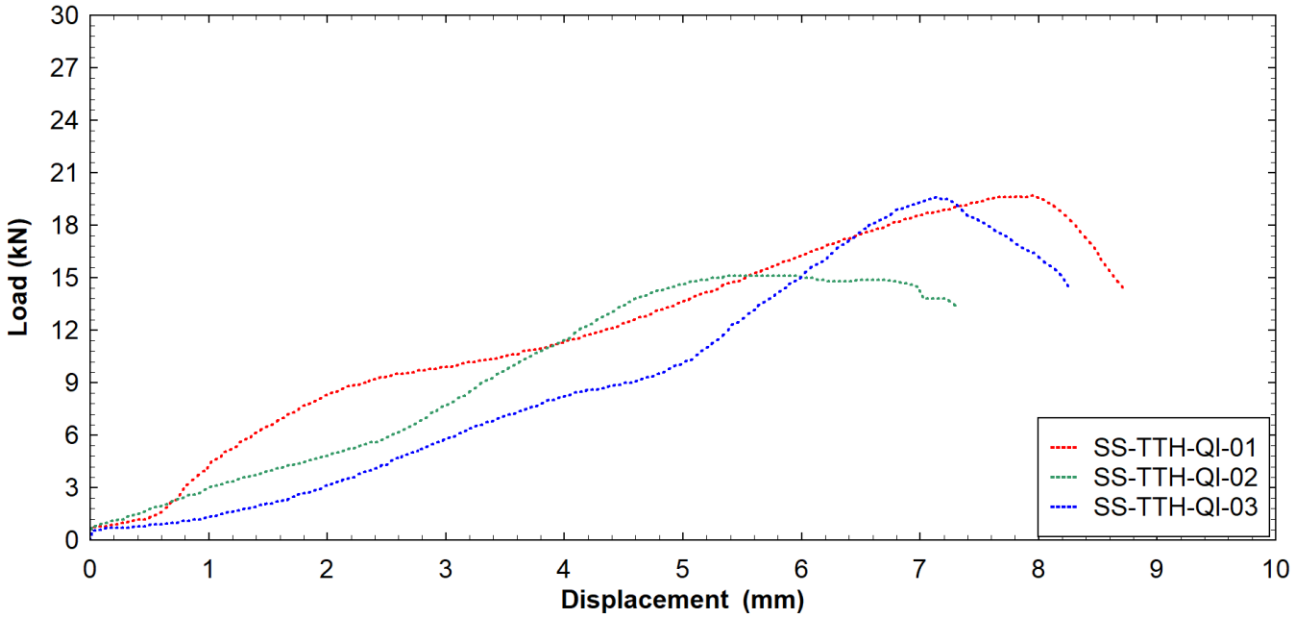

Fig. 4.30: Load-Displacement Curves for 6.4-mm Anchor System in Shear (TTH)

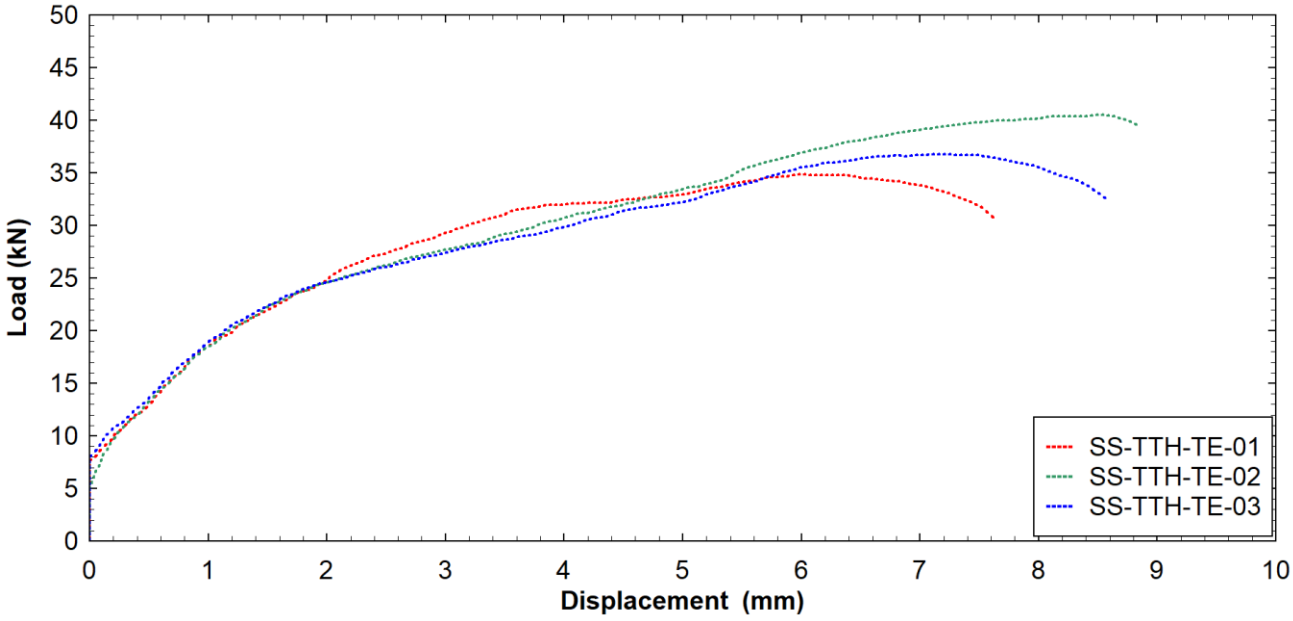

Fig. 4.31: Load-Displacement Curves for 9.5-mm Diameter anchor System in Shear (TTH)

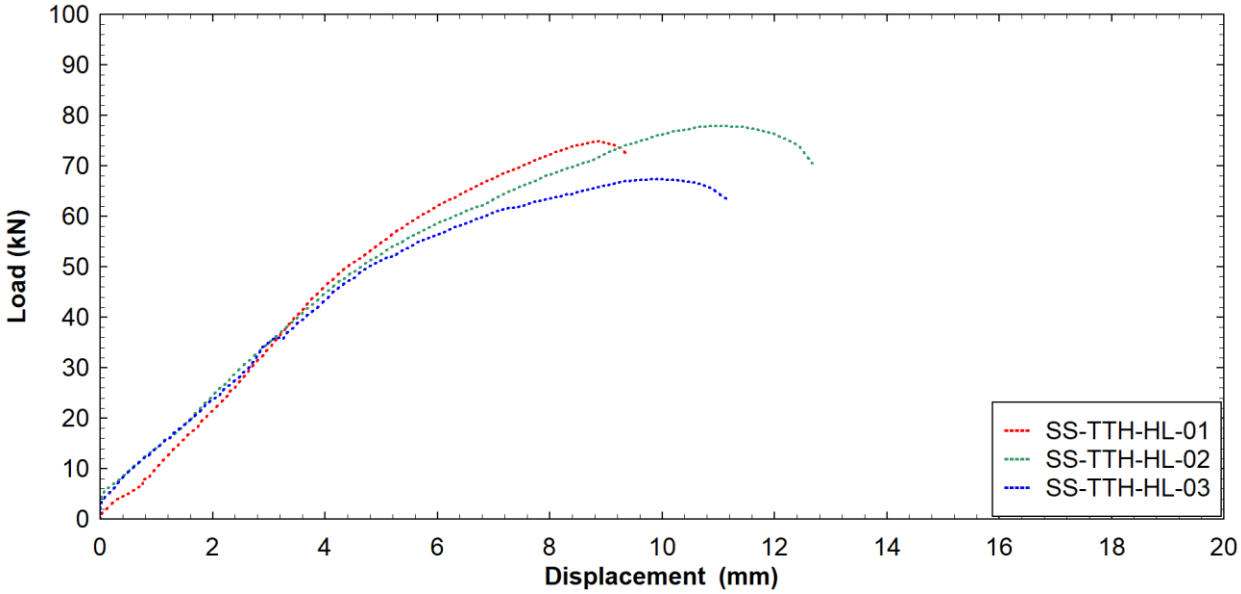

Fig. 4.32: Load-Displacement curves for 12.7-mm Diameter Anchor System in Shear (TTH)

The load-displacement response for the 12.7-mm diameter Titen HD anchors are shown on Fig. 4.32. SS-TTH-HL-01 showed minimal contact friction resistance compared to SS-TTH-HL-02 and SS-TTH-HL-03 which had a frictional resistance of 4 kN. The anchor response shows two regions of stiffness similar to the behavior of the 9.5-mm diameter Titen HD anchors. The early post friction resistance is characterized by an average stiffness of 11 kN/mm while the later region has an average stiffness of 4.3 kN/mm. The peak failure loads of the 12.7-mm diameter Titen HD anchors were 74.9 kN, 77.9 kN and 67.4 kN for SS-TTH-HL-01, SS-TTH-HL-02 and SS-TTH-HL-03 respectively.

4.3 Dynamic Testing

The dynamic impact tests were carried out as described in Section 3.6.2 for both tension and shear. At least three anchor samples for each anchor type and diameter were tested. Also, to obtain the stress-strain response of the anchors, at least one of the anchors in each group was strain-gauged. Data from the strain-gauged anchors also enabled the determination of the rate of strain the anchors were subjected to.

Failure mode of the two expansion anchors (Strong-Bolt® 2 and Wedge-All®) under tension testing was generally pull-through, while mixed failure mode of pull-out and concrete breakout governed the behavior of the screw anchor (Titen HD®). Additional failure modes recorded were steel fracture failure and a pull-through failure followed by splitting of the concrete beam. The stress-strain relationships obtained for the anchors under the drop-mass tests did not extend to the yield point of the anchors. For this matter, the average rate of strains were obtained rather than the standard strain rate defined by UFC-340-02 [80], consequently, the average rate of strain was about 1 /s.

Under shear testing conditions, the predominant failure mode of all the anchors was steel fracture failure, with only one case of splitting of beam preceded by bending of the anchor. Under drop-mass testing, it was not possible to determine the exact failure load since the drop height chosen either resulted in an input energy more than or less than the load required for failure. Unlike the case of static loading, where the anchor was loaded gradually until failure, systems such as drop-mass impact tests are best evaluated by a "Go-No-Go" type of testing such as the Bruceton Method [82]. However, the Bruceton Method requires a large number of samples, making the method time consuming and expensive.

The objective of this investigation was to obtain the highest impulse load that the anchors could absorb without failure and the corresponding peak load. The peak load was taken as the amplitude of the load-time curve while the impulse was calculated as the area under the curve. The peak impact loads were compared with the average failure loads under static testing to obtain the dynamic load ratio (DLR) for each test.

A total of 75 anchors were tested under drop-mass impact testing program. Table 4.14 presents the test matrix for drop-mass testing showing the type and size of anchors and the number of samples tested in the experimental program. Behavior of each type of anchor tested is further discussed in the succeeding sections.

Table 4.14: Test Matrix for Dynamic Anchor Tests

Anchor Type	Diameter (mm)	Number of Samples	
		Tension	Shear
Strong Bolt® 2	6.4	8	3
	9.5	5	3
	12.7	7	3
Wedge-All®	9.5	5	3
	12.7	8	3
Titen HD®	6.4	9	3
	9.5	3	3
	12.7	6	3
Totals		**51**	**24**

4.3.1 Tension Tests

The tension test under dynamic conditions were carried out as described in Section 3.6.2 by subjecting installed anchors to loads from different predetermined drop heights. The first anchor from each anchor type and diameter was subjected to loading from varying drop heights until failure was achieved. The drop height for a subsequent test was based on the drop height that resulted in failure of the preceding test in order to obtain a bracket of the failure load.

Since the load generated from a specific drop height could either lead to failure or non-failure of the test specimen, the behavior of the anchors generally followed two patterns.

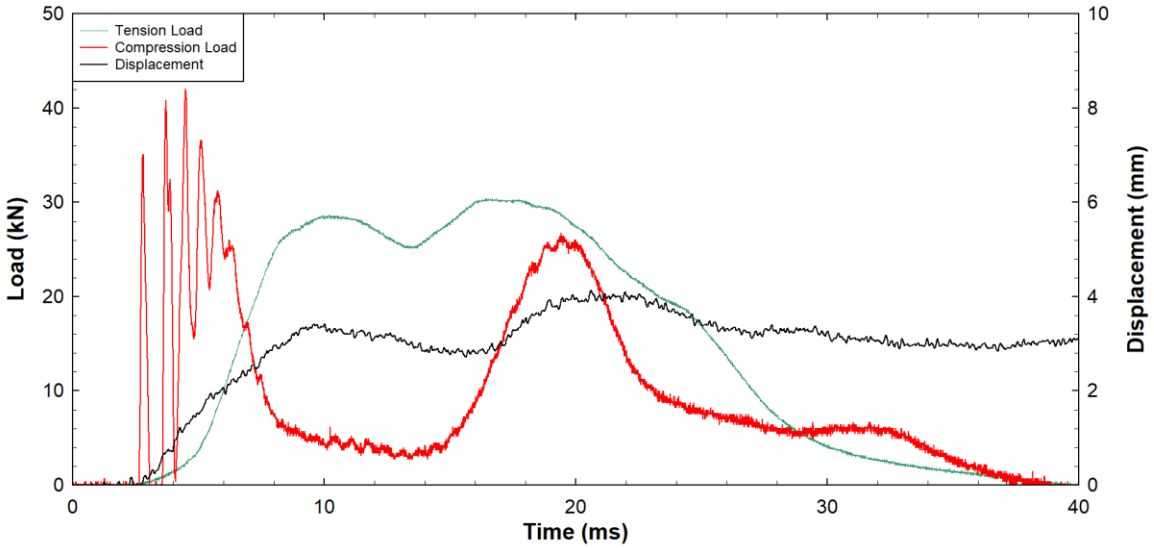

Fig. 4.33: Typical Load Profile for Anchor which Survived Impact Test

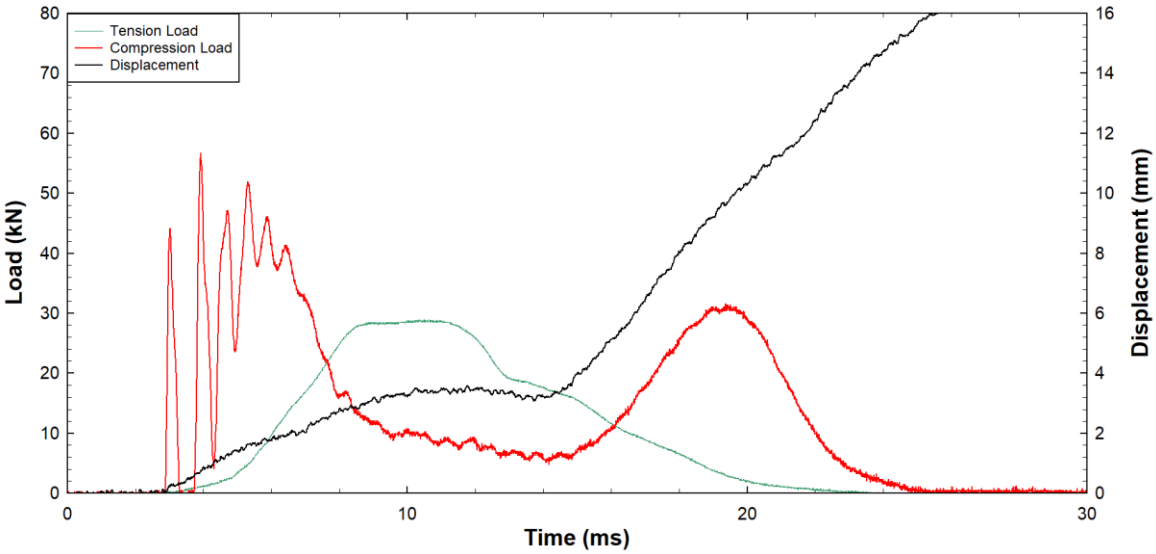

Fig. 4.34: Typical Load Profile for Anchor which did not Survive Impact Test

The first anchor behavior relates to an anchor that survives the impact load and is illustrated in Fig. 4.33. The anchorage system survived the impact load with permanent deformation in terms of displacement, as can be seen from the final displacement after both the "compression" and "tension" loads dissipate. This behavior highlights the "virgin"

capacity of the anchor on the first impact load test or the residual capacity under subsequent tests on the same anchor.

The second anchor behavior (Fig. 4.34) relates to anchors which does not survive the impact load. For this test, the anchor system undergoes increasing displacement of the drop-mass post failure of the anchor in either tension or shear. Both anchor behaviors are considered valid for the purpose of estimating the anchor capacities. The failure modes observed for the dynamic tension tests are summarized on Table 4.15.

Table 4.15: Summary of Recorded Failure Modes for Anchors in Dynamic Tension Test

Anchor Type	Diameter (mm)	Dynamic Failure Mode in Tension			
		Steel Fracture	Concrete Breakout*	Pull-through	Splitting
Strong-Bolt 2	6.4	1		7	
	9.5	1	1	3	
	12.7			7	
Wedge-All	9.5			5	
	12.7			7	1
Titen HD	6.4	1	8		
	9.5		3		
	12.7		5		1

4.3.1.1 Strong-Bolt® 2

Table 4.16: Summary of Dynamic Tension Result for Strong Bolt® 2 Anchor System

Sample	ϕ	Drop height	PE (mgh)	F_{static}	Compression Load				Tension Load				Disp.	DLR	Observation
					P_c	t_r	t_d	Impulse	P_t	t_r	t_d	Impulse			
	(mm)	(mm)	(J)	(kN)	(kN)	(ms)	(ms)	(kN.ms)	(kN)	(ms)	(ms)	(kN.ms)	(mm)		
DT-STB-QI-03-01	6.4	35	81	8.9	49	2.1	10.0	154	7.1	13.2	32.9	145		0.80	PT failure
DT-STB-QI-04-01	6.4	35	81	8.9	53	1.5	12.9	158	9.0	17.9	62.8	341	10	1.02	Not failed
DT-STB-QI-04-02	6.4	35	81	8.9	54	1.6	10.0	161	9.8	3.4	7.7	18.0		1.10	PT failure
DT-STB-QI-05-01	6.4	50	115	8.9	71	1.5	8.3	165	9.2	12.2	33.3	182		1.03	PT failure
DT-STB-QI-07-01	6.4	50	115	8.9	71	1.3	9.3	202	10.0	16.3	71.6	410	10	1.13	Not failed
DT-STB-QI-07-02	6.4	50	115	8.9	64	1.4	10.2	180	11.8	5.0	18.9	97		1.33	PT failure
DT-STB-QI-08-01	6.4	75	173	8.9	81	1.3	9.3	235	9.6	4.4	27.9	181		1.09	PT failure
DT-STB-QI-09-01	6.4	22	51	8.9	39	1.6	53.5	597	9.9	23.3	54.2	357	6	1.12	Not failed
DT-STB-QI-09-02	6.4	35	81	8.9	42	1.2	28.2	331	12.7	5.5	27.4	183		1.43	PT failure
DT-STB-QI-10-01	6.4	35	81	8.9	49	1.1	27.1	384	9.5	9.3	22.1	143		1.07	SF failure
DT-STB-QI-11-01	6.4	30	69	8.9	44	1.7	62.8	611	10.0	20.0	57.7	362	7	1.13	Not failed
DT-STB-QI-11-02	6.4	30	69	8.9	50	1.7	14.1	225	13.2	4.2	9.0	59		1.49	PT failure
DT-SBT-TE-01-01	9.5	70	162	29.3	77	1.6	37.1	642	25.0	18.0	20.7	527	3	0.85	Not failed
DT-SBT-TE-01-04	9.5	100	231	29.3	80	1.3	46.8	683	30.7	13.0	42.1	583	4	1.05	Not failed
DT-SBT-TE-01-05	9.5	110	254	29.3	79	1.3	21.5	376	26.4	5.0	22.3	295		0.90	PT failure
DT-SBT-TE-02-01	9.5	110	254	29.3	89	1.3	41.0	667	23.3	15.5	46.3	603	10	0.80	Not failed
DT-SBT-TE-02-02	9.5	120	277	29.3	85	1.4	46.3	596	27.5	12.3	39.0	550	9	0.94	Not failed
DT-SBT-TE-02-03	9.5	130	300	29.3	68	1.3	10.7	181	26.8	4.2	11.1	92		0.91	PT failure
DT-SBT-TE-03-01	9.5	130	300	29.3	92	1.4	33.8	716	28.2	15.6	36.3	607	9	0.96	Not failed
DT-SBT-TE-03-02	9.5	140	323	29.3	86	1.3	33.8	619	31.5	5.2	35.9	607	8	1.08	Not failed
DT-SBT-TE-03-03	9.5	150	346	29.3	67	1.3	11.5	224	31.0	4.4	16.5	187		1.06	PT failure

Sample	ϕ	Drop height	PE (mgh)	F_{static}	Compression Load				Tension Load				Disp.	DLR	Observation
					P_c	t_r	t_d	Impulse	P_t	t_r	t_d	Impulse			
	(mm)	(mm)	(J)	(kN)	(kN)	(ms)	(ms)	(kN.ms)	(kN)	(ms)	(ms)	(kN.ms)	(mm)		
DT-SBT-TE-04-01	9.5	140	323	29.3	74	0.7	50.7	697	26.5	23.7	47.1	711	14	0.90	Not failed
DT-SBT-TE-04-02	9.5	140	323	29.3	70	0.8	42.5	569	33.2	15.6	38.6	768	11	1.13	Not failed
DT-SBT-TE-04-03	9.5	140	323	29.3	78	0.4	46.7	697	36.6	4.2	44.5	632		1.25	Not failed
DT-SBT-TE-04-04	9.5	140	323	29.3	80	1.2	11.1	254	19.5	3.4	8.8	53		0.67	CC failure
DT-SBT-TE-05-01	9.5	160	369	29.3	66	0.3	38.3	505	32.1	15.9	36.6	747	10	1.10	Not failed
DT-SBT-TE-05-02	9.5	160	369	29.3	66	0.3	38.3	505	32.1	15.9	36.6	747	12	1.10	Not failed
DT-SBT-TE-05-03	9.5	160	369	29.3	83	1.0	21.1	500	38.1	4.8	14.2	343		1.30	SF failure
DT-STB-HL-01-01	12.7	250	577	46.9	55	0.2	35.6	354	43.8	4.7	33.4	937	10	0.93	Not failed
DT-STB-HL-01-02	12.7	270	624	46.9	49	0.2	25.6	263	55.7	4.9	23.4	681		1.19	PT failure
DT-STB-HL-02-01	12.7	270	624	46.9	43	0.2	39.8	390	42.2	15.4	38.7	945	13	0.90	Not failed
DT-STB-HL-02-02	12.7	280	624	46.9	58	0.2	29.5	280	50.8	5.1	48.5	869	16	1.08	Not failed
DT-STB-HL-02-03	12.7	290	670	46.9	43	0.1	10.6	118	19.2	3.5	6.5	39.0		0.41	PT failure
DT-STB-HL-03-01	12.7	300	693	46.9	47	0.2	35.9	377	65.1	4.6	35.8	1016	11	1.39	Not failed
DT-STB-HL-03-02	12.7	340	785	46.9	45	0.2	12.8	138	54.8	4.9	12.3	196		1.17	PT failure
DT-STB-HL-04-01	12.7	300	693	46.9	102	2.1	46.6	1168	36.4	4.3	49.0	1007	23	0.78	Not failed
DT-STB-HL-04-02	12.7	350	808	46.9	95	1.9	12.6	346	35.3	3.4	7.3	74		0.75	PT failure
DT-STB-HL-05-01	12.7	350	808	46.9	66	2.0	46.0	563	46.4	16.6	43.1	1068		0.99	Not failed
DT-STB-HL-05-02	12.7	380	878	46.9	78	1.3	14.1	344	61.6	4.2	11.9	266		1.31	PT failure
DT-STB-HL-06-01	12.7	380	878	46.9	108	0.4	42.7	749	45.9	16.6	41.6	1112	11	0.98	Not failed
DT-STB-HL-06-02	12.7	400	924	46.9	115	0.5	13.0	447	58.1	4.0	10.2	201		1.24	PT failure
DT-STB-HL-07-01	12.7	350	808	46.9	107	1.2	44.9	712	43.0	4.0	47.3	1096	35	0.92	Not failed
DT-STB-HL-07-02	12.7	360	808	46.9	104	1.0	12.1	319	53.0	3.9	12.8	170		1.13	PT failure

Summary of the result for the dynamic tension test for Strong Bolt® 2 is presented on Table 4.16. The test shows the input potential energy corresponding to the specified drop heights. The compression load recorded by the tup on the drop mass, the tension load recorded by the piezoelectric load cell, as well as the rise time and duration of the loads are also presented. The impulse calculated as the areas under the compression and tension load-time plots are also presented. Displacements sustained by anchors which did not fail under the loading are presented as well as observations on the failure modes.

4.3.1.1.1 Behavior Under Dynamic Loading

Eight samples of the 6.4-mm diameter Strong-Bolt® 2 anchors were tested at drop heights ranging from 22 mm to 75 mm (Table 4.16). Fig. 4.35 and Fig. 4.36 show typical recorded failure modes of pull-through and steel fracture for the 6.4-mm diameter anchor system respectively. The anchors survived loading from drop heights of up to 50 mm without failure on the first attempt of loading. DT-STB-QI-03-01 failed under loading from a drop height of 35 mm. The impulse under the tension load was 145 kN.ms while the peak load was 7.1 kN (DLR = 0.80). DT-STB-QI-04-01 on the other hand sustained loading from a drop height of 35 mm without failure. On repeated testing (DT-STB-QI-04-02) at a drop height of 35 mm, the anchor suffered pull-through failure. The impulse and peak load of the sustained load from drop height of 35 mm were 341 kN.ms and 9.0 kN (DLR = 1.02) while sustaining a permanent displacement of 10 mm. DT-STB-QI-05-01 failed at a drop height of 50 mm in pull-through mode with an impulse of 182 kN.ms and peak load of 9.2 kN (DLR = 1.03). At a drop height of 50 mm again, DT-STB-QI-07-01 did not fail, resisting an impulse of 410 kN.ms with a peak load of 10.0 kN (DLR = 1.13) with a residual displacement of 10 mm. The anchor subsequently failed in pull-through at a second attempt

at drop height of 50 mm (DT-STB-QI-07-02). DT-STB-QI-08-01 failed in pull-through mode with an impulse of 181 kN.ms and peak load of 9.6 kN (DLR = 1.09).

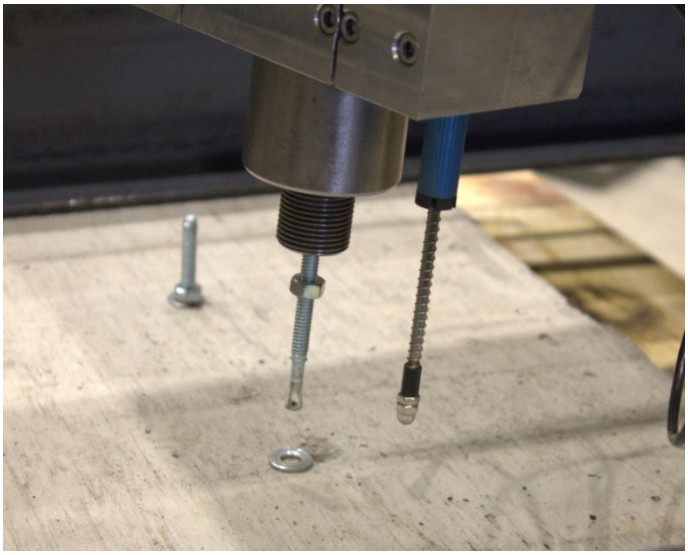

Fig. 4.35: Pull-through Failure for DT-STB-QI-08

Fig. 4.36: Steel Fracture Failure for DT-STB-QI-03

DT-STB-QI-09-01 survived a drop height of 22 mm, generating an impulse of 357 kN.ms, a peak load of 9.9 kN (DLR = 1.12) and residual displacement of 6 mm before failing in pull-through mode at a repeat drop height of 35 mm (DT-STB-QI-09-02). DT-STB-QI-10-01 failed in steel fracture failure on the first attempt, generating an impulse of 143 kN.ms and peak load of 9.5 kN while DT-STB-QI-11-01 sustained a drop height of 30 mm without

failure, generating an impulse and peak load of 362 kN.ms and 10.0 kN (DLR = 1.13) with a residual displacement of 7 mm before failing in pull-through mode on the second attempt at a drop height of 30 mm (DT-STB-QI-11-02).

Five samples of the 9.5-mm diameter Strong-Bolt 2 anchors were tested under impact test. The anchors were tested at drop heights from 70 mm to 160 mm. While three of the anchor systems failed in pull-through mode (Fig. 4.37), one instance each of concrete breakout (Fig. 4.38) and steel fracture failure (Fig. 4.39) were recorded. DT-STB-TE-01 survived impact loads from 70-mm (DT-STB-TE-01-01) to 100-mm (80-mm, 90-mm and 100-mm for DT-STB-TE-01-02, DT-STB-TE-01-03, and DT-STB-TE-01-04 respectively) drop heights and sustained a cumulative residual displacement of 7 mm before failing in pull-through mode under repeated loading at a drop height of 110 mm (DT-STB-TE-01-05). The survived impulse for this anchor for the 100 mm drop height was 583 kN.ms while the peak load was 30.7 kN (DLR = 1.05). DT-STB-TE-02 survived impacts from drop heights of 110-mm (DT-STB-TE-02-01) and 120-mm (DT-STB-TE-02-02) and a cumulative residual displacement of 19 mm before pulling through at a drop height of 130 mm (DT-STB-TE-02-03). The impulse survived under the 120-mm drop height was 550 kN.ms with a peak load of 27.5 kN (DLR = 0.94). DT-STB-TE-03 survived drop heights of 130 mm (DT-STB-TE-03-01) and 140 mm (DT-STB-TE-03-02) with cumulative residual displacement of 17 mm before failing in pull-through mode at drop height of 150 mm (DT-STB-TE-03-03). The impulse survived under the 140-mm drop height was 607 kN.ms with a peak load of 31.5 kN (DLR = 1.08).

DT-STB-TE-04 and DT-STB-TE-05 survived impacts from drop heights of 140 mm and 160 mm respectively, generating DLR of 1.25 and 1.10 (from peak loads of 36.6 kN and

32.1 kN) with cumulative displacements of 25 mm and 22 mm. While DT-STB-TE-04 failed in concrete breakout mode at a repeat drop height of 140 mm (DT-SBT-TE-04-04), DT-STB-TE-05 failed in steel fracture mode (DT-SBT-TE-05-03), generating a DLR of 1.30 (peak load of 38.1 kN) at a drop height of 160 mm. The breakout concrete cone had an average diameter of 220 mm with a depth of 36 mm, resulting in a breakout cone angle of 19°, significantly less than the 35° proposed by the CCD method.

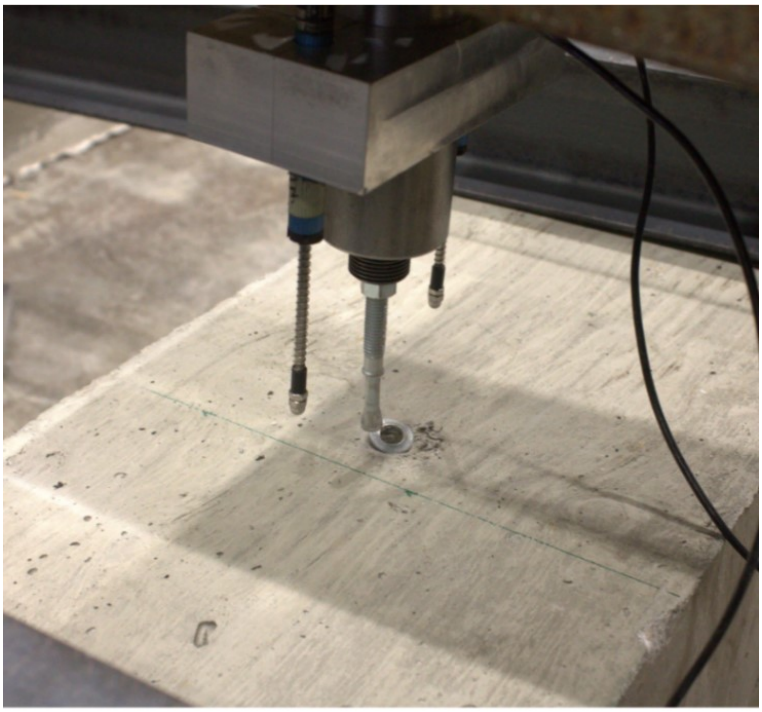

Fig. 4.37: Pull-through Failure for DT-STB-TE-01

Fig. 4.38: Concrete Breakout Failure for DT-STB-TE-01*

Fig. 4.39: Steel Fracture Failure for DT-STB-TE-03

Seven 12.7-mm diameter Strong-Bolt 2 anchors were tested at drop heights from 250 mm to 400 mm. None of the tested anchors failed on the first test, however, repeated testing on the same sample resulted in pull-through failure (Fig. 4.40). DT-STB-HL-01-01 survived

a drop height of 250 mm with residual displacement of 10 mm before failing at a repeated testing at a 270 mm drop height (DT-STB-HL-01-02) in pull-through mode. The DLR calculated from the peak load of 43.8 kN was 0.93 while the survived impulse was 937 kN.ms. For DT-STB-HL-02, drop heights of 270 mm (DT-STB-HL-02-01) and 280 mm (DT-STB-HL-02-02) were survived with a cumulative residual displacement of 29 mm before failing in pull-through mode at a drop height of 290 mm (DT-STB-HL-02-03). The impulse of 870 kN.ms and DLR of 1.08 (peak load of 50.8 kN) were obtained for the 280 mm drop height. DT-STB-HL-03 survived a drop height of 300 mm (DT-STB-HL-03-01), with impulse of 1016 kN.ms and DLR of 1.39 (peak load of 65.1 kN) before failing in pull-through mode at drop height of 340 mm (DT-STB-HL-03-02). The cumulative residual displacement survived before failure was 11 mm.

DT-STB-HL-04 survived drop height of 350 mm (DT-STB-HL-04-01), sustaining a displacement of 23 mm and resisting an impulse of 1007 kN.ms at a DLR of 0.78 (peak load of 36.4 kN) before failing in pull-through mode at 350 mm drop height (DT-STB-HL-04-02). A drop height of 350 mm however was survived by DT-STB-HL-05, resulting in an impulse of 1068 kN.ms at a peak load of 46.4 kN (DLR of 0.99) before failing in pull-through at drop height of 380 mm (DT-STB-HL-05-03).

At 380 mm drop height, DT-STB-HL-06-01 did not fail but resisted an impulse of 1112 kN.ms at a peak load of 45.9 kN (DLR = 0.98) with a residual displacement of 11 mm before failing in pull-through at drop height of 400 mm (DT-STB-HL-06-02). DT-STB-HL-07 also survived a drop height of 350 mm (DT-STB-HL-07-01) before failing at 360 mm (DT-STB-HL-07-02). The resisted impulse for the 350-mm drop height was 1100 kN.ms while the DLR was 0.92 (peak load of 43 kN).

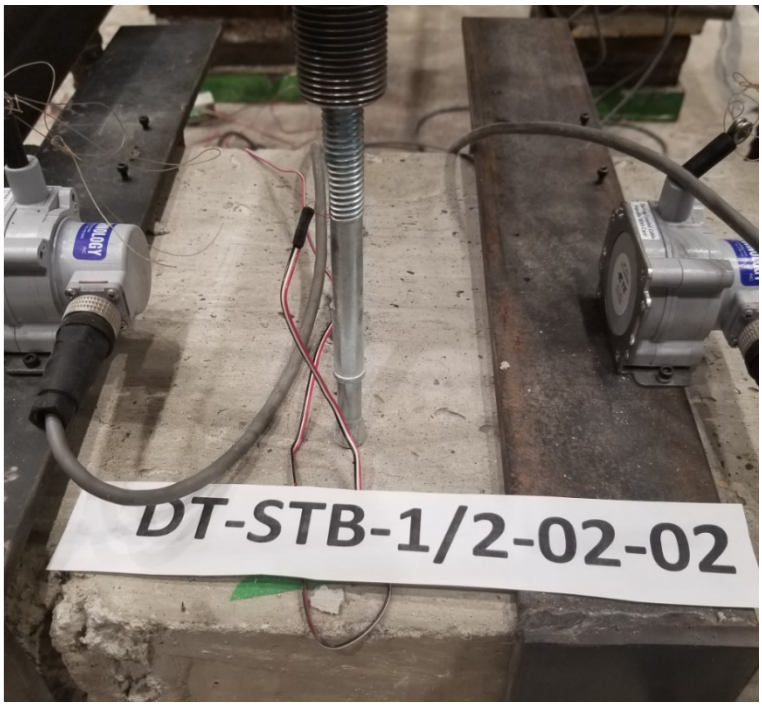

Fig. 4.40: Pull-through Failure for DT-STB-HL-02

4.3.1.1.2 Stress-Strain Behavior

The stress-strain behavior of the Strong-Bolt 2 anchors under the impact load tests are illustrated in Fig. 4.41, Fig. 4.42, and Fig. 4.43 for the 6.4-mm, 9.5-mm and 12.7-mm diameter anchors respectively. The stress-stress responses are plotted with the stress-strain behavior of bare anchor for comparison. Only one strain gauge for the 6.4-mm diameter anchor was functional during the testing. For the 9.5-mm and 12.7-mm diameter anchors only two and three strain-gauged anchors, respectively, remained functional throughout the testing.

The strain-gauged 6.4-mm diameter Strong-Bolt 2 anchor, DT-STB-QI-11, was subjected to impact loading from two drop heights without failure. The stress-strain response under the two impact loads are presented with the stress-strain response of the bare 6.4-mm diameter bare anchor in Fig. 4.41. DT-STB-QI-11-01 exhibited elastic modulus of about 240 GPa while that of DT-STB-QI-11-02 was about 579 GPa compared to the average

elastic modulus of 205 GPa obtained for the bare anchor test under loading rate of 30 mm/s. The average rate of strain obtained for this anchor type was 0.3 /s.

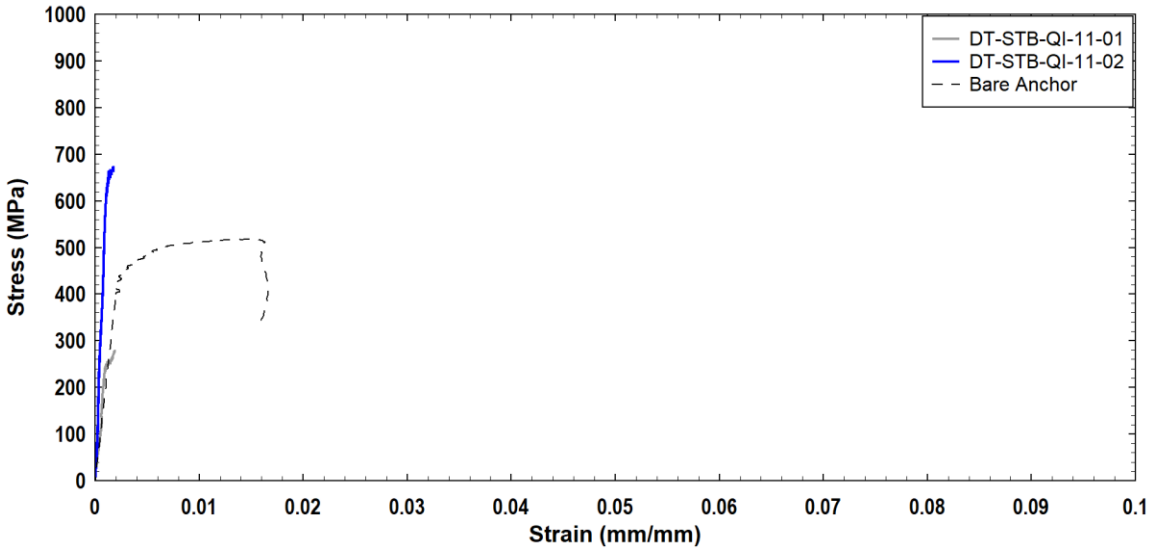

Fig. 4.41: Stress-Strain Curves for 6.4-mm Diameter Anchor System Test in Tension (STB)

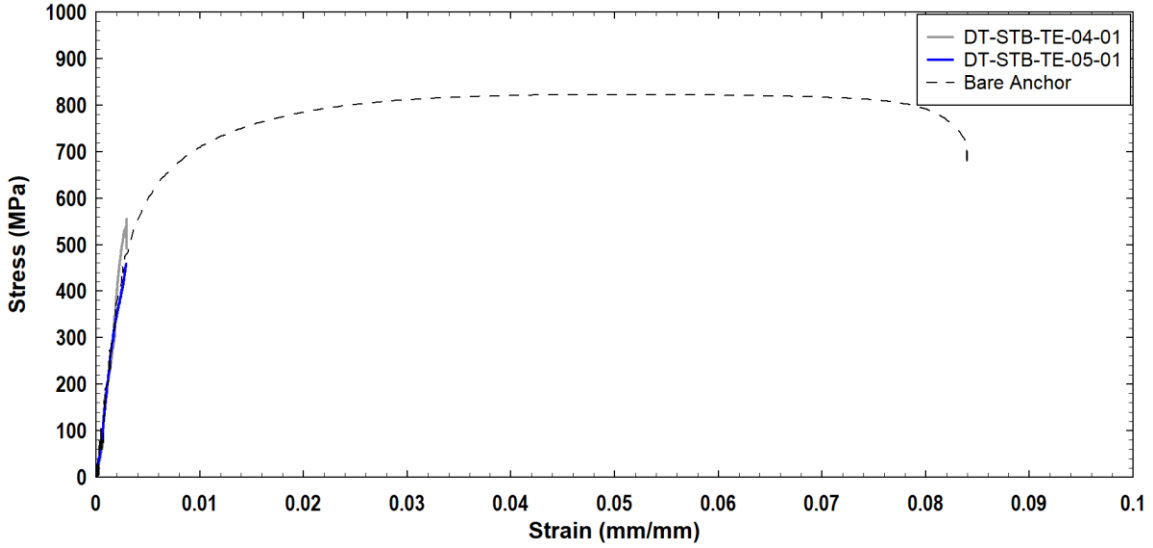

Fig. 4.42: Stress-Strain Curves for 9.5-mm Diameter Anchor System Test in Tension (STB)

For the two strain-gauged 9.5-mm diameter anchors, DT-STB-TE-04-01 failed in concrete breakout mode while DT-STB-TE-05-01 failed in steel fracture failure. The stress-strain behavior for both anchor systems and bare anchor were consistent in the elastic region with

elastic modulus of about 218 GPa, compared with the average value of 201 GPa for the bare anchors. The average rate of strain obtained was 0.7 /s.

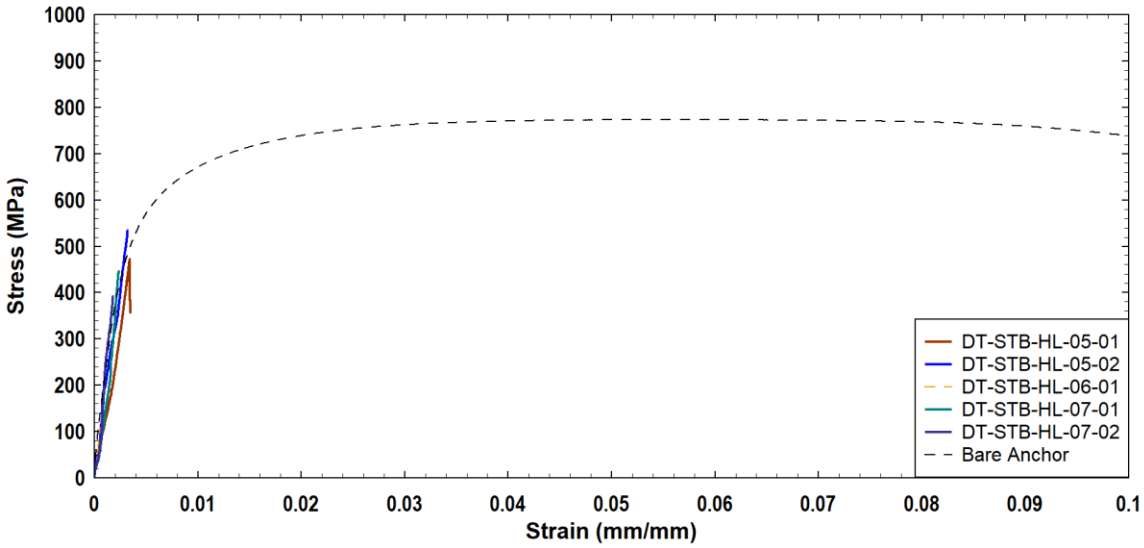

Fig. 4.43: Stress-Strain Curves for 12.7-mm Diameter Anchor System Test in Tension (STB)

For the 12.7-mm diameter Strong-Bolt 2 anchors, the elastic modulus under impact testing varied from 120 GPa for DT-STB-HL-05-01 to 217 GPa for DT-STB-HL-07-02 compared to the average elastic modulus of 210 GPa for the bare anchor under loading rate of 36 mm-/s. Similarly to the 6.4-mm and 9.5-mm diameter anchors, the stress-strain curves for the 12.7-mm diameter anchorage system did not extend into the yield plateau. The average rate of strain obtained for the 12.7-mm diameter anchors was 0.9 /s.

4.3.1.1.3 Summary and Discussion of Results for Strong-Bolt® 2 Anchors

The predominant failure mode for the Strong-Bolt® 2 under dynamic tension test was pull-through failure. However, one steel failure was recorded each for the 6.4-mm and 9.5-mm diameter anchors. The 9.5-mm diameter anchor also recorded one concrete breakout as a mixed failure at a shallow cone depth of 36 mm. The breakout angle was about 19°. The strain rates achieved during the drop test ranged from 0.3 to 1.8 /s. Generally, failure of the anchors occurred on repeated drop testing on the same anchor.

The anchors exhibited an increase in strength under the impact loading (Fig. 4.44), with the 12.7-mm diameter anchor sustaining a peak impact load as much as 140% of the static failure load (DLR = 1.4). No anchor failure was observed under single drop-mass testing of the 9.5-mm and 12.7-mm diameter anchors. The impact loading resulted in DLR values up to 1.2 for the 9.5-mm diameter anchors. The DLR value of the failed test for the 9.5-mm diameter was a repeat test on an anchor that did not fail on the first attempt and is an indication of the residual capacity. For the 6.4-mm diameter anchors, the DLR for the failed and unfailed tests were quite similar, with only one outlier of 0.8.

Based on this data, the DIF for the 6.4-mm diameter anchors at strain rate of 0.3 /s is below 1.0 and is thus not recommended for use in impact load conditions. A DIF value of 1.2 is recommended for the 9.5-mm and 12.7-mm diameter anchors for strain rates of .0.7 and 0.9 /s however the failure mode of anchor pull-through is a concern and needs to be further investigated.

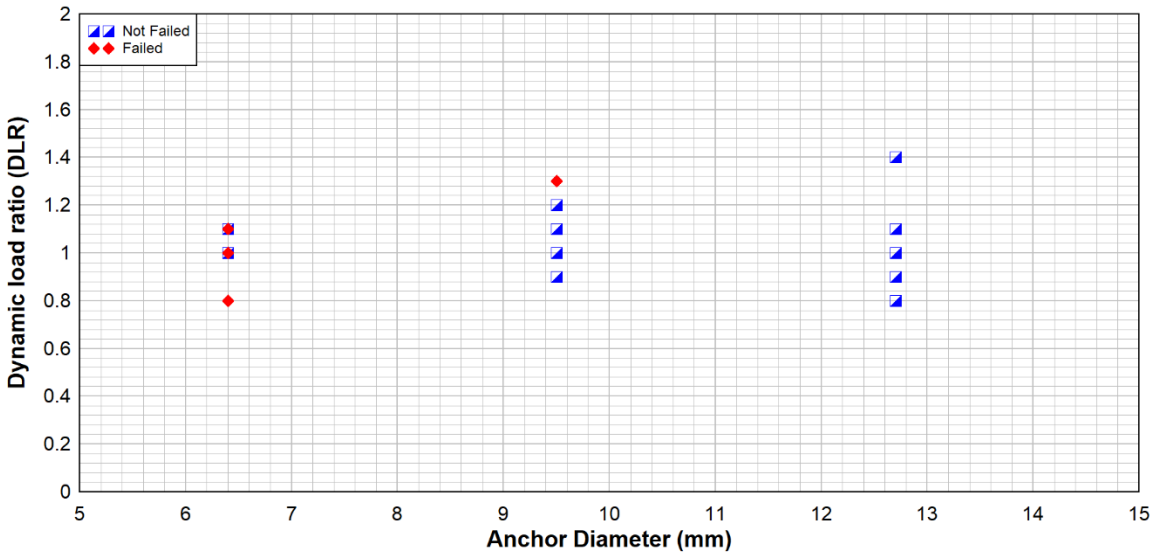

Fig. 4.44: Dynamic Load ratios for Tension Test (STB)

4.3.1.2 Wedge-All®

Summary of the experimental test results of Wedge-All anchor systems under dynamic tension conditions is presented on Table 4.17. While the predominant mode of failure was pull-through, there was one case of beam splitting failure for the 12.7-mm diameter anchor. The dynamic capacities of the Wedge-All anchor systems were found to be, generally, lower than the static capacity as values of DLR less than unity were recorded.

4.3.1.2.1 Behavior Under Dynamic Loading

Five 9.5-mm diameter Wedge-All anchors were tested at drop heights between 130-mm and 150-mm. DT-WA-TE-01-01 failed under 150 mm drop height in pull-through mode. The impulse and peak load from this test were 409 kN.ms and 21.7 kN (DLR = 0.80) respectively. DT-WA-TE-02-01 sustained impact from drop height of 130 mm with residual displacement of 11 mm and failed in pull-through mode upon repeated testing at a drop height of 140 mm. The peak load and associated impulse from the 130 mm drop height were 23.8 kN (DLR = 0.88) and 624 kN.ms respectively. DT-WA-TE-03-01 was then tested at 140 mm drop height. The peak load and associated impulse of 26.4 kN (DLR = 1.0) and 490 kN.ms respectively was survived by the anchor with a residual displacement of 6 mm. The anchor failed in pull-through mode upon retesting at an increased drop height of 150 mm. DT-WA-TE-04-01 failed at 140 mm drop height. The peak load and associated impulse resulting from the impact load were 27.0 kN (DLR = 1.00) and 595 kN.ms respectively. DT-WA-TE-05-01 on the other hand survived a 130-mm drop height with a

residual displacement of 11 mm before failing in pull-through under repeated loading at the same drop height.

Fig. 4.45: Typical Pull-through Failure Mode of Wedge-All Anchor Systems

Table 4.17: Summary of Dynamic Tension Result for Wedge-All® Anchor System

Sample	ϕ	Drop height	PE (mgh)	F_{static}	Compression Load				Tension Load				Disp.	DLR	Observation
					P_c	t_r	t_d	Impulse	P_t	t_r	t_d	Impulse			
	(mm)	(mm)	(J)	(kN)	(kN)	(ms)	(ms)	(kN.ms)	(kN)	(ms)	(ms)	(kN.ms)	(mm)		
DT-WA-TE-01-01	9.5	150	346	27.1	95.0	1.3	25.2	500	21.7	6.4	33.0	409		0.80	PT failure
DT-WA-TE-02-01	9.5	130	300	27.1	93.0	1.4	46.7	665	23.8	13.5	51.0	624	11	0.88	Not failed
DT-WA-TE-02-02	9.5	140	323	27.1	82.8	1.4	10.4	260	25.3	4.5	12.2	110		0.93	PT failure
DT-WA-TE-03-01	9.5	140	323	27.1	86.5	0.9	41.0	693	26.4	16.0	34.2	490	6	0.97	Not failed
DT-WA-TE-04-01	9.5	140	323	27.1	77.4	1.0	23.5	332	27.0	5.0	21.1	256		1.00	PT failure
DT-WA-TE-05-01	9.5	130	300	27.1	70.0	1.0	39.4	604	31.3	15.3	39.5	705	11	1.16	Not failed
DT-WA-TE-05-02	9.5	130	300	27.1	78.0	0.9	21.5	287	30.90	5	16.3	183		1.14	PT failure
DT-WA-HL-01-01	12.7	340	785	48.6	131.3	1.6	12.4	703	38.0	4.4	21.2	529		0.78	PT failure
DT-WA-HL-02-01	12.7	320	739	48.6	120.8	2.2	25.0	690	38.8	4.2	24.6	572		0.80	PT failure
DT-WA-HL-03-01	12.7	250	577	48.6	102.8	2.2	13.1	391	35.1	4.6	15.0	190		0.72	PT/Splitting
DT-WA-HL-04-01	12.7	200	462	48.6	87.9	2.2	34.8	765	38.2	12.8	43.0	850		0.79	Not failed
DT-WA-HL-04-02	12.7	220	508	48.60	113.9	2.2	11.9	402	40.6	4.5	11.9	167		0.84	PT failure
DT-WA-HL-05-01	12.7	220	508	48.6	104.2	1.0	25.2	556	33.6	4.8	27.4	512		0.69	PT failure
DT-WA-HL-06-01	12.7	350	808	48.6	125.3	1.2	24.0	494	35.2	4.1	18.6	338		0.72	PT failure
DT-WA-HL-07-01	12.7	250	577	48.6	92.9	1.1	47.3	575	37.3	13.2	44.9	834		0.77	Not failed
DT-WA-HL-07-02	12.7	250	577	48.60	106.7	1.2	11.6	320	30.7	3.0	7.1	77		0.63	PT failure
DT-WA-HL-08-01	12.7	250	577	48.6	106.7	1.1	37.6	833	42.6	14.3	37.0	890		0.88	Not failed
DT-WA-HL-08-02	12.7	270	624	48.60	107.9	0.9	9.40	303	42.1	2.4	8.3	123		0.87	PT failure

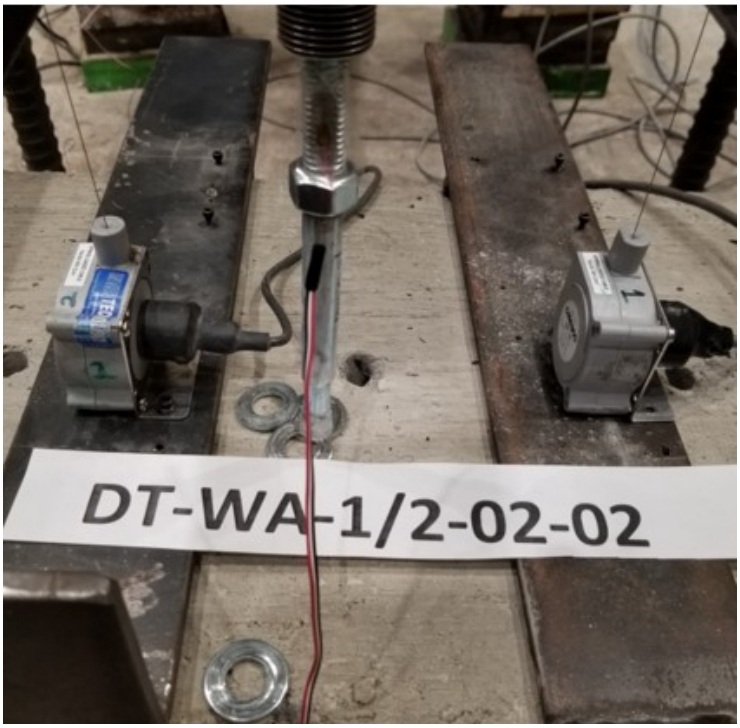

Fig. 4.46: Pull-through Failure for DT-WA-HL-02*

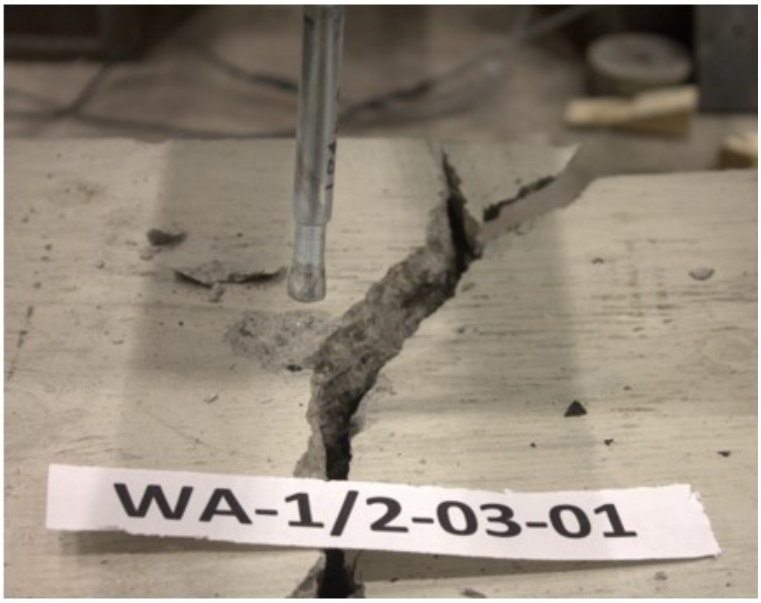

Fig. 4.47: Pull-through and Beam Splitting Failure for DT-WA-HL-03

Eight 12.7-mm diameter Wedge-All anchors were tested from drop heights ranging from 200 mm to 350 mm. Pull-through failure mode (Fig. 4.46) was recorded for all the tested anchors except in DT-WA-HL-03-01 which failed in beam splitting (Fig. 4.47).

DT-WA-HL-01-01 failed at a drop height of 320 mm. The peak load and associated impulse resulting impact load were 38 kN (DLR = 0.78) and 530 kN.ms respectively. DT-WA-HL-02-01 was tested at a drop height of 320 mm and failed in pull-through failure mode. DT-WA-HL-03-01 was then tested at a reduced drop height was reduced to 250 mm and also failed in a pull-through failure mode (with concrete beam splitting) at a peak load and associated impulse of 35.1 kN (DLR = 0.72) and 190 kN.ms respectively For DT-WA-HL-04-01, a drop height of 200 was chosen. The anchor survived the impact from this drop height with a residual displacement of 11 mm before failing in pull-through mode in repeated test at a drop height of 220 mm. The peak impact load and associated impulse resisted under the 200 mm drop height were 38.2 kN (DLR = 0.79) and 850 kN.ms respectively. DT-WA-HL-05 was also tested at a drop height of 220 mm where it failed in pull-through mode, with resulting peak impact load and associated impulse of 33.6 kN (DLR = 0.69) and 512 kN.ms respectively.

DT-WA-HL-06-01, DT-WA-HL-07-01, and DT-WA-HL-08-01 were tested at drop heights of 350 mm, 250 mm, and 250 mm respectively. For DT-WA-HL-06-01, with the peak load of 35.2 kN resulted in pull-through failure of the anchor while DT-WA-HL-07-01 and DT-WA-HL-08-01 both survived the impact loading at the drop height of 250 mm with residual displacements of 15 and 19 mm respectively. The peak loads from the impact loads were 37.3 kN (DLR = 0.77) and 42.6 kN (DLR = 0.88). DT-WA-HL-07-02 and DT-WA-HL-08-02 at drop heights of 260 mm and 270 mm respectively failed in pull-through mode.

4.3.1.2.2 Stress-Strain Behavior

The stress-strain response of the 9.5-mm and 12.7-mm diameter Wedge-All anchor systems tested under the impact load setup are illustrated in Fig. 4.48 and Fig. 4.49 respectively together with the stress-strain response of the bare anchors.

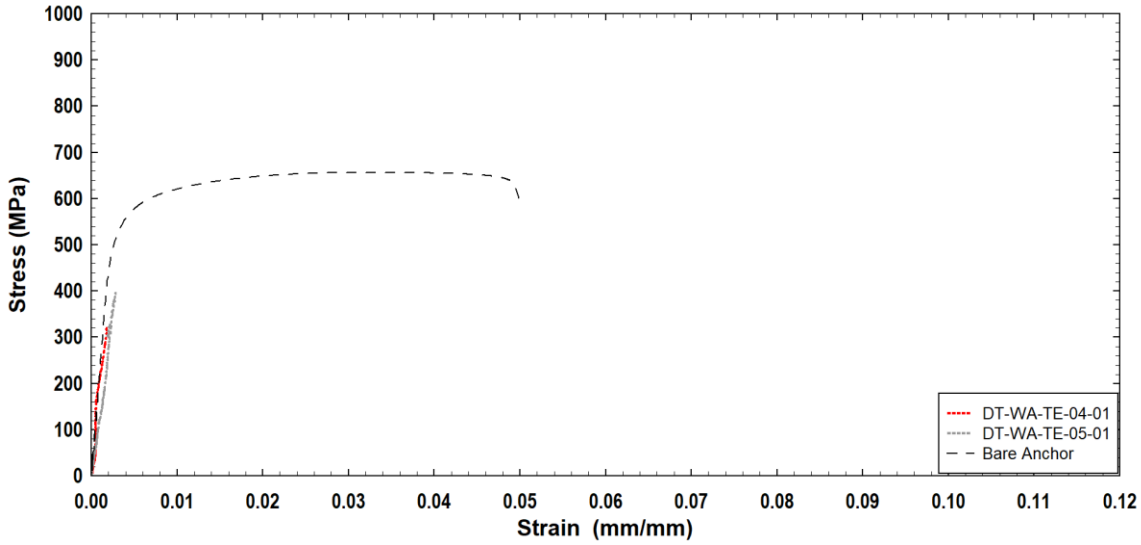

Fig. 4.48: Stress-Strain Curves for 9.5-mm Diameter Anchor System Test in Tension (WA)

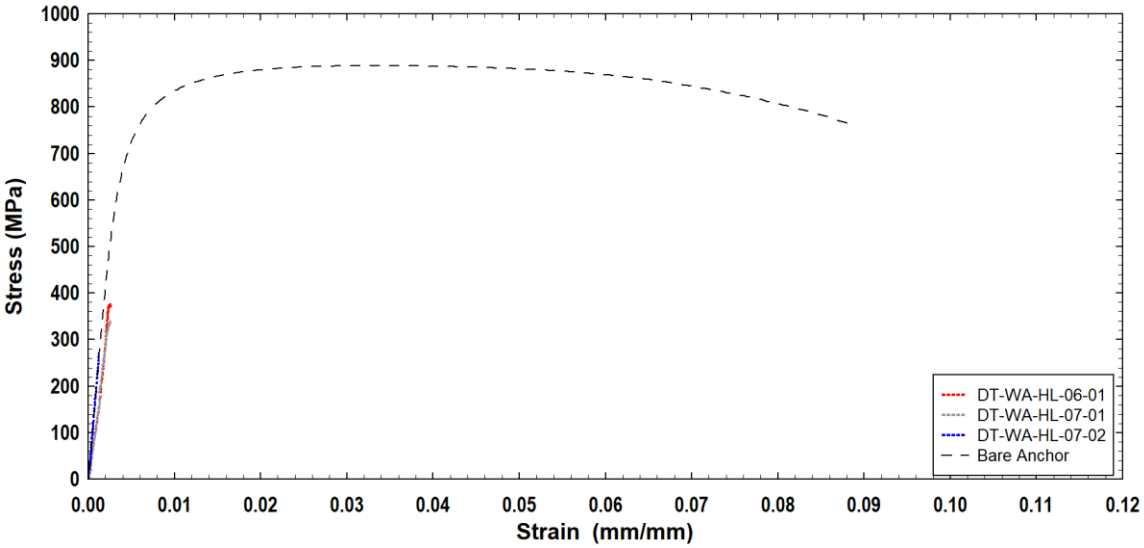

Fig. 4.49:Stress-Strain Curves for 12.7-mm Diameter Anchor System Test in Tension (WA)

For the 9.5-mm diameter anchors, the stress-strain behavior was obtained from DT-WA-TE-04-01 and DT-WA-TE-05-01 while for the 12.7-mm diameter anchors, the stress-strain behavior was obtained from DT-WA-HL-06-01 , DT-WA-HL-07 -01 and DT-WA-HL-07-

02. The stress-strain behavior does not extend beyond the linear elastic region of the stress-strain curves as compared with the bare anchor response because the anchors failed in pull-through mode.

The elastic modulus for DT-WA-TE-04-01 was 190 GPa while the elastic modulus for DT-WA-TE-05-01 was 140 GPa compared to 241 GPa for the bare anchor. Also, the average rate of strain from the impact load testing on the two anchors was 0.9 /s.

For the 12.7-mm diameters, elastic modulus for DT-WA-HL-06-01 and DT-WA-HL-07-01 was 150 GPa while for the repeated drop mass test on DT-WA-HL-07-02 was 220 GPa same as the elastic modulus of the bare anchor. The average rate of strain from the impact load testing on the 12.7-mm diameter Wedge-All anchors was 0.7 /s.

4.3.1.2.3 Summary and Discussion of Results for Wedge-All® Anchors

The dominant failure mode for the 9.5-mm and 12.7-mm diameter Wedge-All anchors was pull-through under the dynamic loading conditions, except in one case where beam splitting failure was observed. The strain rates obtained from the drop-mass testing ranged from 0.5 to 1.0 /s.

Generally, the 12.7-mm diameter anchors showed reduced capacities under the dynamic testing conditions as shown in Fig. 4.50. All failed anchors resulted in DLR values of 1 or lower while only one 9.5-mm diameter anchor system survived impact loading with a DLR more than 1.0.

Based on the drop testing DIF of the anchors at a strain rates of 0.9 and 0.7 /s were observed for the 9.5- and 12.7-mm diameter Wedge-All anchors. Thus the Wedge-All anchors are not recommended for applications where they will be subjected to impact loading. The

reduced capacity of the anchor might be attributed to the short length of sleeve compared to that for Strong-Bolt 2 anchor.

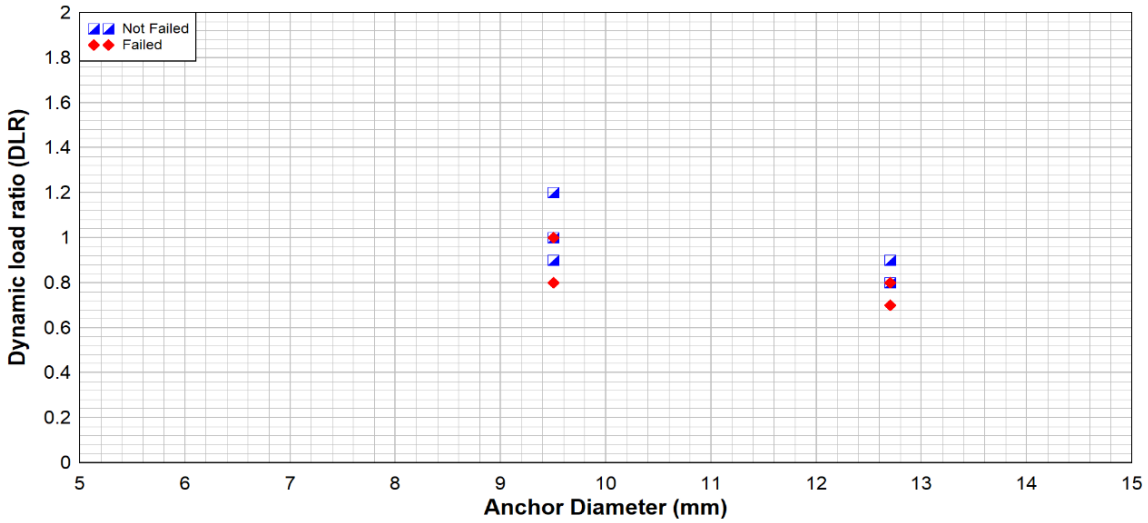

Fig. 4.50: Dynamic Load Ratio for Tension Test (WA)

4.3.1.3 Titen HD®

Table 4.18: Summary of Dynamic Tension Result for Titen HD Anchor System

Sample	ϕ	Drop height	PE (mgh)	F_{static}	Compression Load				Tension Load				Disp.	DLR	Observation
					P_c	t_r	t_d	Impulse	P_t	t_r	t_d	Impulse			
	(mm)	(mm)	(J)	(kN)	(kN)	(ms)	(ms)	(kN.ms)	(kN)	(ms)	(ms)	(kN.ms)	(mm)		
DT-TTH-QI-01-01	6.4	100	231	21.4	89.7	1.4	21.8	539	28.9	14.5	21.4	331		1.35	PO-CC
DT-TTH-QI-02-01	6.4	100	231	21.4	88.2	1.3	11.9	257	26.8	6.3	10.1	101		1.25	PO-CC
DT-TTH-QI-03-01	6.4	100	231	21.4	90.7	1.2	11.3	272	24.2	6.1	9.2	85		1.13	PO-CC
DT-TTH-QI-04-01	6.4	60	139	21.4	61.5	1.3	32.6	479	27.3	15.7	32.9	503		1.28	Not failed
DT-TTH-QI-05-01	6.4	65	150	21.4	66.3	1.3	36.3	476	28.2	16.0	51.6	456		1.32	Not failed
DT-TTH-QI-06-01	6.4	70	162	21.4	75.2	1.6	19.7	363	23.5	6.3	17.2	184		1.10	PO-CC
DT-TTH-QI-07-01	6.4	70	162	21.4	42.1	0.9	35.0	338	30.4	16.0	36.9	542	4	1.42	Not failed
DT-TTH-QI-07-02	6.35	80	185	21.4	49.6	0.7	11.4	152	23.5	4.7	6.3	47		1.10	SF
DT-TTH-QI-08-01	6.4	80	185	21.4	74.0	0.2	20.8	369	29.0	5.7	18.4	254		1.36	PO-CC
DT-TTH-QI-09-01	6.4	70	162	21.4	53.7	1.1	41.6	560	31.2	17.5	39.0	560	4	1.46	Not failed
DT-TTH-TE-01-01	9.5	100	231	42.4	58.8	0.3	36.5	570	48.8	15.3	33.4	766	2	1.15	Not failed
DT-TTH-TE-01-02	9.53	110	254	42.4	65.2	0.1	19.9	281	34.2	6.3	16.3	167		0.81	PO-CC
DT-TTH-TE-02-01	9.53	110	254	42.4	62.3	0.2	35.6	591	53.6	15.6	33.0	800	3	1.26	Not failed
DT-TTH-TE-02-02	9.53	110	254	42.4	64.8	0.1	36.5	642	50.9	15.1	33.9	780	3	1.20	Not failed
DT-TTH-TE-02-03	9.53	115	266	42.4	98.0	0.2	36.5	734	59.3	15.0	32.2	838	3	1.40	Not failed
DT-TTH-TE-02-04	9.5	115	266	42.4	72.9	0.5	36.3	796	59.3	14.8	31.2	840	2	1.40	Not failed
DT-TTH-TE-02-05	9.53	120	277	42.4	73.2	1.2	34.7	759	54.6	6.7	30.6	826	3	1.29	Not failed
DT-TTH-TE-02-06	9.53	125	289	42.4	69.7	1.0	21.3	328	46.6	5.4	24.5	255		1.10	PO-CC
DT-TTH-TE-03-01	9.53	120	277	42.4	69.3	0.3	39.6	654	59.2	18.4	36.2	816	8	1.40	Not failed
DT-TTH-TE-03-02	9.53	125	289	42.4	64.4	1.2	32.9	560	65.9	14.9	31.4	876	6	1.55	Not failed
DT-TTH-TE-03-03	9.53	125	289	42.4	62.0	1.0	32.5	562	67.5	14.7	31.8	878	4	1.59	Not failed

Sample	ϕ	Drop height	PE (mgh)	F_{static}	Compression Load				Tension Load				Disp.	DLR	Observation
					P_c	t_r	t_d	Impulse	P_t	t_r	t_d	Impulse			
	(mm)	(mm)	(J)	(kN)	(kN)	(ms)	(ms)	(kN.ms)	(kN)	(ms)	(ms)	(kN.ms)	(mm)		
DT-TTH-TE-03-04	9.5	150	346	42.4	63.8	0.8	31.2	521	67.2	13.9	28.0	893	2	1.58	Not failed
DT-TTH-TE-03-05	9.53	150	346	42.4	63.0	1.0	33.1	489	64.2	6.9	32.3	901	4	1.51	Not failed
DT-TTH-TE-03-06	9.53	150	346	42.4										0.00	PO-CC
DT-TTH-HL-01-01	12.7	200	462	62.4	97.1	1.6	32.3	989	68.4	14.8	30.0	886	3	1.10	Not failed
DT-TTH-HL-01-02	12.7	250	577	62.4	98.9	0.2	20.4	609	64.0	6.0	21.6	609		1.03	PO-CC
DT-TTH-HL-02-01	12.7	225	520	62.4	66.1	0.2	34.4	446	71.4	15.5	31.8	1055	4	1.14	Not failed
DT-TTH-HL-02-02	12.7	250	577	62.4	67.7	0.2	31.2	351	72.1	5.7	34.9	736		1.16	Not failed
DT-TTH-HL-02-03	12.7	260	600	62.4	50.5	0.2	8.8	146	11.6	3.3	7.0	25		0.19	PO-CC
DT-TTH-HL-03-01	12.7	250	577	62.4	49.2	0.2	23.8	281	69.5	7.6	31.8	686		1.11	PO-CC
DT-TTH-HL-04-01	12.7	250	577	62.4	88.9	0.5	31.9	778	80.8	7.3	29.7	1159		1.29	BS Failure
DT-TTH-HL-05-01	12.7	220	508	62.4	96.9	0.3	32.9	820	89.8	14.8	28.6	1128	8	1.44	Not failed
DT-TTH-HL-05-02	12.7	225	520	62.4	77.5	0.1	33.3	839	70.3	14.8	31.6	877	4	1.13	Not failed
DT-TTH-HL-05-03	12.7	230	531	62.4	71.1	0.3	33.9	728	72.7	15.5	31.9	892	8	1.17	Not failed
DT-TTH-HL-05-04	12.7	240	554	62.4	76.6	0.8	33.8	877	73.6	14.7	29.7	915	7	1.18	Not failed
DT-TTH-HL-05-05	12.7	250	577	62.4	79.5	1.0	34.0	867	69.1	14.2	31.4	945	7	1.11	Not failed
DT-TTH-HL-05-06	12.7	250	577	62.4	103.4	0.3	14.1	402	50.2	4.7	18.3	205		0.80	PO-CC
DT-TTH-HL-06-01	12.7	240	554	62.4	79.5	2.2	34.5	1096	75.9	15.3	31.5	1142	10	1.22	Not failed
DT-TTH-HL-06-02	12.7	240	554	62.4	98.5	0.5	22.5	500	57.8	5.6	38.5	392		0.93	PO-CC

Summary of result from the dynamic tension test of Titen HD anchor system is presented on Table 4.18. The result shows a general increase in dynamic capacity of the anchorage system for all three anchor diameters under impact loading. The anchors were also observed to fail in a mixed mode of pull-out and concrete breakout except for one case of steel fracture failure for the 6.4-mm and concrete splitting of the 12.7-mm diameter anchors. The observed failure mode is consistent with studies by Olsen et al.[15] where an optimized screw undercut leads to a mixture of pullout failure at the bottom of the installed anchor with concrete breakout towards the surface of the anchor.

4.3.1.3.1 Behavior Under Dynamic Loading

Nine 6.4-mm diameter Titen HD anchors were tested at drop heights from 60 mm to 100 mm. DT-TTH-QI-01-01, DT-TTH-QI-02-01, and DT-TTH-QI-03-01 were tested at 100 mm drop height resulting in mixed mode pull-out and concrete breakout failure. The resulting peak loads and associated impulses were 28.9 kN (DLR = 1.35), 26.8 kN (DLR=1.25) and 24.2 kN (DLR=1.13) and 331 kN.ms, 101 kN.ms and 85 kN.ms respectively. DT-TTH-QI-04-01 survived impact loading from a decreased drop height of 60 mm with a residual displacement of 4 mm. The peak load and associated impulse from the 60 mm drop height was 27.3 kN (DLR = 1.28) and 503 kN.ms respectively. The anchor failed on subsequent increase of drop height to 65 mm. DT-TTH-QI-05 survived a drop height of 65 mm (DT-TTH-QI-05-01), successfully resisting peak load and associated impulse of 28.2 kN (DLR = 1.32) and 456 kN.ms respectively. DT-TTH-QI-06 was then tested at 70-mm drop height (DT-TTH-QI-06-01) and suffered failure in mixed pull-out and concrete breakout failure mode. The peak load and associated impulse at the 70-mm drop height were 23.5 kN (DLR = 1.10) and 184 kN.ms respectively.

DT-TTH-QI-07-01, DT-TTH-QI-08-01 and DT-TTH-QI-09-01 were tested at drop heights of 70 mm, 80mm, and 70 mm respectively. DT-TTH-QI-07-01 and DT-TTH-QI-09-01 survived the 70 mm drop height before failing at 80 mm drop height (DT-TTH-QI-07-02 and DT-TTH-QI-09-02) in steel fracture failure and pull-out and concrete breakout respectively. DT-TTH-QI-08-01 on the other hand failed in a mixed pull-out and concrete cone breakout mode. The failure cone properties (Table 4.19) gives an average cone failure angle 30° for the 6.4-mm diameter anchors. The typical failure modes are illustrated in Fig. 4.51 and Fig. 4.52 for the 6.4-mm diameter anchors.

Fig. 4.51: Typical Concrete Breakout Failure for 6.4-mm Diameter Anchor System (TTH)

Table 4.19: Concrete Breakout Features of 6.4-mm Diameter Anchors

Test Sample	Pullout	Cone Properties		
	Depth (mm)	Depth (mm)	Diameter (mm)	Angle (Deg)
DT-TTH-QI-01-01	23	27	106	28
DT-TTH-QI-02-01	26	24	58	43
DT-TTH-QI-03-01	20	30	105	31
DT-TTH-QI-08-01	13	37	229	18
Average	19	31	125	30

Fig. 4.52: Typical Steel Fracture Failure for 6.4-mm Diameter Anchor (TTH)

Three 9.5-mm diameter Titen HD anchors were tested from drop heights ranging from 100 mm to 150 mm. DT-TTH-TE-01-01 sustained loading from a drop height of 100 mm, resulting in a 2 mm anchor pullout from the concrete substrate. The resulting peak load and associated impulse from the 100-mm drop height impact loading were 48.8 kN (DLR=1.15) and 766 kN.ms respectively. The anchor failed, under repeated impact loading from a drop height of 110 mm (DT-TTH-TE-01-02), in a mixed pull-out and concrete breakout failure mode (Fig. 4.53). DT-TTH-TE-02 also survived impact loading from drop heights of 110 mm (DT-TTH-TE-02-01 and DT-TTH-02-02),115 mm (DT-TTH-TE-02-03 and DT-TTH-02-04) and 120 mm (DT-TTH-02-05) before failing at a drop height of 125 mm (DT-TTH-TE-02-06). The peak load and associated impulse from drop height 115 mm (DT-TTH-TE-02-03 and DT-TTH-02-04) were 59.3 kN (DLR=1.40) and 840 kN.ms respectively. The anchor sustained a cumulative residual displacement of 8 mm after the

impact loading from drop height of 115 mm. DT-TTH-TE-03 survived drop heights of 120 mm (DT-TTH-TE-03-01), 125 mm (DT-TTH-TE-03-02 and DT-TTH-TE-03-03) and 150 mm (DT-TTH-TE-03-04 and DT-TTH-TE-305) before failing at a repeated loading at 150 mm (DT-TTH-TE-03-06) drop height. The peak load and associated impulse from the impact at the survived 150 mm (DT-TTH-TE-03-04) drop height were 67.2 kN (DLR=1.58) and 893 kN.ms respectively. The anchor sustained a cumulative residual displacement of 24 mm before a mixed pullout and concrete breakout failure mode was observed. The failure cone properties (Table 4.20) gives an average cone failure angle 27° for the 9.5-mm diameter anchors.

Table 4.20: Concrete Breakout Features of 9.5-mm Diameter Anchors

Test Sample	Pullout	Cone Properties		
	Depth (mm)	Depth (mm)	Diameter (mm)	Angle (Deg)
DT-TTH-TE-01-02	23	38	160	27
DT-TTH-TE-02-06	43	18	80	27
DT-TTH-TE-03-06	19	42	185	26
Average	49	33	82	27

Six 12.7-mm diameter Titen HD anchors were tested at drop heights ranging from 200 mm to 260 mm. DT-TTH-HL-01 sustained a drop height of 200 mm (DT-TTH-HL-01-01) resisting a peak load and associated impulse of 68.4 kN (DLR=1.10) and 886 kN.ms respectively with residual displacement of 3 mm. A repeat test on the anchor at 250 mm (DT-TTH-HL-01-02) drop height resulted in mixed mode failure of pull-out and concrete breakout (Fig. 4.54). DT-TTH-HL-02 sustained drop heights of 225 mm (DT-TTH-HL-02-01) and 250 mm (DT-TTH-HL-02-2) before finally failing at 260-mm (DT-TTH-HL-02-03) drop height. The peak load and associated impulse from the 250 mm drop height were 72.1 kN (DLR=1.16) and 736 kN.ms.

Fig. 4.53: Typical Concrete Breakout Failure for 9.5-mm Diameter Anchor System (TTH)

DT-TTH-HL-03 sustained a drop height of 220 mm (DT-TTH-HL-03-01) before failing at a height of 250 mm (DT-TTH-HL-03-02). The peak load and impulse associated with the 220 mm drop height was 89.8 kN (DLR=1.44) and 1130 kN.ms respectively. DT-TTH-HL-04-01 failed in beam splitting mode under impact loading from a drop height of 250 mm. The peak load and associated from this drop height were 80.8 kN (DLR = 1.29) and 1159 kN.ms respectively.

Fig. 4.54: Typical Concrete Breakout Failure for 12.7-mm Diameter Anchor (TTH)

DT-TTH-HL-05 on the other hand sustained the loading from a reduced drop height of 220 mm (DT-TTH-HL-05-01), 225 mm (DT-TTH-HL-05-02), 230 mm (DT-TTH-HL-05-03), 240 mm (DT-TTH-HL-05-04) and 250 mm (DT-TTH-HL-05-05) with cumulative residual displacement of 34 mm before failing at a drop height of 250 mm (DT-TTH-HL-05-06). The peak load and associated impulse of the 220 mm drop height were 89.8 kN (DLR = 1.44) and 1128 kN.ms. DT-TTH-HL-06-01 was tested at a drop height of 240 mm without failure. Repeated testing at the same drop height however led to failure of the anchor system (DT-TTH-HL-06-02). The peak load and associated impulse from the first drop height of 240 mm were 75.9 kN (DLR = 1.22) and 1142 kN.ms respectively. The failure concrete breakout cone properties for Titen HD anchor systems failing in the mixed pullout and concrete breakout failure mode are presented in Table 4.21 and gives an average cone

failure angle of 34° for the 12.7-mm diameter anchors while the typical failure modes are illustrated in Fig. 4.54 and Fig. 4.55.

Table 4.21: Concrete Breakout Properties of 12.7-mm Diameter Titen HD Anchors

Test Sample	Pullout	Cone Properties		
	Depth (mm)	Depth	Diameter (mm)	Angle (Deg)
DT-TTH-HL-03-01	58	34	140	27
DT-TTH-HL-05-06	68	24	150	19
DT-TTH-HL-06-03	57	35	240	17
Average	61	31	179	21

Fig. 4.55: Typical Concrete Beam Splitting for 12.7-mm Diameter Anchor (TTH)

4.3.1.3.2 Stress-Strain Behavior

The stress-strain relationship for the anchors tested in tension showed significant variability in the behavior under impact load tests. For the 6.4-mm diameter anchors (Fig. 4.56), the recorded stress-strain behavior of DT-TTH-QI-08-01 was very different from that of DT-TTH-QI-09-01 in terms of the elastic modulus. DT-TTH-QI-08-01 had an average elastic

modulus of about 55 GPa compared to the average of 230 GPa for DT-TTH-QI-09-01. The elastic modulus of the bare anchor was 206 GPa. The average rate of strain obtained for the 6.4-mm diameter Titen HD anchors was 1.2 /s.

For the 9.5-mm diameter Titen HD anchors (Fig. 4.57), only DT-TTH-TE-01-01 and DT-TTH-TE-01-02 exhibited elastic modulus similar to that of the bare anchor of about 230 GPa. DT-TTH-TE-02-01 and DT-TTH-TE-02-02 exhibited an average elastic modulus of about 100 GPa on the other hand. The average rate of strain obtained for the 9.5-mm diameter anchors was 0.9 /s.

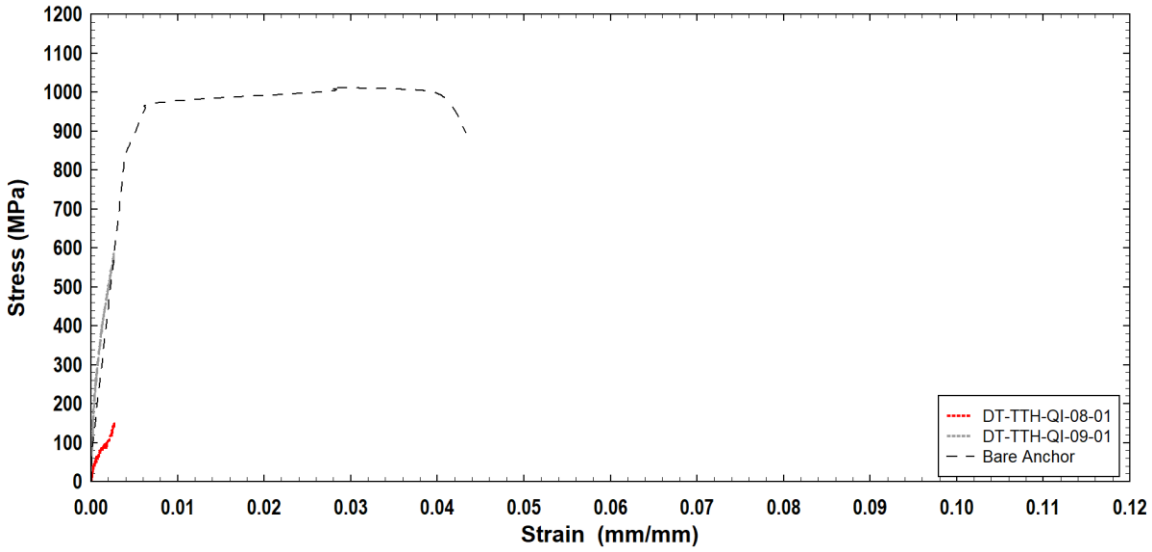

Fig. 4.56: Stress-Strain Response of 6.4-mm Diameter Anchor System in Tension (TTH)

For the 12.7-mm diameter anchor systems (Fig. 4.58), the average elastic modulus was about 45 GPa compared to the average of 230 GPa for the bare anchor tested at a loading rate 36 mm/s.

The average rate of strain for the 12.7-mm diameter anchors was 1.1 /s respectively.

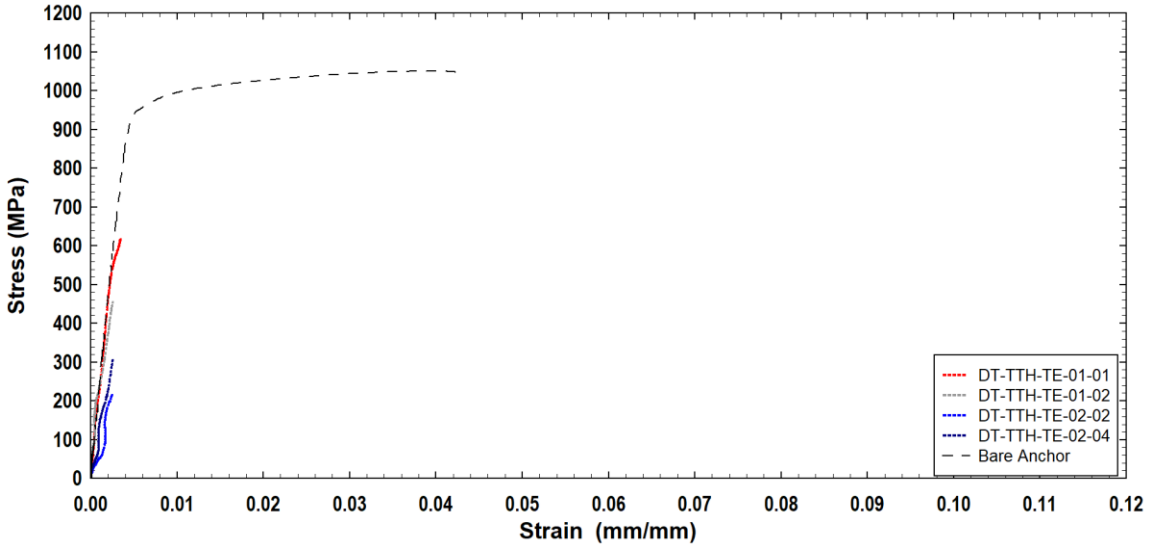

Fig. 4.57: Stress-Strain behavior of 9.5-mm Diameter Anchor System in Tension (TTH)

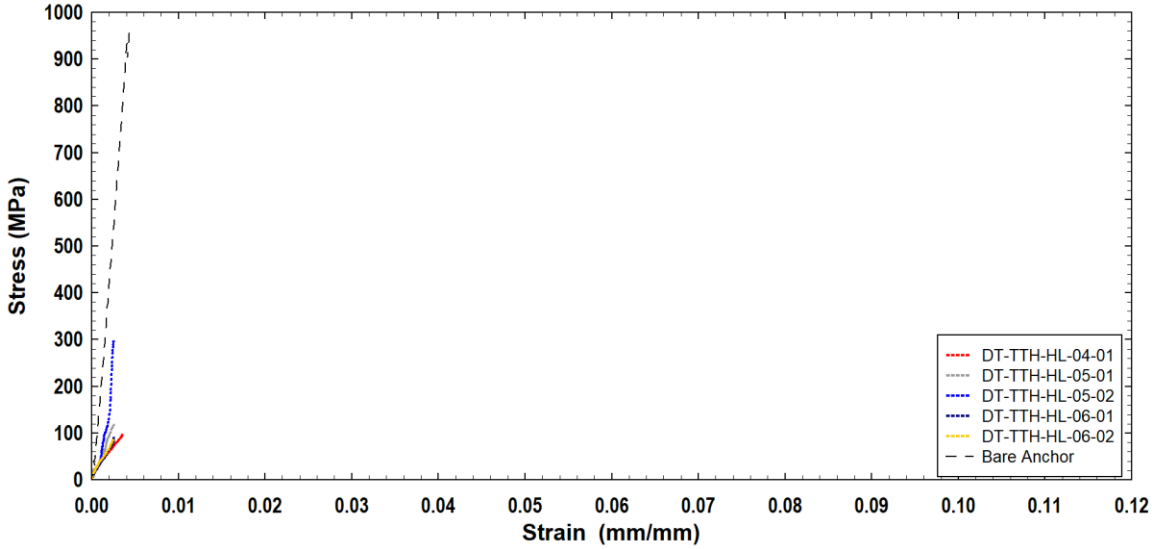

Fig. 4.58: Stress-Strain behavior of 12.7-mm Diameter Anchor System in Tension (TTH)

4.3.1.3.3 Summary and Discussion of Results for Titen HD® Anchors

Generally, the Titen HD anchors showed higher capacity in tension under the dynamic impact loading compared with loading under static conditions, resulting in DLR values greater than 1.0 (Fig. 4.59). A summary of the DLR values plotted against the anchor diameter is shown on Fig. 4.59. The strain rates obtained for these tests ranged from 0.7 to 1.7 /s.

For the 6.4-mm diameter anchors, the minimum DLR that resulted in failure was 1.1 while the maximum DLR that did not result in failure was about 1.5. For the 9.5-mm diameter anchors, the highest DLR that did not result in failure was about 1.6. No 9.5-mm diameter anchors failed under the initial drop mass test. The 12.7-mm diameter anchors failed at DIF of 1.1, however some anchor systems were capable of resisting loading with DIF as high as 1.4, The strain rates achieved for the Titen HD anchor systems varied between 0.9 and 1.2 /s.

Based on the drop testing, a DIF of 1.1 at a strain rate of 1.0 /s is recommended for Titen HD anchors.

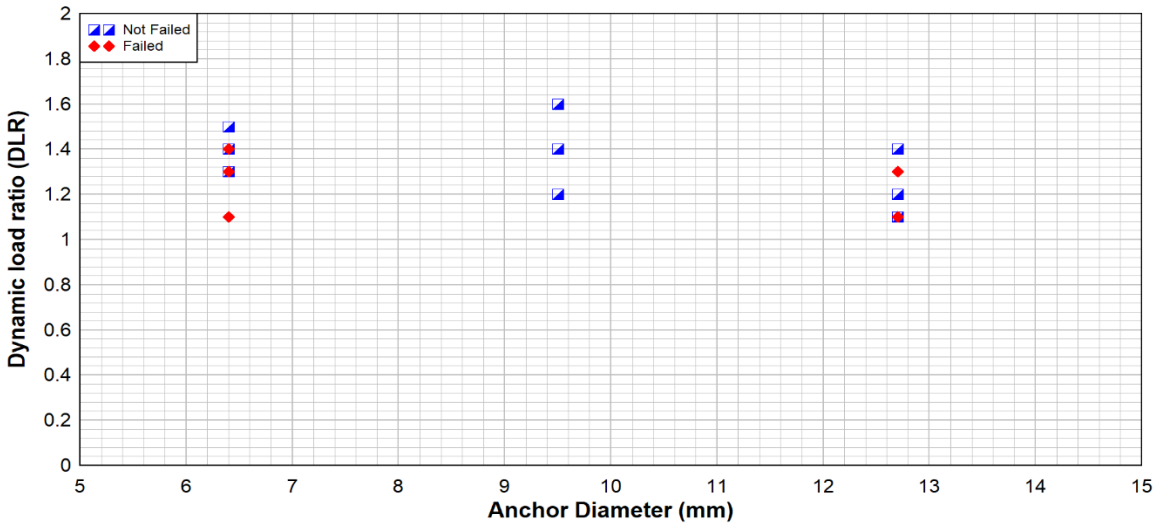

Fig. 4.59: Dynamic Load ratio for Tension Test (TTH)

4.3.2 Shear Test

The dynamic shear tests were carried out as described in Section 3.6.2. The test matrix involved three samples for each type and diameter of the anchors, as presented in Table 4.14.

4.3.2.1 Strong Bolt® 2

The summary of test results for the Strong Bolt® 2 anchors is presented in Table 4.22. The only failure mode recorded under impact drop-mass testing in shear was steel fracture.

4.3.2.1.1 Behavior Under Dynamic Loading

The anchors were tested at drop heights ranging from 15 to 30 mm. DS-STB-QI-01-01 failed in steel fracture mode at a drop height of 30 mm. The peak load and associated impulse were 6.9 kN (DLR = 0.93) and 81 kN.ms respectively. DS-STB-QI-02-01 survived shear loading from a drop height of 15 mm before failing in steel fracture failure under loading from an increased drop height of 20 mm (DS-STB-QI-02-02). The peak load and associated impulse from the impact load at the drop height of 15 mm were 7.0 kN (DLR = 0.95) and 299 kN.ms respectively while for the 20 mm drop height, the peak load was 7.3 kN (DLR = 0.99) with impulse of 40 kN.ms. DS-STB-QI-03-01 also failed under shear loading from a drop height of 20 mm and peak load and associated impulse of 6.8 kN (DLR = 0.92) and 110 kN.ms respectively.

The 9.5-mm diameter Strong Bolt 2 anchors were subjected to impact loading from drop heights ranging from 40 mm to 65 mm. In general, anchor systems failure was recorded at drop heights of 60 mm and 65 mm while no failure was observed under loading from drop heights below 60 mm.

DS-STB-TE-01 survived shear loading from drop height of 40 mm (DS-STB-TE-01-01), 45 mm (DS-STB-TE-01-02), and 50 mm (DS-STB-TE-01-03) before failing in steel fracture failure at a height of 60 mm. The impact loading survived by the anchor at a 50 mm drop height was a peak load of 27.1 kN (DLR = 1.09) and associated impulse of 515 kN.ms. DS-STB-TE-02-01 and DS-STB-TE-02-02 survived a drop heights of 50 and 60 mm respectively before failing at a drop height of 65 mm (DS-STB-TE-02-03).The peak load of 25.8 kN (DLR = 1.04) and an associated impulse of 487 kN.ms were survived at the 60 mm drop height. The anchor failed in steel fracture mode when the drop height was increased to 65 mm (DS-STB-TE-02-03). The impulse and peak load associated with this drop height was 113 kN.ms and 26.2 (DLR = 1.06).

Table 4.22: Summary of Dynamic Shear Results for Strong Bolt 2 Anchors in Shear

Sample	ϕ	h_{ef}	Drop height	PE (mgh)	F_{static}	Compression Load				Tension Load				Disp.	DLR	Observation
						P_c	t_r	t_d	Impulse	P_t	t_r	t_d	Impulse			
	(mm)	(mm)	(mm)	(J)	(kN)	(kN)	(ms)	(ms)	(kN.ms)	(kN)	(ms)	(ms)	(kN.ms)	(mm)		
DS-STB-QI-01-01	6.4	38.1	30	69	7.4	36.9	1.58	11.36	107	6.9	6.0	21.5	81		0.93	SF Failure
DS-STB-QI-02-01	6.4	38.1	15	35	7.4	14.8	2.30	59.80	127	7.0	32.0	56.0	299	5	0.95	Not Failed
DS-STB-QI-02-02	6.4	38.1	20	46	7.4	16.0	2.30	11.50	49	7.3	7.8	15.3	40		0.99	SF Failure
DS-STB-QI-03-01	6.4	38.1	20	46	7.4	18.9	2.00	10.10	92	6.80	18.0	25.8	110		0.92	SF Failure
DS-STB-TE-01-01	9.5	63.5	40	92	24.8	47.7	1.60	59.70	419	19.2	23.2	50.4	435	6	0.77	Not Failed
DS-STB-TE-01-02	9.5	63.5	45	104	24.8	49.0	1.40	48.10	467	24.5	15.7	44.5	505	3	0.99	Not Failed
DS-STB-TE-01-03	9.5	63.5	50	115	24.8	53.0	1.34	47.80	466	27.1	16.2	44.5	515	2	1.09	Not Failed
DS-STB-TE-01-04	9.5	63.5	60	139	24.8	57.6	1.34	11.95	178	21.7	6.4	8.9	69		0.88	SF Failure
DS-STB-TE-02-01	9.5	63.5	50	115	24.8	48.6	1.48	37.00	483	19.9	22.8	56.0	490	8	0.80	Not Failed
DS-STB-TE-02-02	9.5	63.5	60	139	24.8	60.7	1.26	37.20	537	25.8	15.1	45.2	487	3	1.04	Not failed
DS-STB-TE-02-03	9.5	63.5	65	150	24.8	64.0	0.70	19.20	280	26.2	7.1	10.5	113		1.06	SF Failure
DS-STB-TE-03-01	9.5	63.5	60	139	24.8	41.4	1.50	44.80	480	20.5	22.2	48.2	476	7	0.83	Not failed
DS-STB-TE-03-02	9.5	63.5	65	150	24.8	50.8	2.00	22.00	396	24.8	6.6	17.7	253		1.00	SF Failure
DS-STB-HL-01-03	12.7	85.7	210	485	42.5	101.9	0.60	39.44	1063	56.9	17.4	39.0	966	10	1.34	Not failed
DS-STB-HL-01-04	12.7	85.7	230	531	42.5	117.0	0.67	22.20	743	59.4	5.5	17.9	514		1.40	SF Failure
DS-STB-HL-02 -01	12.7	85.7	220	508	42.5	91.6	0.60	41.90	970	49.4	17.4	44.0	995	9	1.16	Not Failed
DS-STB-HL-02 -02	12.7	85.7	230	531	42.5	116.7	0.78	35.80	1097	61.1	5.5	39.3	1083	2	1.44	Not failed
DS-STB-HL-02 -03	12.7	85.7	250	577	42.5	116.0	1.23	22.90	858	62.3	14.0	17.2	612		1.47	SF Failure
DS-STB-HL-03 -01	12.7	85.7	240	554	42.5	111.0	1.45	41.00	858	58.6	16.2	41.7	1182	4	1.38	Not Failed
DS-STB-HL-03 -02	12.7	85.7	250	577	42.5	118.0	0.80	38.80	1019	65.3	13.3	34.2	1079	2	1.54	Not failed
DS-STB-HL-03 -03	12.7	85.7	260	600	42.5	120.0	0.72	13.50	456	61.1	5.5	8.0	220		1.44	SF Failure

DS-STB-TE-03 also survived a drop height of 60 mm (DS-STB-TE-03-01) before failing at a drop height of 65 mm (DS-STB-TE-03-02) in steel fracture failure. The sustained impulse was 476 kN.ms while a peak load of 20.5 kN resulted in DLR of 0.83. The impulse resulting from the failed test however was 253 kN.ms with a peak load of 24.8 kN leading DLR of 1.00.

The 12.7-mm diameter Strong-Bolt 2 anchors were tested at drop heights ranging from 120 mm to 260 mm. All of the anchors survived the first drop height before failing on subsequent test. DS-STB-HL-01 survived a drop height of 120 mm (DS-STB-HL-01-01), 150 mm (DS-STB-HL-01-02) and 210 mm (DS-STB-HL-01-03) before failing at 230 mm. The impulse sustained at the 210-mm (DS-STB-HL-01-03) drop height was 966 kN.ms while the peak load of 56.9 kN resulted in a DLR of 1.34. For the 230-mm drop height where the anchor failed, the impulse was 514 kN.ms while the DLR was 1.4 was obtained from the peak load of 59.4 kN.

For DS-STB-HL-02, testing started at 220 mm (DS-STB-HL-02-01) and increased to 230 mm (DS-STB-HL-02-02) and finally to 250 mm (DS-STB-HL-02-03) when failure occurred. The impulse resisted at the drop height of 230 mm was 1083 kN.ms while the peak load of 61.1 kN resulted in DLR of 1.44. An impulse and peak load of 612 kN-ms and 62.3 kN (DLR = 1.47) respectively were observed for the test at 250-mm drop height.

For DS-STB-HL-03, testing commenced at a drop height of 240 mm (DS-STB-HL-03-01), increased to 250 mm (DS-STB-HL-03-02) before failing finally at a height of 260 mm (DS-STB-HL-03-03). The impulse sustained at the 250 mm drop height was 1079 while the peak load was 65.3 kN (DLR = 1.54). For the 260-mm drop height, the impulse was 220 kN.ms while the peak load was 61.1 kN (DLR = 1.44).

4.3.2.1.2 Summary and Discussion of Results for Strong Bolt® Anchors

The Strong-Bolt 2 anchors exhibited consistent steel fracture failure mode for all three anchor diameters tested. Failure loads however exhibited some level of variability. While the 6.4-mm and 9.5-mm diameter anchors showed shear capacities close to the static failure load, the 12.7-mm diameter anchors consistently showed capacities substantially higher than the static failure load, even in cases of retesting of the anchors at increased drop heights.

The results also showed that anchors that did not fail were able to sustain higher impulse than anchors that failed even though, in general, peak loads for anchors that did not fail were less than those that resulted in anchor failure .Fig. 4.60 illustrates the variation of the DLR with the anchor diameter tested under dynamic shear conditions. The minimum DLR that resulted in failure for the 6.4-mm diameter anchors was the same as the maximum recorded DLR that resulted in failure. In this regard, a DIF of 0.9 is recommended for of the 6.4-mm diameter anchor. For the 9.5-mm diameter anchors, the minimum DLR that led to failure was 1.0 while the maximum DLR that did not result in failure was about 1.1. For the 12.7-mm diameter anchors, the minimum DLR that resulted in failure was 1.4 while the maximum DLR that did not result in failure was 1.5.

Based on the drop-mass test, a DIF of 0.8 is recommended for the 6.4 mm and 9.5 mm diameter anchors while DIF 1.2 are recommended for the 12.7 mm diameter anchors.

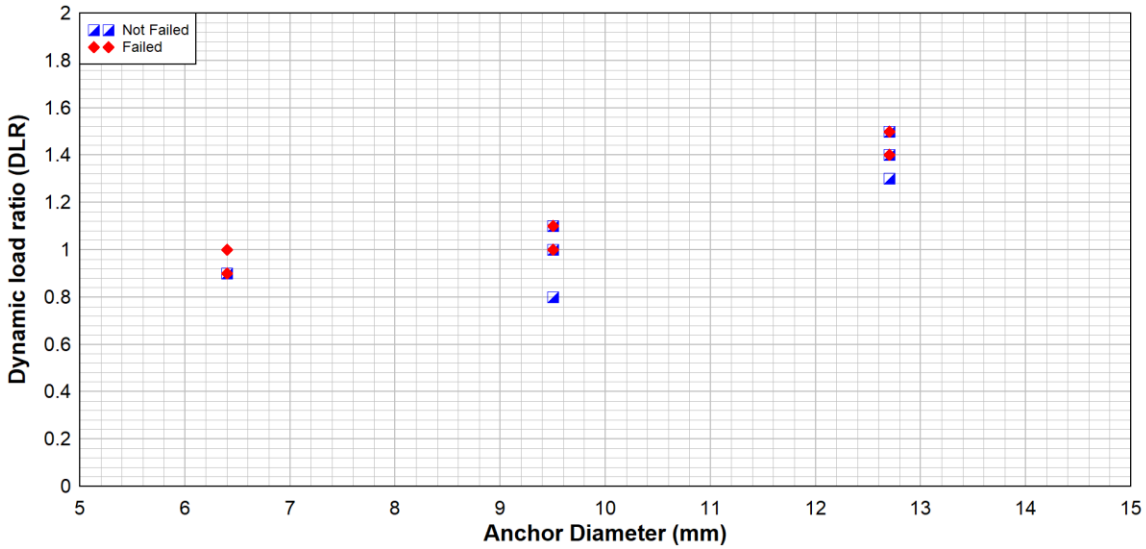

Fig. 4.60: Dynamic Load Ratio for Shear Test (STB)

4.3.2.2 Wedge-All®

Table 4.23 provides a summary of the experimental results for the Wedge-All anchors tested under shear loading. Similar to the Strong Bolt 2 anchors, all the anchors failed in steel fracture mode except for one 12.7-mm diameter anchor system where beam splitting failure was observed (Fig. 4.61).

4.3.2.2.1 Behavior Under Dynamic Loading

The 9.5-mm diameter Wedge-All anchors were tested at drop heights ranging from 40 mm to 60 mm. DS-WA-TE-01 sustained impact loads from drop heights of 40 mm (DS-WA-TE-01-01) and 50 mm (DS-WA-TE-01-02) before failing in steel fracture mode at a drop height of 60 mm (DS-WA-TE-01-03). The 50-mm drop height resulted in a peak load and associated impulse of 21.2 kN (DLR = 1.02) and 497 kN.ms respectively. The loading from the drop height that resulted in failure consisted of a peak load of 22.5 kN (DLR = 1.08) and associated impulse of 128 kN.ms .

Table 4.23: Summary of Dynamic Shear Test Results for Wedge-All Anchors

Sample	ϕ	h_{ef}	Drop height	PE (mgh)	F_{static}	Compression Load				Tension Load				Disp.	DLR	Observation
						P_c	t_r	t_d	Impulse	P_t	t_r	t_d	Impulse			
	(mm)	(mm)	(mm)	(J)	(kN)	(kN)	(ms)	(ms)	(kN.ms)	(kN)	(ms)	(ms)	(kN.ms)	(mm)		
DS-WA-TE-01-01	9.5	67.0	40	92	20.8	26.3	1.6	46.4	430	16.6	22.4	50.0	325	5	0.80	Not failed
DS-WA-TE-01-02	9.5	67.0	50	115	20.8	39.3	1.3	43.0	523	21.2	17.0	50.7	497	2	1.02	Not failed
DS-WA-TE-01-03	9.5	67.0	60	139	20.8	48.0	1.3	19.5	221	22.5	7.0	12.6	128		1.08	SF Failure
DS-WA-TE-02-01	9.5	67.0	55	127	20.8	34.4	1.4	46.7	325	19.7	22.4	54.5	501	6	0.95	Not failed
DS-WA-TE-02-02	9.5	67.0	60	139	20.8	46.4	1.3	22.9	277	24.1	15.8	19.7	306		1.16	SF Failure
DS-WA-TE-03-01	9.5	67.0	55	127	20.8	38.9	1.2	48.5	466	20.9	22.6	56.8	525	7	1.01	Not failed
DS-WA-TE-03-02	9.5	67.0	60	139	20.8	54.0	1.2	23.4	427	24.0	6.5	19.3	285		1.15	SF Failure
DS-WA-HL-01-01	12.7	86.0	250	577	51.5	99.1	1.3	33.9	695	62.0	15.1	36.0	1078	7	1.20	Not failed
DS-WA-HL-01-02	12.7	86.0	260	600	51.5	112.3	1.5	11.3	334	70.8	5.0	7.5	176		1.37	SF Failure
DS-WA-HL-02-03	12.7	86.0	260	600	51.5	121.7	1.2	31.3	1155	73.5	13.8	32.6	1217	15	1.43	Not failed
DS-WA-HL-02-04	12.7	86.0	260	599	51.5	128.0	0.7	26.4	1050	76.2	13.1	26.9	924		1.48	BS Failure
DS-WA-HL-03-01	12.7	86.0	255	588	51.5	94.0	1.7	39.9	711	58.1	16.8	39.4	1087	10	1.13	Not failed
DS-WA-HL-03-02	12.7	86.0	260	599	51.5	85.7	0.2	38.5	757	70.0	13.9	36.5	1172	4	1.36	Not failed
DS-WA-HL-03-03	12.7	86.0	270	622	51.5	86.4	0.1	24.7	580	72.8	13.8	18.9	702		1.41	SF Failure

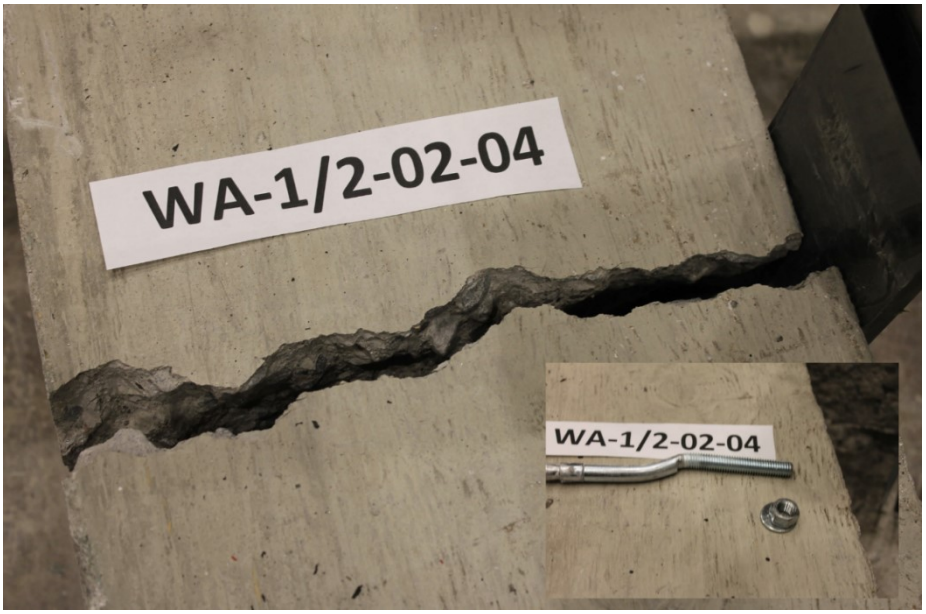

Fig. 4.61: Beam Split Failure Preceded by Excessive Bending of Anchor

Testing of DS-WA-TE-02 commenced at a drop height of 55 mm (DS-WA-TE-02-01) without failure. An increase in drop height to 60 mm (DS-WA-TE-02-02) resulted in steel fracture failure. The impact loading resisted at the 55-mm drop height consisted of a peak load of 19.7 kN (DLR = 0.95) and impulse of 501 kN.ms. The impact loading from the drop height that resulted in failure on the other hand consisted of a peak load of 24.1 kN (DLR = 1.16) and impulse of 306 kN.ms . Drop-mass testing of DS-WA-TE-03 also commenced at 55-mm drop height (DS-WA-TE-03-01) before also failing at 60-mm drop height (DS-WA-TE-03-02). The impulse and peak load from the sustained drop height were 525 kN.ms and 20.9 kN (DLR = 1.01), while those from the drop height that resulted in failure were 285 kN.ms and 24 kN (DLR = 1.15).

The 12.7-mm diameter anchors were tested at drop heights ranging from 250 mm to 270 mm. DS-WA-HL-01 sustained drop height of 250 mm (DS-WA-HL-01-01) before failing in steel fracture mode at a drop height of 260 mm (DS-WA-HL-01-02). The impact loading sustained at the 250-mm drop height consisted of a peak load of 62 kN (DLR = 1.20) and

impulse of 1078 kN.ms. The shear loading resulting from the drop height that resulted in failure was a peak load of 70.8 kN (DLR = 1.37) and impulse of 176 kN.ms. DS-WA-HL-02 on the other hand survived three impact loading from a drop heights of 250 mm (DS-WA-HL-02-01), 255 mm (DS-WA-HL-02-02) and 260 mm (DS-WA-HL-02-03) before failing on the fourth impact loading by concrete beam splitting from the same drop height of 260 mm (DS-WA-HL-02-04). The failure resulted in bending of the anchor. The maximum impact loading sustained by the anchor before failure were a peak load of 73.5 kN (DLR = 1.43) and impulse of 1217 kN.ms. The impact load that resulted in beam splitting was a peak load of 76.2 kN (DLR = 1.48) and impulse of 924 kN.ms. DS-WA-HL-03 sustained impact loads from drop heights of 255 mm (DS-WA-HL-03-01) and 260 mm (DS-WA-HL-03-02) before failing in steel fracture failure at a drop height of 270 mm (DS-WA-HL-03-03). The impulse and peak load associated with the 260-mm drop height were 70 kN (DLR = 1.36) and 1172 kN.ms. The impact loading associated with the 270 mm drop height consisted of a peak load of 72.8 kN (DLR = 1.41) and impulse of 702 kN.ms.

4.3.2.2.2 Summary and Discussion of Results for Wedge-All®

Except for one case where the shear test resulted in beam fracture with considerable bending of a 12.7-mm diameter anchor, all the Wedge-All anchors failed in steel fracture mode under dynamic shear loading. The failure mode was consistent with the failure mode recorded under the static testing condition.

In all the tests, the anchor capacities under dynamic testing were greater than the static capacities, resulting in DLR values of anchor systems that resulted in failure to be more than unity (Fig. 4.62).

For the 9.5-mm diameter anchors, the minimum DLR that resulted in failure was 1.1 while the maximum DLR that did not result in failure was 0.95. For the 12.7-mm diameter anchors, maximum DLR of 1.4 did not result in failure while a minimum DLR of 1.4 resulted in failure of an anchor that did not fail on the first attempt.

Based on the result of the drop-mass test, a DIF of 1.0 is recommended for the 9.5-mm diameter while a DIF of 1.2 may be recommended for the 12.7-mm diameter anchors in shear.

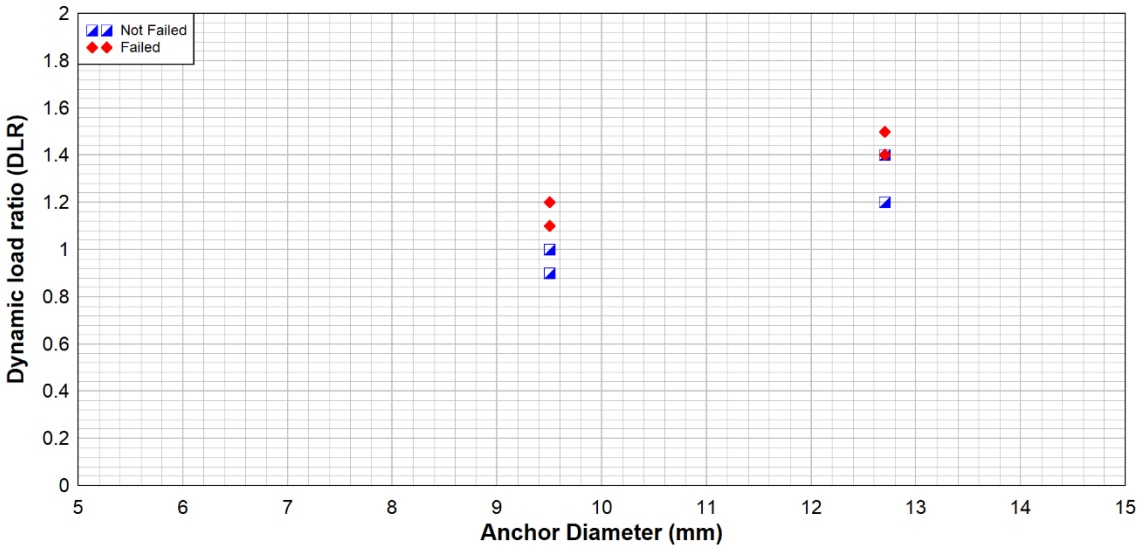

Fig. 4.62: Dynamic Load Ratio for Shear Test (WA)

4.3.2.3 Titen HD®

The experimental test results for the Titen HD tested under dynamic shear loading are summarized in Table 4.24 shows consistent steel fracture failure for all the anchors. The table also shows that except for the 6.4-mm diameter anchors, the 9.5-mm and 12.7-mm diameters have higher dynamic capacities than static capacities with DLRs greater than 1.0.

Table 4.24: Summary of Dynamic Shear Test Results for Titen HD Anchor

Sample	ϕ	h_{ef}	Drop height	PE (mgh)	F_{static}	Compression Load				Tension Load				Disp	DLR	Observation
						P_c	t_r	t_d	Impulse	P_t	t_r	t_d	Impulse			
	(mm)	(mm)	(mm)	(J)	(kN)	(kN)	(ms)	(ms)	(kN.ms)	(kN)	(ms)	(ms)	(kN.ms)	(mm)		
DS-TTH-QI-01-01	6.4	49.3	20	46	18.1	26.9	1.1	76.6	293	9.2	39.4	75.6	344	5	0.51	Not failed
DS-TTH-QI-01-02	6.4	49.3	30	69	18.1	38.4	1.4	68.8	346	13.1	22.1	63.7	425	3	0.72	SF Failure
DS-TTH-QI-01-03	6.4	49.3	40	92	18.1	47.2	1.4	27.4	284	15.9	17.6	24.7	234		0.88	SF Failure
DS-TTH-QI-02-01	6.4	49.3	30	69	18.1	44.2	1.5	64.5	380	14.6	26.6	57.6	428	5	0.81	Not failed
DS-TTH-QI-02-02	6.4	49.3	40	92	18.1	43.0	1.6	27.3	270	18.8	16.9	24.0	247		1.04	SF Failure
DS-TTH-QI-03-01	6.4	49.3	30	69	18.1	40.3	1.4	68.5	300	11.3	36.4	65.9	401	5	0.62	Not failed
DS-TTH-QI-03-02	6.4	49.3	35	81	18.1	36.0	1.6	51.7	283	14.2	21.0	55.1	398	5	0.78	Not failed
DS-TTH-QI-03-03	6.4	49.3	35	81	18.1	31.7	1.6	23.7	195	16.5	15.7	19.2	160		0.91	SF Failure
DS-TTH-TE-01-02	9.5	61.0	50	115	37.4	62.3	1.4	44.4	754	28.6	15.6	40.1	508	5	0.76	Not failed
DS-TTH-TE-01-03	9.5	61.0	70	162	37.4	67.8	1.4	44.2	793	33.4	16.5	42.4	618	2	0.89	Not failed
DS-TTH-TE-01-04	9.5	61.0	120	277	37.4	96.4	0.2	25.6	707	44.0	15.1	20.2	467		1.18	SF Failure
DS-TTH-TE-02-01	9.5	61.0	80	185	37.4	46.5	0.9	45.2	503	29.4	21.2	46.0	589	5	0.79	Not failed
DS-TTH-TE-02-02	9.5	61.0	100	231	37.4	58.8	1.6	40.9	535	37.6	14.8	37.6	669	1	1.01	Not failed
DS-TTH-TE-02-03	9.5	61.0	120	277	37.4	66.0	0.6	39.4	584	44.9	14.8	38.5	756	2	1.20	Not failed
DS-TTH-TE-02-04	9.5	61.0	140	323	37.4	76.6	0.1	21.8	332	40.0	7.1	16.5	413		1.07	SF Failure
DS-TTH-TE-03-01	9.5	61.0	140	323	37.4	60.0	1.4	40.4	545	38.9	18.9	41.1	796	8	1.04	Not failed
DS-TTH-TE-03-02	9.5	61.0	150	346	37.4	71.4	0.3	37.1	623	50.1	15.3	38.7	883	2	1.34	Not failed
DS-TTH-TE-03-03	9.5	61.0	160	369	37.4	75.0	0.3	19.1	306	47.4	6.9	10.6	198		1.27	SF Failure
DS-TTH-HL-01-01	12.7	75.9	250	577	73.4	93.9	1.2	34.6	767	73.8	14.5	23.7	1107	4	1.01	Not failed
DS-TTH-HL-01-02	12.7	75.9	270	622	73.4	99.3	1.6	30.5	892	84.8	12.7	28.8	1188	1	1.16	Not failed
DS-TTH-HL-01-03	12.7	75.9	300	693	73.4	110.6	0.4	31.0	985	92.7	12.4	29.1	1262	1	1.26	Not Failed
DS-TTH-HL-01-04	12.7	75.9	330	762	73.4	108.6	2.2	20.4	776	97.4	13.0	14.4	675		1.33	SF Failure
DS-TTH-HL-02-01	12.7	75.9	310	716	73.4	96.3	0.5	36.0	870	69.2	18.6	32.7	1222	7	0.94	Not failed
DS-TTH-HL-02-02	12.7	75.9	330	762	73.4	92.4	0.4	32.4	990	83.9	11.6	31.4	1376	1	1.14	Not failed
DS-TTH-HL-02-03	12.7	75.9	360	831	73.4	122.8	0.2	34.7	1107	95.0	11.7	30.6	1453	1	1.29	Not Failed
DS-TTH-HL-02-04	12.7	75.9	370	854	73.4	123.4	0.32	20.9	767	89.9	12.1	15.0	662		1.22	SF Failure
DS-TTH-HL-03-01	12.7	75.9	350	807	73.4	108.1	1.7	37.3	950	76.2	14.8	35.2	1342	7	1.04	Not failed
DS-TTH-HL-03-02	12.7	75.9	370	854	73.4	107.7	1.5	32.3	980	94.0	13.0	31.9	1436	2	1.28	Not Failed
DS-TTH-HL-03-03	12.7	75.9	390	901	73.4	109.1	1.9	20.5	671	95.6	4.6	14.4	705		1.30	SF Failure

4.3.2.3.1 Behavior Under Dynamic Loading

Three 6.4-mm diameter Titen HD anchors were tested at drop heights ranging from 20 mm to 40 mm. All the anchors survived the initial drop-mass testing and failed in steel fracture mode under repeated impact loading.

DS-TTH-QI-01 survived impacts from drop heights of 20 mm (DS-TTH-QI-01-01) and 30 mm (DS-TTH-QI-01-02) before failing at a drop height of 40 mm (DS-TTH-QI-01-03). The impulse load sustained from the 30-mm drop height consisted of an impulse of 425 kN.ms and peak load of 13.1 kN (DLR = 0.72) The impact loading causing failure of the anchor at a drop height of 40 mm was an impulse of 234 kN.ms and peak load of 15.9 kN (DLR = 0.88). DS-TTH-QI-02 also sustained the impact loading from a drop height of 30 mm (DS-TTH-QI-02-01) before failing at the increased drop height of 40 mm (DS-TTH-QI-02-02). The impact load from the drop height of 30 mm consisted of a peak load of 14.6 kN (DLR = 0.81) and associated impulse of 428 kN.ms while the peak load and associated impulse of drop height causing failure was 18.8 kN (DLR = 1.04) and 247 kN.ms respectively. For DS-TTH-QI-03, drop heights of 30 mm (DS-TTH-QI-03-01) and 35 mm (DS-TTH-QI-03-02) were sustained without failure. Upon retesting at the drop height of 35 mm (DS-TTH-QI-03-03), the anchor system suffered steel fracture failure. The impact loading from DS-TTH-QI-03-02 drop height resulted in an impulse of 398 kN.ms and peak load of 14.2 kN (DLR = 0.78). For the drop height that resulted in failure (DS-TTH-QI-03-03), the impulse was 160 kN.ms while the peak load was 16.5 kN (DLR = 0.91).

The 9.5-mm diameter Titen HD anchors were tested at drop heights from 50 mm to 160 mm. Similar to the 6.4-mm diameter anchors, the 9.5-mm diameter anchors survived the loading from the initial impact tests before failing on repeated impact tests.

DS-TTH-TE-01 resisted the impact loading from drop heights of 50 mm (DS-TTH-TE-01-01 and DS-TTH-TE-01-02) and 70 mm (DS-TTH-TE-03) before finally failing at a drop height of 120 mm (DS-TTH-TE-01-04). The impulse survived under the 70-mm drop height was 618 kN.ms while a DLR of 0.89 was calculated from the peak load of 33.4 kN. The impulse and peak load recorded when the anchor failed at the drop height of 120 mm were 467 kN.ms and 44.0 kN (DLR = 1.18).

DS-TTH-TE-02 was then tested starting from drop height of 80 mm (DS-TTH-TE-02-01), increasing to 100 mm (DS-TTH-TE-02-02), and 120 mm (DS-TTH-TE-02-03) before it failed at 140 mm (DS-TTH-TE-02-04). The impulse from the 120-mm drop height was 756 kN.ms with peak load of 44.9 kN (DLR = 1.20). For the 140-mm drop height where the anchor failed, the impulse was 413 kN.ms with peak load of 40 kN (DLR = 1.07). Since the result of DS-TTH-TE-02-04 showed lower residual capacity compared to DS-TTH-TE-03, it was not considered in determining the capacity of the anchor. DS-TTH-TE-03 sustained impact from drop heights of 140 mm (DS-TTH-TE-03-01) and 150 mm (DS-TTH-TE-03-02) before failing at a drop height of 160 mm (DS-TTH-TE-03-03). The impulse and peak load for the 150-mm drop height were 883 kN.ms and 50.1 kN (DLR = 1.34) while the impulse and peak load from the 160-mm drop height were 198 kN.ms and 47.4 kN (DLR = 1.27).

The 12.7-mm diameter anchors were tested at drop heights from 250 mm to 390 mm. All the anchors failed in steel fracture mode after surviving at least one impact from varied drop heights.

DS-TTH-HL-01 survived impacts from drop heights of 250 mm (DS-TTH-HL-01-01), 270 mm (DS-TTH-HL-01-02) and 300 mm (DS-TTH-HL-01-03) before failing at a drop height

of 330 mm (DS-TTH-HL-01-04). The impulse and peak load of the 300-mm drop height were 1262 kN.ms and 92.7 kN (DLR = 1.26), while the impulse from the failed anchor was 675 kN.ms with peak load of 97.4 kN, (DLR = 1.33). DS-TTH-HL-02 survived impact loading from drop heights of 310 mm (DS-TTH-HL-02-01), 330 mm (DS-TTH-HL-02-02) and 360 mm (DS-TTH-HL-02-03) before failing at a drop height of 370 mm (DS-TTH-HL-02-04). The resulting impulse and peak load from the 360-mm sustained drop height were 1453 kN.ms and 95 kN (DLR = 1.29). For the 370-mm drop height that resulted in failure, the impulse was 662 kN.ms while the peak load of 95.0 kN resulted in a DLR of 1.23. Again, DS-TTH-HL-02-04 was not considered in assessing the anchor capacity as the peak load was less than DS-TTH-HL-02-03. DS-TTH-HL-03 sustained impacts from drop heights of 350 (DS-TTH-HL-03-01) and 370 mm (DS-TTH-HL-03-02) before failing at 390 mm (DS-TTH-HL-03-03). The sustained impulse at 370-mm drop height was 1436 kN.ms with peak load of 94 kN (DLR = 1.28). For the drop height that resulted in failure, the impulse and peak load were 705 kN.ms and 95.6 kN (DLR = 1.30) respectively.

4.3.2.3.2 Summary and Discussion of Results for Titen HD®

All anchors failed in steel fracture mode for all three diameters of anchors. However, except for the 6.4-mm diameter anchors, the anchors exhibited higher capacities under dynamic loading conditions compared to the static loading as can be seen from Fig. 4.63.

The 6.4-mm diameter anchors show a maximum DLR that did not result in failure of 0.81 while the minimum DLR that resulted in failure was 0.88. For the 9.5-mm diameter anchors, the maximum DLR that did not result in failure was 1.34 while the minimum DLR that resulted in failure was 1.18. For the 12.7-mm diameter, the maximum DLR that did not result in failure was 1.29 while the minimum DLR that resulted in failure was 1.30.

Again, it has been pointed out that the DLRs corresponding to failed tests were a representation of the residual capacity as the anchor had sustained loads from other drop heights.

Based on the experimental test results. DIF of 0.8 is recommended for the 6.4-mm diameter anchors, while a value of 1.2 is recommended for the 9.5- and 12.7-mm diameters.

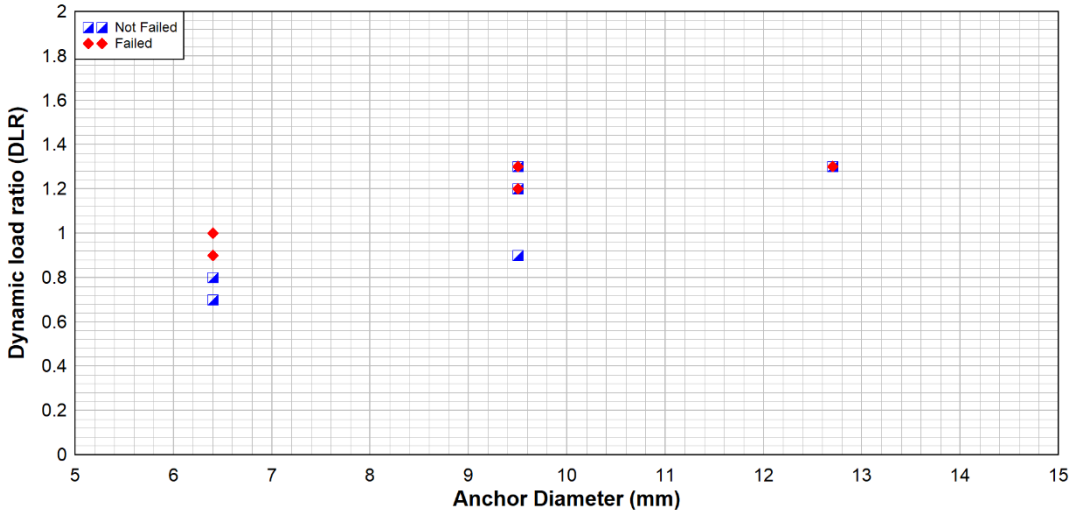

Fig. 4.63: Dynamic Load Ratio for Shear Test (TTH)

4.4 Summary and Discussion of the Experimental Results

4.4.1 Failure Mode

The anchors exhibited consistent failure modes in shear, with all the anchors failing in steel fracture failure, except in one case in the 12.7-mm diameter Wedge-All® where concrete beam splitting failure was preceded by bending of the anchor without fracture. The steel fracture failure was expected as the edge distance was chosen to preclude concrete breakout failure with effective bearing lengths out of the range that would lead to pryout failure.

For the tensile test, a variety of failure modes were recorded with respect to the static and dynamic tests. For the torque-controlled expansion anchors (Strong-Bolt 2 and Wedge-All), all the 6.4-mm and 9.5-mm diameter anchors failed in steel fracture failure under static conditions. Under the same static test conditions, two of the 12.7-mm diameter

Strong-Bolt 2 anchors failed in concrete breakout failure while one failed in splitting of the beam. For the 12.7-mm diameter Wedge-All anchors under static testing conditions, all the anchors failed in pull-through mode.

Under dynamic testing conditions in tension, 29 out of 32 tested torque-controlled expansion anchors failed in pull-through mode. Two steel fracture failures were recorded, one each for the 6.4-mm and 9.5-mm diameter Strong Bolt® 2 anchors with one 9.5-mm diameter Strong Bolt® failing in concrete breakout mode. Additionally, one sample of the 12.7-mm diameter Strong Bolt® 2 anchor resulted in splitting of the testing beam.

For the screw anchors, except for one case of steel fracture and beam splitting, all tested anchors failed in a mixed mode of pull-out and concrete break under both static and dynamic test conditions in tension. The average cone failure for angles for the static test were 27°, 25° and 18° for the 6.4-mm, 9.5-mm and 12.7-mm diameter anchors while the failure cone angles for the dynamic tests were slightly higher at 29°, 26° and 21° for the 6.4-mm, 9.5-mm and 12.7-mm diameters respectively.

4.4.2 Failure Loads

The anchors showed a general increase in dynamic failure loads in tension compared with the failure loads under static conditions. The 12.7-mm diameter Wedge-All® anchors however had lower dynamic capacities compared to the static capacities in tension. Again, among the torque-controlled expansion anchors, it was the 12.7-mm diameter Wedge-All® anchors that exhibited the same mode of failure under both static and dynamic loading conditions.

For shear loading, the anchor capacity under dynamic conditions were lower than those for the static condition for the 6.4-mm diameter Strong-Bolt 2 and Titen HD. However, for the

9.5-mm and 12.7-mm diameter anchors, all the three different anchor types showed higher dynamic capacities than static capacities.

5 Chapter: Conclusions and Recommendations

5.1 Summary

The research was carried out to assess the effects of impact loading on three different proprietary post-installed anchors, namely Strong Bolt® 2, Wedge-All® and Titen HD® using a drop-mass system. The first two anchors were torque-controlled expansion anchors while the third anchor was a screw anchor. Three different diameters (6.4 mm, 9.5 mm and 12.7 mm) of Strong-Bolt 2 and Titen HD were tested while only two different diameters (9.5 mm and 12.7mm) of the Wedge-All anchors were tested.

The first part of the test involved establishing the static capacities of each anchor while the second part of the testing involved establishing the dynamic capacity of the anchors. The static test was carried out in a static loading frame with the main force imparting unit being a 245-kN double-acting hydraulic actuator. The dynamic capacity was established using a 235-kg drop-mass tower in conjunction with a lever system designed generate a mechanical advantage of 1. The strain rate for the static test was in the order of 10^{-4} /s, while the strain rate observed in the dynamic test was in the order of 10^{0} /s.

The static capacities and failure modes were compared with predictions of the CCD method. The failure modes under dynamic conditions were assessed and compared qualitatively with the failure modes under the static tests.

For anchor capacities, the dynamic failure loads were compared with the average static capacities to obtain a DLR. A DIF value was then recommended from the range of DLR values to ensure safe designs based on both the anchor diameter and the stress on the anchor.

5.2 Conclusions

The following conclusions were arrived at from the results of the experimental investigation:

- For the screw anchors, the predominant mode of failure in tension under both static and dynamic conditions is a mix mode of anchor pull-out and concrete cone breakout.
- For torque-controlled expansion anchors, while different modes of failure were observed under static loading conditions, the predominant failure mode under dynamic conditions was anchor pull-through.
- Increased loading rate results in increased anchor capacity in tension for the screw anchors tested. For torque-controlled expansion anchors when the failure in static and dynamic conditions are pull-through, the dynamic capacity is lower.
- For Strong Bolt® 2, DIFs of 0.6, 1.2 and 1.2 are recommended for 6.4-mm, 9.5-mm and 12.7-mm diameter anchors in tension and 0.8, 1.0 and 1.2 for the 6.4-mm, 9.5-mm, and 12.7-mm diameter anchors in shear.
- For Wedge-All, DIF of 0.6 is recommended for the 9.5-mm and 12.7-mm diameter anchors in tension and DIFs of 1.0 and 1.2 are recommended for the 9.5-mm and 12.7-mm diameter anchors in shear.
- For Titen HD, DIF of 1.1 is recommended for 6.4-mm, 9.5-mm and 12.7-mm diameter anchors in tension while DIFs of 0.8, 1.2 and 1.2 are recommended for the 6.4-mm, 9.5-mm, and 12.7-mm diameters in shear.

5.3 Research Limitations

The following are the limitations associated with the research:

I. The research presented only assessed the capacity of the anchors under manufacturer defined embedment depths. These presents a limitation as those depths may not adequately reflect the required depths for a preferred failure mode under dynamic conditions as the reaction of the concrete and steel anchor responds differently to change in strain rate.

II. Failure loads under dynamic testing were bracketed between the lowest load that caused failure on the anchor and the highest load that did not cause the anchor to fail. This was quite challenging as it is obvious that an un-failed anchor would retain a capacity, albeit lower than the capacity of an untested one. Numerous tests with closely spaced parameter changes would have to be performed in order to adequately estimate the exact failure load under dynamic conditions. This would be extremely time consuming as well as expensive as more anchors and concrete substrate materials would be employed.

III. Though strain rates in the order of 10^{-4} /s obtained under the static loading condition was within the quasi-static range, those achieved under the dynamic condition were of the order of 10^{0} /s, which would describe rates only under Impulsive regime. Tests under higher strain rates may lead to different results. Test setup that would achieve these rates would need to be explored for further research.

5.4 Recommendations

The following are recommendation for further research:

- Different embedment to ensure concrete breakout failure should be explored for each anchor to fully understand the concrete failure capacities.
- Further testing of Titen HD anchors to confirm the concrete cone breakout angles
- Pull-through capacities for the torque-controlled expansive anchors should be investigated under static loading conditions in order to compare with the dynamic capacities under similar failure modes.
- Higher loading rates should be explored in future research as the strain-rate obtained in the current research is only in the order of 10^0 /s.

References

[1] M. Lee Marsh and E. G. Burdette, “Anchorage of Steel Building Components To Concrete.,” *Eng. J.*, vol. 22, no. 1, pp. 33–39, 1985.

[2] CSA (Canadian Standards Association), “Design of Concrete Structures,” *CAN/CSA S23.3- 14*, 2014.

[3] ACI Committee 318, *Building Code Requirements for Structural Concrete (ACI 318-08)*. 2008.

[4] ACI Committe 349, “ACI 349-06: Code Requirements for Nuclear Safety-Related Concrete Structures and Commentary.” p. 196, 2014.

[5] W. Fuchs, R. Eligehausen, and J. E. Breen, “Concrete capacity design (CCD) approach for fastening to concrete,” *ACI Struct. J.*, vol. 92.1, pp. 73–94, 1995.

[6] S. Mallonee, S. Shariat, G. Stennies, R. Waxweiler, D. Hogan, and F. Jordan, “Physical Injuries Resulting From the Oklahoma City Bombing,” *JAMA*, vol. 276, no. 5, pp. 382–287, 1996.

[7] B. H. S. Norville and E. J. Conrath, “Consideration for Blast -Resistant Glazing Design,” *J. Archit. Eng.*, vol. 7, no. September, pp. 80–86, 2001.

[8] M. Rodriguez, D. Lotze, J. H. Gross, Y. G. Zhang, R. E. Klingner, and H. L. Graves, “Dynamic behavior of tensile anchors to concrete,” *ACI Struct. J.*, vol. 98, no. 4, pp. 511–524, 2001.

[9] R. Nilforoush, “Anchorage in Concrete Structures: Numerical and Experimental Evaluation of Load-Carrying Capacity of Cast-in-Place Headed Anchors and Post-Installed Adhesive Anchors,” Lulea, Lulea, 2017.

[10] T. Gurbuz and A. Ilki, “Pullout performance of fully and partially bonded retrofit

anchors in low-strength concrete," *ACI Struct. J.*, vol. 108, no. 1, pp. 61–70, 2011.

[11] K. H. Yang and A. F. Ashour, "Mechanism analysis for concrete breakout capacity of single anchors in tension," *ACI Struct. J.*, vol. 105, no. 5, pp. 609–616, 2008.

[12] M. Gesoglu, T. Özturan, M. Özel, and E. Güneyisi, "Tensile behavior of post-installed anchors in plain and steel fiber-reinforced normal-and high-strength concretes," *ACI Struct. J.*, vol. 102, no. 2, pp. 224–231, 2005.

[13] D. F. Meinheit, A. E. N. Osborn, and M. R. Krueger, "Pullout Strength of L-Bolt Anchors - Revisiting Design Equations," *Spec. Publ.*, vol. 296, pp. 1–30.

[14] B. T. Eligehausen, Rolf., "Behaviour of Fasteners Loaded in Tension in Cracked Concrete," *Struct. J.*, vol. 92(3), pp. 365–379, 1995.

[15] J. Olsen, T. Pregartner, and A. J. Lamanna, "Basis for Screw Anchors in Concrete," *ACI Struct. J.*, vol. 109, no. 4, 2012.

[16] M. Saleem and T. Tsubaki, "Multi-layer Model for Pull-out behavior of Post-installed Anchor," 2010.

[17] K. Jebara, J. Ožbolt, and J. Hofmann, "Pryout failure capacity of single headed stud anchors," *Mater. Struct. Constr.*, vol. 49, no. 5, pp. 1775–1792, 2016.

[18] B. S. Hamad, R. Al Hammoud, and J. Kunz, "Evaluation of Bond Strength of Bonded-In or Post-Installed Reinforcement," *ACI Mater. J.*, vol. 103, no. 2, p. 207, 2006.

[19] M. Kwon, J. Kim, H. Seo, and W. Jung, "Long-term performance of mechanically post-installed anchor systems," *Adv. Struct. Eng.*, vol. 20, no. 3, pp. 288–298, 2017.

[20] R. Nilforoush, M. Nilsson, G. Söderlind, and L. Elfgren, "Long-term performance

of adhesive bonded anchors," *ACI Struct. J.*, vol. 113, no. 2, pp. 251–261, 2016.

[21] P. H. Bischoff and S. H. Perry, "Compressive behaviour of concrete at high strain rates," *Mater. Struct.*, vol. 24, no. 6, pp. 425–450, 1991.

[22] W. L. Cowell, "Dynamic Properties of Plain Cement Concrete."

[23] L. J. Malvar and J. E. Crawford, "Dynamic Increase Factors," *28th DDESB Semin. Orlando*, pp. 1–17, 1998.

[24] L. J. Malvar and J. E. Crawford, "Dynamic Increase Factors for Steel Reinforcing Bars," *Proc. Twenty-Eighth DoD Explos. Saf. Semin.*, pp. 1–18, 1998.

[25] A. Braimah, E. Contestabile, and R. Guilbeault, "Behaviour of adhesive steel anchors under impulse-type loading," *Can. J. Civ. Eng.*, vol. 36, no. 11, pp. 1835–1847, 2009.

[26] R. Eligehausen, R. Mallée, and J. Silva, "Anchorage in Concrete Construction," *John Wiley Sons*, vol. 10, 2006.

[27] L. T. Ahmed and A. Braimah, "Behaviour of undercut anchors subjected to high strain rate loading," *Procedia Eng.*, vol. 210, pp. 326–333, 2017.

[28] G. Solomos and M. Berra, "Testing of anchorages in concrete under dynamic tensile loading," *Mater. Struct. Constr.*, vol. 39, no. 7, pp. 695–706, 2006.

[29] C. Allen Ross, "Split-Hopkinson pressure bar tests," *No. AFESC/ESL-TR-88-82. AIR FORCE Eng. Serv. Cent. TYNDALL AFB FL Eng. Serv. LAB*, 1989.

[30] M. Rodriguez, "Tensile and shear behavior of anchors in uncracked and cracked concrete under static and dynamic loading," University of Texas at Austin, 1996.

[31] H. Sato, K. Fujikake, and S. Mindess, "Study on dynamic pullout strength of anchors based on failure modes," *13th world Conf. Earthq. Eng.*, no. 854, pp. 1–7,

2004.

[32] ACI Committee 355, *ACI 355.2-07 Qualification of Post-Installed Mechanical Anchors in Concrete & Commentary*. 2007.

[33] ICC Evaluation Services, “Acceptance Criteria for Mechanical Anchors in Concrete,” no. 800. 2009.

[34] ASTM International, “Standard Terminology for Anchors and Fasteners in Concrete and Masonry (ASTM E2265),” pp. 1–4, 2009.

[35] ASTM Internationa, “ASTM E488 - Standard Test Methods for Strength of Anchors in Concrete Elements,” *Astm*, pp. 1–21, 2015.

[36] R. Eligehausen, R. A. Cook, and J. Appl, “Behavior and design of adhesive bonded anchors,” *ACI Struct. J.*, vol. 103, no. 6, pp. 822–831, 2006.

[37] R. Cook, Ronald ; Konz, “Anchoring with bonded fasteners,” *Connect. between Steel Concr.*, vol. 1, pp. 361–370, 2001.

[38] S. Cattaneo and G. Muciaccia, “Adhesive anchors in high performance concrete,” *Mater. Struct. Constr.*, vol. 49, no. 7, pp. 2689–2700, 2016.

[39] J. Chen, “Static Behaviour and Strenght of Adhesively Bonded - Chen.pdf,” Carleton University, 2004.

[40] M. Marcon, K. Ninčević, I. Boumakis, L. M. Czernuschka, and R. Wan-Wendner, “Aggregate effect on the concrete cone capacity of an undercut anchor under quasi-static tensile load,” *Materials (Basel).*, vol. 11, no. 5, 2018.

[41] E. J. Primavera, J. P. Pinelli, and E. H. Kalajian, “Tensile behavior of cast-in-place and undercut anchors in high-strength concrete,” *ACI Struct. J.*, vol. 94, no. 5, pp.

583–594, 1997.

[42] A. R. E. Jorg, “Design Method for Splitting Failure Mode of Fastening,” in *International Symposium on Connections Between Steel and Concrete (Rilem Publication)*, 2001, pp. 80–89.

[43] F. Delhomme, B. Pallud, and N. Rouane, “Tightening Torque Influence on Pullout Behavior of Post-installed Expansion Anchors,” *KSCE J. Civ. Eng.*, vol. 22, no. 10, pp. 3931–3939, 2018.

[44] R. Eligehausen, “Anchorage to Concrete by Metallic Expansion Anchors,” 1987.

[45] M. J. M. and Z. K. Karmazinova and Z. Kala, “Design of Expansion Anchors to Concrete Based on Results of Experimental Verification,” *Adv. Steel Constr.*, vol. 5, no. 4, pp. 390–405, 2009.

[46] G. Muciaccia, “Behavior of post-installed fastening under seismic action,” *ACI Struct. J.*, vol. 114, no. 1, pp. 75–86, 2017.

[47] T. Kuenzlen, Jurgen; Sippel, “Behaviour and Design of Fastenings with Concrete Screws,” *Int. Simp. Connect. between Concr. Steel*, vol. 1, pp. 919–929, 2001.

[48] J. H. Kuenzlen, “Load-Bearing Behaviour of Screw Anchors under Axial Tension (Doctoral Dissertation, Doctoral Thesis, The University of Stuttgart, Stuttgart, Germany),” University of Stuttgart, 2004.

[49] A. Mohyeddin, E. F. Gad, K. Yangdon, R. Khandu, and J. Lee, “Tensile load capacity of screw anchors in early age concrete,” *Constr. Build. Mater.*, vol. 127, pp. 702–711, 2016.

[50] L. Li, “Load Bearing Capacity of Torque-Controlled Anchors,” *Int. Simp. Connect.*

between Concr. Steel, vol. 1, pp. 170–177, 2001.

[51] J. W. Ollgaard, J. G.; Slutter, R. G.; Fisher, "Shear strength of stud connectors in lightweight and normal weight concrete," *AISC Eng. J.*, vol. 71, no. 10, 1971.

[52] A. F. Shaikh and W. Yi, "In-Place Strength of Welded Headed Studs," *PCI J.*, vol. 30, no. 2, pp. 56–81, 1985.

[53] M. Anderson, Neal; Donald, "Pryout capacity of cast-in headed stud anchors," *PCI J.*, vol. 50, no. 2, pp. 90–112, 2005.

[54] N. Subramanian, "Recent developments in the design of anchor bolts," *Indian Concr. J.*, vol. 74, no. 7, pp. 407–414, 2000.

[55] R. Eligehausen and J. Ozbolt, "Size effect in anchorage behavior," 1990.

[56] Z. P. Bažant, J. Kim, and P. A. Pfeiffer, "Nonlinear Fracture Properties from Size Effect Tests," *J. Struct. Eng.*, vol. 112, no. 2, pp. 289–307, 1986.

[57] R. Eligehausen and G. Sawade, "A fracture mechanics based description of the pull-out behavior of headed studs embedded in concrete," *Fract. Mech. Concr. Struct.*, pp. 281–299, 1989.

[58] J. Eligehausen, R ; Ozbolt, "Fastening Elements in Concrete Structures - Numerical Simulations," 1993.

[59] R. Cook, RA; Kunz, J; Fuchs, W; Konz, "Behavior and design of single adhesive anchors under tensile load in uncracked concrete," *Struct. J.*, vol. 95, no. 1, pp. 9–26, 1998.

[60] H. Muratli, R. E. Klingner, and H. L. Graves, "Breakout capacity of anchors in concrete - Part 2: Shear," *ACI Struct. J.*, vol. 101, no. 6, pp. 821–829, 2004.

[61] R. A. Cook, "Strength Design of Anchorage to Concrete," *Portl. Cem. Assoc.*,

1999.

[62] N. S. Anderson and D. F. Meinheit, “Design criteria for headed stud groups in shear: Part 1 — Steel capacity and back edge effects,” *PCI J.*, vol. 45, no. 5, pp. 46–75, 2000.

[63] K. Jebara, J. Ožbolt, and J. Hofmann, “Pryout failure of single headed stud anchor: 3D numerical FE analysis,” *Mater. Struct. Constr.*, vol. 49, no. 11, pp. 4551–4563, 2016.

[64] K. Jebara, “Pryout capacity and bearing behavior of stocky headed stud anchorages,” 2018.

[65] G. Zhao, “‘Tragverhalten von randfernen Kopfbolzenverankerungen bei Betonbruch (Load-Carrying Behavior of Headed Stud Anchors in Concrete Breakout Away From an Edge).,’” Stuttgart, 1994.

[66] J. Hofmann, R. Eligehausen, and J. Ozbolt, “Behavior and design of fastenings with headed anchors at the edge under tension and shear load,” *Swets & Zeitlinger*, vol. 90, pp. 2651–825, 2001.

[67] N. Hawkins, “Strength in shear and tension of cast-in-place anchor bolts,” *Am. Concr. Inst.*, vol. SP 103, pp. 233–257, 1987.

[68] W. Wang, Y. Ma, M. Yang, P. Jiang, F. Yuan, and X. Wu, “Strain Rate Effect on Tensile Behavior for a High Specific Strength Steel: From Quasi-Static to Intermediate Strain Rates,” *Metals (Basel).*, vol. 8, no. 1, p. 11, 2017.

[69] N. R. Nagaraja Rao, M. Lohrmann, and L. Tall, “Effect of strain rate on the yield stress of structural steels,” *J. Mater.*, vol. 1, no. 1, pp. 241–262, 1966.

[70] B. H. C. Fu, M. A. Erki, and M. Seckin, “Review o f effects of loading rate on

reinforced concrete. Tech. Rep. No. R642, U.S. Naval Civ. Engrg. Lab., Calif.," *J. Struct. Eng.*, vol. 117, no. 12, pp. 3660–3679, 1991.

[71] C. Mahrenholtz and R. Eligehausen, "Dynamic performance of concrete undercut anchors for Nuclear Power Plants," *Nucl. Eng. Des.*, vol. 265, pp. 1091–1100, 2013.

[72] P. Mahrenholtz, "Experimental Performance and Recommendations for Qualification of Post-installed Anchors for Seismic Applications," 2013.

[73] ASTM, "ASTM C143/143M - 15a," 2015.

[74] A. International, "Standard Test Method for Compressive Strength of Cylindrical Concrete Specimens 1," *ASTM Int.*, pp. 1–7, 2006.

[75] ASTM International, "ASTM C469/469M - 14."

[76] ICC Evaluation Services, "ICC-ES Evaluation Report ESR-3037," no. 800, 2018.

[77] S. Strong-Tie, "Wedge All Anchor - Submittal / Substitution Request," 2011.

[78] S. Strong-Tie, "Catalog: Anchoring and Fastening Systems for Concrete and Masonry 2012-2013 (C-SAS-2012)."

[79] ASTM International, "Specification ASTM E8M - 13a - Standard test methods for tension testing of metallic materials," *Specification*, no. C, pp. 1–27, 2009.

[80] U. S. DoD, "UFC 3-340-02 Unified Facilities Criteria (UFC) Structures to resist the effects of accidental explosions.," no. December, 2008.

[81] S. Strong-tie, "Catalog: Anchoring and Fastening Systems for Concrete and Masonry (C-A-2016)," pp. 10–13.

[82] ASTM International, "ASTM D2463 Standard Test Method for Drop Impact

Resistance of Blow-Molded Thermoplastic,” pp. 1–6, 2015.

Appendices

Appendix A : Plots

A.1 : Dynamic Tension Plots

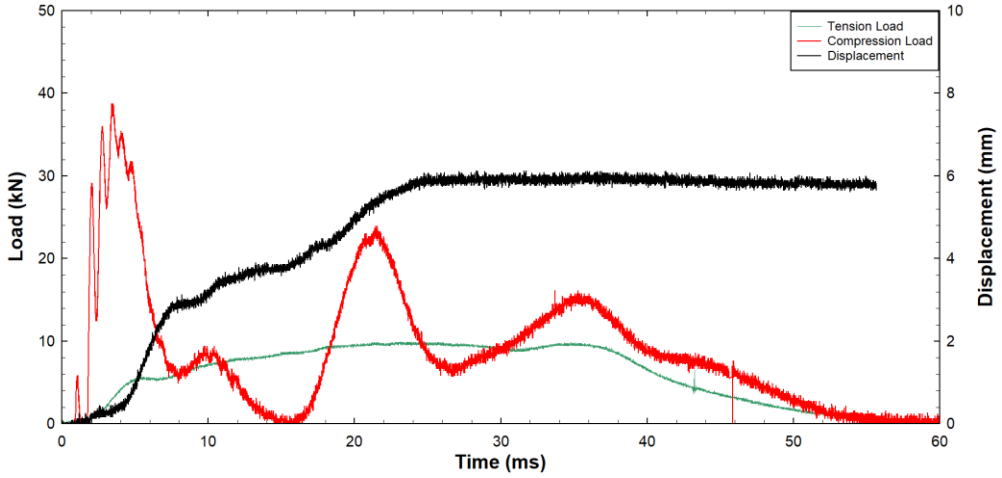

Fig. A1.1: Test Result for DT-STB-QI-01-01

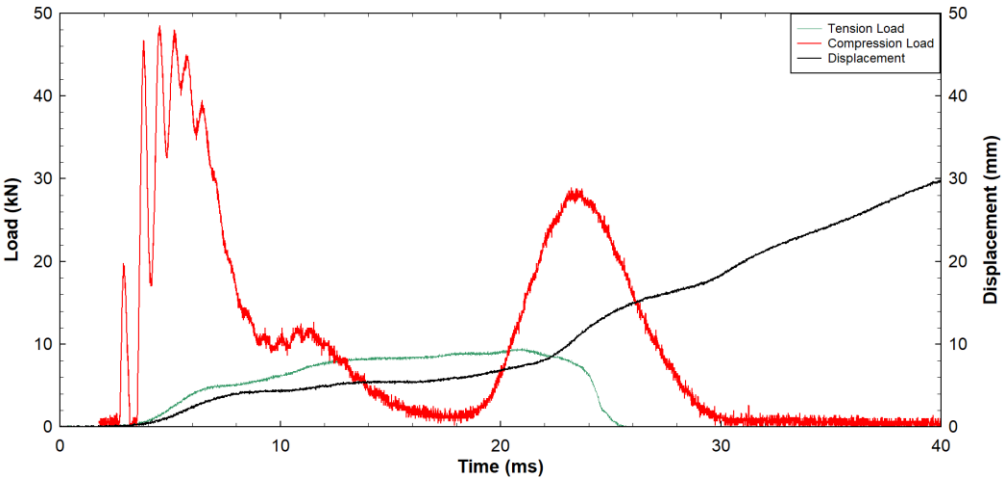

Fig. A1.2: Test Result for DT-QI-02-01

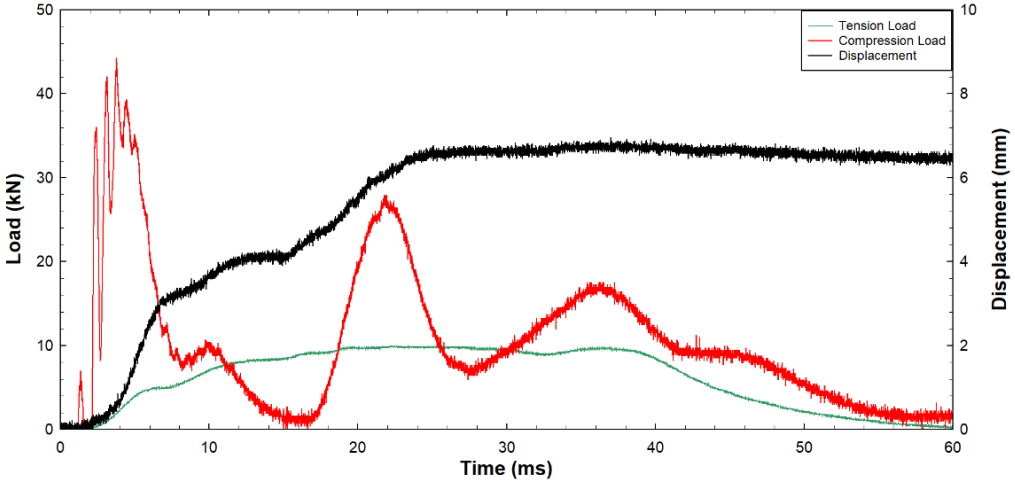

Fig. A1.3: Test Result for DT-QI-03-01

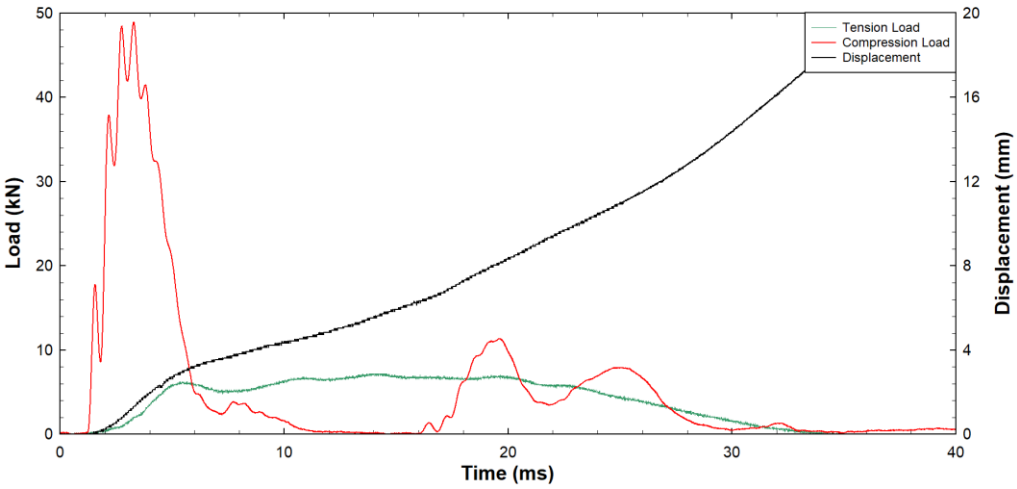

Fig. A1.4: Test Result for DT-QI-03-01

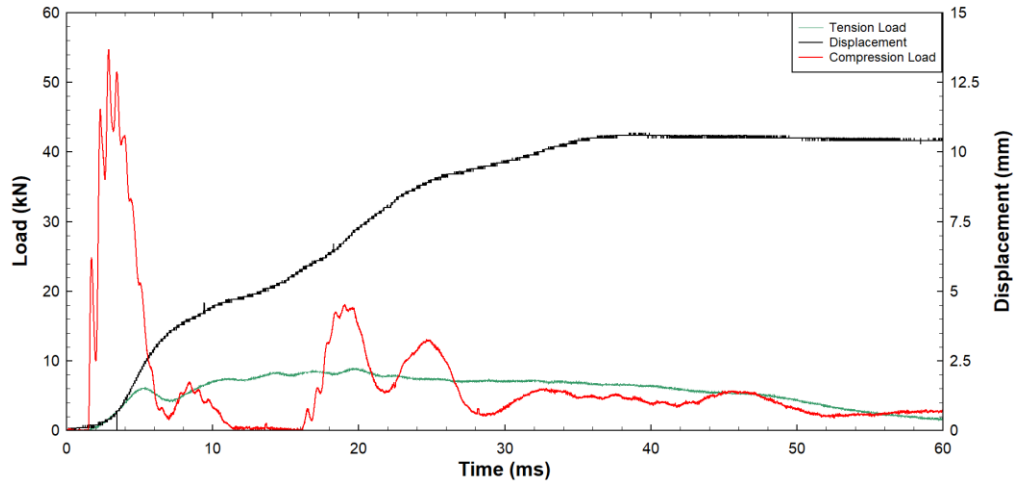

Fig. A1.5: Test Result for DT-STB-QI-04-01

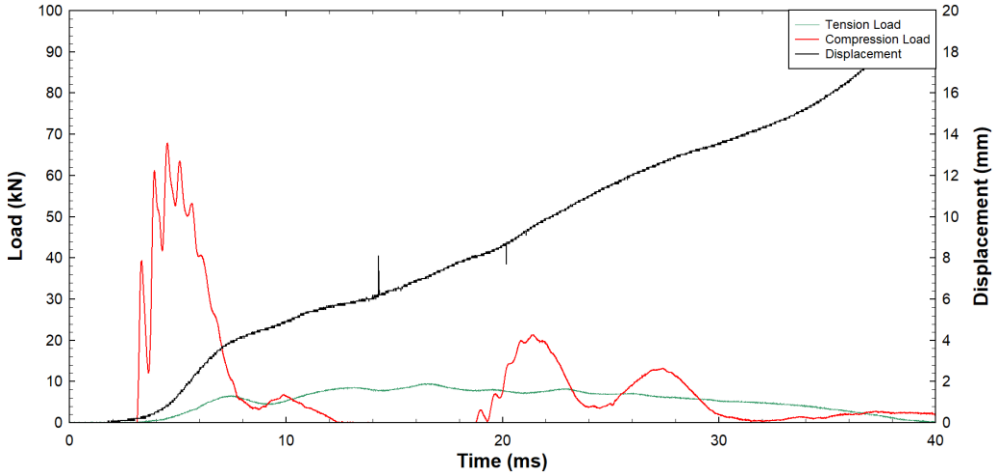

Fig. A1.6: Test Result for DT-STB-QI-05-01

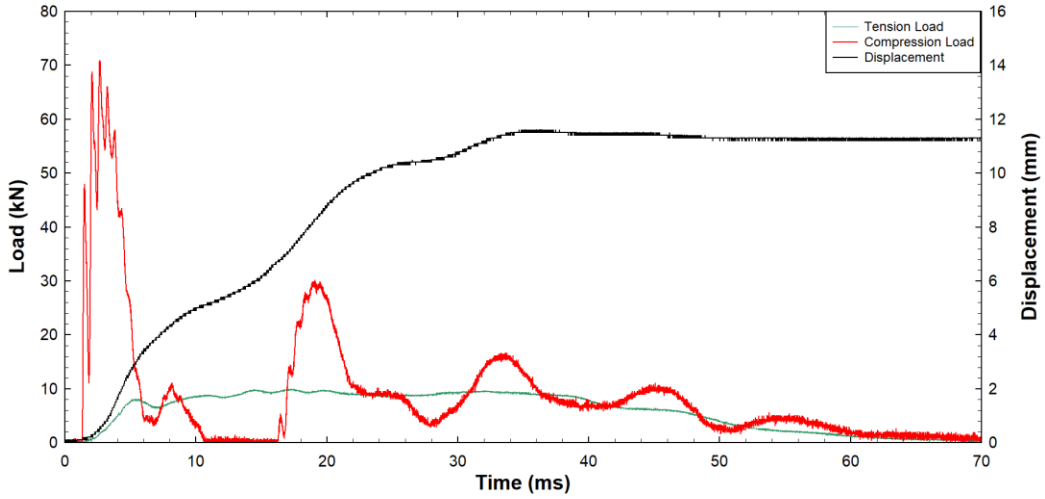

Fig. A1.7: Test Result for DT-STB-QI-07-01

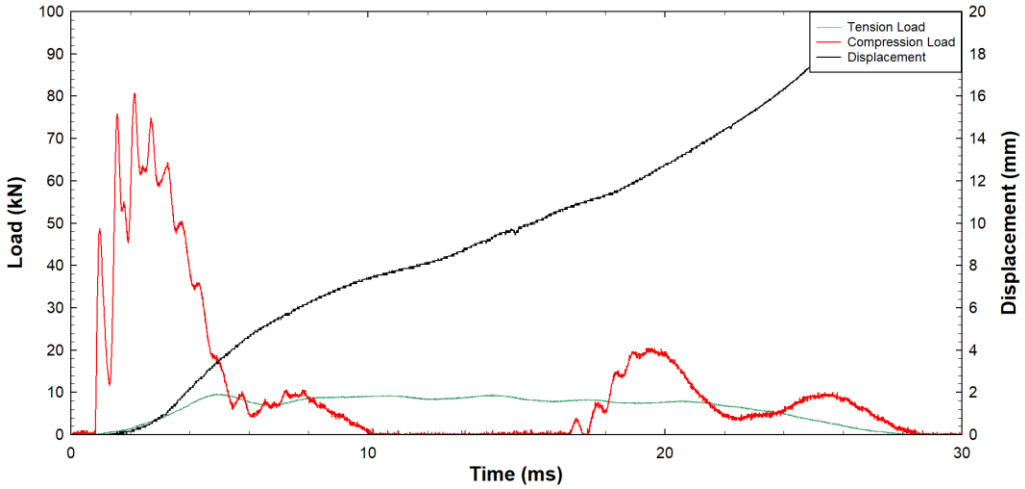

Fig. A1.8: Test Result for DT-STB-QI-08-01

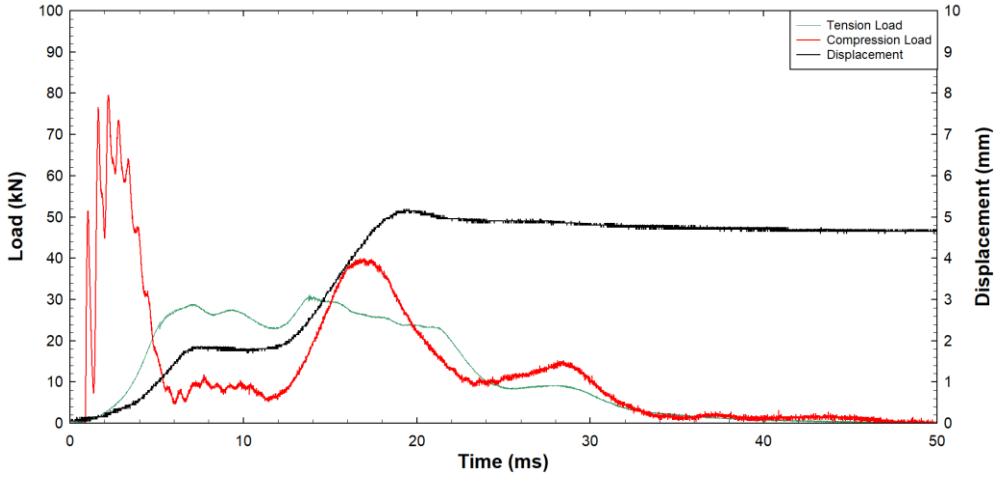

Fig. A1.9: Test Result for DT-STB-TE-01-04

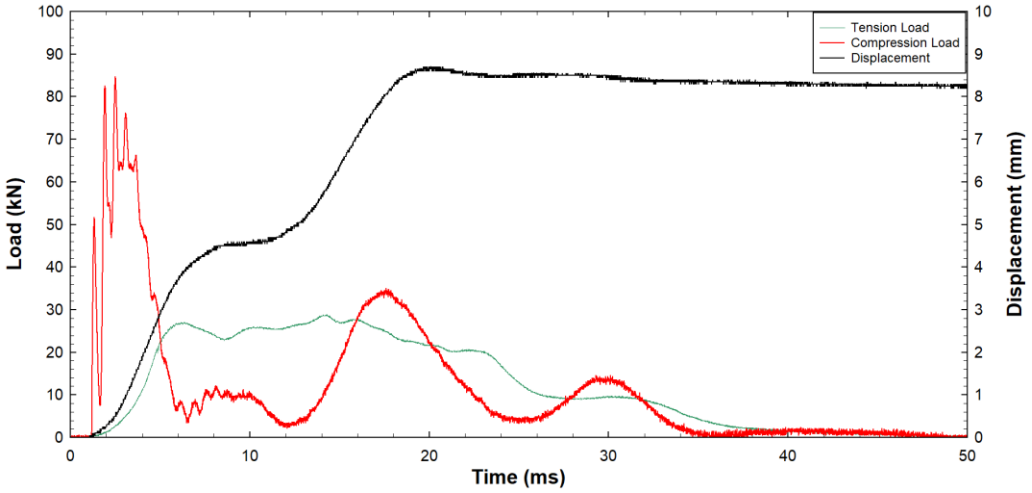

Fig. A1.10: Test Result for DT-STB-TE-02-02

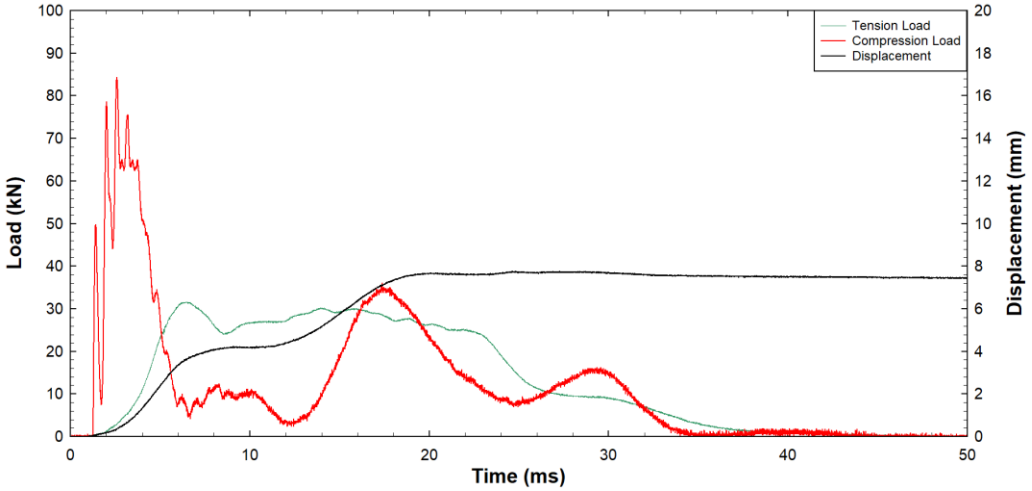

Fig. A1.11: Test Result for DT-STB-TE-03-02

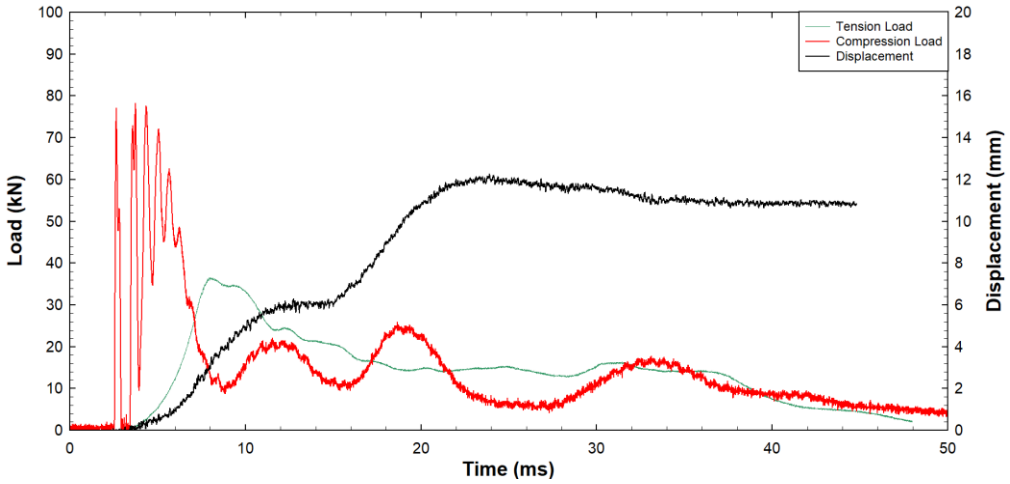

Fig. A1.12: Test Result for DT-STB-TE-01-03

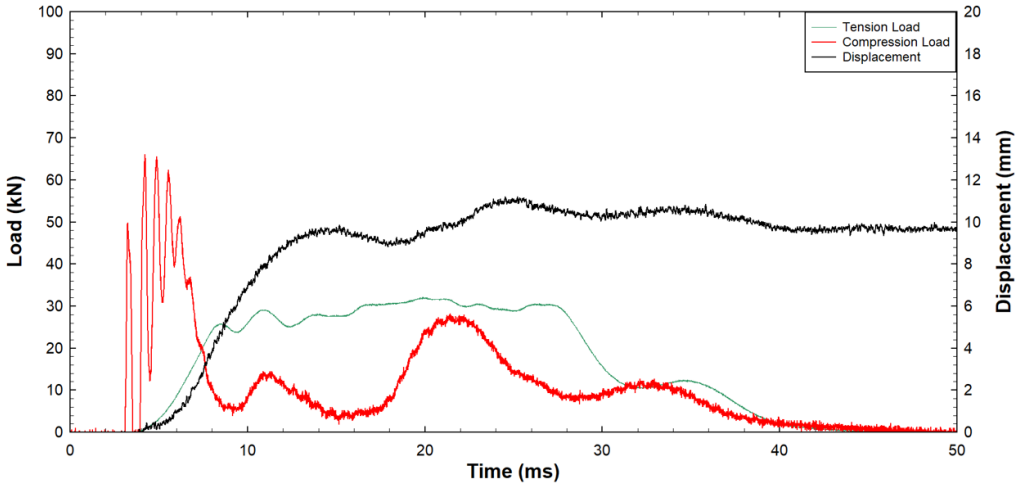

Fig. A1.13: Test Result for DT-STB-TE-03-01

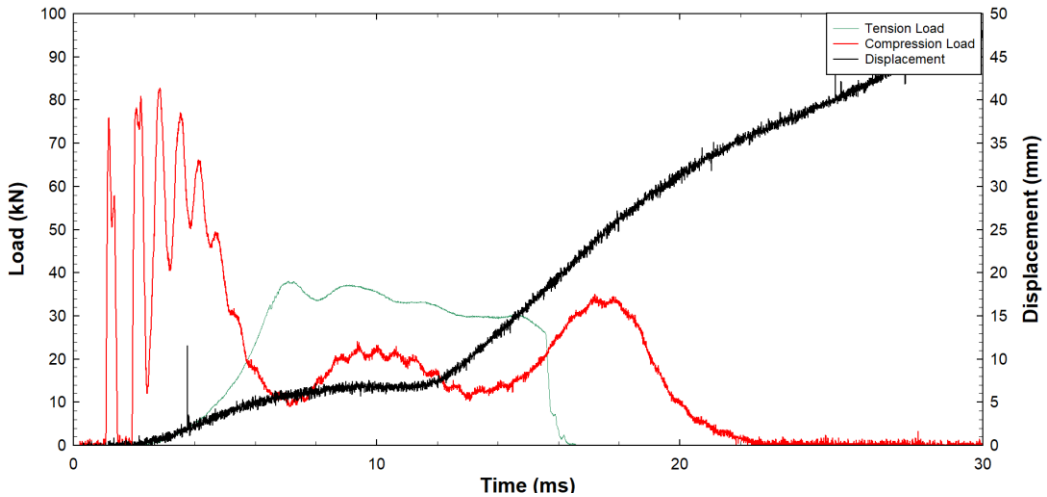

Fig. A1.14: Test Result for DT-STB-TE-03-02

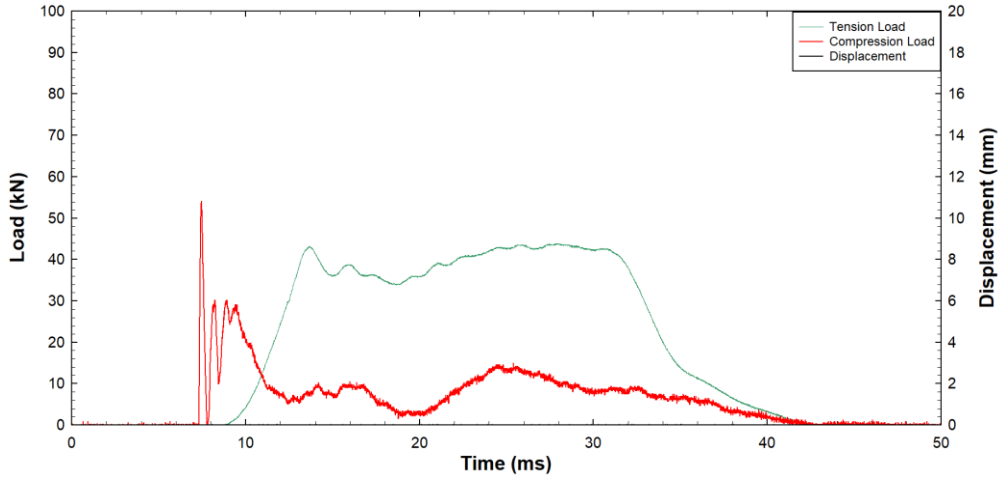

Fig. A1.15: Test Result for DT-STB-HL-01-01

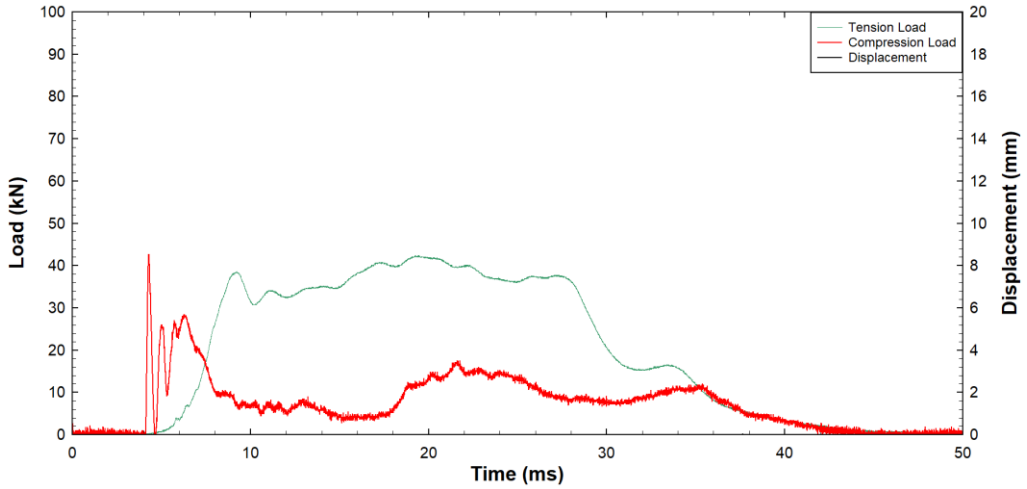

Fig. A1.16: Test Result for DT-STB-HL-02-01

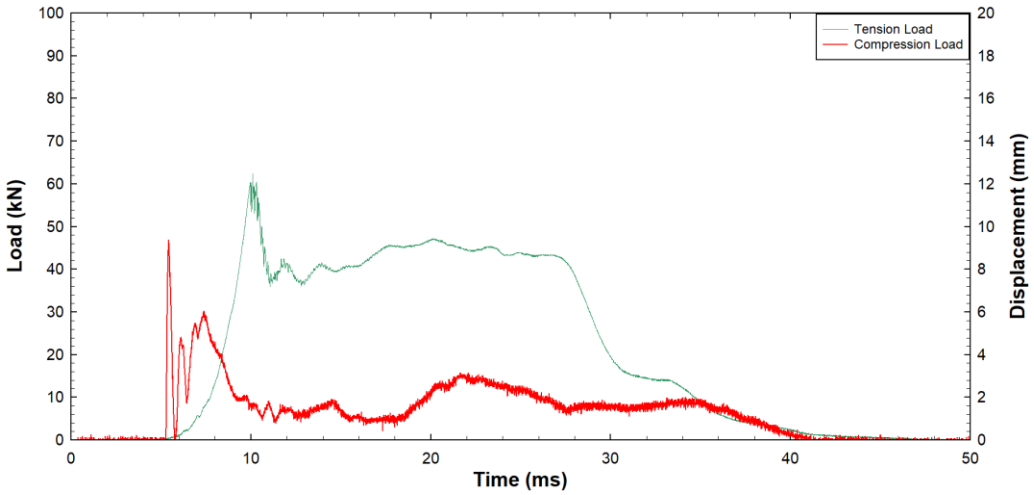

Fig. A1.17: Test Result for DT-STB-HL-03-01

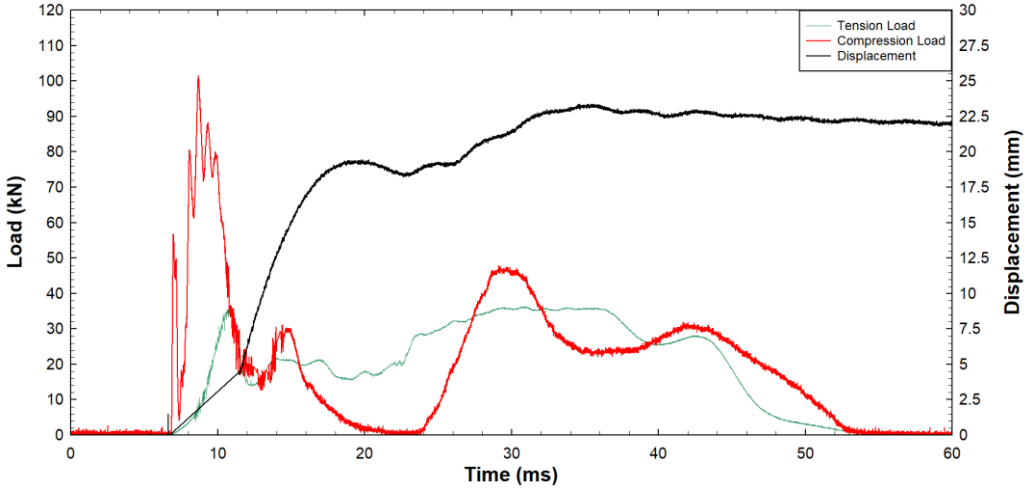

Fig. A1.18: Test Result for DT-STB-HL-04-01

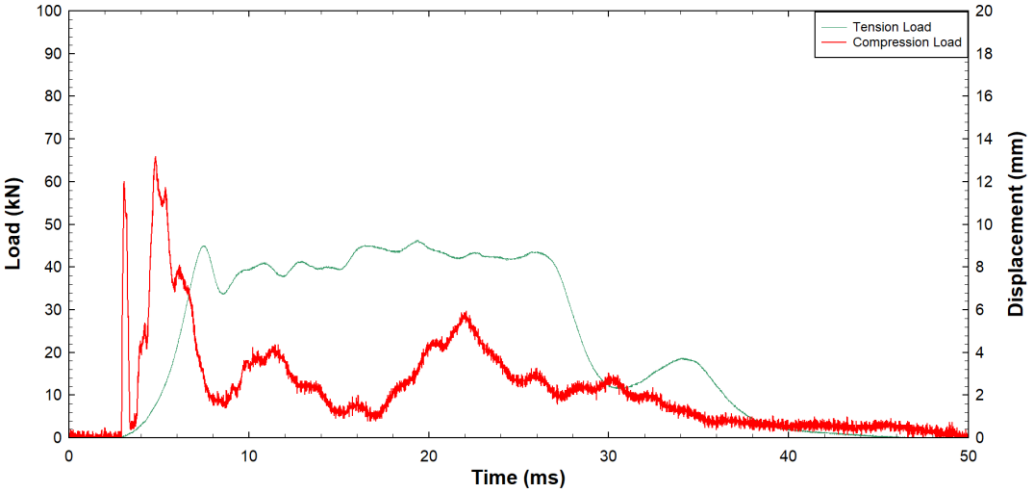

Fig. A1.19: Test Result for DT-STB-HL-05-01

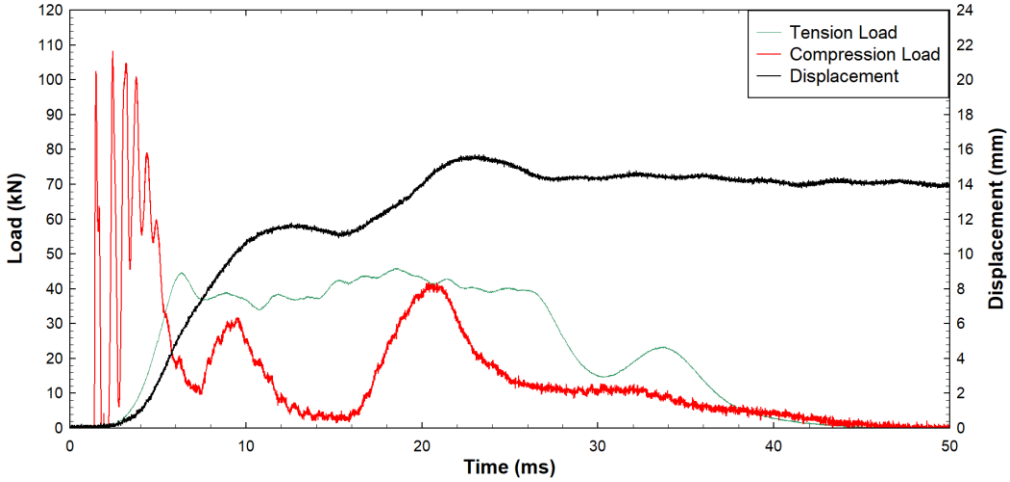

Fig. A1.20: Test Result for DT-STB-HL-06-01

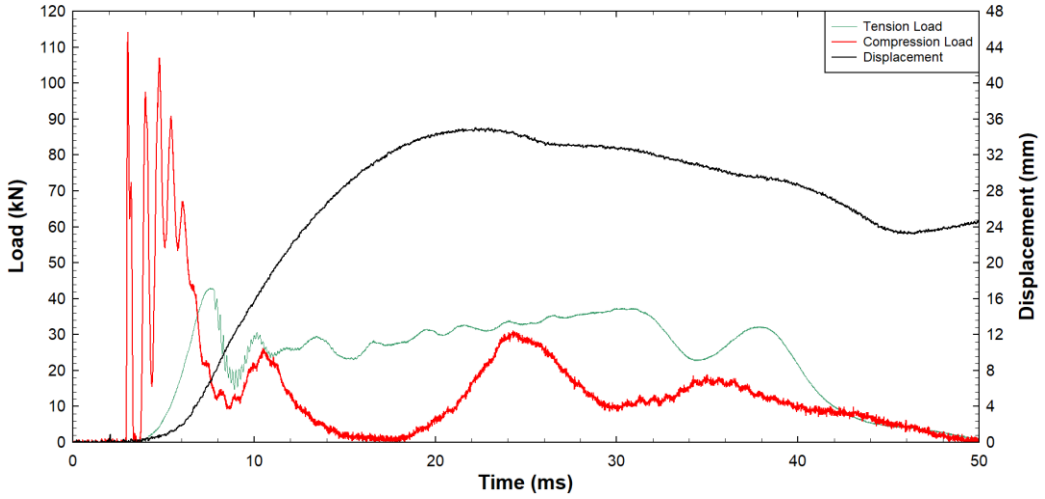

Fig. A1.21: Test Result for DT-STB-HL-04-01

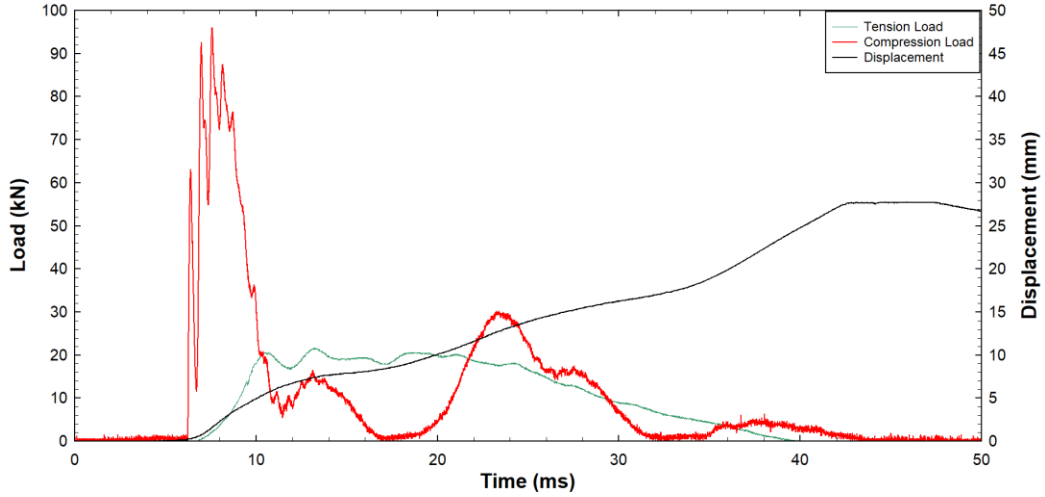

Fig. A1.22: Test Result for DT-WA-TE-01-01

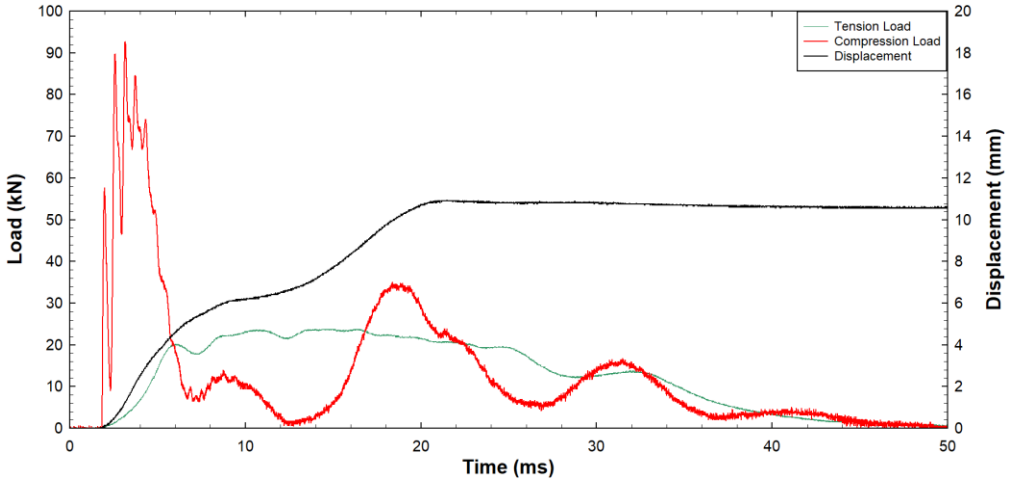

Fig. A1.23: Test Result for DT-WA-TE-02-01

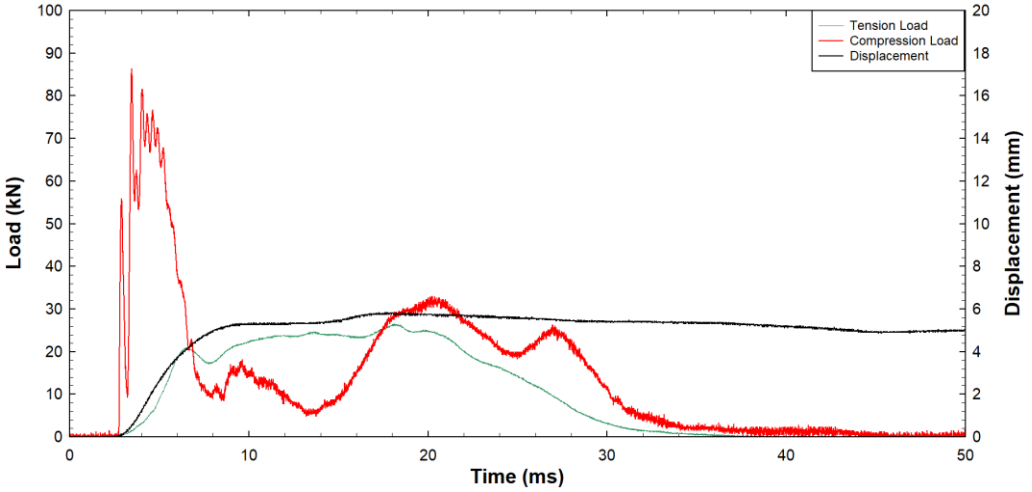

Fig. A1.24: Test Result for DT-WA-TE-03-01

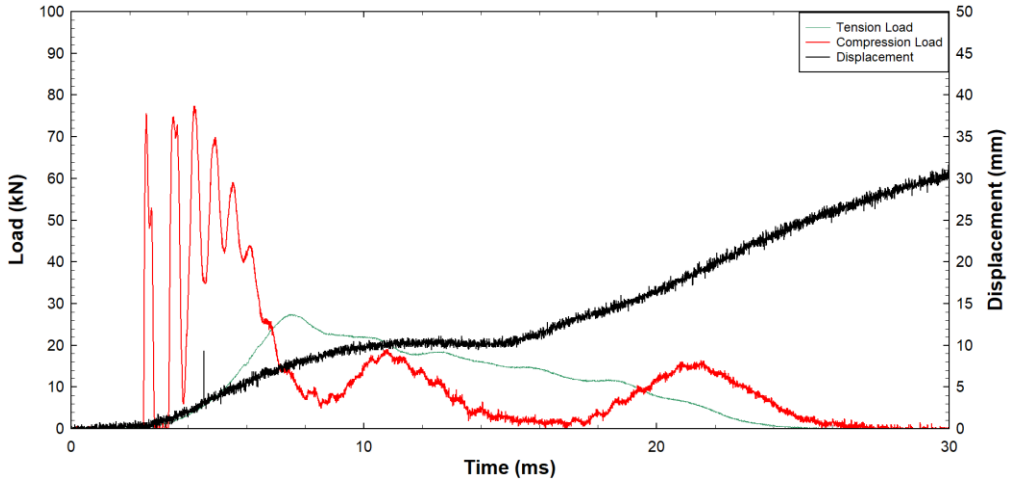

Fig. A1.25: Test Result for DT-WA-TE-01-01*

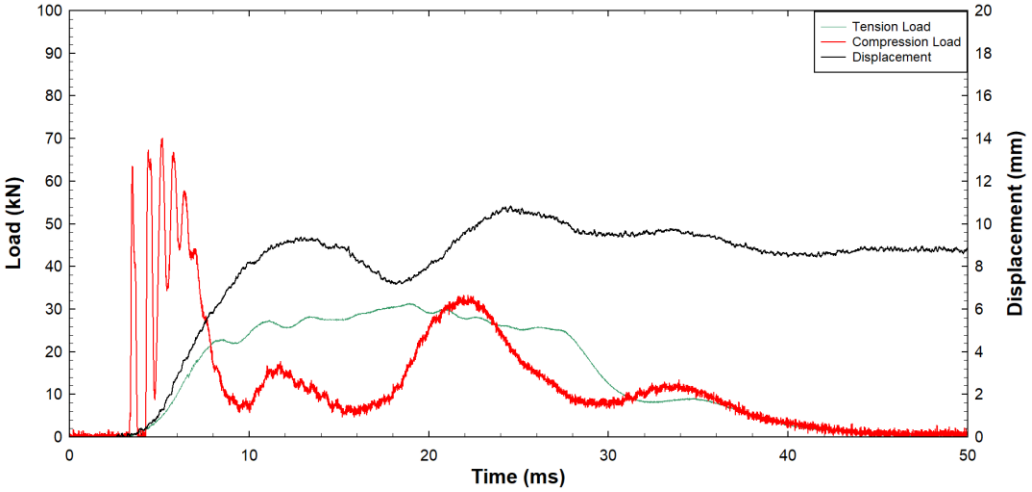

Fig. A1.26: Test Result for DT-WA-TE-02-01

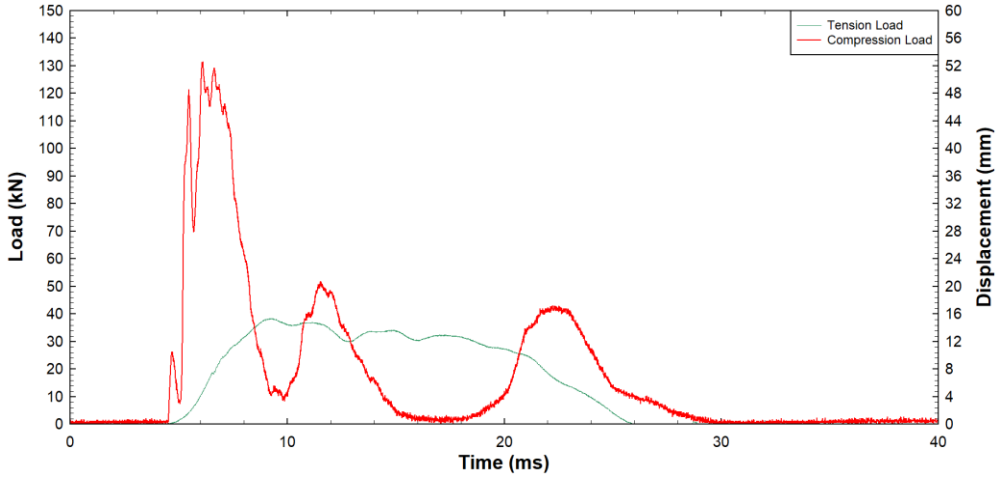

Fig. A1.27: Test Result for DT-WA-HL-01-01

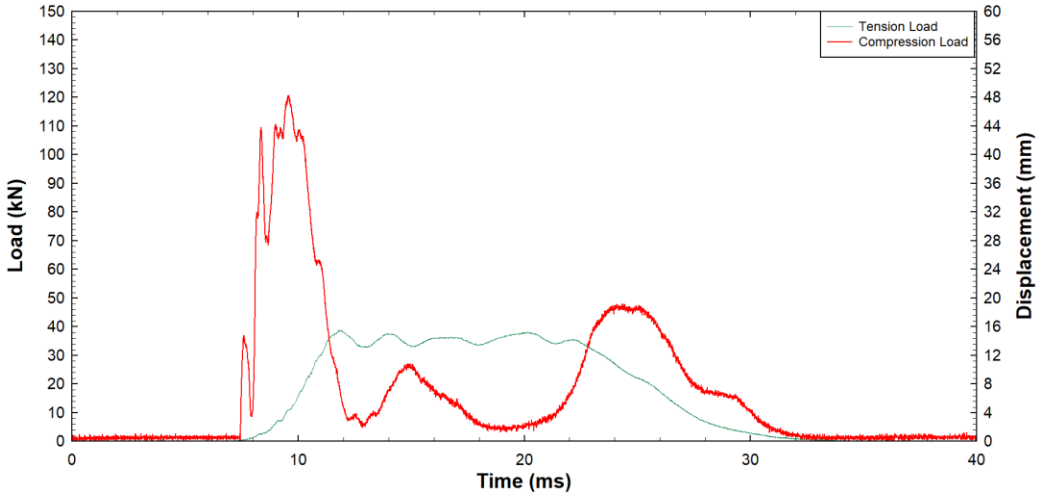

Fig. A1.28: Test Result for DT-WA-HL-02-01

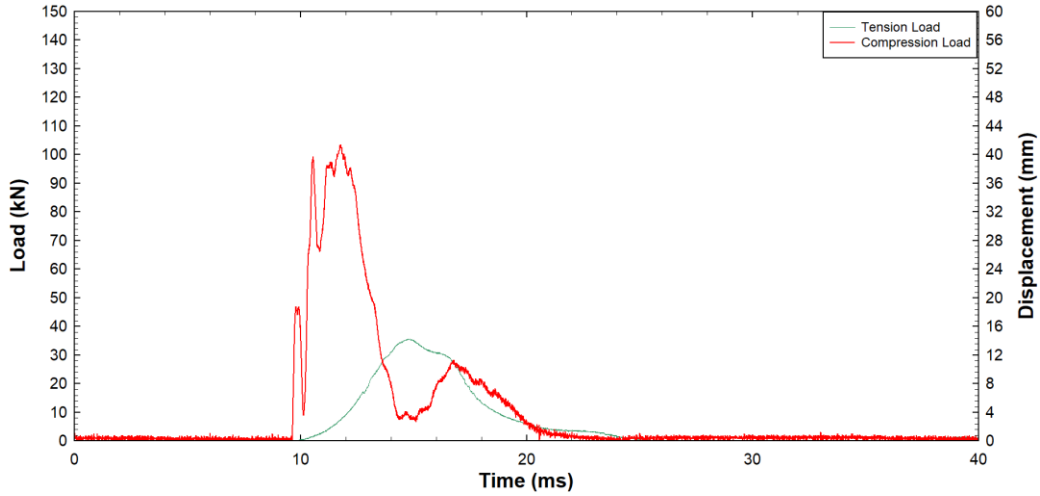

Fig. A1.29: Test Result for DT-WA-HL-03-01

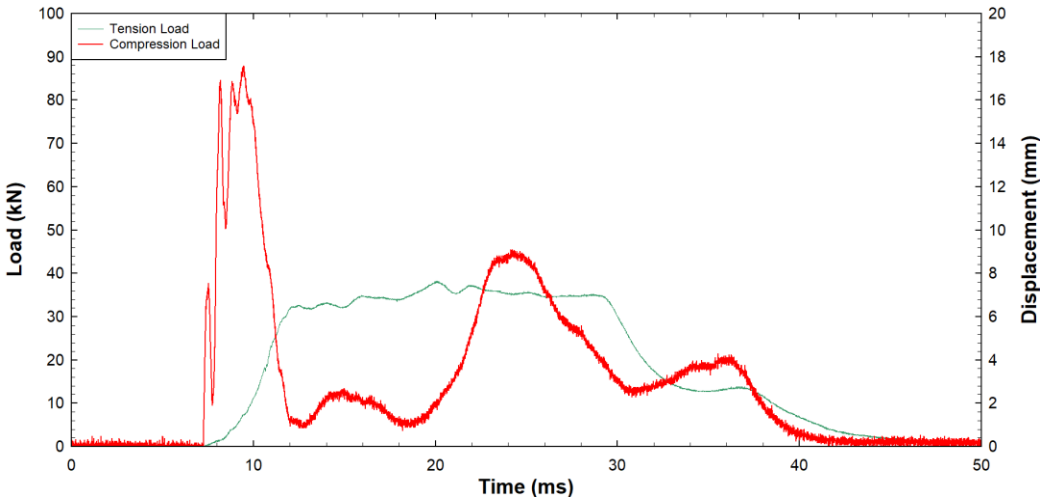

Fig. A1.30: Test Result for DT-WA-HL-04-01

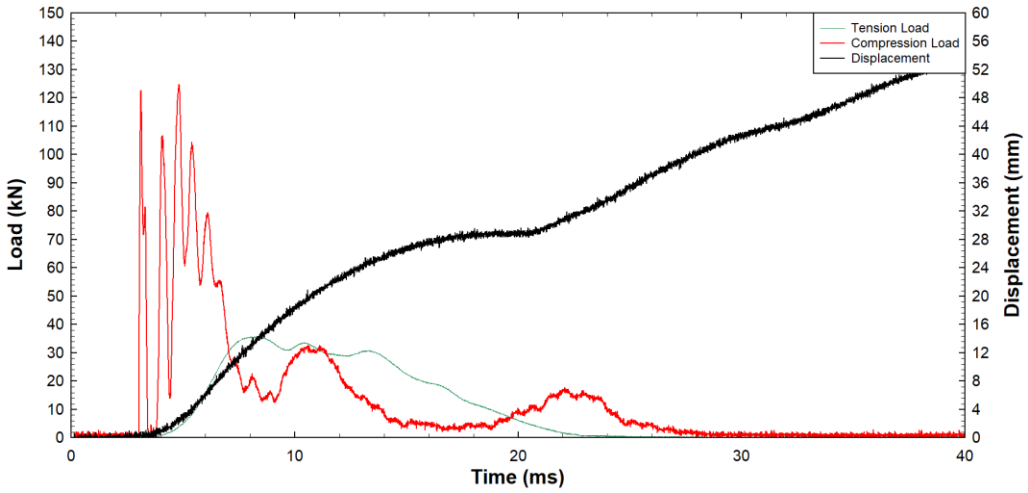

Fig. A1.31: Test Result for DT-WA-HL-01-01

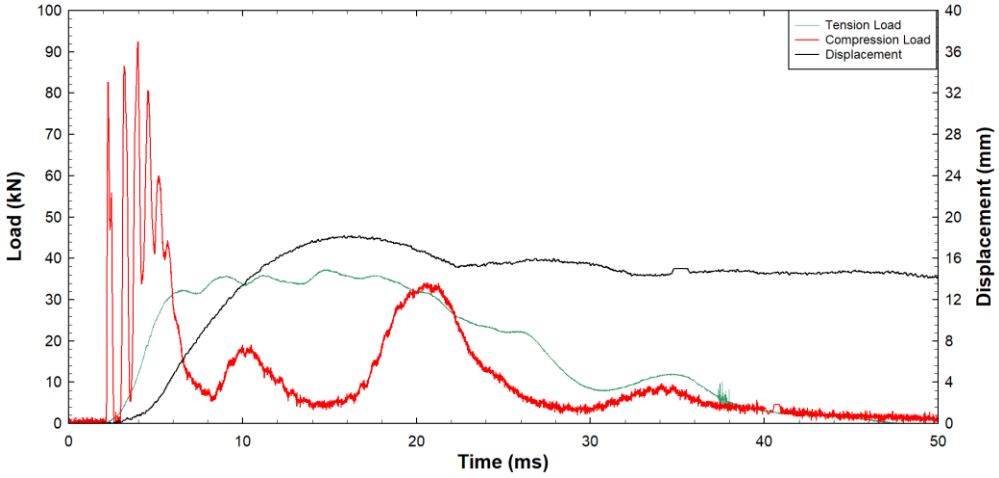

Fig. A1.32: Test Result for DT-WA-HL-02-01

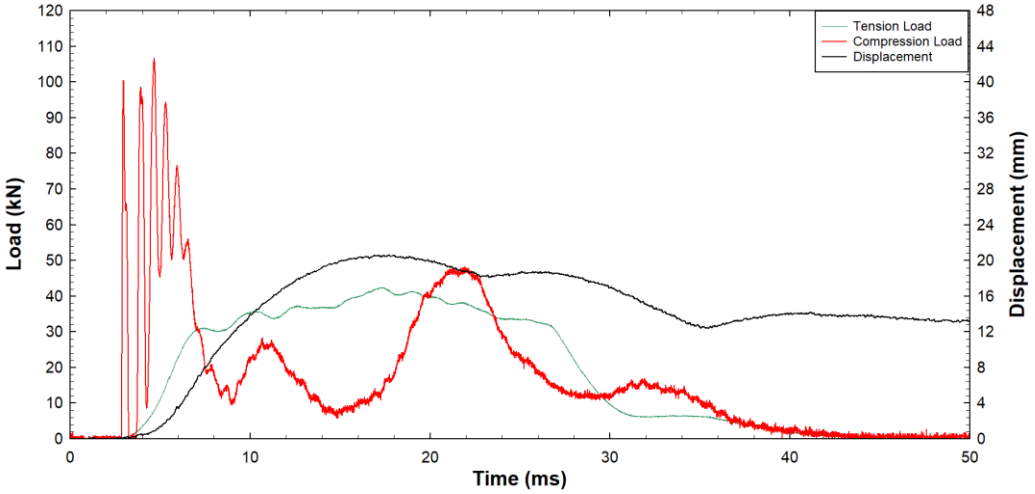

Fig. A1.33: Test Result for DT-WA-HL-03-01

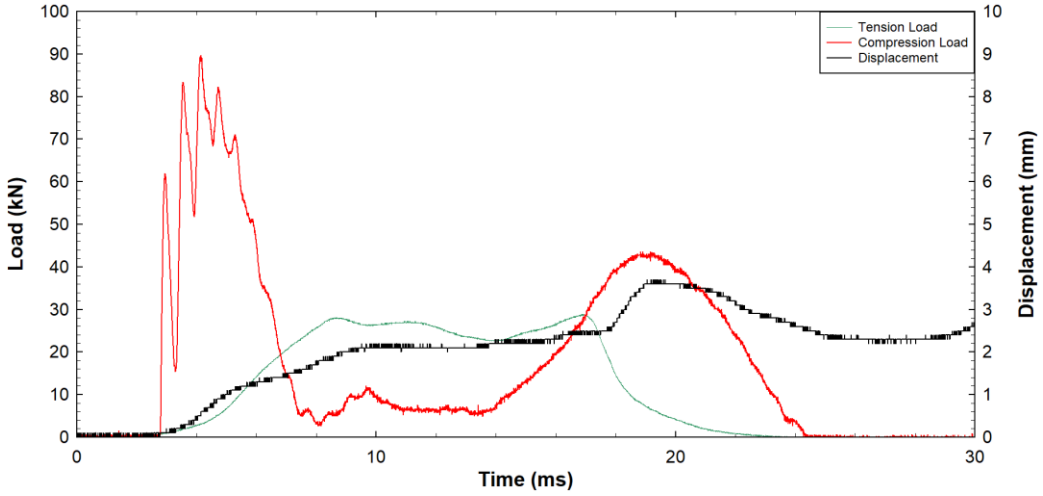

Fig. A1.34: Test Result for DT-TTH-QI-01-01

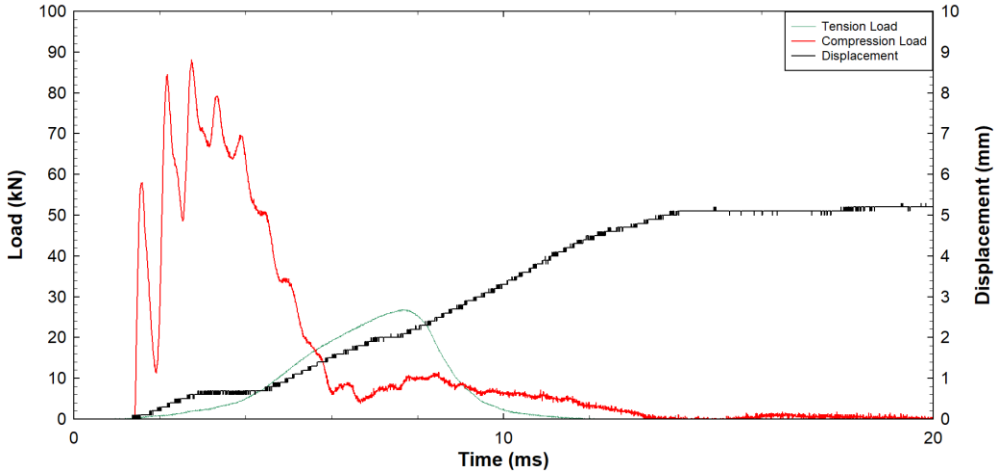

Fig. A1.35: Test Result for DT-TTH-QI-02-01

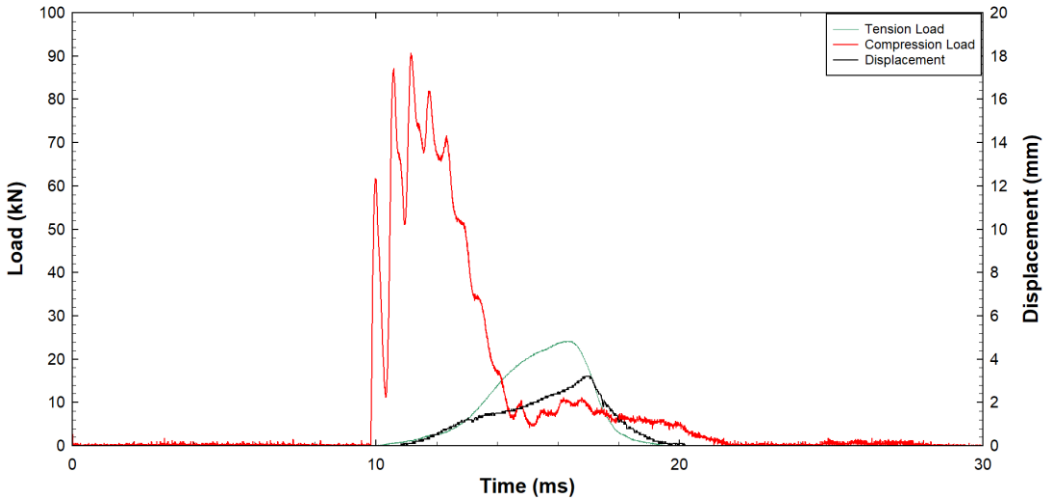

Fig. A1.36: Test Result for DT-TTH-QI-03-01

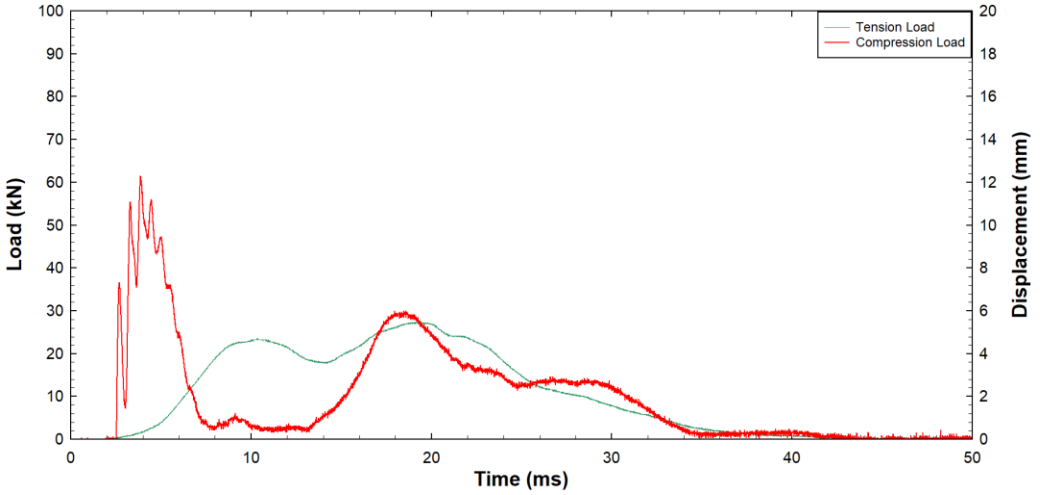

Fig. A1.37: Test Result for DT-TTH-QI-04-01

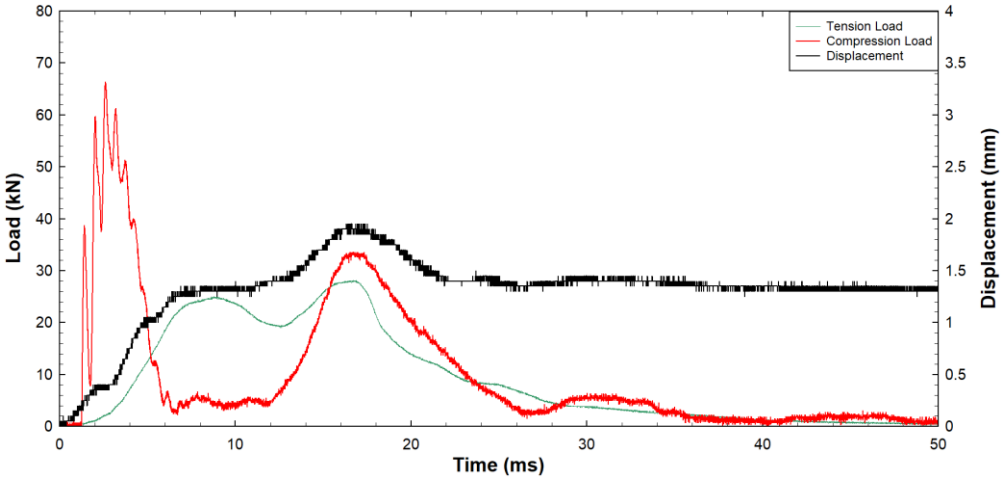

Fig. A1.38: Test Result for DT-TTH-QI-05-01

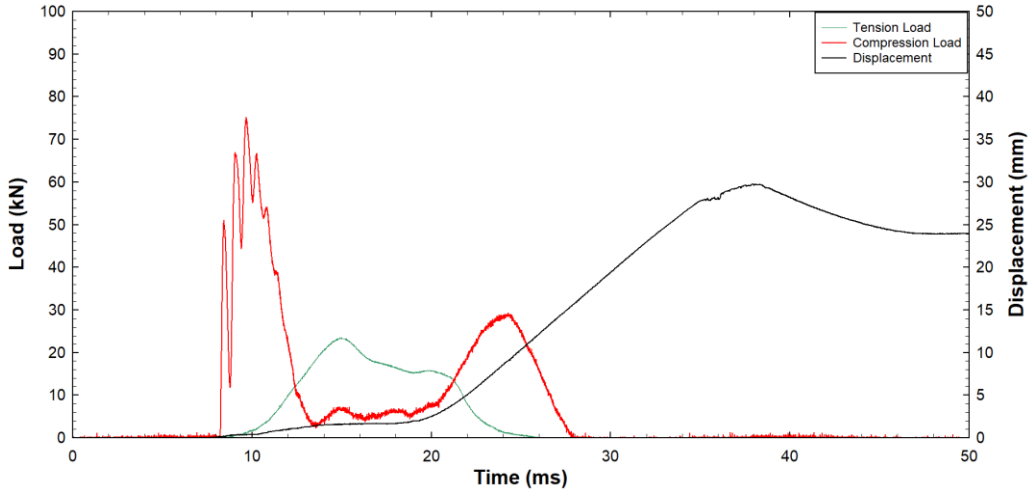

Fig. A1.39: Test Result for DT-TTH-QI-06-01

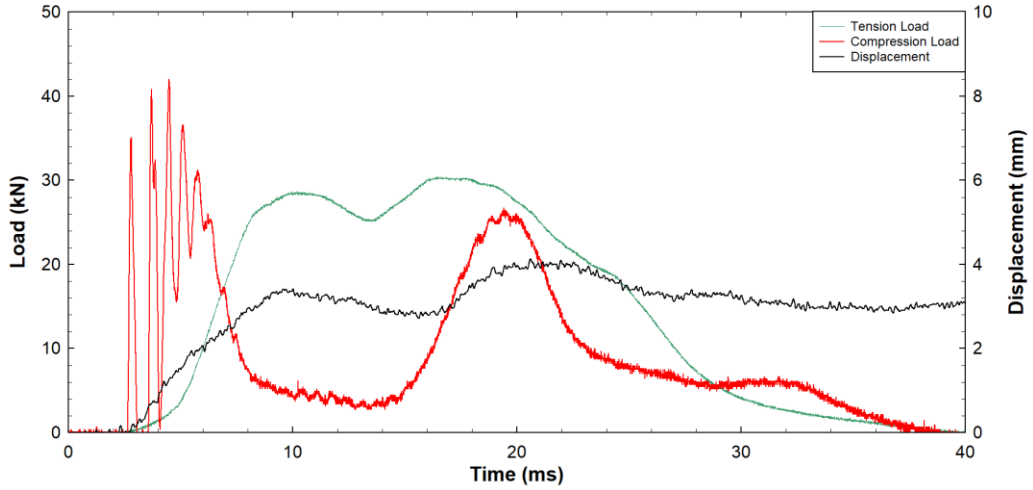

Fig. A1.40: Test Result for DT-TTH-QI-01-01

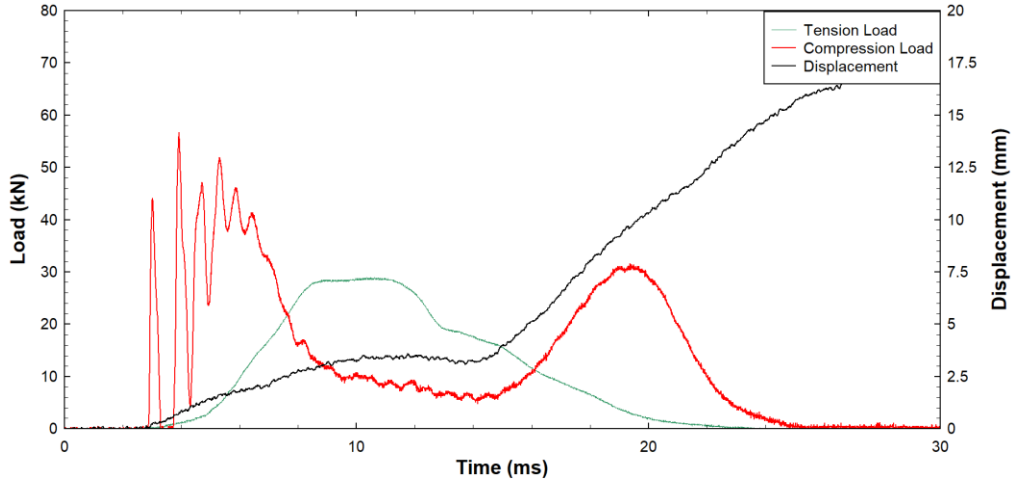

Fig. A1.41: Test Result for DT-TTH-QI-02-01

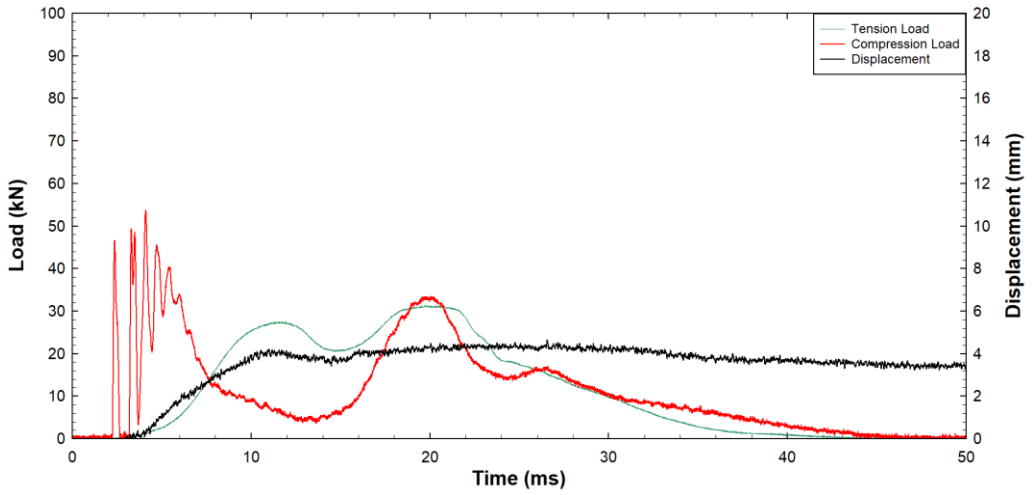

Fig. A1.42: Test Result for DT-TTH-QI-03-01

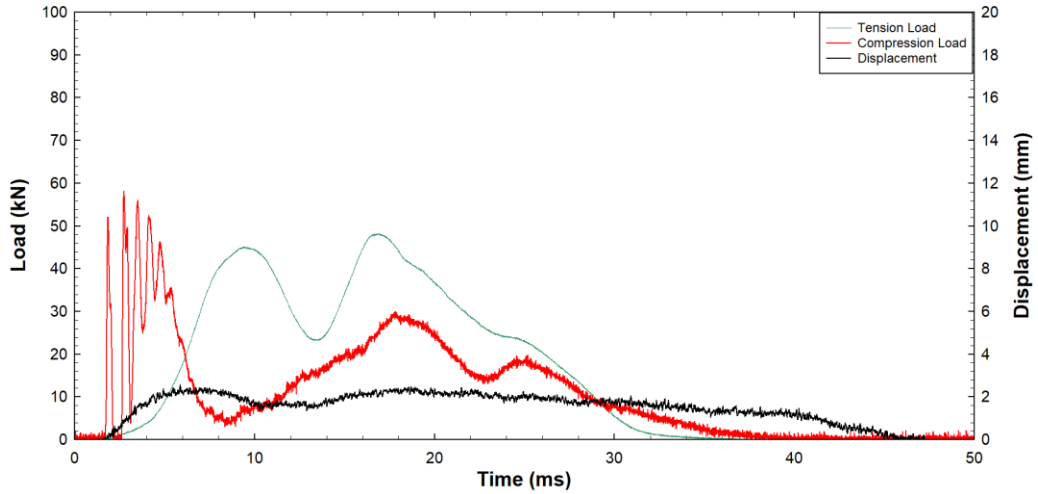

Fig. A1.43: Test Result for DT-TTH-TE-01

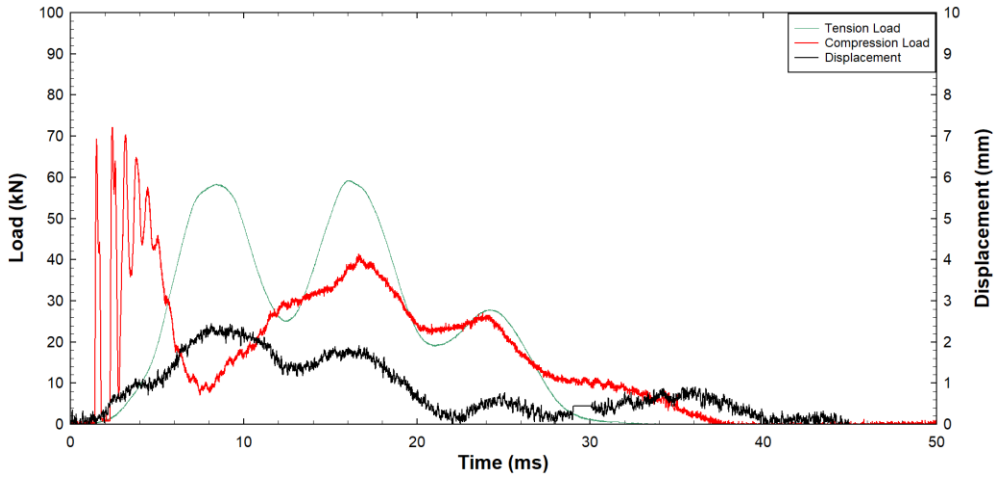

Fig. A1.44: Test Result for DT-TTH-TE-02

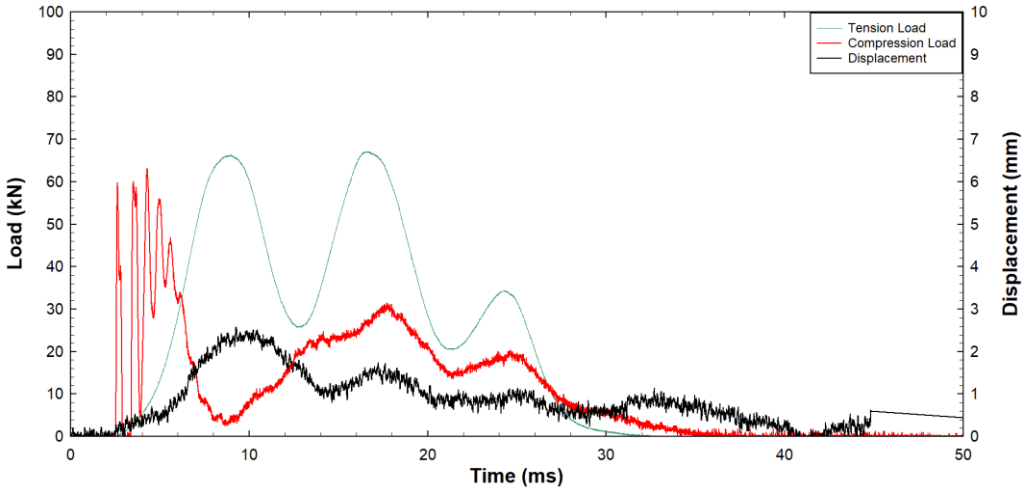

Fig. A1.45: Test Result for DT-TTH-TE-03

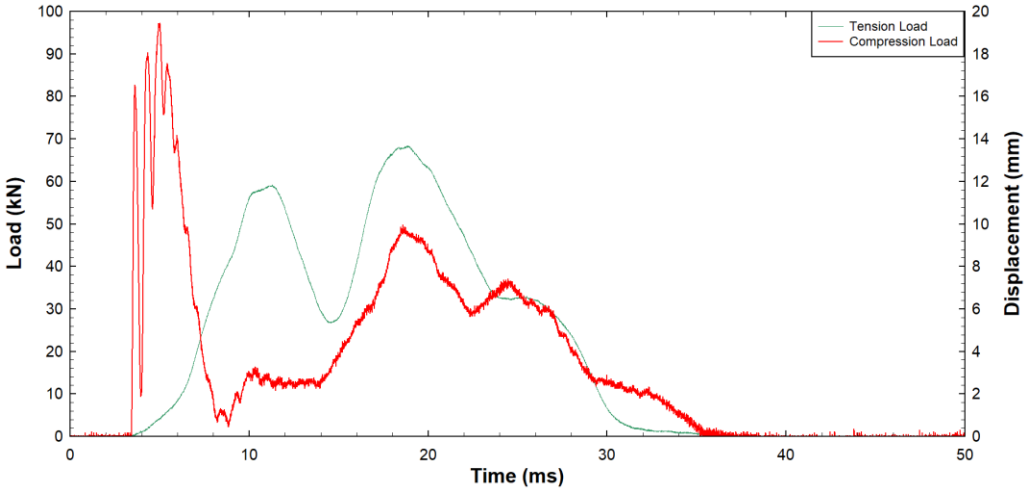

Fig. A1.46: Test Result for DT-TTH-HL-01-01

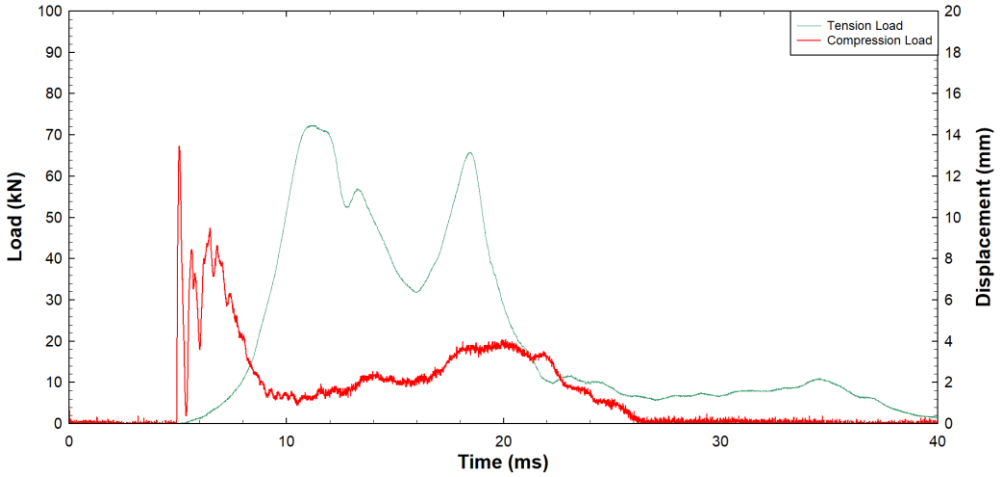

Fig. A1.47: Test Result for DT-TTH-HL-02-02

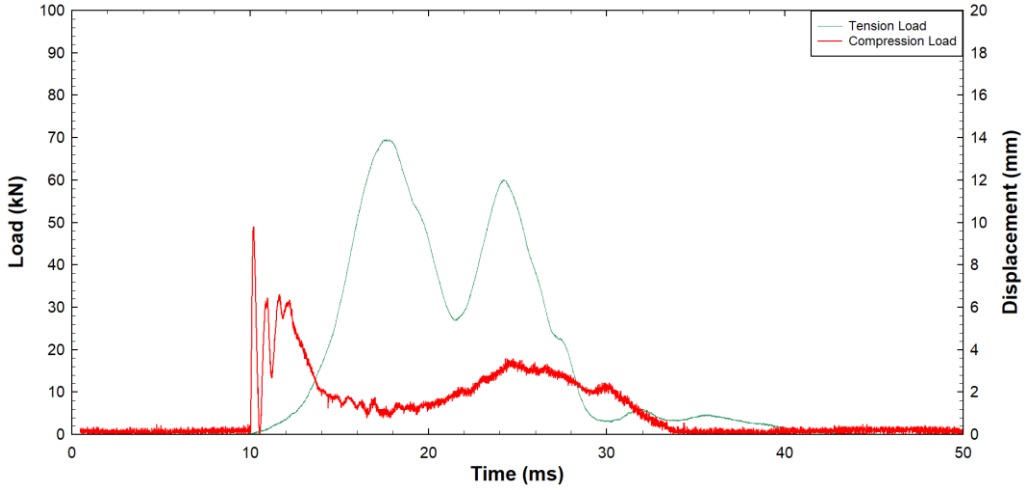

Fig. A1.48: Test Result for DT-TTH-HL-03-01

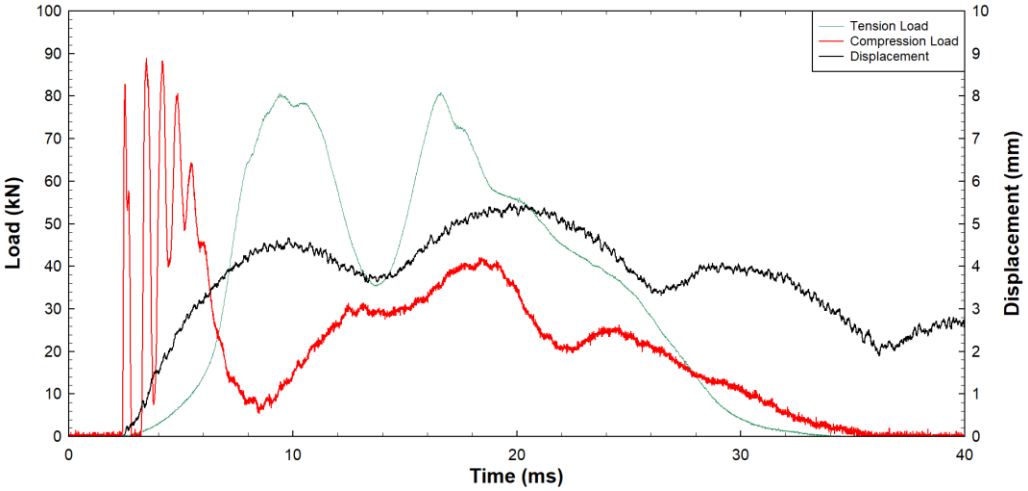

Fig. A1.49: Test Result for DT-TTH-HL-01-01

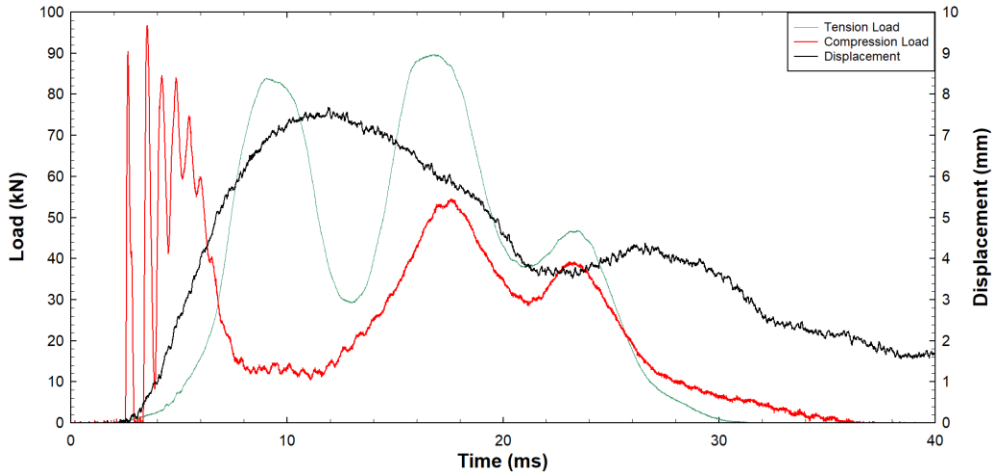

Fig. A1.50: Test Result for DT-TTH-HL-02-01

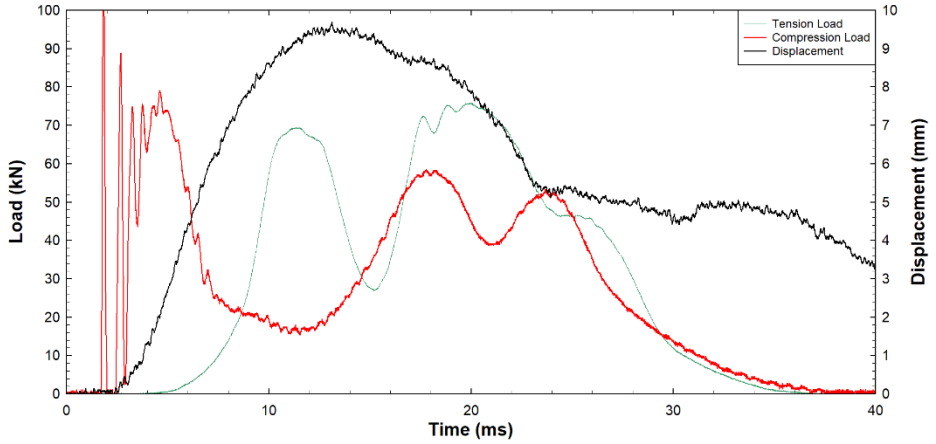

Fig. A1.51: Test Result for DT-TTH-HL-03-01

A.2 : Dynamic Shear Plots

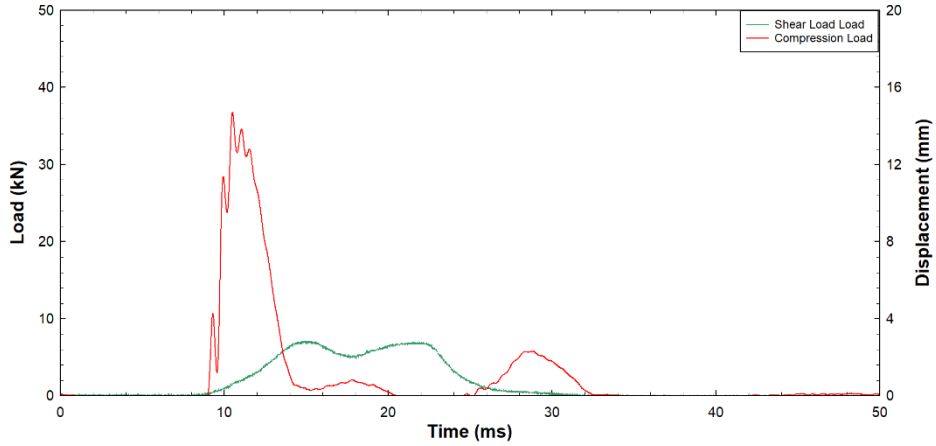

Fig. A2.1 : Test Result for DS-STB-QI-01-01

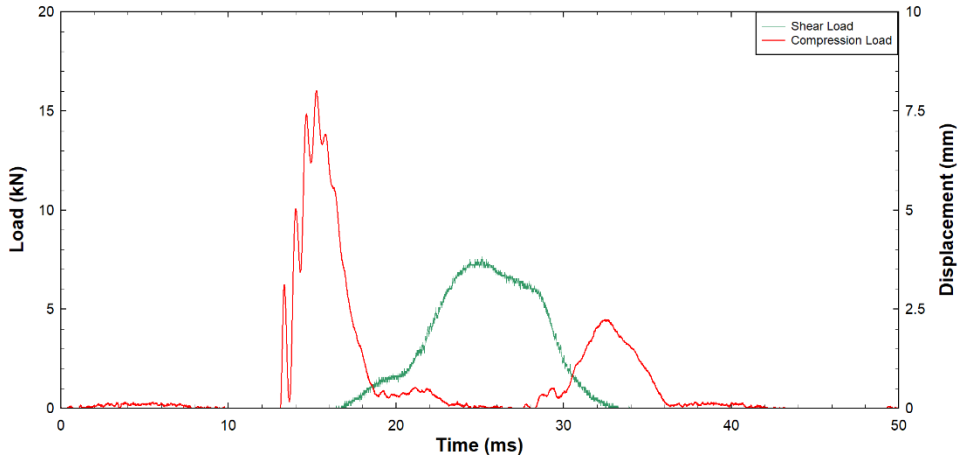

Fig. A2.2: Test Result for DS-STB-QI-02-01

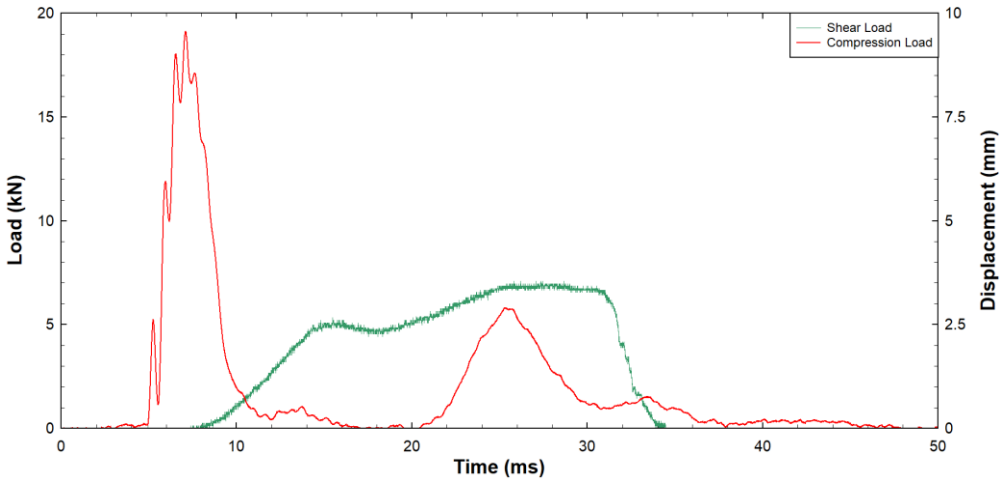

Fig. A2.3: Test Result for DS-STB-QI-03-01

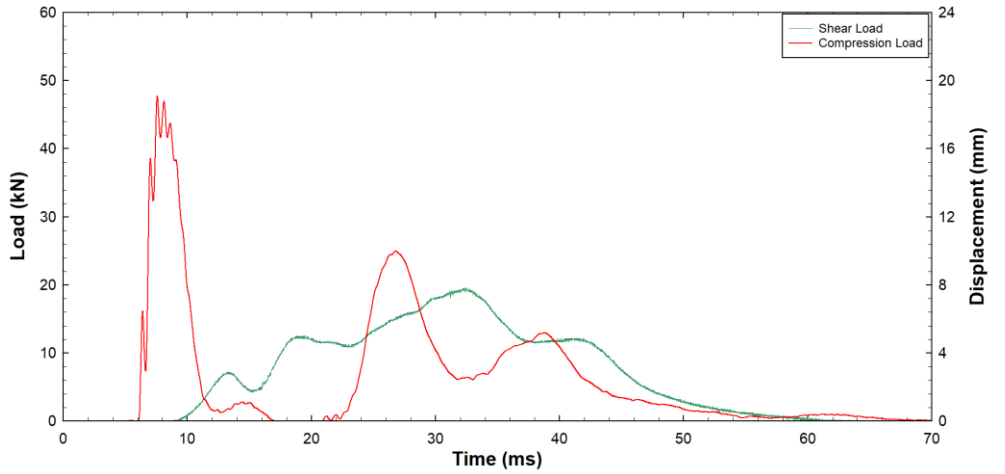

Fig. A2.4: Test Result for DS-STB-TE-01-01

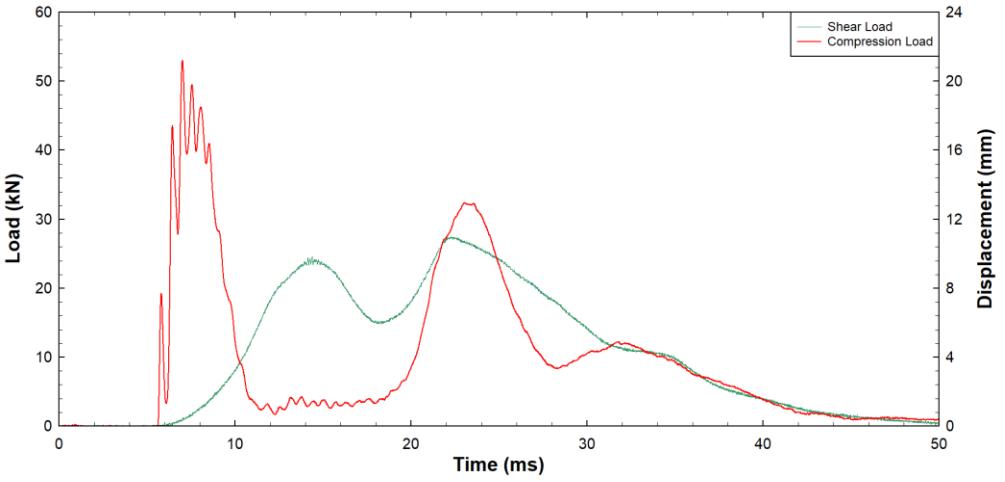

Fig. A2.5: Test Result for DS-STB-TE-01-03

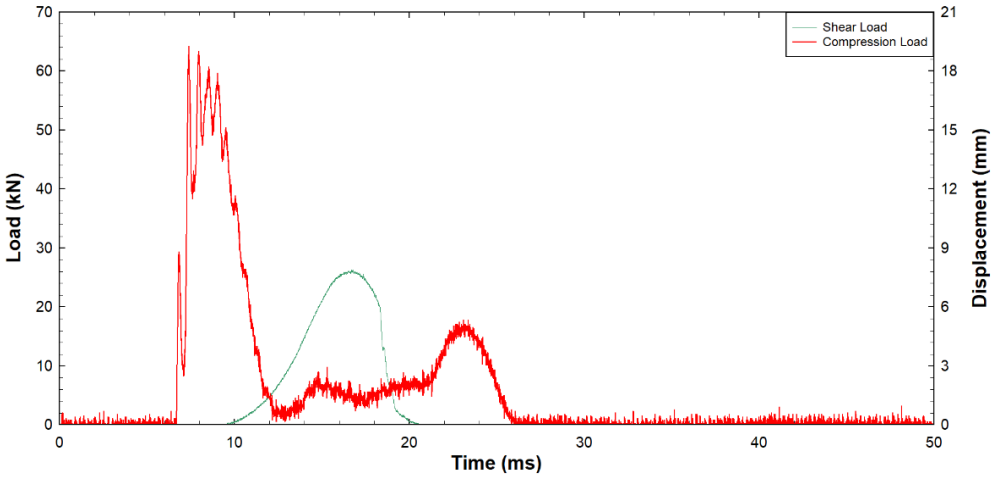

Fig. A2.6: Test Result for DS-STB-TE-02-03

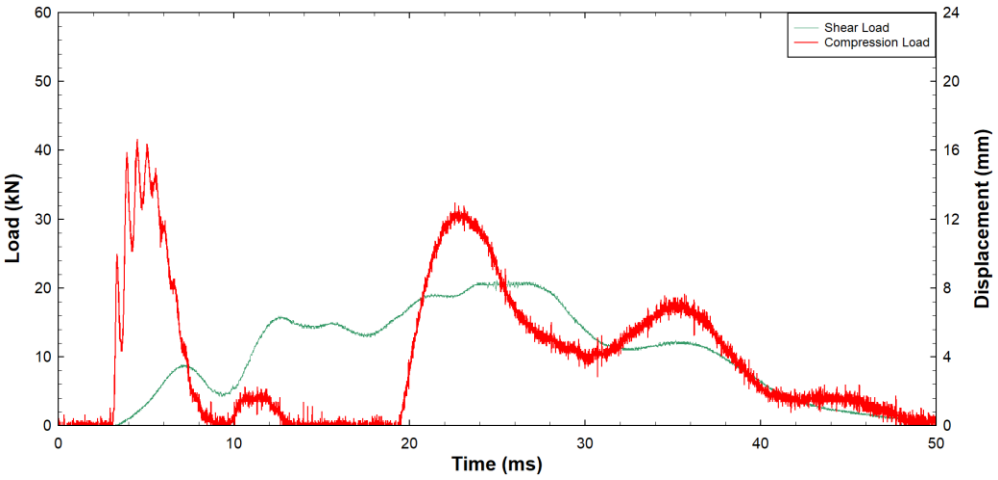

Fig. A2.7: Test Result for DS-STB-TE-03-01

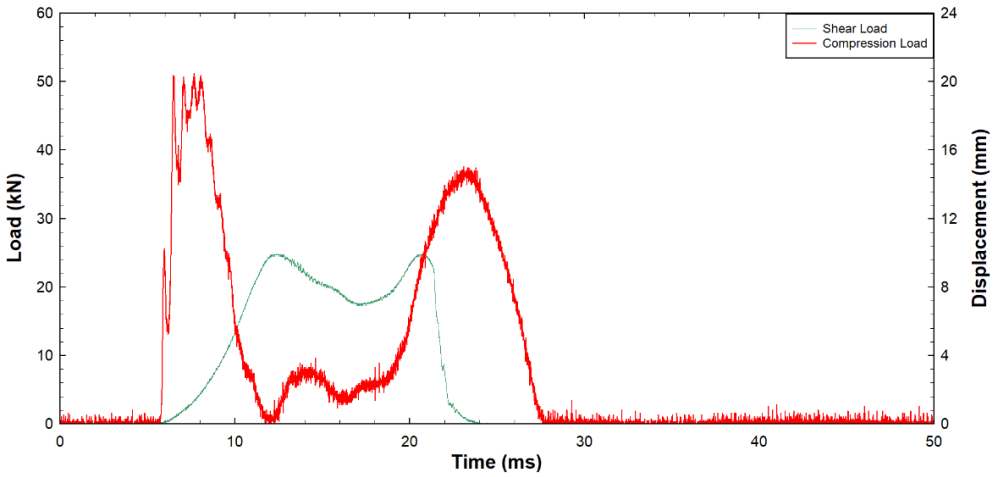

Fig. A2.8: Test Result for DS-STB-TE-03-02

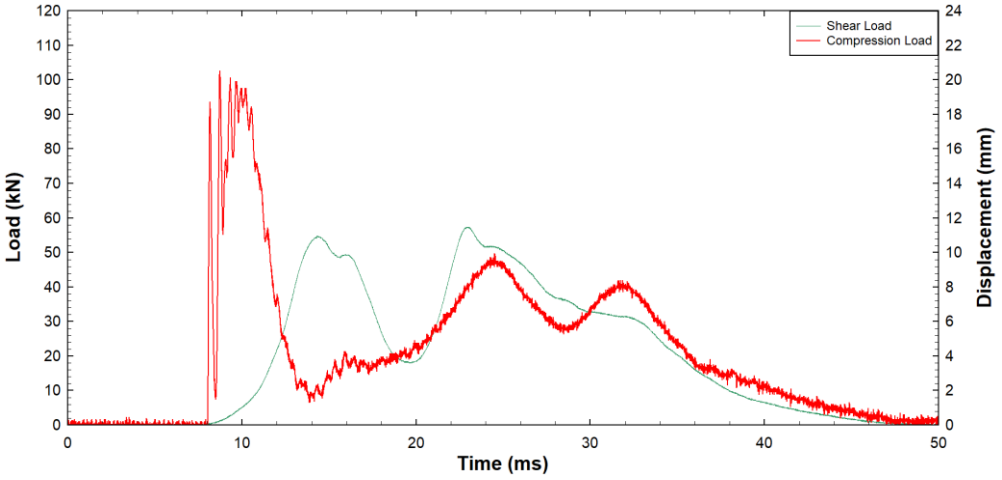

Fig. A2.9: Test Result for DS-STB-HL-01-03

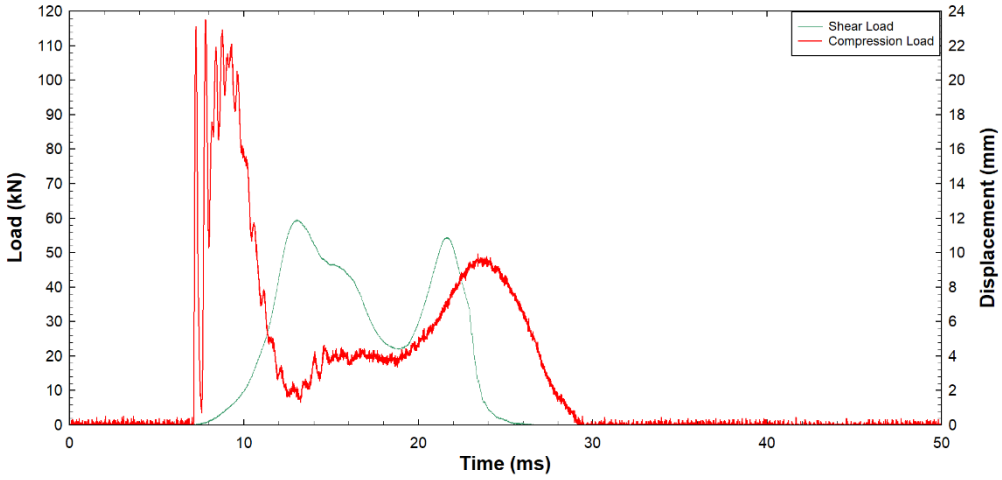

Fig. A2.10: Test Result for DS-STB-HL-01-04

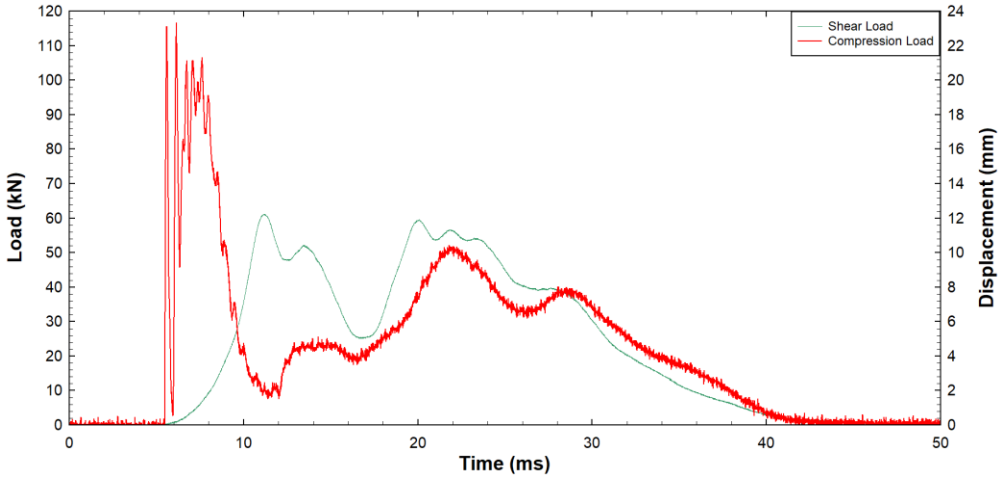

Fig. A2.11: Test Result for DS-STB-HL-02-02

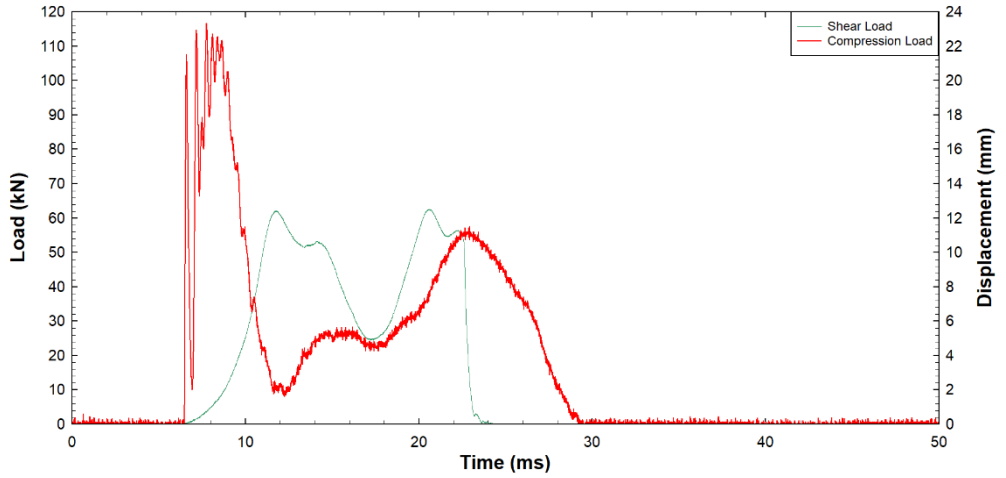

Fig. A2.12: Test Result for DS-STB-HL-02-04

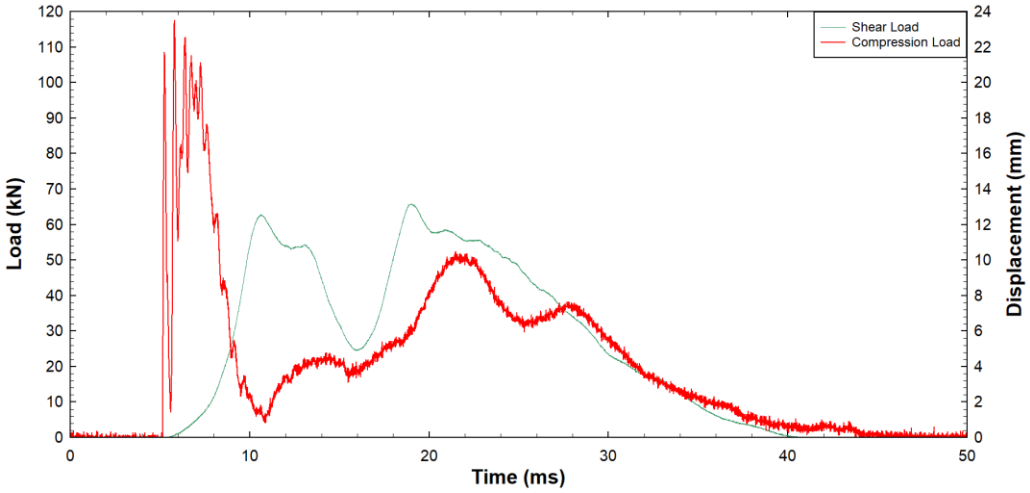

Fig. A2.13: Test Result for DS-STB-HL-03-02

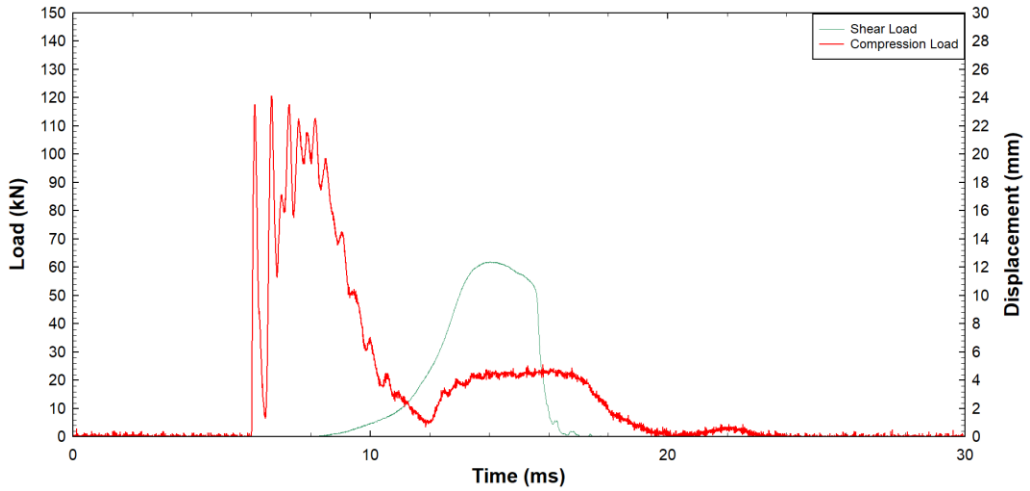

Fig. A2.14: Test Result for DS-STB-HL-03-03

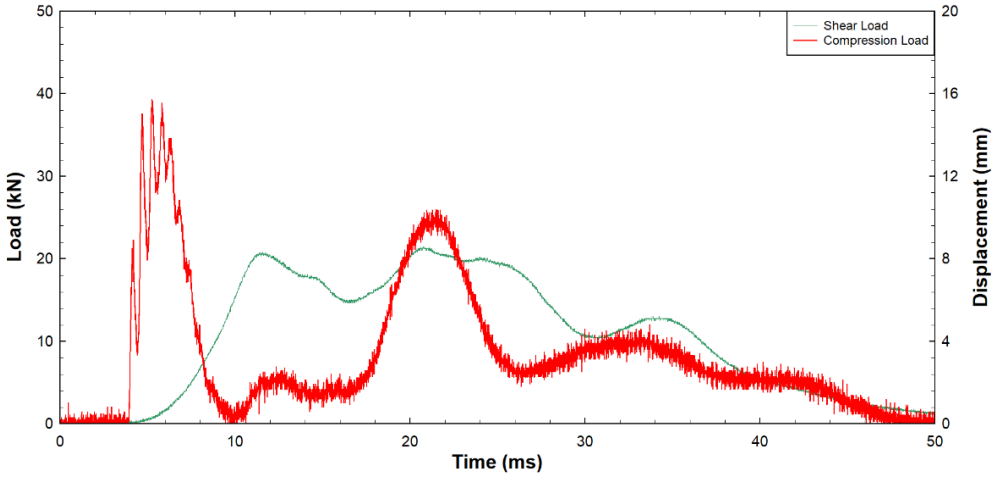

Fig. A2.15: Test Result for DS-WA-TE-01-02

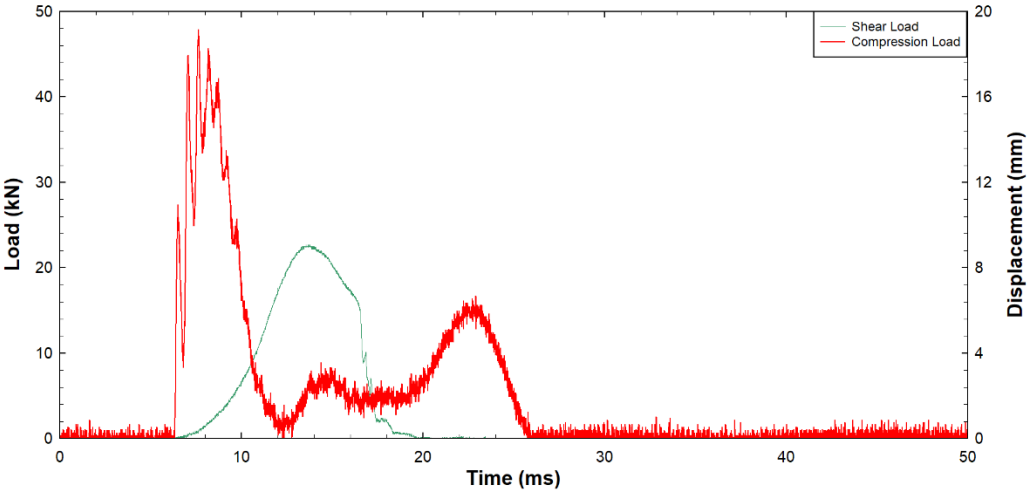

Fig. A2.16: Test Result for DS-WA-TE-01-03

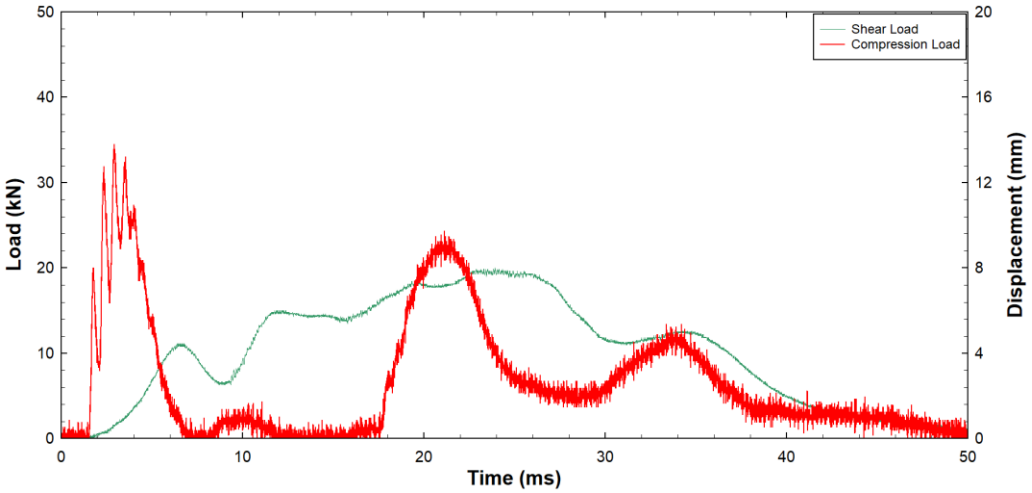

Fig. A2.17: Test Result for DS-WA-TE-02-01

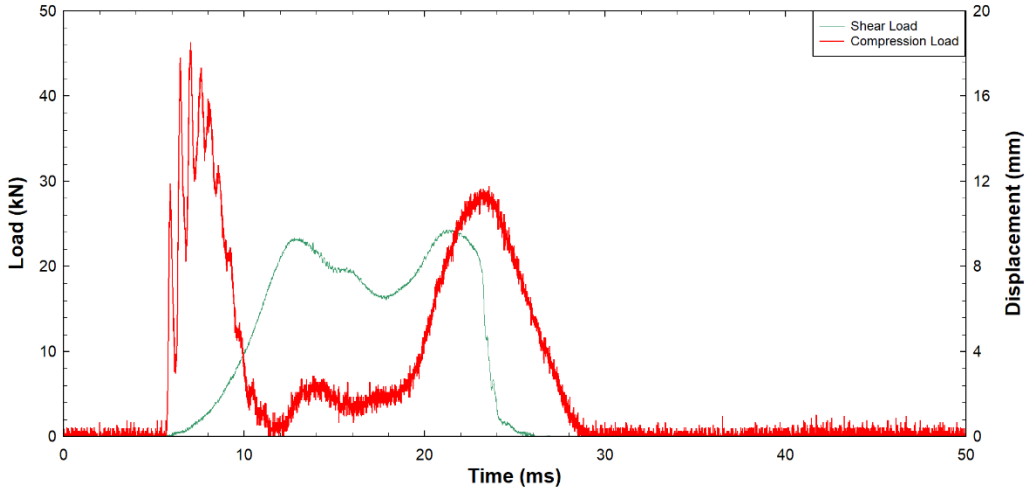

Fig. A2.18: Test Result for DS-WA-TE-02-02

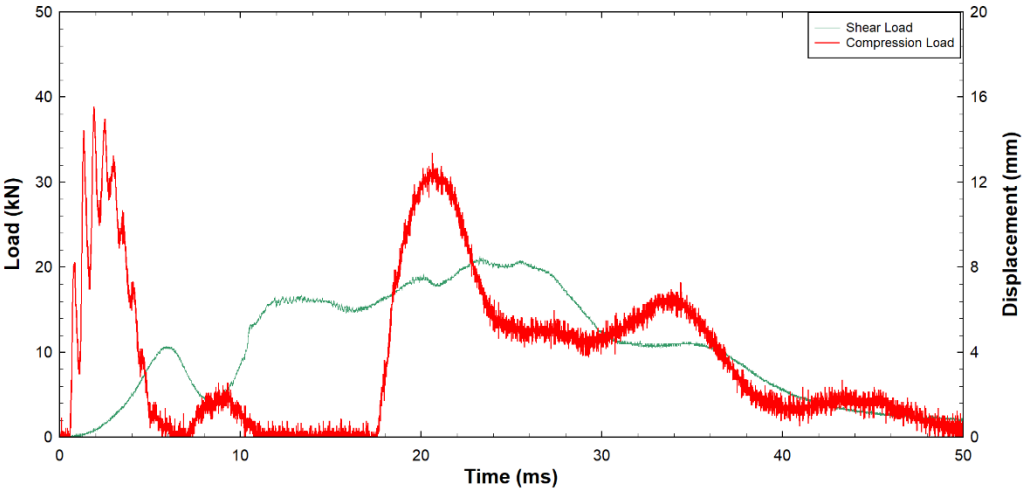

Fig. A2.19: Test Result for DS-WA-TE-03-01

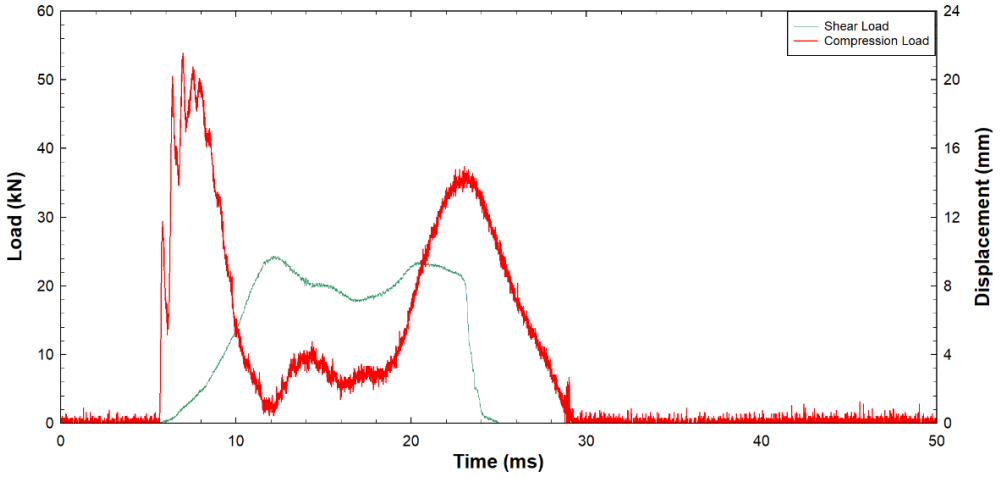

Fig. A2.20: Test Result for DS-WA-TE-03-02

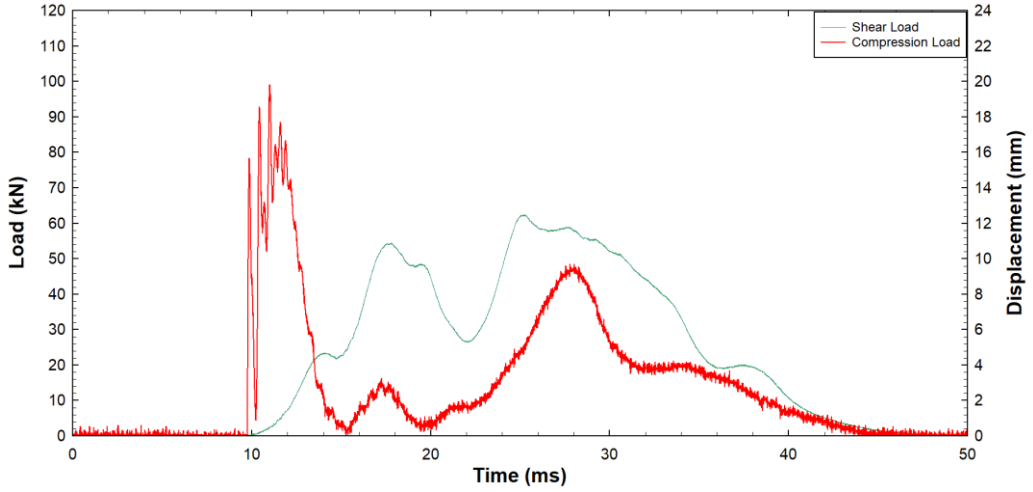

Fig. A2.21: Test Result for DS-WA-HL-01-01

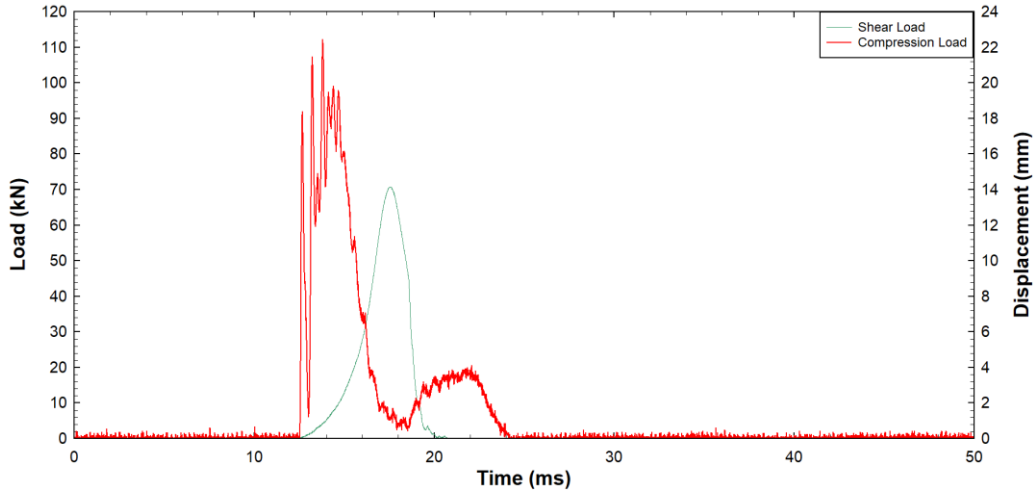

Fig. A2.22: Test Result for DS-WA-HL-01-02

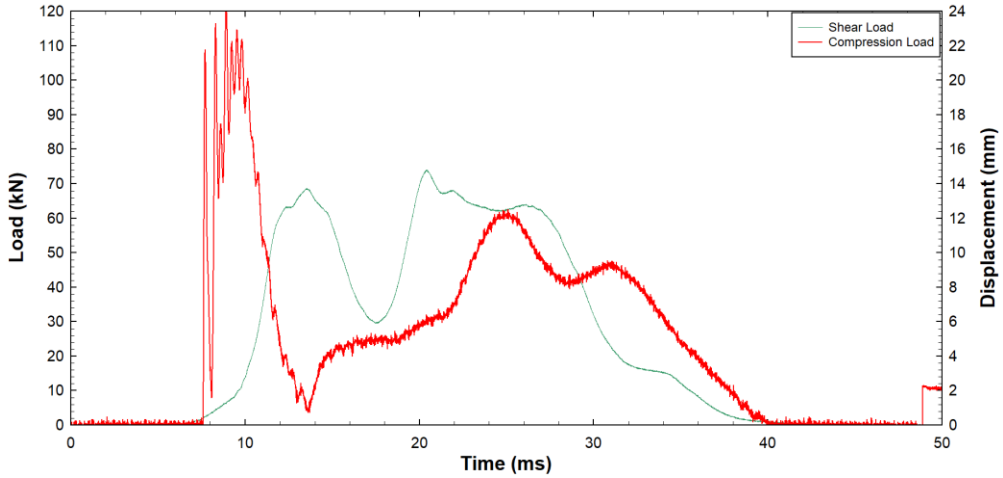

Fig. A2.23: Test Result for DS-WA-HL-02-03

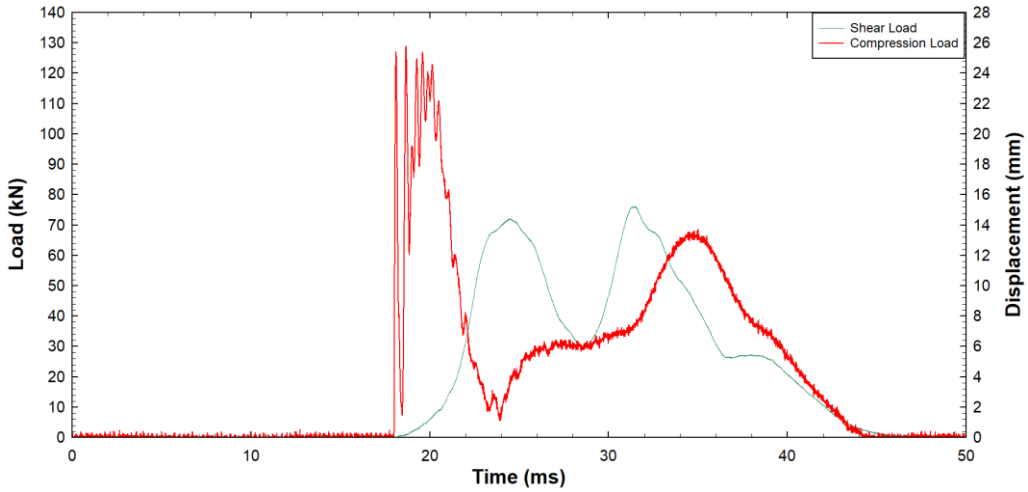

Fig. A2.24: Test Result for DS-WA-HL-02-04

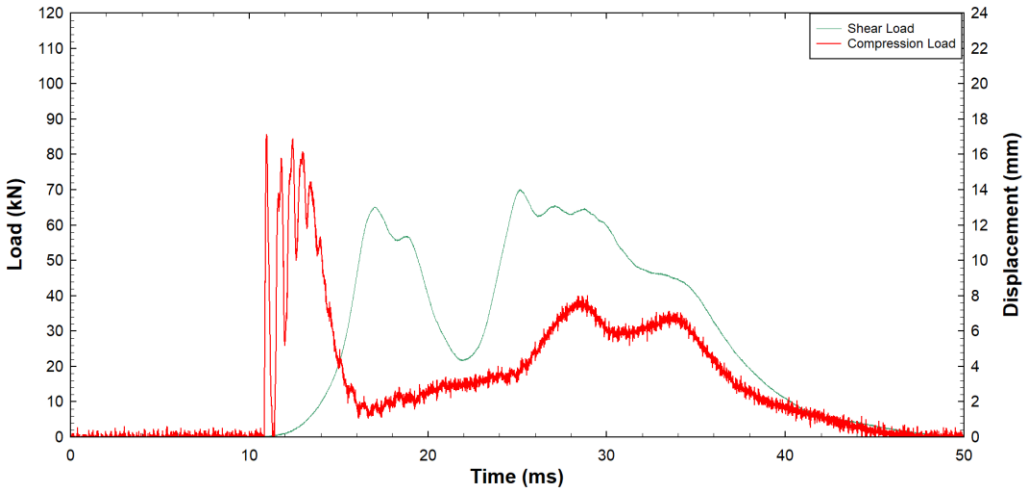

Fig. A2.25: Test Result for DS-WA-HL-03-02

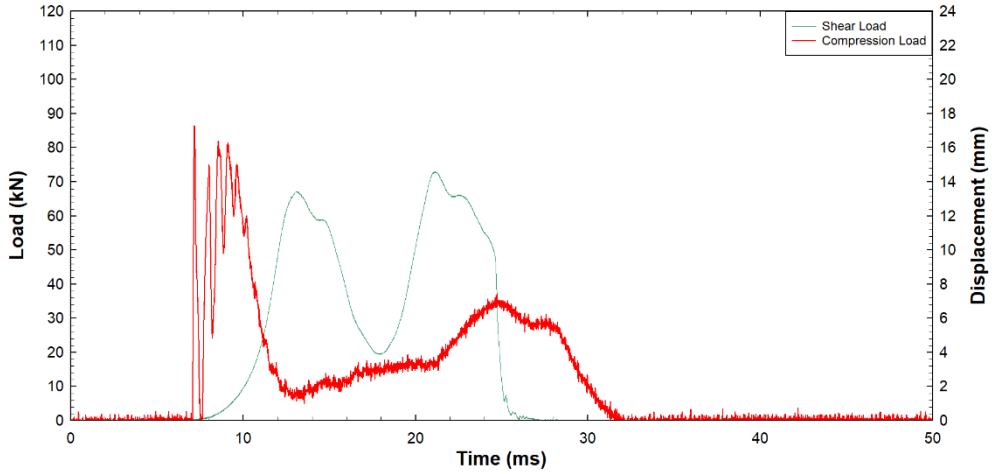

Fig. A2.26: Test Result for DS-WA-HL-03-03

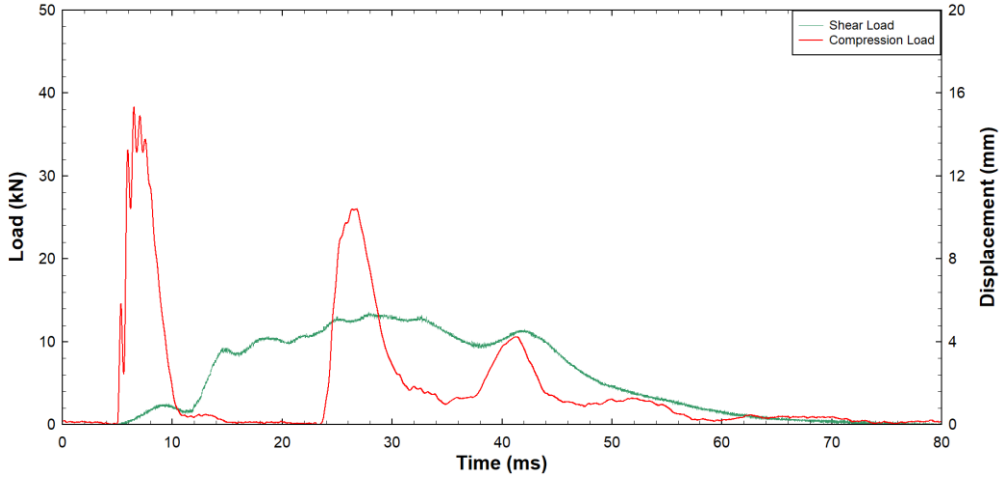

Fig. A2.27: Test Result for DS-TTH-QI-01-02

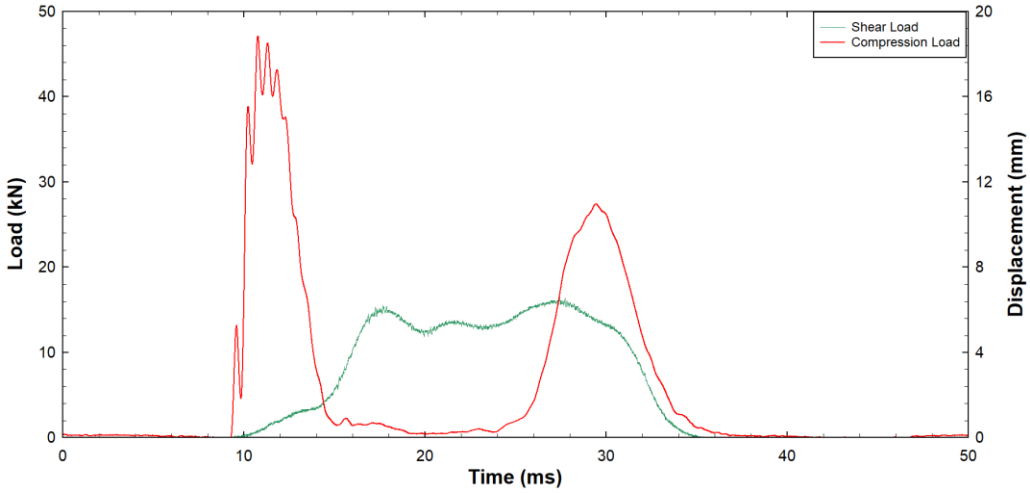

Fig. A2.28: Test Result for DS-TTH-QI-01-03

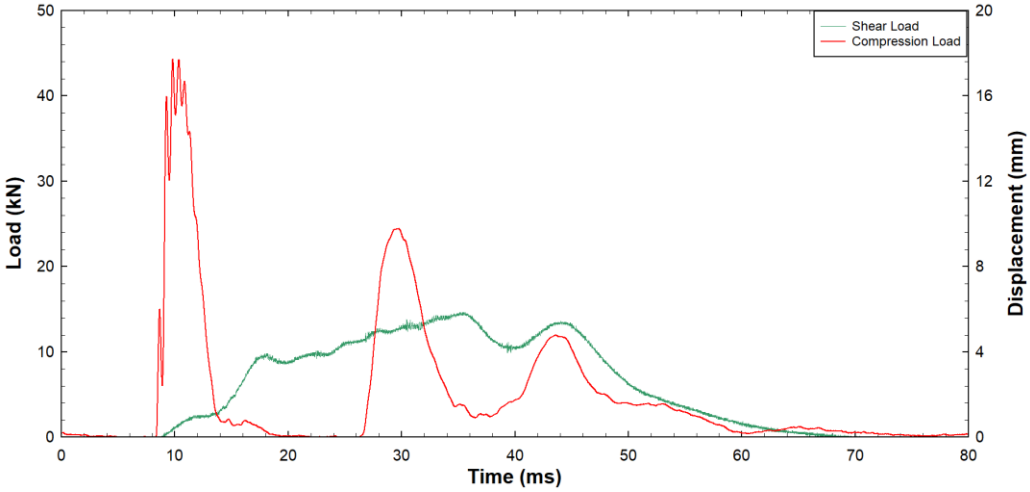

Fig. A2.29: Test Result for DS-TTH-QI-02-01

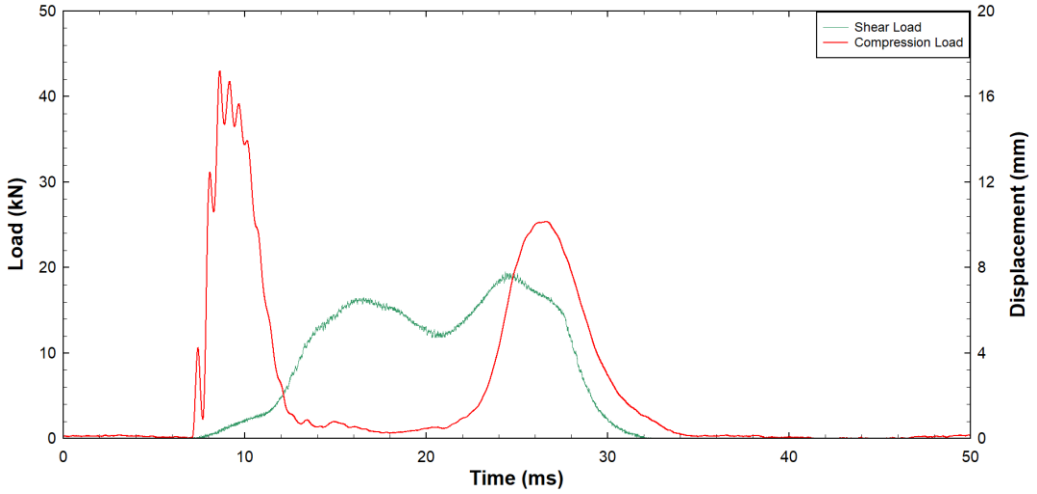

Fig. A2.30: Test Result for DS-TTH-QI-02-02

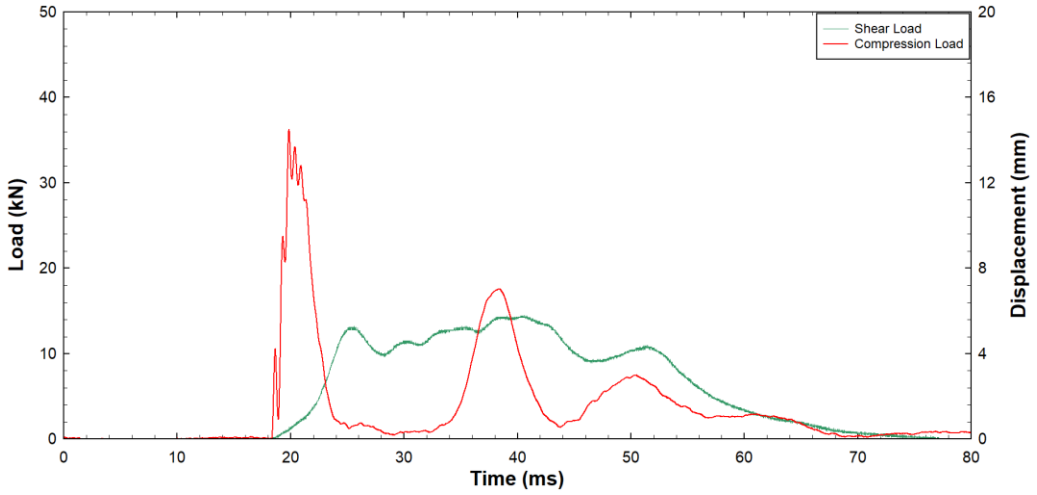

Fig. A2.31:Test Result for DS-TTH-QI-03-02

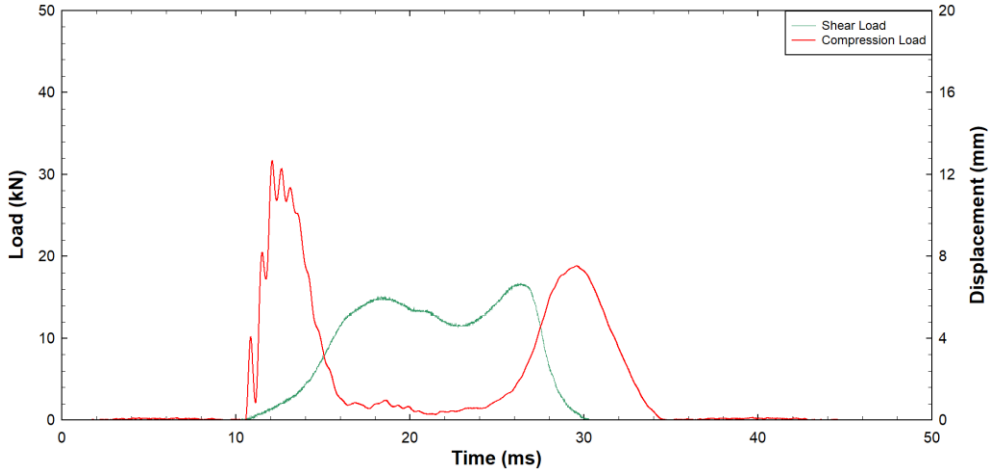

Fig. A2.32: Test Result for DS-TTH-QI-03-03

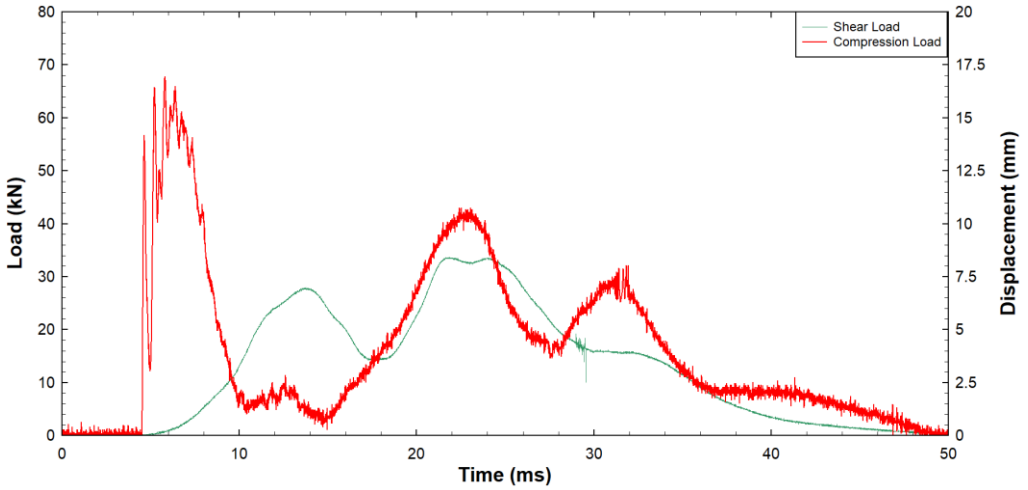

Fig. A2.33: Test Result for DS-TTH-TE-01-03

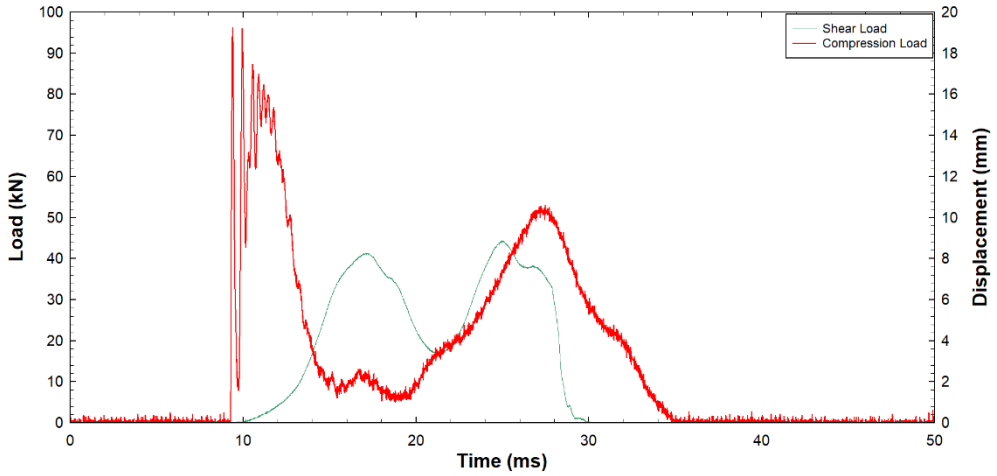

Fig. A2.34: Test Result for DS-TTH-TE-01-04

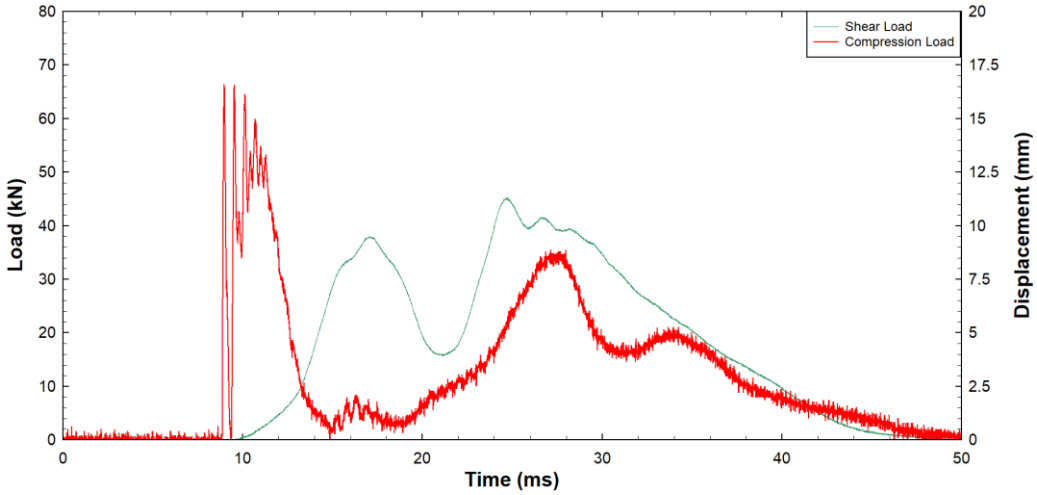

Fig. A2.35: Test Result for DS-TTH-TE-02-03

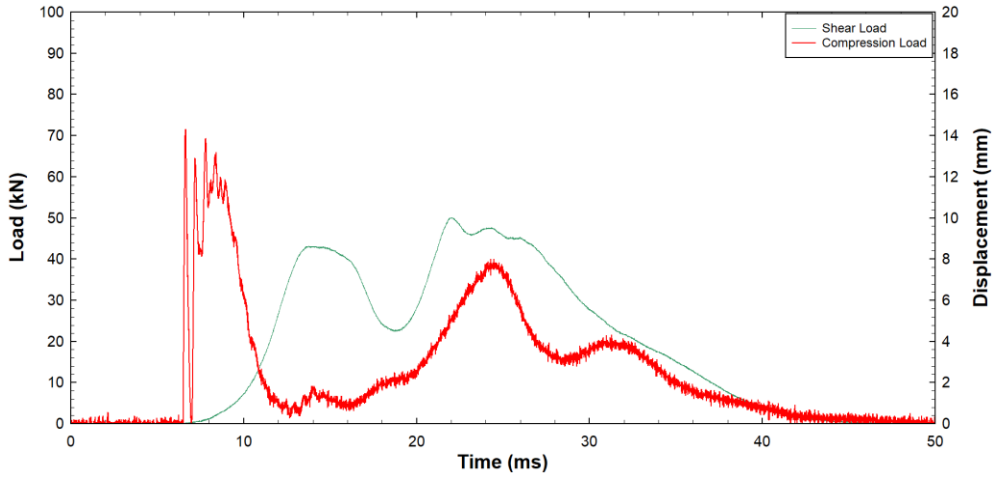

Fig. A2.36: Test Result for DS-TTH-TE-03-02

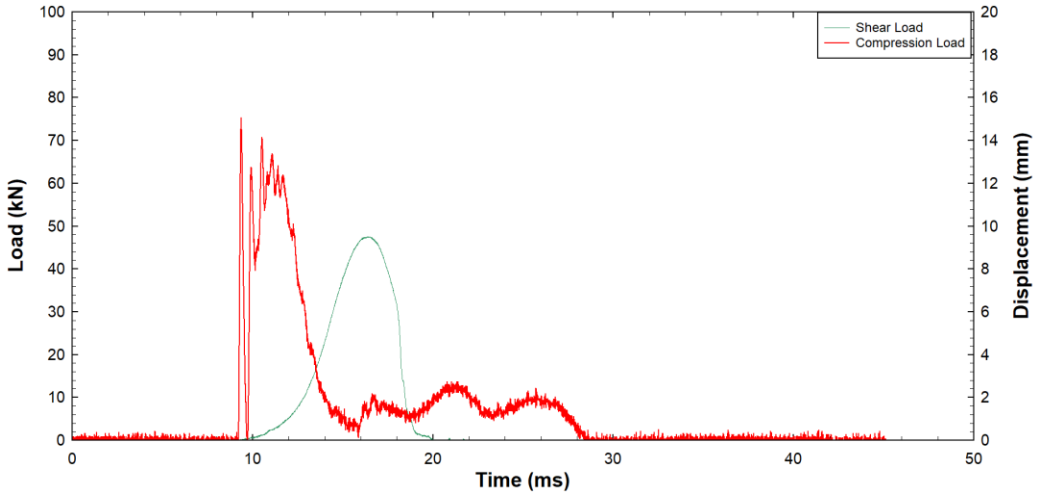

Fig. A2.37: Test Result for DS-TTH-TE-03-03

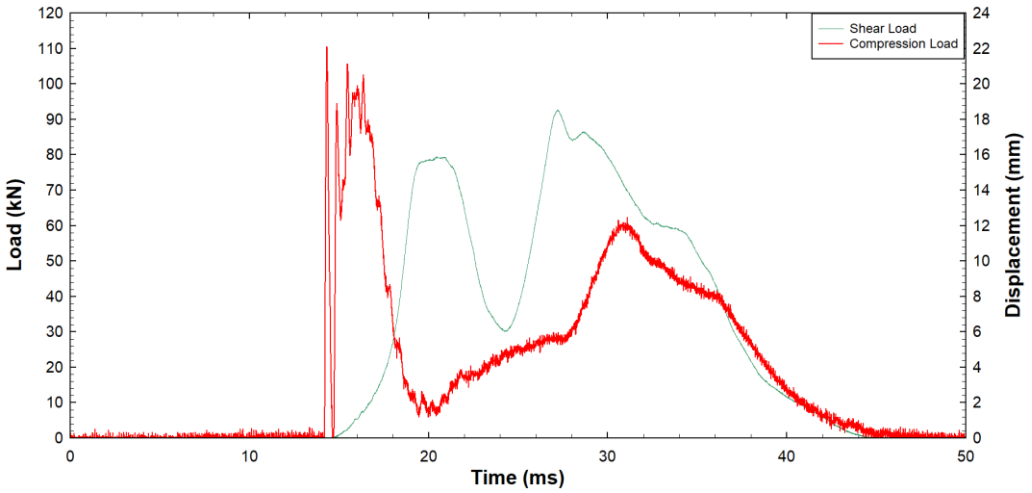

Fig. A2.38: Test Result for DS-TTH-HL-01-03

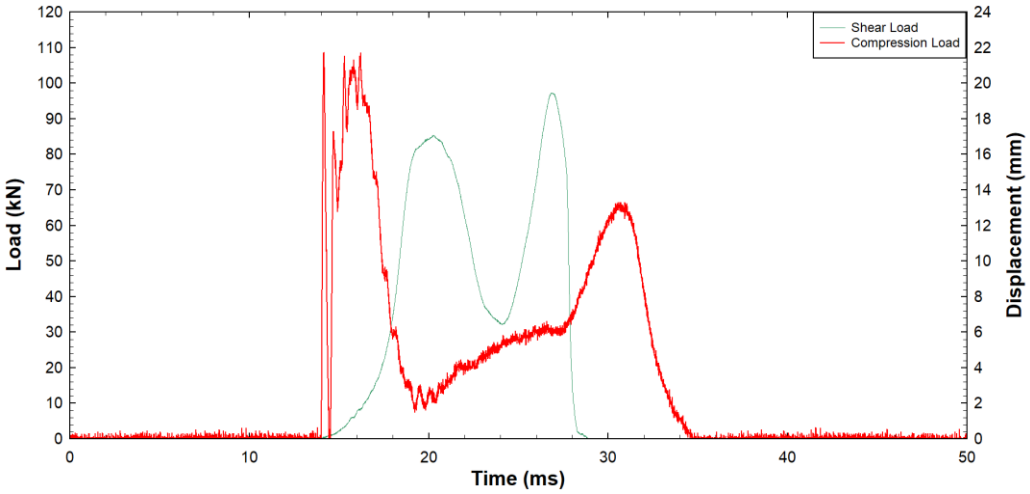

Fig. A2.39: Test Result for DS-TTH-HL-01-04

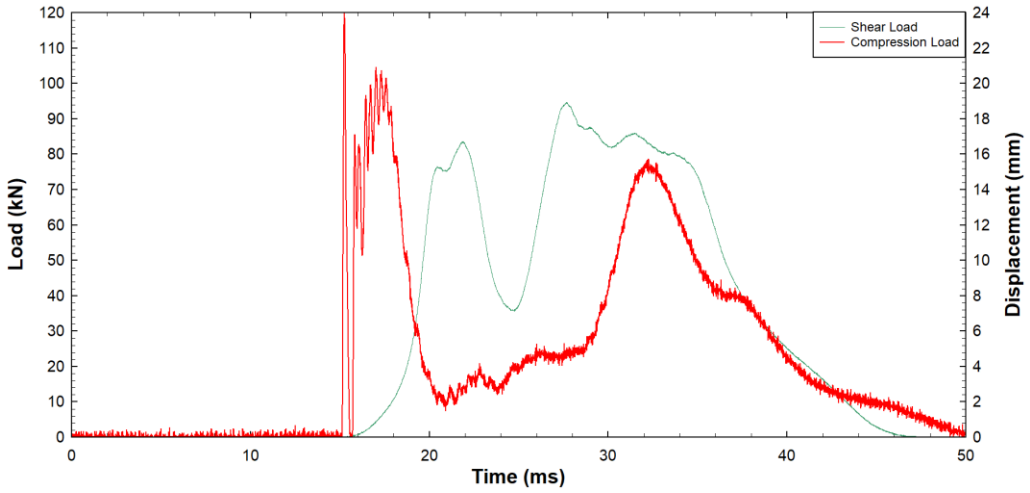

Fig. A2.40: Test Result for DS-TTH-HL-02-03

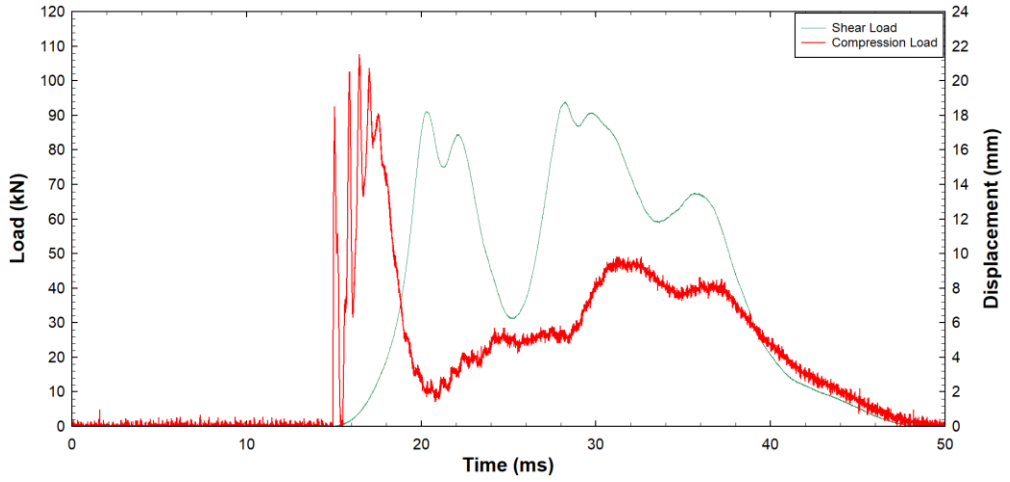

Fig. A2.41: Test Result for DS-TTH-HL-03-02

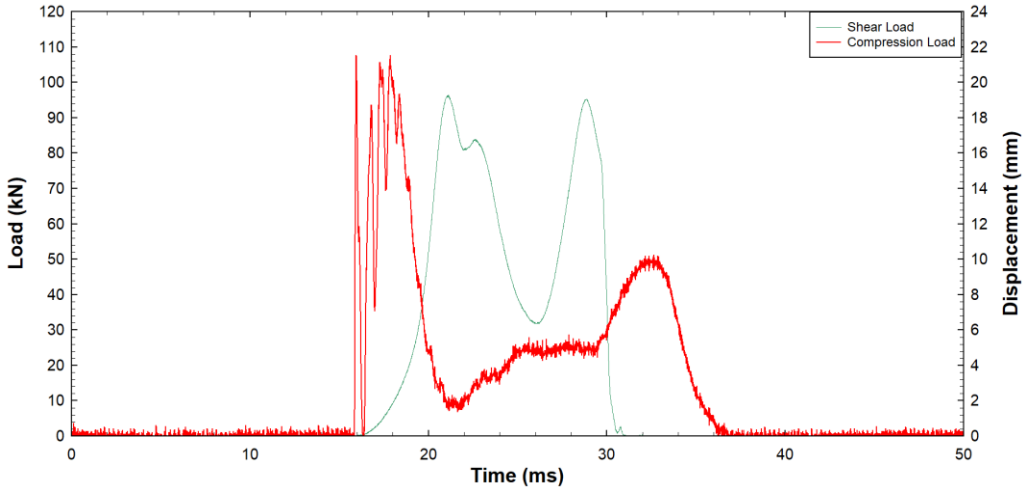

Fig. A2.42: Test Result for DS-TTH-HL-03-03

Appendix B : Pictures

B.1 : Static Test Pictures

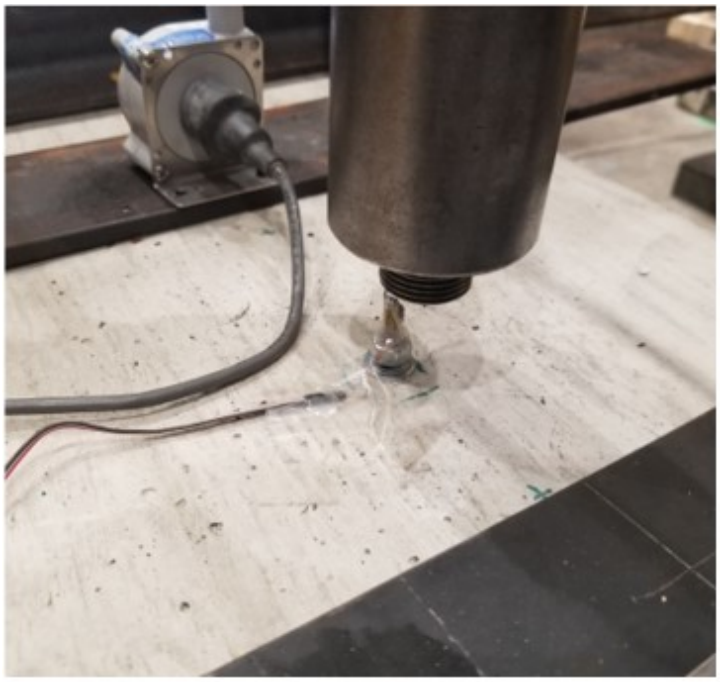

Fig. B1.1: Steel Fracture Failure for ST-STB-QI-01

Fig. B1.2: Steel Fracture Failure for ST-STB-QI-02

Fig. B1.3: Steel Fracture Failure for ST-STB-QI-03

Fig. B1.4: Steel Fracture Failure for ST-STB-TE-01

Fig. B1.5: Steel Fracture Failure for ST-STB-TE-02

Fig. B1.6: Steel Fracture Failure for ST-STB-TE-03

Fig. B1.7: Concrete Breakout and Pull-through Failure for ST-STB-HL-01

Fig. B1.8: Beam Splitting Failure for ST-STB-TE-02

Fig. B1.9: Concrete Breakout Failure for ST-STB-HL-03

Fig. B1.10: Steel Fracture Failure for ST-WA-TE-01

Fig. B1.11: Steel Fracture Failure for ST-WA-TE-02

Fig. B1.12: Steel Fracture Failure for ST-WA-TE-03

Fig. B1.13: Pull-through Failure for ST-WA-HL-01

Fig. B1.14: Pull-through Failure for ST-WA-HL-02

Fig. B1.15: Pull-through Failure for ST-WA-HL-03

Fig. B1.16: Mixed Pullout and Concrete Breakout Failure for ST-TTH-QI-01

Fig. B1.17: Mixed Pullout and Concrete Breakout Failure for ST-TTH-QI-02

Fig. B1.18: Mixed Pullout and Concrete Breakout Failure for ST-TTH-QI-03

Fig. B1.19: Mixed Pullout and Concrete Breakout Failure for ST-TTH-TE-01

Fig. B1.20: Mixed Pullout and Concrete Breakout Failure for ST-TTH-TE-02

Fig. B1.21: Mixed Pullout and Concrete Breakout Failure for ST-TTH-TE-03

Fig. B1.22: Mixed Pullout and Concrete Breakout Failure for ST-TTH-HL-01

Fig. B1.23: Mixed Pullout and Concrete Breakout Failure for ST-TTH-HL-02

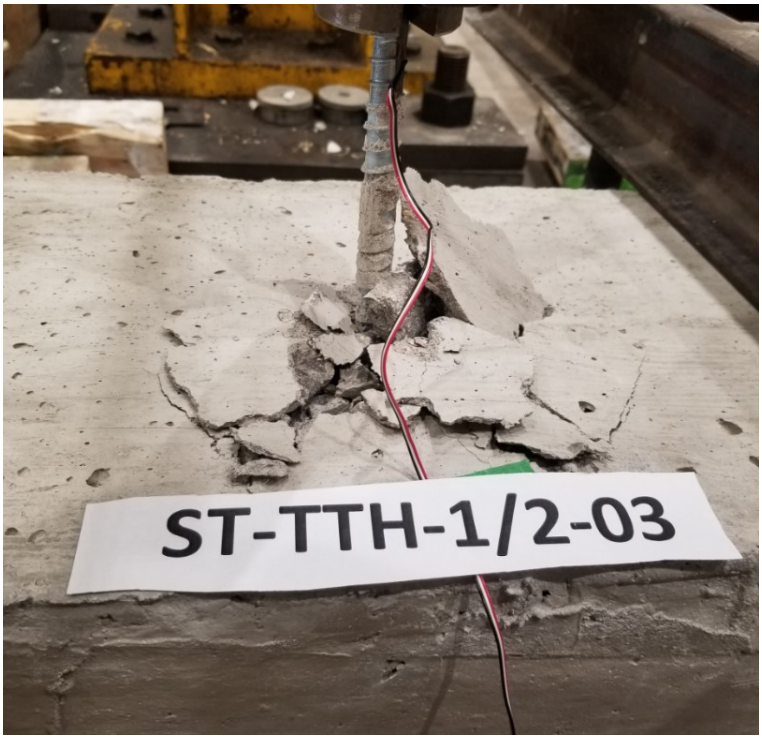

Fig. B1.24: Mixed Pullout and Concrete Breakout Failure for ST-TTH-HL-03

B.2 : Dynamic Test Pictures

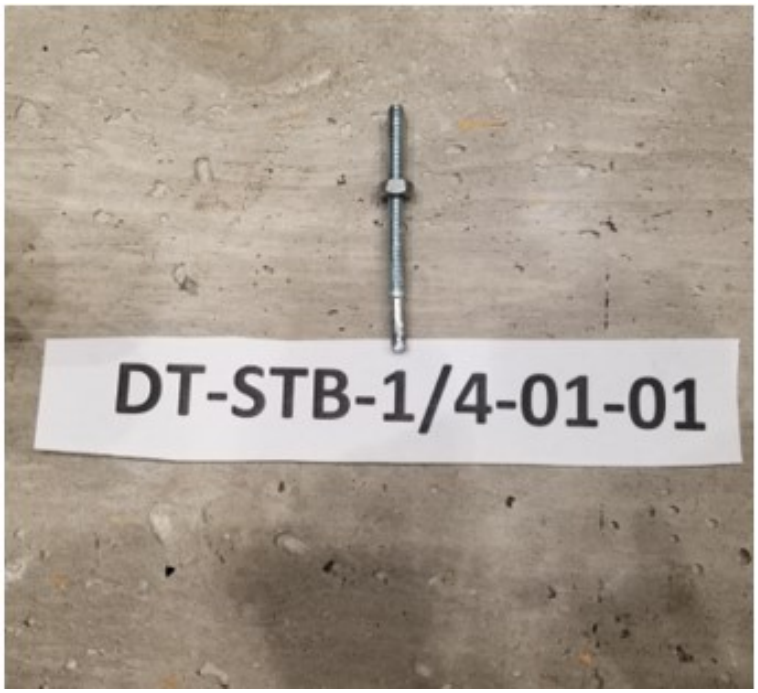

Fig. B2.1: Pull-through Failure for DT-STB-QI-01

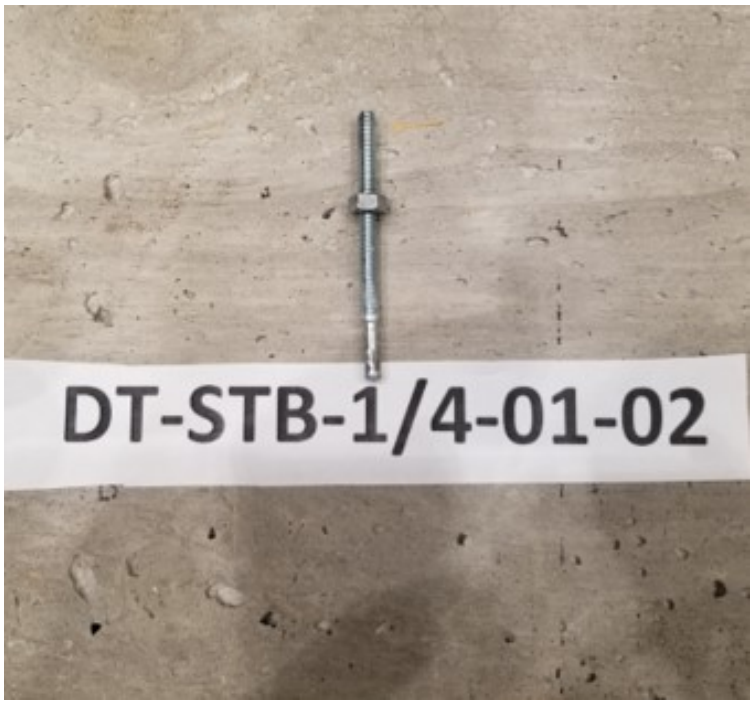

Fig. B2.2: Pull-through Failure for DT-STB-QI-02

Fig. B2.3: Pull-through Failure for DT-STB-QI-03

Fig. B2.4: Pull-through Failure for DT-STB-QI-04

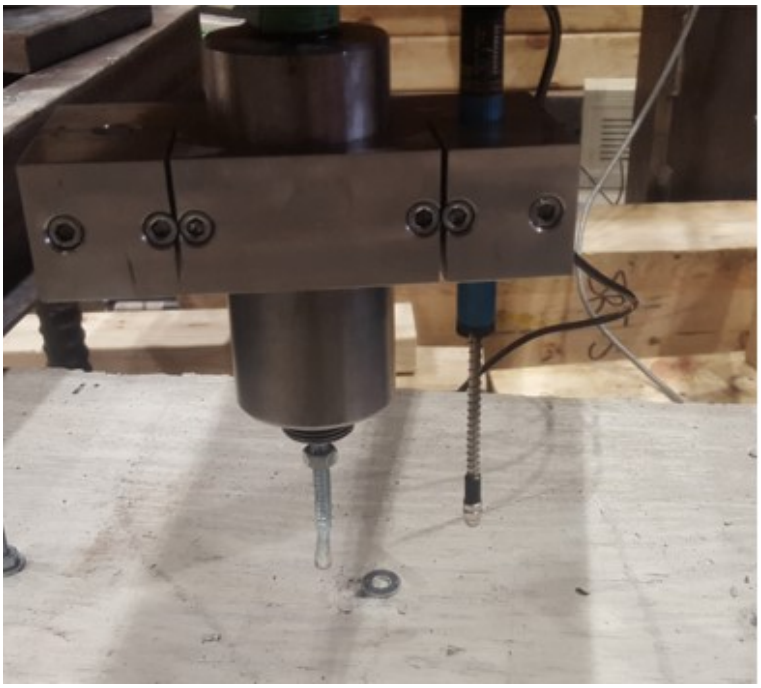

Fig. B2.5: Pull-through Failure for DT-STB-QI-05

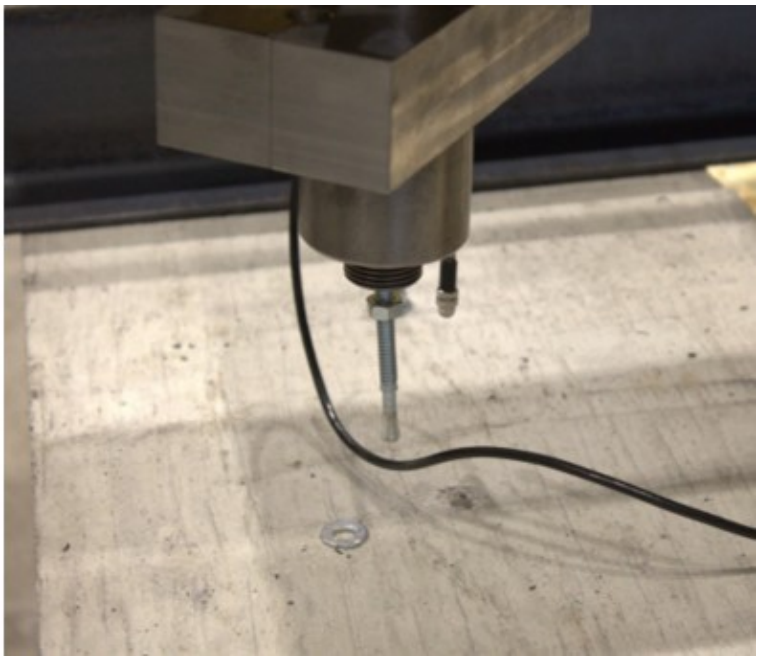

Fig. B2.6: Pull-through Failure for DT-STB-QI-07

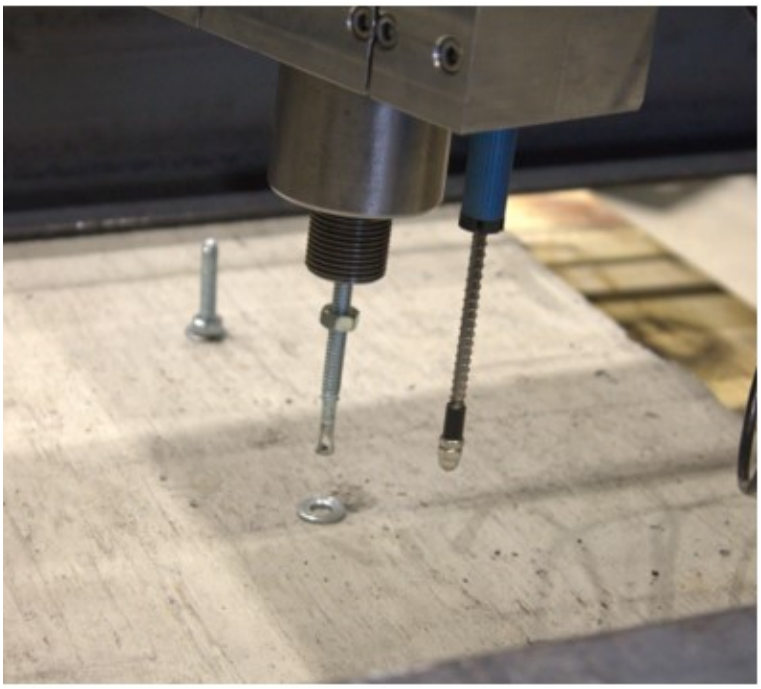

Fig. B2.7: Pull-through Failure for DT-STB-QI-08

Fig. B2.8: Concrete Breakout Failure for DT-STB-TE-01

Fig. B2.9: Steel Fracture Failure for DT-STB-TE-03*

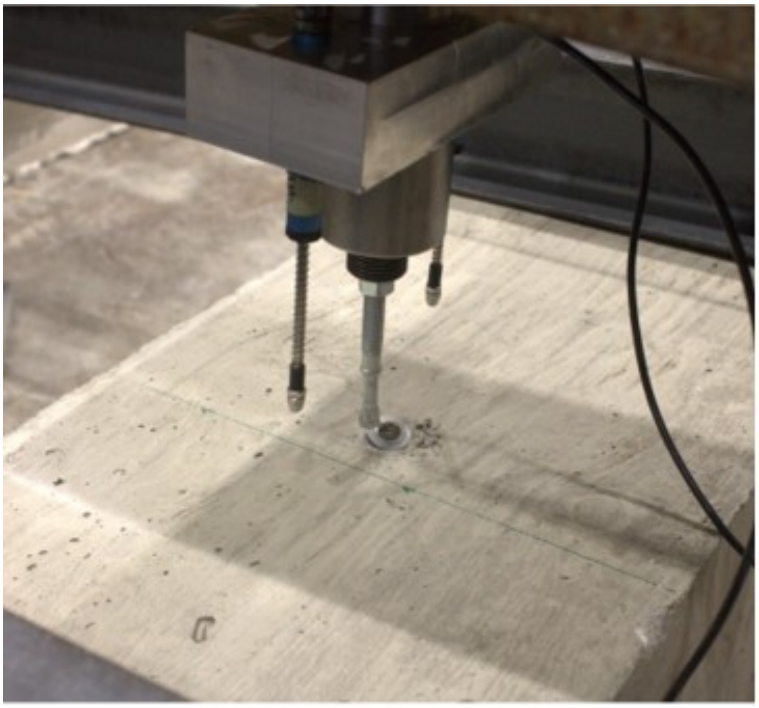

Fig. B2.10: Pull-through Failure for DT-STB-TE-01

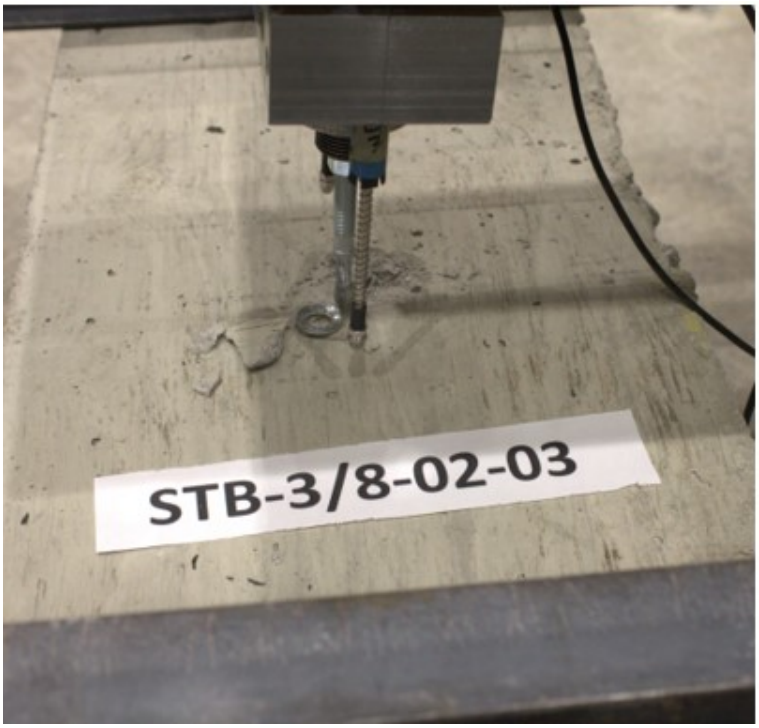

Fig. B2.11: Pull-through Failure for DT-STB-TE-02

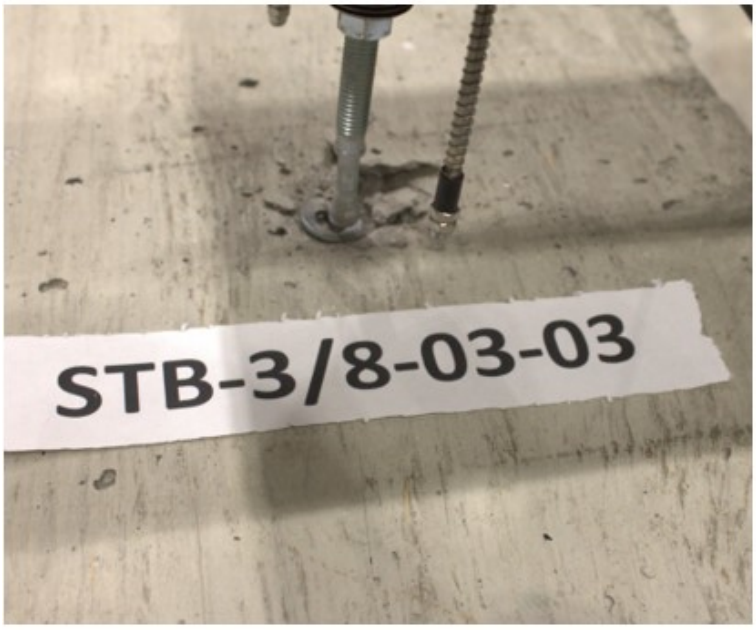

Fig. B2.12: Pull-through Failure for DT-STB-TE-01

Fig. B2.13: Pull-through Failure for DT-STB-HL-01

Fig. B2.14: Pull-through Failure for DT-STB-HL-02

Fig. B2.15: Pull-through Failure for DT-WA-TE-01

Fig. B2.16: Pull-through Failure for DT-WA-TE-02

Fig. B2.17: Pull-through Failure for DT-WA-TE-03

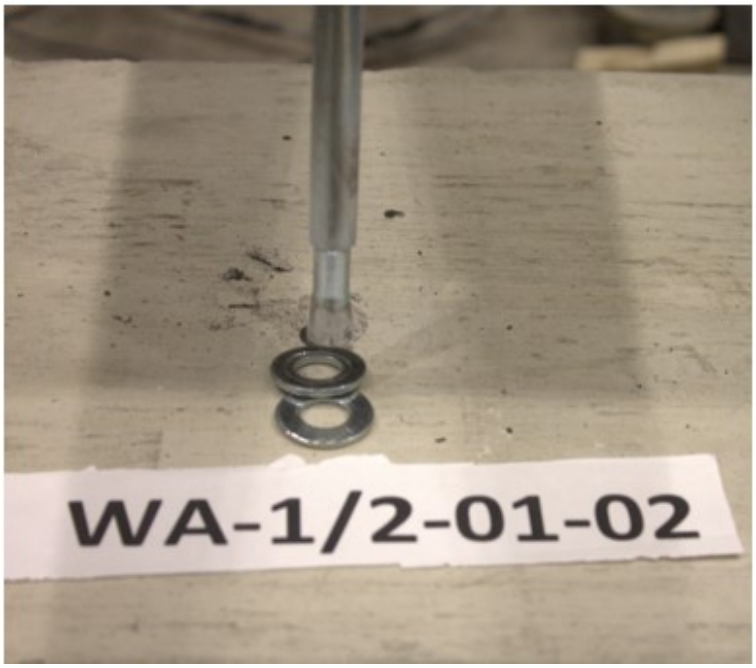

Fig. B2.18: Pull-through Failure for DT-WA-HL-01

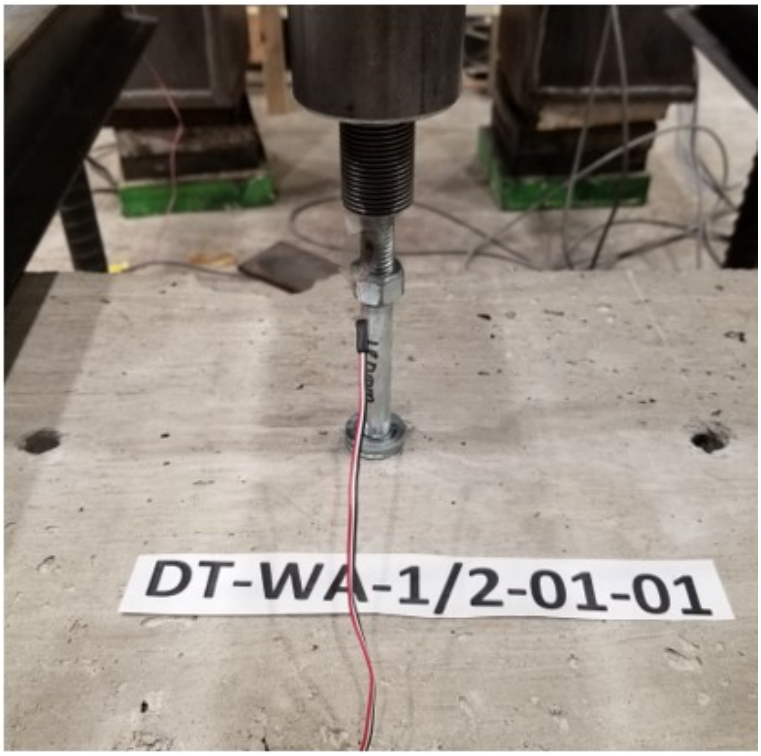

Fig. B2.19: Pull-through Failure for DT-WA-HL-01

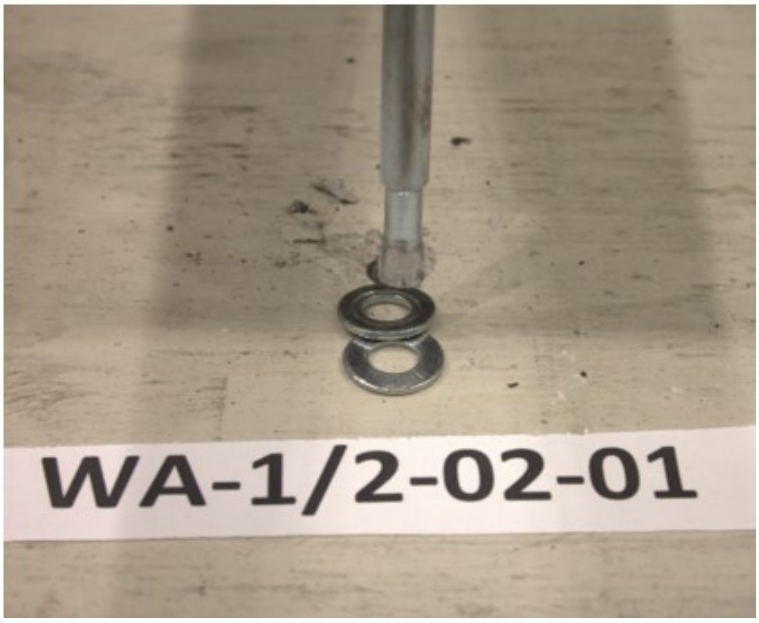

Fig. B2.20: Pull-through Failure for DT-WA-HL-02

Fig. B2.21: Pull-through Failure for DT-WA-HL-02

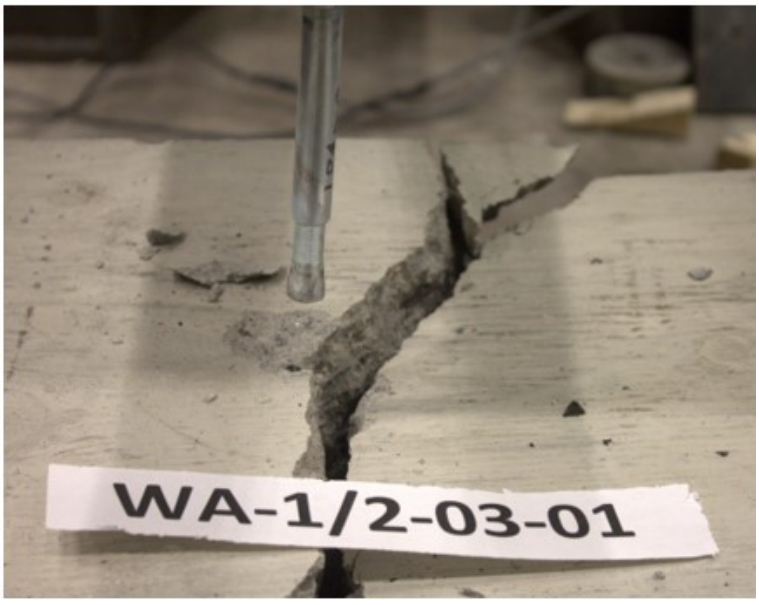

Fig. B2.22: Pull-through and Beam Splitting Failure for DT-WA-HL-03

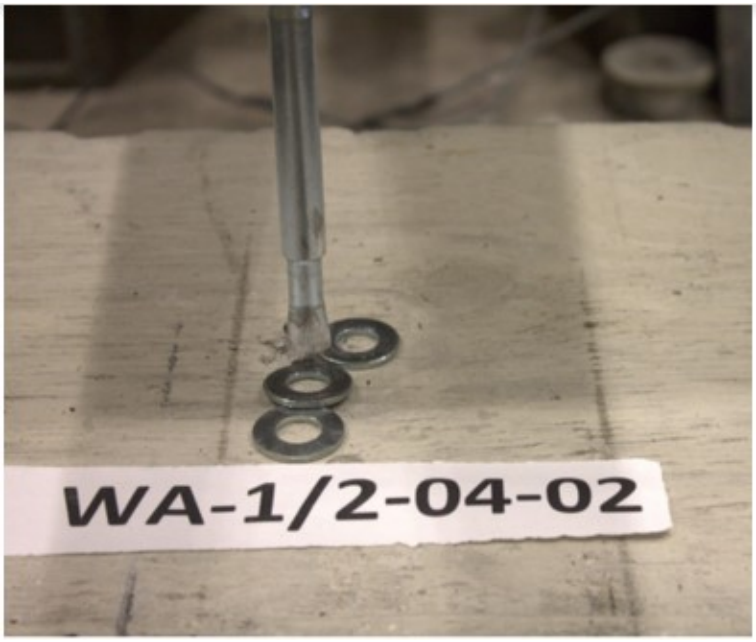

Fig. B2.23: Pull-through Failure for DT-WA-HL-04

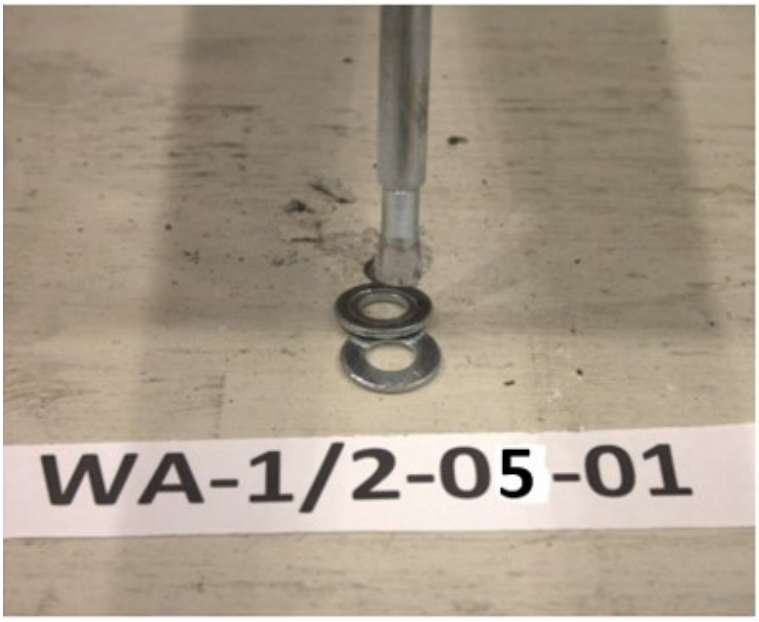

Fig. B2.24: Pull-through Failure for DT-WA-HL-05

Fig. B2.25: Concrete Breakout Failure of DT-TTH-QI-01

Fig. B2.26: Steel Fracture Failure of DT-TTH-QI-01

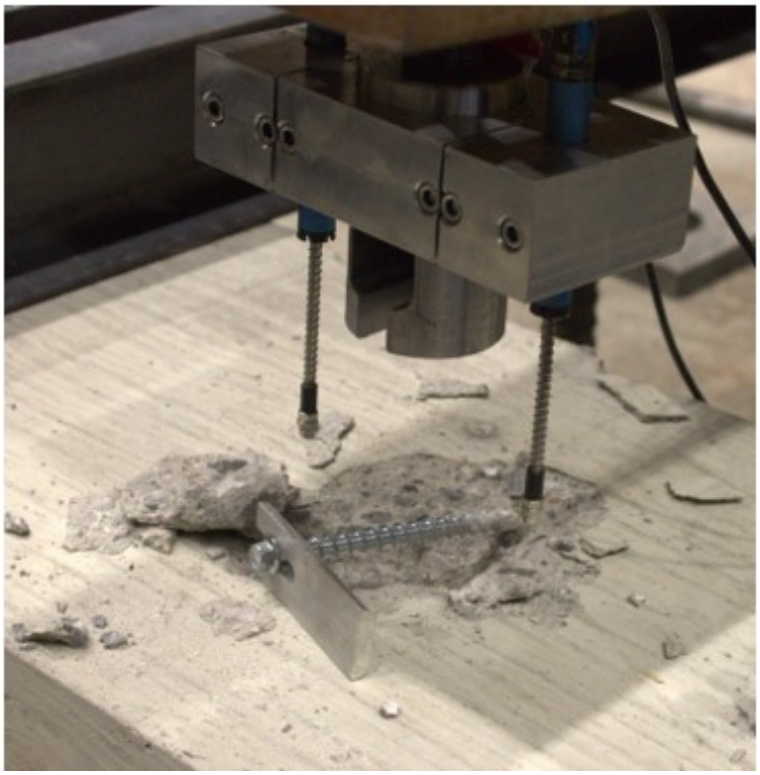

Fig. B2.27: Concrete Breakout Failure of DT-TTH-QI-02

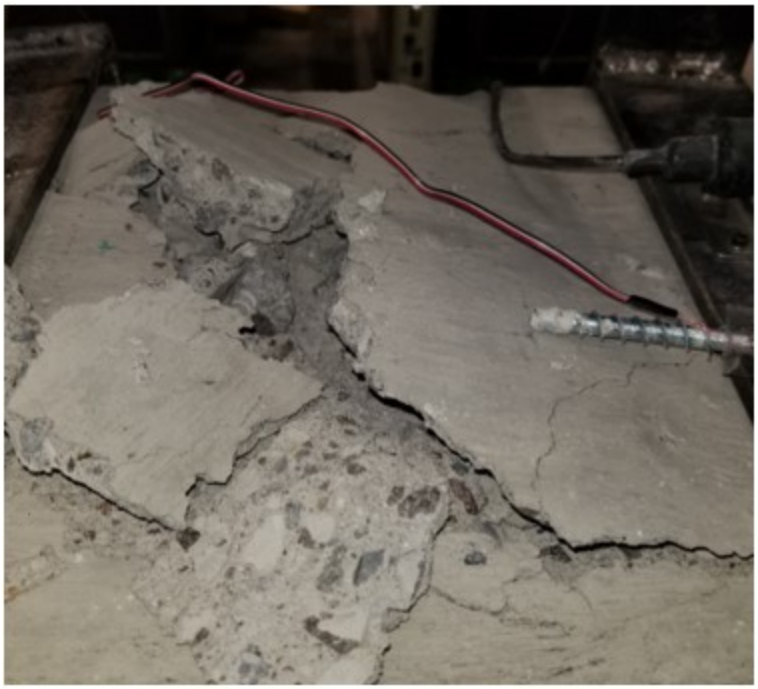

Fig. B2.28: Concrete Breakout Failure of DT-TTH-QI-02

Fig. B2.29: Concrete Breakout Failure of DT-TTH-QI-03

Fig. B2.30: Concrete Breakout Failure of DT-TTH-QI-03

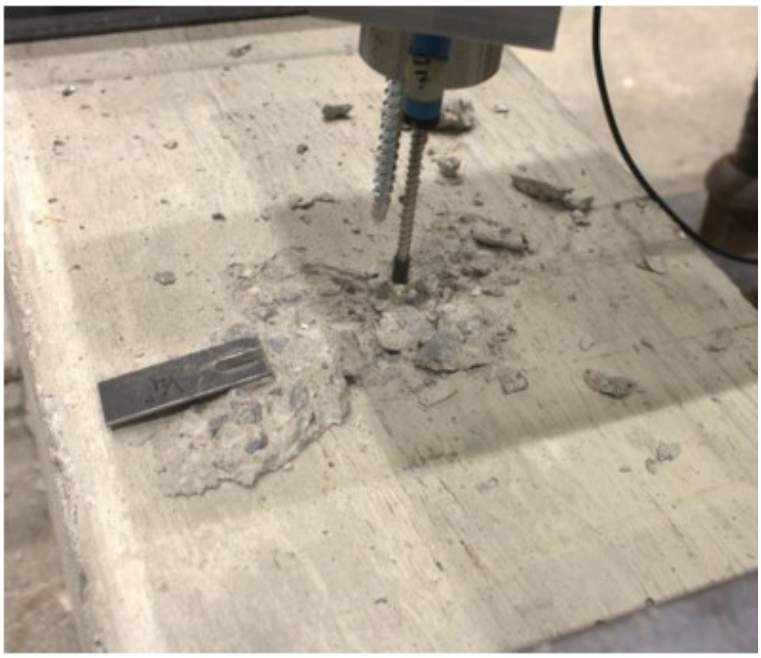

Fig. B2.31: Concrete Breakout Failure of DT-TTH-QI-06

Fig. B2.32: Concrete Breakout Failure of DT-TTH-TE-01

Fig. B2.33: Concrete Breakout Failure of DT-TTH-TE-02

Fig. B2.34: Concrete Breakout Failure of DT-TTH-TE-03

Fig. B2.35: Beam Splitting Failure of DT-TTH-HL-01

Fig. B2.36: Concrete Breakout Failure of DT-TTH-HL-02

Fig. B2.37: Concrete Breakout Failure for DT-TTH-HL-03